IOWA STATE UNIVERSITY
Digital Repository

Retrospective Theses and Dissertations

Iowa State University Capstones, Theses and Dissertations

1969

A theoretical study on the postbuckling strength of webplates in steel plate girders

Eiichi Watanabe
Iowa State University

Follow this and additional works at: https://lib.dr.iastate.edu/rtd

 Part of the Civil Engineering Commons

Recommended Citation
Watanabe, Eiichi, "A theoretical study on the postbuckling strength of webplates in steel plate girders " (1969). *Retrospective Theses and Dissertations*. 4162.
https://lib.dr.iastate.edu/rtd/4162

This Dissertation is brought to you for free and open access by the Iowa State University Capstones, Theses and Dissertations at Iowa State University Digital Repository. It has been accepted for inclusion in Retrospective Theses and Dissertations by an authorized administrator of Iowa State University Digital Repository. For more information, please contact digirep@iastate.edu.

www.manaraa.com

70-13,642

WATANABE, Eiichi, 1942-
A THEORETICAL STUDY ON THE POST-BUCKLING STRENGTH OF WEBPLATES IN STEEL PLATE GIRDERS.

Iowa State University, Ph.D., 1969
Engineering, civil

University Microfilms, Inc., Ann Arbor, Michigan

THIS DISSERTATION HAS BEEN MICROFILMED EXACTLY AS RECEIVED

A THEORETICAL STUDY ON THE POST-BUCKLING STRENGTH OF WEBPLATES IN STEEL PLATE GIRDERS

by

Eiichi Watanabe

A Dissertation Submitted to the
Graduate Faculty in Partial Fulfillment of
The Requirements for the Degree of
DOCTOR OF PHILOSOPHY

Major Subject: Structural Engineering

Approved:

Signature was redacted for privacy.

In Charge of Major Work

Signature was redacted for privacy.

Head of Major Department

Signature was redacted for privacy.

Dean of Graduate College

Iowa State University
Ames, Iowa

1969

TABLE OF CONTENTS

NOTATION

a	Distance between vertical stiffeners or panel length
A	Amplitude of total initial deflection at the center of plate
A_f, A'_f	Cross sectional areas of upper and lower flanges, respectively
A_s, A'_s	Cross sectional areas of left and right stiffeners, respectively
b	Distance between flanges or panel depth
c_f	Half width of the compression flange
d_f,d'_f	Widths of the upper and lower flanges, respectively
D	Flexural rigidity of plate
E	Modulus of elasticity of steel
$f_w^{(k)}$	Functions of $w^{(k)}$ where k = 1,2,3
$g_w^{(k)}$	Functions of $w^{(k)}$ where k = 1,2,3
h	Thickness of webplate
$h_w^{(k)}$	Functions of $w^{(k)}$ where k = 1,2,3
i_f,i'_f	Flexural rigidities in y-direction of upper and lower flanges, respectively
J_f,J'_f	Torsional rigidities of upper and lower flanges, respectively
J_s,J'_s	Torsional rigidities of left and right stiffeners, respectively
ℓ_k	Lateral buckling length
M	Bending moment

N	Dimension of the mesh point system
P	Load
P_{cr}	Buckling load
P_u	Ultimate load
S	Shearing force on a beam
t_f, t_f'	Thicknesses of upper and lower flanges, respectively
u_i	Displacement vector component
u,v,w	Displacement components in x-, y- and z-directions, respectively
$u^{(k)}, v^{(k)}, w^{(m)}$	k-th order displacement components in x-, y- and z-directions, respectively
$\tilde{u}^{(k)}, \tilde{v}^{(k)}, \tilde{w}^{(k)}$	Nondimensionalized k-th order displacement components in x-, y- and z-directions, respectively
u^T, v^T, w^T	Total displacement components in x-, y- and z-directions, respectively
$w^{(0)}$	0-th order elastic deflection
w_o	Total initial deflection
$\tilde{w}_o$	Nondimensionalized total initial deflection
w^T	Total deflection
w_e^T	Total elastic deflection
x, y, z	Coordinates
α	σ_o/E
β, β'	a/h and b/h respectively (slenderness ratios of webplate)

β_f	Slenderness ratio of compression flange
β_v	Critical slenderness ratio of plate for vertical buckling of flange
Δ	Nondimensionalized load
Δ_{cr}^{L}, Δ_{cr}^{T}	Nondimensionalized lateral and torsional buckling loads, respectively
Δ_{wcr}	Nondimensionalized plate buckling load
Δ_u	Nondimensionalized ultimate load
ε_{ij}	Strain tensor component
$\bar{\varepsilon}_x$, $\bar{\varepsilon}_y$, $\bar{\varepsilon}_{xy}$	Strain tensor components in the plane of plate
ε_{bx}, ε_{by}, ε_{bxy}	Bending strain components
ζ	σ_o/σ_{Yw}
Θ	$\lambda M/(aS)$
κ_f, κ_f'	Nondimensionalized flexural rigidities of upper and lower flanges, respectively
λ	Aspect ratio of panel (b/a)
μ	Nondimensionalized amplitude of total initial deflection (A/h)
ν	Poisson's ratio of steel
ξ, η	Nondimensionalized coordinates
$\bar{\sigma}_x$, $\bar{\sigma}_y$, $\bar{\tau}_{xy}$	In-plane stress components
$\bar{\sigma}_x^{(k)}$, $\bar{\sigma}_y^{(k)}$, $\bar{\tau}_{xy}^{(k)}$	k-th order in-plane stress components
$\tilde{\sigma}_x^{(k)}$, $\tilde{\sigma}_y^{(k)}$, $\tilde{\sigma}_{xy}^{(k)}$	Nondimensionalized k-th order in-plane stress components

$\bar{\sigma}_x^T$, $\bar{\sigma}_y^T$, $\bar{\sigma}_{xy}^T$	Total in-plane stress components
σ_{xo}, σ_{yo}, σ_{xyo}	Initial stress components
$\tilde{\sigma}_{xo}$, $\tilde{\sigma}_{yo}$, $\tilde{\sigma}_{xyo}$	Nondimensionalized initial stress components
σ_{bx}, σ_{by}, τ_{bxy}	Bending stress components
σ_{bxo}, σ_{byo}, σ_{bxyo}	Initial bending stress components
σ_f, σ'_f	Stresses in upper and lower flanges, respectively
σ_f, σ'_f	Nondimensionalized stresses in upper and lower flanges, respectively
σ_o	σ_{yo} at $x = a/2$ and $y = 0$
σ_s, σ'_s	Stresses in left and right stiffeners, respectively
$\tilde{\sigma}_s$, $\tilde{\sigma}'_s$	Nondimensionalized stresses in left and right stiffeners, respectively
σ_{Yf}, σ'_{Yf}	Tensile strengths of upper and lower flanges, respectively
σ_{Yw}	Tensile strength of webplate
τ	Average external edge shearing stress
ϕ_f, ϕ'_f	Nondimensionalized cross sectional areas of upper and lower flanges, respectively
ϕ_s, ϕ'_s	Nondimensionalized cross sectional areas of left and right stiffeners, respectively
ψ_f, ψ'_f	Nondimensionalized torsional rigidities of upper and lower flanges, respectively

ψ_s, ψ'_s	Nondimensionalized torsional rigidities of left and right stiffeners, respectively
ω	$2\pi/(N-1)$

CHAPTER ONE: INTRODUCTION

Purpose of Study

The frequent use of steel in bridges, buildings, ships and aircraft makes it necessary to consider instability problems in these structures. With recent increase in the use of high strength steel, the instability problems are becoming even more important in the design of steel structures. It is true that structures made of high strength steel can be designed so that their weights are reduced compared with those made of ordinary carbon steel. However, the structures made of high strength steel tend to be more flexible and less stable because of reduction in cross sectional areas with the modulus of elasticity remaining the same.

One of the most important and interesting problems of this kind is found in the design of webplates in steel plate girders. Since the end of the 19th century, many attempts have been made to design webplates of steel girders considering their buckling stresses based on the small deflection theory of plates. It has been a well-known fact, however, that buckling stress of webplate has little bearing on the true load carrying capacity of webplate. Furthermore, buckling of webplate seldom occurs because of the existence of initial deflection in the webplate. This gives rise to the following question: "If the buckling of the webplate is not important, is it possible to design a

really flexible webplate without having instability problems?" Currently, it is believed that even a very flexible webplate can carry a considerable load if the girder is well designed. For this reason, the specifications for the design of webplates are being subjected to reconsideration in various countries.

The purpose of this study is to investigate the significance of plate buckling on the behavior of plate girders and the behavior of girder panels beyond their buckling loads.

Specific points of interest in this study are:

1. Effect of initial stresses due to some causes such as welding,

2. Effect of initial deflections due to some causes such as welding,

3. Effect of rigidities of the boundary members such as flanges and stiffeners,

4. Load carrying capacity of webplate in pure shear condition,

5. Load carrying capacity of webplate in pure bending condition,

6. Load carrying capacity of webplate in combined shear and bending condition,

7. Effect of yield strength of steel,

A method of analysis based on the large deflection theory of plates is proposed for the purpose of this study. It is

noted that several attempts were made to analyze webplates with simple boundary conditions in the past. In the proposed analysis, plate girder panels are considered as elastic systems consisting of webplates and their surrounding members. The boundary conditions, therefore, include various interactions between the webplates and their surrounding members. It is necessary to establish, first, how well the proposed analysis predicts the behavior of the panels and secondly, how it may be used to predict the ultimate loads of panels. Elasto-plastic analysis of the webplates is beyond the scope of the proposed analysis; however, it is important to know under what load yielding initiates in the panel.

The large deflection theory of plates is a nonlinear theory and its mathematical natures are not yet completely known. Two major problems exist in the proposed analysis: (1) how to linearize the nonlinear partial differential equations, and (2) how to meet complex boundary conditions imposed on the panels. For the first problem, a method similar to perturbation method is applied. For the second problem, the finite difference method is used since analytical solution is extremely difficult.

Definition of a Plate Girder

A plate girder can be defined as a deep flexural member consisting of webplate, flanges (with or without cover plates)

and stiffeners. The girder elements such as webplate, flange plates, cover plates and stiffeners are connected to each other by means of welding, riveting or bolting. Plate girders are frequently used in bridges and large span buildings whenever and wherever the cross sections are considered to be economical. Unlike rolled beams, the design of plate girders requires special considerations on the problems of instability. Figure 1 shows some typical plate girders for highway bridges, and Figure 2 shows some possible cross sections for plate girders.

Summary of Previous Work

It is amazing to note that the first instability problem was formulated both theoretically and experimentally by Euler about two centuries ago when structures were mainly made of stones, bricks and wood. Euler's concept slept and was not brought into practice for a long time until steel began to be used for buildings and bridges. Euler investigated the instability problem of columns subjected to axial compressive load. Since the end of the 19th century, great efforts were made by many investigators to solve the buckling problems of flexible structures mainly made of steel. The concept used for column buckling was also applied to plate buckling problems and plate buckling was believed to govern the load carrying capacity of webplates of steel plate girders. Later, through

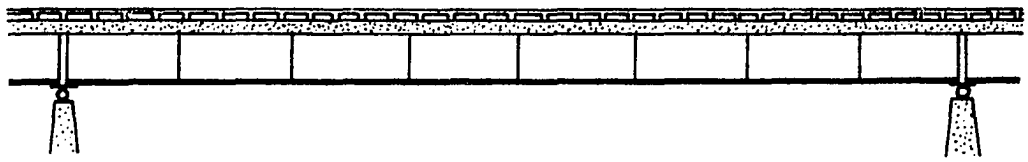

(a) Straight plate girder with vertical stiffeners

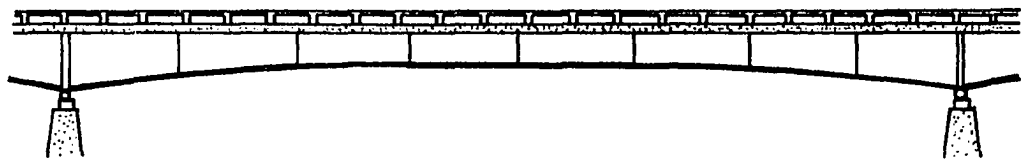

(b) Haunched plate girder with vertical stiffeners

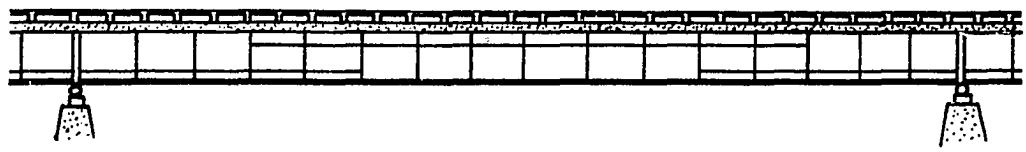

(c) Straight plate girder with vertical and horizontal stiffeners

Figure 1. Typical plate girders used for highway bridges

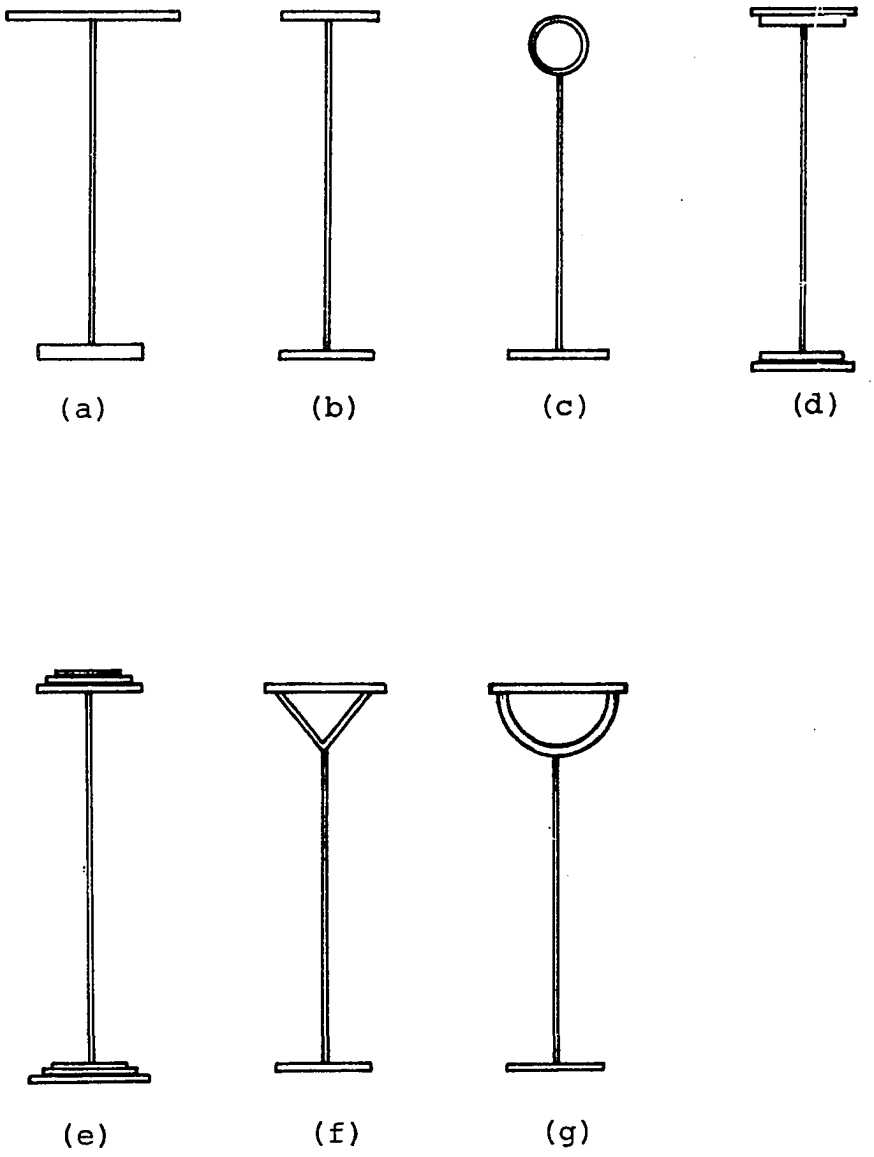

Figure 2. Possible cross sections for plate girders

practices and experiments, the phenomenon of plate buckling proved to be significantly different from that of column buckling, and the existence of postbuckling strength in plates became gradually recognized.

In order to have the mathematical explanation of the post-buckling behavior of webplates, von Kármán first formulated the large deflection theory of plates (15) and later introduced the concept of effective width for plate in compression (16). After von Kármán, many investigators solved the post-buckling problems mathematically using Fourier series or using energy approach (11, 25, 29, 30, 31). Alexeev (1) made use of a successive approximation method in solving the nonlinear equations of large deflection theory of plates.

Basler and others (2, 3, 4, 5, 13) performed an extensive investigation on welded plate girders experimentally and established the concepts of load carrying capacity of steel girders subjected to bending, shear, or both combined. The analysis they proposed and used is not highly theoretical. Yet it is quite simple and accurate in the prediction of load carrying capacities so that fairly good design can be expected from the design formulas they derived. In a panel subjected to bending moment, some portion of the webplate in compression zone is assumed to offer no resistance to the bending because of the buckling of the webplate. On the other hand, in a panel subjected to shearing forces, a diagonal tension field is

assumed in such a way that the flanges do not provide the anchor for the tension field. Their method is a limit analysis method since a failure mode is assumed in computing ultimate load. The only drawback of this method is that it cannot provide the behavioral informations of girder panels throughout its loading stage.

Cooper and others (10) investigated the load carrying capacity of welded constructional alloy steel plate girders. The emphasis was placed on the effects of high strength steel and the effects of residual stress in girder panels.

Massonnet and others (19, 20) investigated experimentally the effect of stiffeners intensively and established the minimum rigidity required for stiffeners to maintain girder panels in stable conditions.

Rockey, Cook and Leggett (7, 8, 9, 24) investigated experimentally the buckling loads of panels with horizontal stiffeners and the optimum rigidity for the stiffeners to keep the panels stable.

Škaloud and Donea (25) investigated the effect of the residual stress on the post-buckling behavior of webplates. The large deflection theory of plates was used in the analysis. The effect of the initial deflection and the minimum requirement for the flange rigidity in the post-buckling range of webplate were also studied.

A method quite similar to perturbation method was used by Stein (26, 27) to investigate the post-buckling behavior of

simply supported rectangular plates subjected to longitudinal compression and subjected to a uniform temperature rise. The basis of his approach is the expansion of unknown displacement components into a power series in terms of an arbitrary parameter. This expansion enables the conversion of the non-linear large deflection equations of von Kármán into a set of linear equations. Stein states that the method of solution he used is similar to a perturbation method and that in a true perturbation method, consideration is restricted to solutions which involve only small values of the arbitrary parameter. Furthermore, he explains that the smallness of the arbitrary parameter is not required in his analysis since the coefficients of the higher powers are small. Mansfield made use of a method similar to Stein's to analyze the post-buckling behavior of a compressed square plate (17, 18).

CHAPTER TWO: PROPOSED THEORETICAL ANALYSIS

Basic Assumptions for the Analysis

Figure 3 shows a panel of steel plate girder surrounded by two flanges and two vertical stiffeners and subjected to a combination of bending moment, M, and shear. The shearing stress, τ, is assumed to be constant over the cross sectional area of webplate.

The girder panel system is assumed to be linearly elastic until yielding occurs. The initiation of yielding is predicted by von Mises yield criterion.

The analysis requires solution of displacement components u, v and w in x-, y- and z-directions, respectively. For convenience, the rigid body motion displacement components should be eliminated from the system. Thus, the degree of freedom of the system is six, of which three refer to the displacement components u and v; while the other three refer to the displacement components, w. For convenience, it is assumed that displacement components u vanish at corner points (0,0) and (0,b) (See coordinates shown in Figure 3), and the displacement component v vanishes at corner point (0,0). On the other hand, displacement component w is assumed to vanish at any three of four corner points.

The flexural rigidities of the boundary members are quite large compared with the flexural rigidity of the plate so that

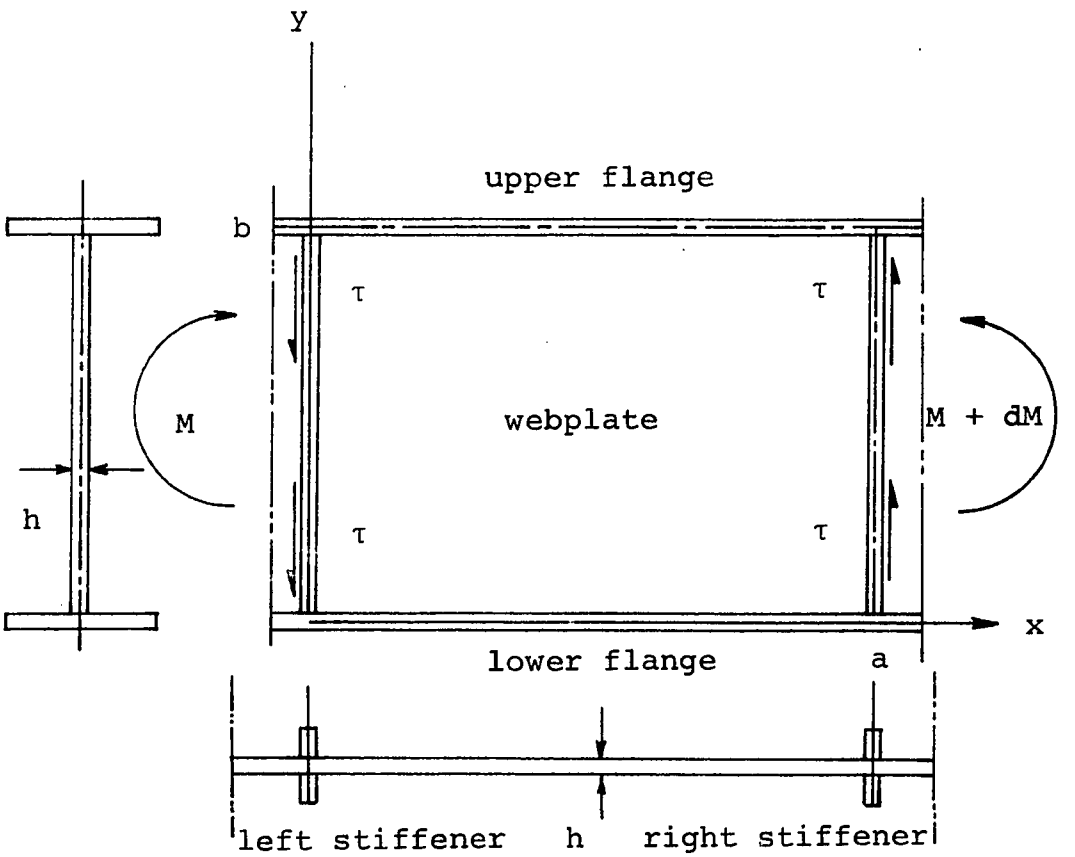

Figure 3. Steel plate girder panel

the curvatures of displacement component w are assumed to be negligible along the boundaries. Hence, combining with the assumptions mentioned above, the displacement component w vanishes along the boundary members. Similarly, the flexural rigidities of boundary members consisting of a stiffener and the adjacent panel are quite large so that the curvature associated with displacement u in y-direction can be assumed to be negligible. Combining with the assumptions previously made, the displacement component u is assumed to vanish along the edge $x = 0$.

Based on the above-mentioned assumptions, the girder panel shown in Figure 3 can be represented by the mechanical model shown in Figure 4. Analytical description of boundary and loading conditions associated with this model is given in a later section.

Basic Relations

The purpose of this section is to define certain relationships among stresses, strains, and displacements, which are used in the development of the proposed analysis.

Stresses

The stresses can be divided into in-plane stresses and bending stresses.

In-plane stresses The in-plane stresses can be further divided into two: the initial stresses and the stresses due to loading. Let the initial in-plane stresses

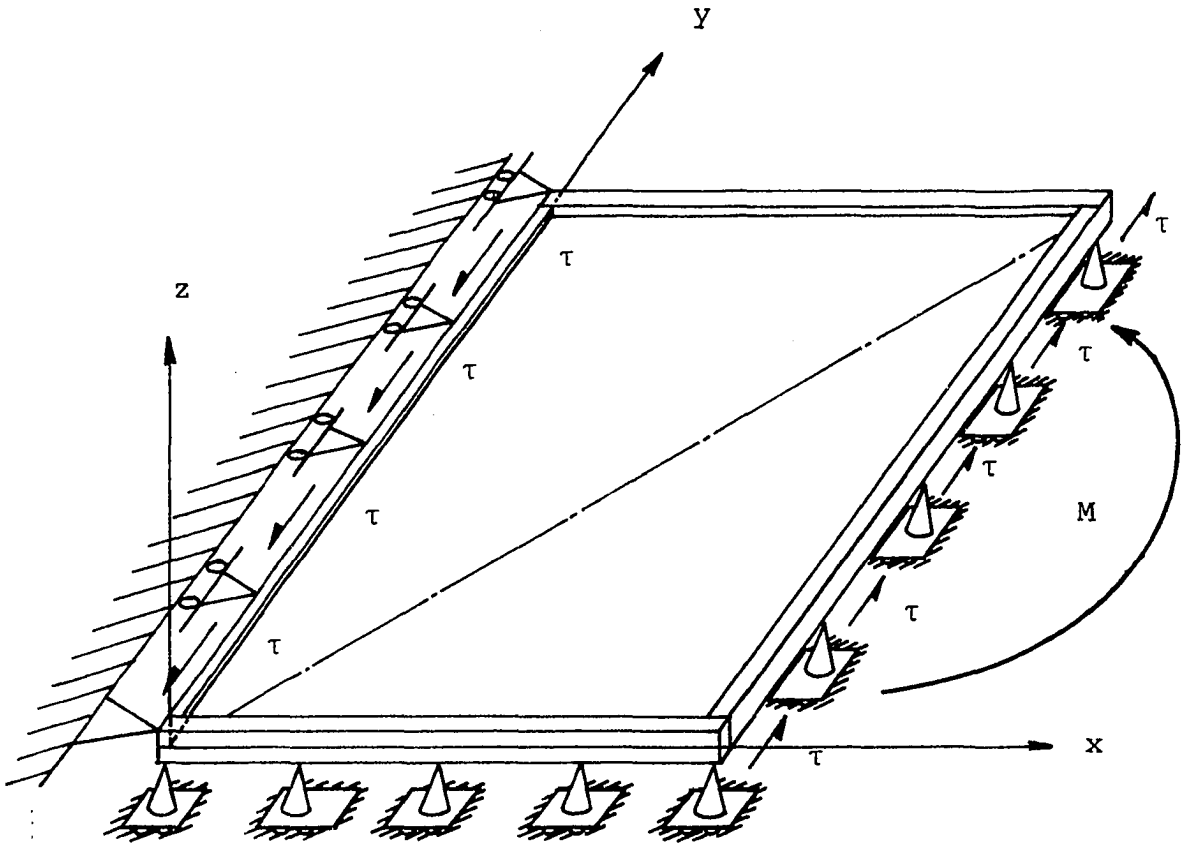

Figure 4. Simplified mechanical model of webplate panel

be designated as follows:

$$\sigma_{xo}, \quad \sigma_{yo}, \quad \tau_{xyo}$$

Let the in-plane stresses due to loading be designated as follows:

$$\bar{\sigma}_x, \quad \bar{\sigma}_y, \quad \bar{\tau}_{xy}$$

Then, the total in-plane stresses $\bar{\sigma}_x^T$, $\bar{\sigma}_y^T$ and $\bar{\tau}_{xy}^T$ are:

$$\begin{aligned} \bar{\sigma}_x^T &= \sigma_{xo} + \bar{\sigma}_x \\ \bar{\sigma}_y^T &= \sigma_{yo} + \bar{\sigma}_y \\ \bar{\tau}_{xy}^T &= \tau_{xyo} + \bar{\tau}_{xy} \end{aligned} \tag{1}$$

The sign convention for these stresses is shown in Figure 5.

Bending stresses Similarly, the initial bending stresses are designated by:

$$\sigma_{bxo}, \quad \sigma_{byo}, \quad \tau_{bxyo},$$

and the bending stresses caused by the loading are designated by:

$$\sigma_{bx}, \quad \sigma_{by}, \quad \tau_{bxy}$$

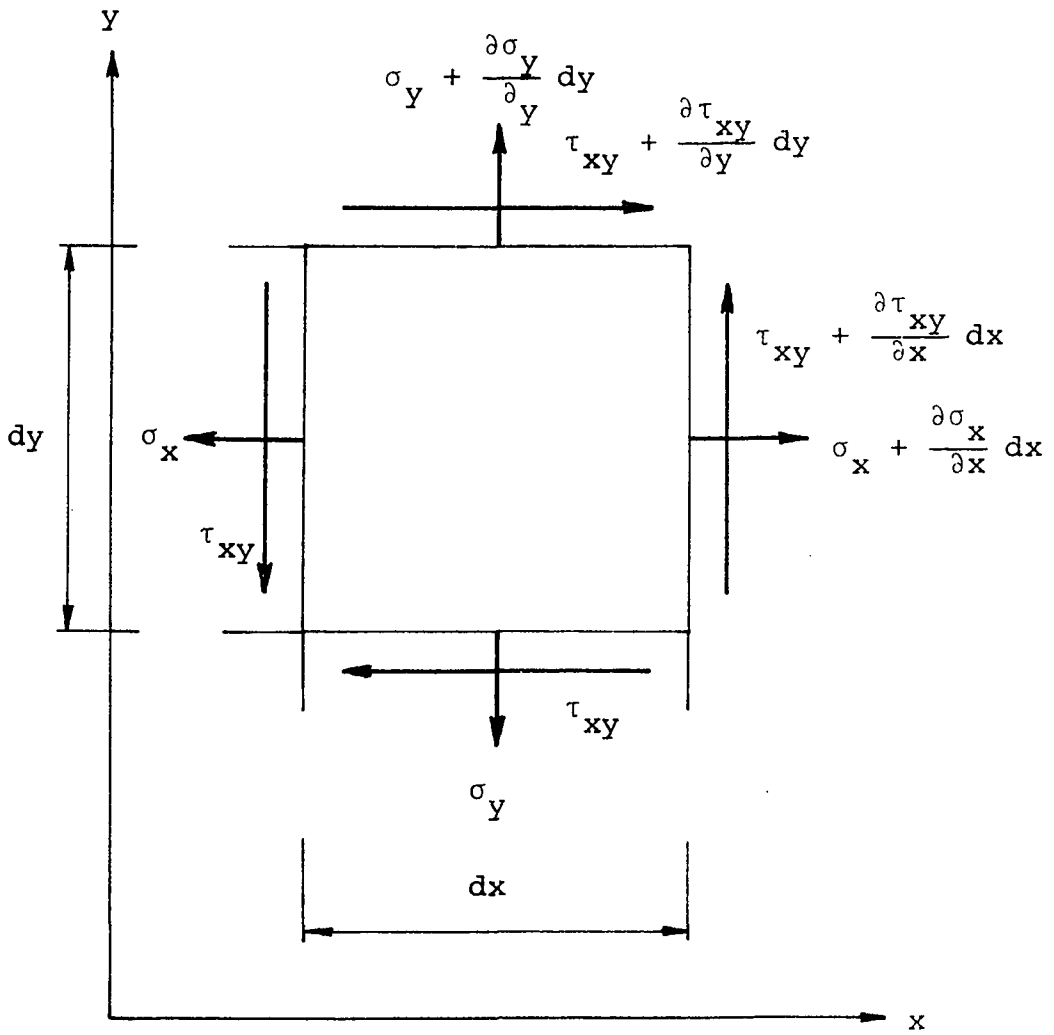

Figure 5. Sign convention for stresses

Stress-strain relationship

According to the Hooke's law, the in-plane stress-strain relationship is given by the following equation in matrix form:

$$\begin{Bmatrix} \bar{\sigma}_x \\ \bar{\sigma}_y \\ \bar{\tau}_{xy} \end{Bmatrix} = E \begin{bmatrix} \frac{1}{1-\nu^2} & \frac{\nu}{1-\nu^2} & 0 \\ \frac{\nu}{1-\nu^2} & \frac{1}{1-\nu^2} & 0 \\ 0 & 0 & \frac{1}{2(1+\nu)} \end{bmatrix} \begin{Bmatrix} \bar{\varepsilon}_x \\ \bar{\varepsilon}_y \\ \bar{\gamma}_{xy} \end{Bmatrix} \tag{2}$$

Similarly, in bending

$$\begin{Bmatrix} \sigma_{bx} \\ \sigma_{by} \\ \tau_{bxy} \end{Bmatrix} = E \begin{bmatrix} \frac{1}{1-\nu^2} & \frac{\nu}{1-\nu^2} & 0 \\ \frac{\nu}{1-\nu^2} & \frac{1}{1-\nu^2} & 0 \\ 0 & 0 & \frac{1}{2(1+\nu)} \end{bmatrix} \begin{Bmatrix} \varepsilon_{bx} \\ \varepsilon_{by} \\ \gamma_{bxy} \end{Bmatrix} \tag{3}$$

where $\bar{\varepsilon}_x$, $\bar{\varepsilon}_y$ and $\bar{\gamma}_{xy}$ refer to in-plane strains, and ε_{bx}, ε_{by} and γ_{bxy} refer to bending strains, both due to loading.

Displacement vector components

The displacement can be expressed by a vector which has three components u, v and w in x-, y- and z-directions,

respectively. In general, initial (or residual) deflection exists in a webplate due to welding process. Let this initial deflection be designated by w_o. Then, the total deflection w^T is given as follows:

$$w^T = w + w_o \tag{4}$$

The initial displacement components in the plane of the plate u_o and v_o are assumed to be zero. Therefore, the total displacement can be expressed by the following equation:

$$\begin{Bmatrix} u^T \\ v^T \\ w^T \end{Bmatrix} = \begin{Bmatrix} 0 \\ 0 \\ w_o \end{Bmatrix} + \begin{Bmatrix} u \\ v \\ w \end{Bmatrix} \tag{5}$$

Strain-displacement relationship

Again, there are two different strain-displacement relationships: one for in-plane and the other for bending.

In-plane strain-displacement relationship The etching of the neutral plane corresponding to the non-linear portion of the strains is also considered. Using Lagrange's displacement-strain tensor concept, the relationship is symbolically written as follows:

$$\varepsilon_{ij} = 1/2\ (u_{i,j} + u_{j,i} + u_{k,i}\ u_{k,j})$$

where

$$u_{i,j} = \frac{\partial u_i}{\partial x_j}$$

and $$u_{k,i}\, u_{k,j} = \sum_{k=1}^{3} \frac{\partial u_k}{\partial x_i} \cdot \frac{\partial u_k}{\partial x_j} \,. \tag{6}$$

ε_{ij} refer to the strain tensor components; while u_i refer to the displacement vector components.

The term $u_{k,i}\, u_{k,j}$ represents the nonlinear strain component due to large deflection. However, it is generally assumed that the in-plane displacement components u, v are quite small compared with the deflection w so that

$$u_{k,i}\, u_{k,j} \doteq w_{,i}\, w_{,j} = \frac{\partial w}{\partial x_i} \cdot \frac{\partial w}{\partial x_j} \tag{7}$$

In terms of x,y coordinates, the components of the total in-plane strain as applied to the cases of thin plate with large deflection can now be written as:

$$\begin{aligned} \bar{\varepsilon}_x^T &= \frac{\partial u^T}{\partial x} + \frac{1}{2} \frac{\partial w^T}{\partial x} \cdot \frac{\partial w^T}{\partial x} \\ \bar{\varepsilon}_y^T &= \frac{\partial v^T}{\partial y} + \frac{1}{2} \frac{\partial w^T}{\partial y} \cdot \frac{\partial \bar{w}^T}{\partial y} \\ \bar{\gamma}_{xy}^T &= \frac{\partial u^T}{\partial y} + \frac{\partial v^T}{\partial x} + \frac{\partial w^T}{\partial x} \cdot \frac{\partial w^T}{\partial y} \end{aligned} \tag{8}$$

where $\bar{\varepsilon}_x^T$, $\bar{\varepsilon}_y^T$ and $\bar{\gamma}_{xy}^T$ are total in-plane strain components. Substituting the displacement vector components given in Equation 5, the following equations are obtained:

$$\bar{\varepsilon}_x^T = \bar{\varepsilon}_x + \varepsilon_{xo}$$

$$\bar{\varepsilon}_y^T = \bar{\varepsilon}_y + \varepsilon_{yo} \tag{9}$$

$$\bar{\gamma}_{xy}^T = \bar{\gamma}_{xy} + \gamma_{xyo}$$

where

$$\bar{\varepsilon}_x \equiv \frac{\partial u}{\partial x} + \frac{1}{2}\left(\frac{\partial w}{\partial x}\right)^2 + \frac{\partial w_o}{\partial x}\cdot\frac{\partial w}{\partial x}$$

$$\bar{\varepsilon}_y \equiv \frac{\partial v}{\partial y} + \frac{1}{2}\left(\frac{\partial w}{\partial y}\right)^2 + \frac{\partial w_o}{\partial y}\cdot\frac{\partial w}{\partial y}$$

$$\bar{\gamma}_{xy} \equiv \frac{\partial u}{\partial y} + \frac{\partial v}{\partial x} + \frac{\partial w}{\partial x}\cdot\frac{\partial w}{\partial y} + \frac{\partial w_o}{\partial x}\cdot\frac{\partial w}{\partial y} + \frac{\partial w_o}{\partial y}\frac{\partial w}{\partial x} \tag{10}$$

and

$$\varepsilon_{xo} = \frac{1}{2}\left(\frac{\partial w_o}{\partial x}\right)^2$$

$$\varepsilon_{yo} = \frac{1}{2}\left(\frac{\partial w_o}{\partial y}\right)^2 \tag{11}$$

$$\gamma_{xyo} = \frac{\partial w_o}{\partial x}\cdot\frac{\partial w_o}{\partial y}$$

Bending strain-displacement relationship According to the theory of plates,

$$\varepsilon_{bx} = -z\,\frac{\partial^2 w}{\partial x^2}$$

$$\varepsilon_{by} = -z \frac{\partial^2 w}{\partial y^2}$$

$$\gamma_{bxy} = -2z \frac{\partial^2 w}{\partial x \partial y} \tag{12}$$

Stress-displacement relationship

Making use of the stress-strain relationships and the strain-displacement relationships, the stress-displacement relationships are obtained for both the in-plane and bending stresses.

In-plane stress-displacement relationship

$$\bar{\sigma}_x = \frac{E}{1-\nu^2}\left[\frac{\partial u}{\partial x} + \nu\frac{\partial v}{\partial y} + \left(\frac{\partial w_o}{\partial x}\frac{\partial}{\partial x} + \nu\frac{\partial w_o}{\partial y}\frac{\partial}{\partial y}\right) w \right.$$

$$\left. + \frac{1}{2}\left(\frac{\partial w}{\partial x}\right)^2 + \frac{\nu}{2}\left(\frac{\partial w}{\partial y}\right)^2\right]$$

$$\bar{\sigma}_y = \frac{E}{1-\nu^2}\left[\frac{\partial v}{\partial y} + \nu\frac{\partial u}{\partial x} + \left(\frac{\partial w_o}{\partial y}\frac{\partial}{\partial y} + \nu\frac{\partial w_o}{\partial x}\frac{\partial}{\partial x}\right) w \right.$$

$$\left. + \frac{1}{2}\left(\frac{\partial w}{\partial y}\right)^2 + \frac{\nu}{2}\left(\frac{\partial w}{\partial x}\right)^2\right] \tag{13}$$

$$\bar{\tau}_{xy} = \frac{E}{2(1+\nu)}\left[\frac{\partial u}{\partial y} + \frac{\partial v}{\partial x} + \left(\frac{\partial w_o}{\partial x}\frac{\partial}{\partial y} + \frac{\partial w_o}{\partial y}\frac{\partial}{\partial x}\right) w \right.$$

$$\left. + \frac{\partial w}{\partial x}\cdot\frac{\partial w}{\partial y}\right]$$

Bending stress-displacement relationship

$$\sigma_{bx} = \frac{-Ez}{1-\nu^2}\left(\frac{\partial^2 w}{\partial x^2} + \nu\frac{\partial^2 w}{\partial y^2}\right)$$

$$\sigma_{by} = \frac{-Ez}{1-\nu^2}\left(\frac{\partial^2 w}{\partial y^2} + \nu\frac{\partial^2 w}{\partial x^2}\right) \qquad (14)$$

$$\tau_{bxy} = \frac{-Ez}{1+\nu}\frac{\partial^2 w}{\partial x \partial y}$$

Criterion of yielding

Among several yielding criteria, von Mises' yield criterion is generally accepted for steel. To determine the initiation of yielding in the webplate the following von Mises comparison stresses are first defined:

$$\sigma_{vM} = \sqrt{\bar{\sigma}_x^2 + \bar{\sigma}_y^2 - \bar{\sigma}_x \cdot \bar{\sigma}_y + 3\,\bar{\tau}_{xy}^2}$$

$$\sigma_{vM1} = \sqrt{\sigma_{x1}^2 + \sigma_{y1}^2 - \sigma_{x1} \cdot \sigma_{y1} + 3\,\tau_{xy1}^2} \qquad (15)$$

$$\sigma_{vM2} = \sqrt{\sigma_{x2}^2 + \sigma_{y2}^2 - \sigma_{x2} \cdot \sigma_{y2} + 3\,\tau_{xy2}^2}$$

If σ_{vM}, σ_{vM1} and σ_{vM2} are less than the yield strength of the webplate, σ_{yw}, the webplate is elastic. The subscripts 1 and 2 refer to upper and lower surfaces of the plate, respectively. The terms without numerical subscript are for the middle plane

of the plate. Thus, σ_{vM}, σ_{vM1} and σ_{vM2} correspond to von Mises comparison stresses at mid-depth, on upper surface and on lower surface of the webplate, respectively. Naturally, bending and in-plane stress components are added for stress components with numerical subscripts.

If the appropriate von Mises comparison stress is smaller than the yield strength of the webplate, σ_{Yw}, the point in question is considered to be elastic.

Formulation of the Problem

Large deflection theory of plates

The small deflection theory of thin plates established by Lagrange is based on the following assumptions:

1. Points of the plate lying initially on a normal-to-the-middle plane of the plate remain on the normal-to-the-middle surface of the plate after bending.

2. The normal stresses in the direction transverse to the plate can be ignored.

3. The middle plane of plate remains neutral during bending of plate.

4. The deflection of plate is very small compared with the thickness of plate.

In the large deflection theory of plates, assumptions 1 and 2 are retained; however, assumptions 3 and 4 are not retained any more. It is believed that if the deflection is

less than 40% of the thickness of plate, then the stretching of the middle surface can be neglected without a substantial error in the magnitude of maximum bending stress (29).

Theoretically, the stretching of the middle surface is accompanied by terms which are proportional to the square products of the deformational slopes. Mathematically, these terms are referred to as nonlinear strain components.

The large deflection theory of plates in which the stretching of the middle plane is taken into account was formulated by von Kármán (15). It should be noted, however, that the lateral displacement or the deflection of plate is assumed to be the only displacement component that gives rise to the nonlinear components.

If there is no lateral load acting on the plate, the basic equations of equilibrium of plate are given as follows:

$$\frac{\partial \bar{\sigma}_x^T}{\partial x} + \frac{\partial \bar{\tau}_{xy}^T}{\partial y} = 0$$

$$\frac{\partial \bar{\tau}_{xy}^T}{\partial x} + \frac{\partial \bar{\sigma}_y^T}{\partial y} = 0$$

$$\nabla^4 w_e^T = \frac{h}{D} \left(\bar{\sigma}_x^T \frac{\partial^2}{\partial x^2} + \bar{\sigma}_y^T \frac{\partial^2}{\partial y^2} + 2 \bar{\tau}_{xy}^T \frac{\partial^2}{\partial x \partial y} \right) w^T \qquad (16)$$

where:

$w_e^T = w + w^{(0)}$, and

$w^T = w + w_o$, also,

D = flexural rigidity of plate = $\frac{Eh^3}{12(1-\nu^2)}$

h = thickness of plate

w = deflection of plate due to loading

$w^{(0)}$ = initial elastic deflection of plate

w_o = total initial deflection

w_e^T = total elastic deflection

$\bar{\sigma}_x^T, \bar{\sigma}_y^T, \bar{\tau}_{xy}^T$ = total in-plane stresses

The coordinate system is shown in Figure 4 and the sign convention for stresses is indicated in Figure 5.

Equations 16 are the governing differential equations for the postbuckling behavior of a girder panel model shown in Figure 4. A set of boundary conditions associated with the model is described in the next subsection.

Boundary conditions

Support conditions for w_e^T Kirchhoff established two relationships for the interaction of the plate element and an adjacent boundary element (29). One relates torsion of the plate element to bending of the boundary element; and, another relates bending of the plate element to torsion of the boundary element. In the structural model presented previously, however,

the flexural rigidities of boundary members in the direction perpendicular to the plane of plate are so large that the deflection w_e^T vanishes along every boundary. From this viewpoint, the following relationships are obtained:

1. Along $x = 0$:

$$w_e^T = 0, \quad \text{and} \quad GJ_s \frac{\partial}{\partial y}\left(\frac{\partial^2 w_e^T}{\partial x \partial y}\right) = D\left(\frac{\partial^2 w_e^T}{\partial x^2} + \nu \frac{\partial^2 w_e^T}{\partial y^2}\right)$$

2. Along $x = a$:

$$w_e^T = 0, \quad \text{and} \quad GJ'_s \frac{\partial}{\partial y}\left(\frac{\partial^2 w_e^T}{\partial x \partial y}\right) = -D\left(\frac{\partial^2 w_e^T}{\partial x^2} + \nu \frac{\partial^2 w_e^T}{\partial y^2}\right) \tag{17}$$

3. Along $y = 0$:

$$w_e^T = 0, \quad \text{and} \quad GJ'_f \frac{\partial}{\partial x}\left(\frac{\partial^2 w_e^T}{\partial x \partial y}\right) = D\left(\frac{\partial^2 w_e^T}{\partial y^2} + \nu \frac{\partial^2 w_e^T}{\partial x^2}\right)$$

4. Along $y = b$:

$$w_e^T = 0, \quad \text{and} \quad GJ_f \frac{\partial}{\partial x}\left(\frac{\partial^2 w_e^T}{\partial x \partial y}\right) = -D\left(\frac{\partial^2 w_e^T}{\partial y^2} + \nu \frac{\partial^2 w_e^T}{\partial x^2}\right)$$

where: G = Modulus of rigidity

J_s, J'_s = Torsional rigidities for stiffeners

J_f, J'_f = Torsional rigidities for flanges

Boundary conditions for in-plane displacements, u and v

In general, two relationships can be obtained to designate the interaction of the plate element and an adjacent boundary element. One refers to the longitudinal equilibrium of a

boundary element, and the other refers to the equilibrium of this element in the direction perpendicular to the axis of the boundary member. These two relationships can be expressed explicitly along y = 0 or y = b. The longitudinal equilibrium conditions along x = 0 and x = a, however, are replaced by different and simpler conditions because the curvatures of the vertical stiffeners in y-direction are assumed to vanish. The boundary conditions are given as follows:

1. Along x = 0:

$$u = 0, \quad \text{and} \quad \frac{\partial \sigma_s}{\partial y} + \frac{h}{A_s} \bar{\tau}^T_{xy} = \frac{h}{A_s} \tau$$

2. Along x = a:

$$\frac{\partial^2 u}{\partial y^2} = 0, \text{ and } \frac{\partial \sigma'_s}{\partial y} - \frac{h}{A'_s} \bar{\tau}^T_{xy} = - \frac{h}{A'_s} \tau \qquad (18)$$

3. Along y = 0:

$$Ei'_f \frac{\partial^4 v}{\partial x^4} = h \bar{\sigma}^T_y , \quad \text{and} \quad \frac{\partial \sigma'_f}{\partial x} + \frac{h}{A'_f} \bar{\tau}^T_{xy} = 0$$

4. Along y = b:

$$Ei_f \frac{\partial^4 v}{\partial x^4} = -h \bar{\sigma}^T_y, \quad \text{and} \quad \frac{\partial \sigma_f}{\partial x} - \frac{h}{A_f} \bar{\tau}^T_{xy} = 0$$

where:

σ_s, σ'_s = Stresses in left and right stiffeners, respectively

σ_f, σ'_f = Stresses in upper and lower flanges, respectively

A_s, A'_s = Cross sectional areas of left and right stiffeners, respectively

A_f, A'_f = Cross sectional areas of upper and lower flanges, respectively

i_f, i'_f = Flexural rigidities in y-direction of upper and lower flanges, respectively

Conditions of zero net resultant forces Since there is no external load acting perpendicular to a boundary member, the corresponding resultant force should vanish at each of the boundaries.

These conditions are given by the following equations:

1. Along $x = 0$

$$h\int_0^b \bar{\sigma}_x^T \, dy \Big|_{x=0} + A_f \sigma_f \Big|_{x=0} + A'_f \sigma'_f \Big|_{x=0} = 0$$

2. Along $x = a$

$$h\int_0^b \bar{\sigma}_x^T \, dy \Big|_{x=a} + A_f \sigma_f \Big|_{x=a} + A'_f \sigma'_f \Big|_{x=a} = 0$$

3. Along $y = 0$

$$h\int_0^a \bar{\sigma}_y^T \, dx \Big|_{y=0} + A_s \sigma_s \Big|_{y=0} + A'_s \sigma'_s \Big|_{y=0} = 0$$

4. Along $y = b$

$$h \int_0^a \bar{\sigma}_y^T \, dx \Big|_{y=b} + A_s \sigma_s \Big|_{y=b} + A_s' \sigma_s' \Big|_{y=b} = 0 \qquad (19)$$

Bending moment conditions The bending moment at $x = a$ should be of uniquely assigned value. The condition is given as follows:

$$M \Big|_{x=a} = -h \int_0^b \bar{\sigma}_x^T \, y \, dy \Big|_{x=a} - b \, A_f \, \sigma_f \Big|_{x=a} \qquad (20)$$

However, there are no external torques acting along two horizontal edges: $y = 0$ and $y = b$. Hence, the following conditions should be satisfied:

$$M \Big|_{\substack{y=0 \\ (y=b)}} = -h \int_0^a \bar{\sigma}_y^T \, x \, dx \Big|_{\substack{y=0 \\ (y=b)}} - a \, A_s' \, \sigma_s' \Big|_{\substack{y=0 \\ (y=b)}} = 0 \qquad (21)$$

Problem Formulation by Means of an Expansion of Displacement Components in Terms of an Arbitrary Parameter

The large deflection theory of plates is a nonlinear theory in a geometric sense, and its mathematical nature is still not well known at the present time. A rigorous analytical solution to the problem is extremely difficult. Because

of this, an attempt is made herein to solve the problem approximately with the experimental evidence as a guide. A method of expanding the solutions of Equation 16 into polynomial series is proposed in this thesis. It is seen that this method enables the linearization of the nonlinear equations and that the solution process is systematic. This polynomial series expansion is based on an engineering judgement on the load-displacement relationships experimentally obtained.

Displacements, stresses and stress-displacement relations in terms of an arbitrary parameter

The displacement components u, v and w may be expanded into the following forms in terms of an arbitrary parameter, Δ:

$$u = \sum_{k=1}^{\infty} u^{(k)} \Delta^k$$

$$v = \sum_{k=1}^{\infty} v^{(k)} \Delta^k$$

$$w = \sum_{k=1}^{\infty} w^{(k)} \Delta^k$$

where $u^{(k)}$, $v^{(k)}$ and $w^{(k)}$ $(k = 1,2,3,...)$ are unknowns yet to be determined. The terms corresponding to the first power may be identified as those which can be considered in the usual small deflection theory of plates. The terms corresponding to

the second power will be found to introduce the first approximation to the large deflection of plates. Solutions of additional higher power equations will give the second and then higher approximations (26, 27). In this thesis, however, consideration will be limited only up to the third order because of great complexity involved in the solution process for the powers higher than the third. By keeping the third power terms it is possible to evaluate the relative significance of terms corresponding to the first through the third powers. Thus, the expansion of displacement components mentioned previously may be rewritten in the following manner:

$$\begin{Bmatrix} u \\ v \\ w \end{Bmatrix} = \begin{bmatrix} u^{(1)} & u^{(2)} & u^{(3)} \\ v^{(1)} & v^{(2)} & v^{(3)} \\ w^{(1)} & w^{(2)} & w^{(3)} \end{bmatrix} \begin{Bmatrix} \Delta \\ \Delta^2 \\ \Delta^3 \end{Bmatrix} \tag{22}$$

Similarly, the in-plane and the bending stress components may be expanded into the following form:

$$\begin{Bmatrix} \bar{\sigma}_x \\ \bar{\sigma}_y \\ \bar{\tau}_{xy} \\ \sigma_{bx} \\ \sigma_{by} \\ \tau_{bxy} \end{Bmatrix} = \begin{bmatrix} \bar{\sigma}_x^{(1)} & \bar{\sigma}_x^{(2)} & \bar{\sigma}_x^{(3)} \\ \bar{\sigma}_y^{(1)} & \bar{\sigma}_y^{(2)} & \bar{\sigma}_y^{(3)} \\ \bar{\tau}_{xy}^{(1)} & \bar{\tau}_{xy}^{(2)} & \bar{\tau}_{xy}^{(3)} \\ \sigma_{bx}^{(1)} & \sigma_{bx}^{(2)} & \sigma_{bx}^{(3)} \\ \sigma_{by}^{(1)} & \sigma_{by}^{(2)} & \sigma_{by}^{(3)} \\ \tau_{bxy}^{(1)} & \tau_{bxy}^{(2)} & \tau_{bxy}^{(3)} \end{bmatrix} \begin{Bmatrix} \Delta \\ \Delta^2 \\ \Delta^3 \end{Bmatrix} \tag{23}$$

Substitution of Equation 22 and Equation 23 into Equation 13 yields the following relationship:

$$\begin{bmatrix} \bar{\sigma}_x^{(1)} & \bar{\sigma}_x^{(2)} & \bar{\sigma}_x^{(3)} \\ \bar{\sigma}_y^{(1)} & \bar{\sigma}_y^{(2)} & \bar{\sigma}_y^{(3)} \\ \bar{\tau}_{xy}^{(1)} & \bar{\tau}_{xy}^{(2)} & \bar{\tau}_{xy}^{(3)} \end{bmatrix}$$

$$= \frac{E}{1-\nu^2} \begin{bmatrix} \frac{\partial}{\partial x}, & \nu\frac{\partial}{\partial y}, & \frac{\partial w_o}{\partial x}\frac{\partial}{\partial x} + \nu\frac{\partial w_o}{\partial y}\frac{\partial}{\partial y} \\ \nu\frac{\partial}{\partial x}, & \frac{\partial}{\partial y}, & \frac{\partial w_o}{\partial y}\frac{\partial}{\partial y} + \nu\frac{\partial w_o}{\partial x}\frac{\partial}{\partial x} \\ \frac{1-\nu}{2}\frac{\partial}{\partial y}, & \frac{1-\nu}{2}\frac{\partial}{\partial x}, & \frac{1-\nu}{2}\left(\frac{\partial w_o}{\partial x}\frac{\partial}{\partial y} + \frac{\partial w_o}{\partial y}\frac{\partial}{\partial x}\right) \end{bmatrix}$$

$$\cdot \begin{bmatrix} u^{(1)} & u^{(2)} & u^{(3)} \\ v^{(1)} & v^{(2)} & v^{(3)} \\ w^{(1)} & w^{(2)} & w^{(3)} \end{bmatrix}$$

$$+ \begin{bmatrix} 0, & \frac{1}{2}\left(\frac{\partial w^{(1)}}{\partial x}\right)^2 + \frac{\nu}{2}\left(\frac{\partial w^{(1)}}{\partial y}\right)^2, & \frac{\partial w^{(1)}}{\partial x}\frac{\partial w^{(2)}}{\partial x} + \nu\frac{\partial w^{(1)}}{\partial y}\frac{\partial w^{(2)}}{\partial y} \\ 0, & \frac{1}{2}\left(\frac{\partial w^{(1)}}{\partial y}\right)^2 + \frac{\nu}{2}\left(\frac{\partial w^{(1)}}{\partial x}\right)^2, & \frac{\partial w^{(1)}}{\partial y}\frac{\partial w^{(2)}}{\partial y} + \nu\frac{\partial w^{(1)}}{\partial x}\frac{\partial w^{(2)}}{\partial x} \\ 0, & \frac{1-\nu}{2}\frac{\partial w^{(1)}}{\partial x}\frac{\partial w^{(1)}}{\partial y}, & \frac{1-\nu}{2}\left(\frac{\partial w^{(1)}}{\partial x}\frac{\partial w^{(2)}}{\partial y} + \frac{\partial w^{(1)}}{\partial y}\frac{\partial w^{(2)}}{\partial x}\right) \end{bmatrix}$$

(24)

Since $w_e^T = w + w^{(0)}$, the substitution of Equation 22 into Equation 14 yields the following relationship:

$$\begin{bmatrix} \sigma_{bxo} & \sigma_{bx}^{(1)} & \sigma_{bx}^{(2)} & \sigma_{bx}^{(3)} \\ \sigma_{byo} & \sigma_{by}^{(1)} & \sigma_{by}^{(2)} & \sigma_{by}^{(3)} \\ \tau_{bxyo} & \tau_{bxy}^{(1)} & \tau_{bxy}^{(2)} & \tau_{bxy}^{(3)} \end{bmatrix}$$

$$= -\frac{E\,z}{1-\nu^2} \begin{Bmatrix} \frac{\partial^2}{\partial x^2} + \nu\frac{\partial^2}{\partial y^2} \\ \frac{\partial^2}{\partial y^2} + \nu\frac{\partial^2}{\partial x^2} \\ (1-\nu)\frac{\partial^2}{\partial x \partial y} \end{Bmatrix} \left(w^{(0)},\ w^{(1)},\ w^{(2)},\ w^{(3)}\right) \qquad (25)$$

Equations of equilibrium in terms of polynomial series

Upon substitutions of the polynomial series for both displacement components, Equation 22, and the in-plane stresses, Equation 23, into Equation 16, the following sets of simultaneous equations are obtained.

Zero order approximation

$$\frac{\partial \sigma_{xo}}{\partial x} + \frac{\partial \tau_{xyo}}{\partial y} = 0$$

$$\frac{\partial \tau_{xyo}}{\partial x} + \frac{\partial \sigma_{yo}}{\partial y} = 0$$

$$\nabla^4 w^{(0)} = \frac{h}{D}\left[\sigma_{xo}\frac{\partial^2}{\partial x^2} + \sigma_{yo}\frac{\partial^2}{\partial y^2} + 2\tau_{xyo}\frac{\partial^2}{\partial x \partial y}\right] w_o \qquad (26)$$

1st order approximation

$$\frac{\partial \bar{\sigma}_x^{(1)}}{\partial x} + \frac{\partial \bar{\tau}_{xy}^{(1)}}{\partial y} = 0$$

$$\frac{\partial \bar{\tau}_{xy}^{(1)}}{\partial x} + \frac{\partial \bar{\sigma}_y^{(1)}}{\partial y} = 0 \qquad (27)$$

$$\nabla^4 w^{(1)} = \frac{h}{D}\left[\left(\bar{\sigma}_x^{(1)}\frac{\partial^2}{\partial x^2} + \bar{\sigma}_y^{(1)}\frac{\partial^2}{\partial y^2} + 2\bar{\tau}_{xy}^{(1)}\frac{\partial^2}{\partial x \partial y}\right) w_o + \left(\sigma_{xo}\frac{\partial^2}{\partial x^2} + \sigma_{yo}\frac{\partial^2}{\partial y^2} + 2\tau_{xyo}\frac{\partial^2}{\partial x \partial y}\right) w^{(1)}\right]$$

2nd order approximation

$$\frac{\partial \bar{\sigma}_x^{(2)}}{\partial x} + \frac{\partial \bar{\tau}_{xy}^{(2)}}{\partial y} = 0$$

$$\frac{\partial \bar{\tau}_{xy}^{(2)}}{\partial x} + \frac{\partial \bar{\sigma}_y^{(2)}}{\partial y} = 0$$

(28)

$$\nabla^4 w^{(2)} = \frac{h}{D}\left[\left(\bar{\sigma}_x^{(2)}\frac{\partial^2}{\partial x^2} + \bar{\sigma}_y^{(2)}\frac{\partial^2}{\partial y^2} + 2\bar{\tau}_{xy}^{(2)}\frac{\partial^2}{\partial x \partial y}\right) w_o\right.$$

$$+ \left(\bar{\sigma}_x^{(1)}\frac{\partial^2}{\partial x^2} + \bar{\sigma}_y^{(1)}\frac{\partial^2}{\partial y^2} + 2\bar{\tau}_{xy}^{(1)}\frac{\partial^2}{\partial x \partial y}\right) w^{(1)}$$

$$\left. + \left(\sigma_{xo}\frac{\partial^2}{\partial x^2} + \sigma_{yo}\frac{\partial^2}{\partial y^2} + 2\tau_{xyo}\frac{\partial^2}{\partial x \partial y}\right) w^{(2)}\right]$$

3rd order approximation

$$\frac{\partial \bar{\sigma}_x^{(3)}}{\partial x} + \frac{\partial \bar{\tau}_{xy}^{(3)}}{\partial y} = 0$$

$$\frac{\partial \bar{\tau}_{xy}^{(3)}}{\partial x} + \frac{\partial \bar{\sigma}_y^{(3)}}{\partial y} = 0$$

$$\nabla^4 w^{(3)} = \frac{h}{D}\left[\left(\bar{\sigma}_x^{(3)}\frac{\partial^2}{\partial x^2} + \bar{\sigma}_y^{(3)}\frac{\partial^2}{\partial y^2} + 2\bar{\tau}_{xy}^{(3)}\frac{\partial^2}{\partial x \partial y}\right) w_o\right.$$

$$+ \left(\bar{\sigma}_x^{(2)} \frac{\partial^2}{\partial x^2} + \bar{\sigma}_y^{(2)} \frac{\partial^2}{\partial y^2} + 2\bar{\tau}_{xy}^{(2)} \frac{\partial^2}{\partial x \partial y}\right) w^{(1)}$$

$$+ \left(\bar{\sigma}_x^{(1)} \frac{\partial^2}{\partial x^2} + \bar{\sigma}_y^{(1)} \frac{\partial^2}{\partial y^2} + 2\bar{\tau}_{xy}^{(1)} \frac{\partial^2}{\partial x \partial y}\right) w^{(2)}$$

$$+ \left(\sigma_{xo} \frac{\partial^2}{\partial x^2} + \sigma_{yo} \frac{\partial^2}{\partial y^2} + 2\tau_{xyo} \frac{\partial^2}{\partial x \partial y}\right) w^{(3)}\Big] \quad (29)$$

Boundary conditions in terms of polynomial series

Substitutions of Equation 22 and Equation 23 into the boundary conditions shown in Equations 17 through Equation 21 make it possible to expand these conditions into series forms.

Support conditions for w_e^T The support conditions are linear with respect to the perturbation; therefore,

1. Along x = 0:

$$w^{(k)} = 0, \quad GJ_s \frac{\partial}{\partial y}\left(\frac{\partial^2 w^{(k)}}{\partial x \partial y}\right) = D\left(\frac{\partial^2 w^{(k)}}{\partial x^2} + \nu \frac{\partial^2 w^{(k)}}{\partial y^2}\right)$$

2. Along x = a:

$$w^{(k)} = 0, \quad GJ'_s \frac{\partial}{\partial y}\left(\frac{\partial^2 w^{(k)}}{\partial x \partial y}\right) = -D\left(\frac{\partial^2 w^{(k)}}{\partial x^2} + \nu \frac{\partial^2 w^{(k)}}{\partial y^2}\right)$$

3. Along y = 0: (30)

$$w^{(k)} = 0, \quad GJ'_f \frac{\partial}{\partial x}\left(\frac{\partial^2 w^{(k)}}{\partial x \partial y}\right) = D\left(\frac{\partial^2 w^{(k)}}{\partial y^2} + \nu \frac{\partial^2 w^{(k)}}{\partial x^2}\right)$$

4. Along y = b:

$$w^{(k)} = 0, \quad GJ_f \frac{\partial}{\partial x}\left(\frac{\partial^2 w^{(k)}}{\partial x \partial y}\right) = -D\left(\frac{\partial^2 w^{(k)}}{\partial y^2} + \nu \frac{\partial^2 w^{(k)}}{\partial x^2}\right)$$

where

$k = 0,1,2,3.$

Boundary conditions for in-plane displacements u, v

Stresses in flanges and stiffeners have the following relationships:

$$\sigma_s \text{ (or } \sigma_s') = E \frac{\partial v}{\partial y}; \quad \sigma_f \text{ (or } \sigma_f') = E \frac{\partial u}{\partial x} . \tag{31}$$

Therefore, these stresses can be expanded into series forms by virtue of Equation 23. For example, σ_s can be expanded as follows:

$$\sigma_s = E \frac{\partial}{\partial y} \left(v^{(1)} \; v^{(2)} \; v^{(3)}\right) \begin{Bmatrix} \Delta \\ \Delta^2 \\ \Delta^3 \end{Bmatrix} . \tag{32}$$

The externally applied shearing stress, τ can be expanded into a series:

$$\tau = \tau^{(1)} \Delta + \tau^{(2)} \Delta^2 + \tau^{(3)} \Delta^3 . \tag{33}$$

Upon substitutions of Equations 1, 23, 33 and the equations similar to Equation 32 into Equation 18 provide the necessary boundary conditions.

Zero order The zero order boundary conditions are obtained as follows:

1. Along $x = 0$: $\tau_{xyo} = 0$
2. Along $x = a$: $\tau_{xyo} = 0$
3. Along $y = 0$: $\sigma_{yo} = 0$ and $\tau_{xyo} = 0$
4. Along $y = b$: $\sigma_{yo} = 0$ and $\tau_{xyo} = 0$

(34)

Higher order The higher order boundary conditions are obtained as follows:

1. Along $x = 0$: $u^{(k)} = 0$ and

$$E \frac{\partial^2 v^{(k)}}{\partial y^2} + \frac{h}{A_s} \bar{\tau}_{xy}^{(k)} = \frac{h}{A_s} \tau^{(k)}$$

2. Along $x = a$: $\frac{\partial^2 u^{(k)}}{\partial y^2} = 0$ and

$$E \frac{\partial^2 v^{(k)}}{\partial y^2} - \frac{h}{A_s} \bar{\tau}_{xy}^{(k)} = \frac{-h}{A_s} \tau^{(k)}$$

3. Along $y = 0$:

$$Ei_f' \frac{\partial^4 v^{(k)}}{\partial x^4} = h \bar{\sigma}_y^{(k)} \quad \text{and} \tag{35}$$

$$E \frac{\partial^2 u^{(k)}}{\partial x^2} + \frac{h}{A_f'} \bar{\tau}_{xy}^{(k)} = 0$$

4. Along $y = b$:

$$Ei_f \frac{\partial^4 v^{(k)}}{\partial x^4} = -h\ \bar{\sigma}_y^{(k)} \quad \text{and}$$

$$E \frac{\partial^2 u^{(k)}}{\partial x^2} - \frac{h}{A_f} \bar{\tau}_{xy}^{(k)} = 0$$

where k = 1,2,3.

Conditions of no net resultant force Upon substitutions of Equations 1, 24 and the equations similar to Equation 32 into Equation 19 provide the following conditions.

Zero order

$$h \int_0^b \sigma_{xo}\, dy = 0 \quad \text{along } x = 0 \text{ and } x = a, \text{ and}$$

$$h \int_0^a \sigma_{yo}\, dx = 0 \quad \text{along } y = 0 \text{ and } y = b. \tag{36}$$

Higher order

$$h \int_0^b \bar{\sigma}_x^{(k)}\, dy + E \frac{\partial}{\partial x} \left(A_f u^{(k)} \Big|_{y=b} + A_f' u^{(k)} \Big|_{y=0} \right) = 0$$

along x = 0 and x = a, and

$$h \int_0^a \bar{\sigma}_y^{(k)}\, dx + E \frac{\partial}{\partial y} \left(A_s v^{(k)} \Big|_{x=0} + A_s' v^{(k)} \Big|_{x=a} \right) = 0 \tag{37}$$

along y = 0 and y = b, where k = 1,2,3.

Bending moment conditions The externally applied bending moment, M, can also be expanded into a polynomial series:

$$M = M^{(1)}\ \Delta + M^{(2)}\ \Delta^2 + M^{(3)}\ \Delta^3. \tag{38}$$

The bending moment conditions for zero order and higher order approximations are obtained as follows:

Zero order

$$\int_0^b \sigma_{xo}\ y\ dy = 0 \qquad \text{along } x = a, \text{ and}$$

$$\int_0^a \sigma_{yo}\ x\ dx = 0 \qquad \text{along } y = 0 \text{ and } y = b \tag{39}$$

Higher order

$$M^{(k)} = -h \int_0^b \bar{\sigma}_x^{(k)}\ y\ dy - EA_f b \left.\frac{\partial u^{(k)}}{\partial x}\right|_{y=b} \qquad \text{along } x = a,$$

$$\text{and} \int_0^a \bar{\sigma}_y^{(k)}\ x\ dx + EA_s' a \left.\frac{\partial v^{(k)}}{\partial y}\right|_{x=a} = 0 \text{ along } y = 0 \text{ and } y = b. \tag{40}$$

Choice of polynomial expansion parameter

Figure 6 indicates typical load-displacement curves for webplates with initial deflections subjected to externally applied loads in the plane of the webplates (5, 21, 22, 26, 27,

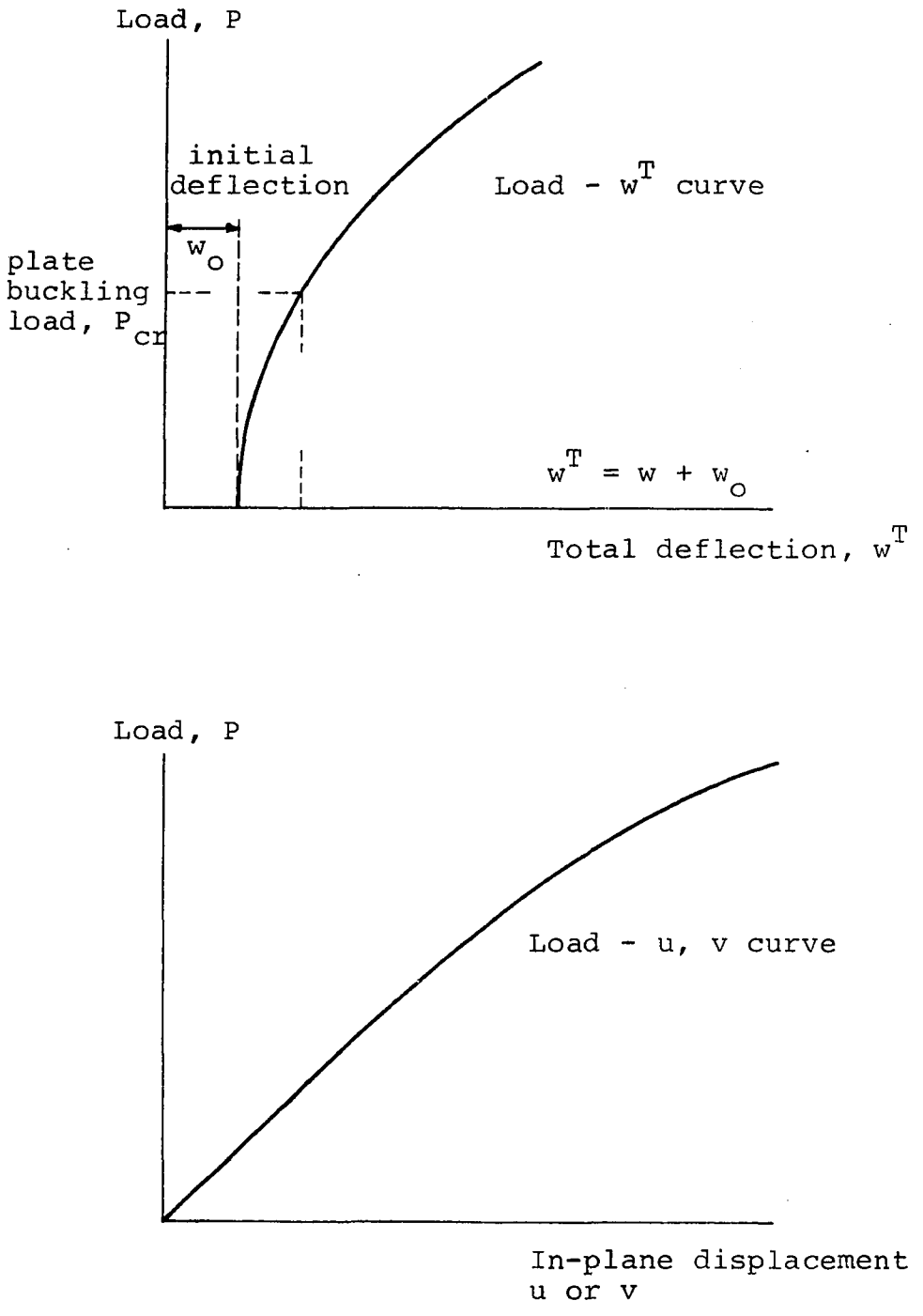

Figure 6. Typical load-displacement curves

28). The fact that deflection w may be expressed in polynomial series with first, second and third powers in terms of the magnitude of load suggests that the magnitude of load could be taken as parameter Δ. The third equation in Equation 22 corresponds to the load-deflection curve shown in Figure 6. On the other hand, it is seen from Figure 6 that the in-plane displacement components u and v may also be expressed in terms of the load parameter. A question exists regarding the maximum power that should be assigned to the expansions of the in-plane displacement components u and v. They may be expanded only up to the quadratic term rather than up to the cubic term. If the quadratic series are used for the in-plane displacement components u and v, the deflection w may also be conveniently expanded only up to the quadratic term. Then, the expansion of the displacement components u, v and w in Equation 22 can be replaced by the following simpler expansion:

$$\begin{Bmatrix} u \\ v \\ w \end{Bmatrix} = \begin{bmatrix} u^{(1)} & u^{(2)} \\ v^{(1)} & v^{(2)} \\ w^{(1)} & w^{(2)} \end{bmatrix} \begin{Bmatrix} \Delta \\ \Delta^2 \end{Bmatrix}. \tag{41}$$

Consequently, Equations 23, 24 and 25 can be simplified also. Since the simplification of these equations is an obvious one, it is not presented herein. A detailed discussion on the number of terms in the expansions of displacement components

is provided in Appendix D.

If the average edge shearing stress, τ is taken as the load parameter, then Δ, its nondimensionalized form can be conveniently defined in the following manner:

$$\Delta = \frac{\tau}{\sigma_{Yw}} , \tag{42}$$

where σ_{Yw} refers to the yield strength of webplate. Then, from Equations 33 and 42, the following equations are obtained:

$$\tau^{(1)} = \sigma_{Yw}, \quad \tau^{(2)} = 0 \quad \text{and} \quad \tau^{(3)} = 0. \tag{43}$$

If the externally applied bending moment, M, is taken as the load parameter, then Δ can be conveniently defined in the following manner:

$$\Delta = \frac{M}{\sigma_{Yw}\, h\, a^2} . \tag{44}$$

Then, from Equations 38 and 42, the following equations are obtained:

$$M^{(1)} = \sigma_{Yw}\, h\, a^2, \quad M^{(2)} = 0 \quad \text{and} \quad M^{(3)} = 0. \tag{45}$$

Method of solution

It is seen that by expansion of displacements in polynomial forms, the equations of equilibrium indicated by Equation 16 have been linearized into sets of equations given

in Equations 26 through 29. The form of these sets of equations indicates that the solution to the problem consists of solving the basic set of equations four times, from zero order to third order. After a set of equations is solved, the solutions are substituted into the next higher order equations and the solution to this new set of equations is obtained. This process of solution is repeated from zero order approximation through third order approximation, each time satisfying an appropriate set of boundary conditions. In Equations 26 through 29, the first two approximations, i.e., zero and first order approximations, Equations 26 and 27, represent the linear portion of the large deflection equations and the second and third order approximations, Equations 28 and 29, correspond to the nonlinear portion of the same equations. Also while the displacement components are expanded into cubic polynomial forms in terms of the load parameter, the in-plane stresses in terms of the same parameter have powers as high as twice of those for displacements because of the nonlinear products appearing in Equation 6. However, since the boundary conditions are met only four times, i.e., for zero order through third order, the stresses corresponding to orders higher than the third have no meaning. Because of this, every mechanical quantity is totaled from zero through third order components.

It is necessary to determine the initial in-plane stresses σ_{xo}, σ_{yo} and τ_{xyo} first. Because of the nature of these initial stresses, the precise analytical determination of them is not feasible. An approximate solution developed by Škaloud (25) is used in this thesis. The detailed description of initial stress distribution is given in the following section. The remaining zero order equations and all sets of higher order equations are too complicated to be solved analytically. In the section following the next, all equations in this group, including the boundary conditions, are expressed in terms of displacement components and nondimensionalized. The last section in this chapter describes the numerical solution of the third equation in the zero order approximation, and of individual sets of equations in the higher order approximations, by means of finite differences.

Initial In-plane Stresses

The purpose of this section is to obtain the distribution of the initial in-plane stress components σ_{xo}, σ_{yo} and τ_{xyo}. The basic differential equations are the first and the second equations in Equation 26. The boundary conditions for these stresses are given in Equations 34, 36 and 39.

Figure 7 shows a typical initial (or residual) in-plane stress distribution in a plate girder cross section when the flanges are continuously welded along the webplate (6, 10, 12,

22). If vertical stiffeners are welded on top of it, the stress distribution will be affected by this additional welding and become as illustrated in Figure 8 (25). Thus, taking a particular coordinate system as shown in Figure 8, the stress distribution may be reasonably approximated by the following equations:

$$\sigma_{xo} = -16 \frac{C}{b^2} \left[1 - 4 \left(\frac{x'}{a}\right)^2\right]^2 \left[1 - 12 \left(\frac{y'}{b}\right)^2\right]$$

$$\sigma_{yo} = -16 \frac{C}{a^2} \left[1 - 12 \left(\frac{x'}{a}\right)^2\right] \left[1 - 4 \left(\frac{y'}{b}\right)^2\right]^2 \qquad (46, 47)$$

$$\tau_{xyo} = -256 \frac{C\, x' y'}{a^2\, b^2} \left[1 - 4 \left(\frac{x'}{a}\right)^2\right] \left[1 - 4 \left(\frac{y'}{b}\right)^2\right]$$

where $x = x' + \frac{1}{2} a$ and $y = y' + \frac{1}{2} b$

It is seen that Equations 46, 47 satisfy all boundary conditions for the in-plane stresses, Equations 34, 36 and 39, as well as the in-plane equilibrium equations, the first two of Equations 26.

It is an experimental fact (6, 10, 12, 22, 25) that

$$\sigma_{yo} \equiv \sigma_o > 0 \text{ at } x' = \frac{1}{2} a \text{ and } y' = 0. \qquad (48)$$

In terms of σ_o, the initial in-plane stresses are obtained as follows:

$$\sigma_{xo} = -\frac{1}{2} \left(\frac{a}{b}\right)^2 \sigma_o \left[1 - 4 \left(\frac{x'}{a}\right)^2\right]^2 \left[1 - 12 \left(\frac{y'}{b}\right)^2\right] \qquad (49)$$

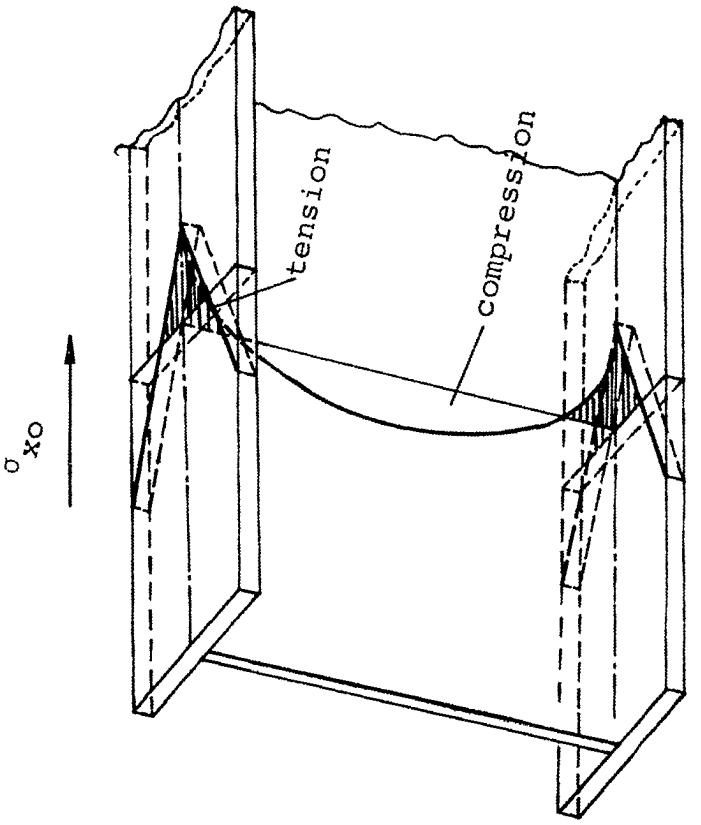

Figure 7. Typical residual stress distribution due to continuous longitudinal weld

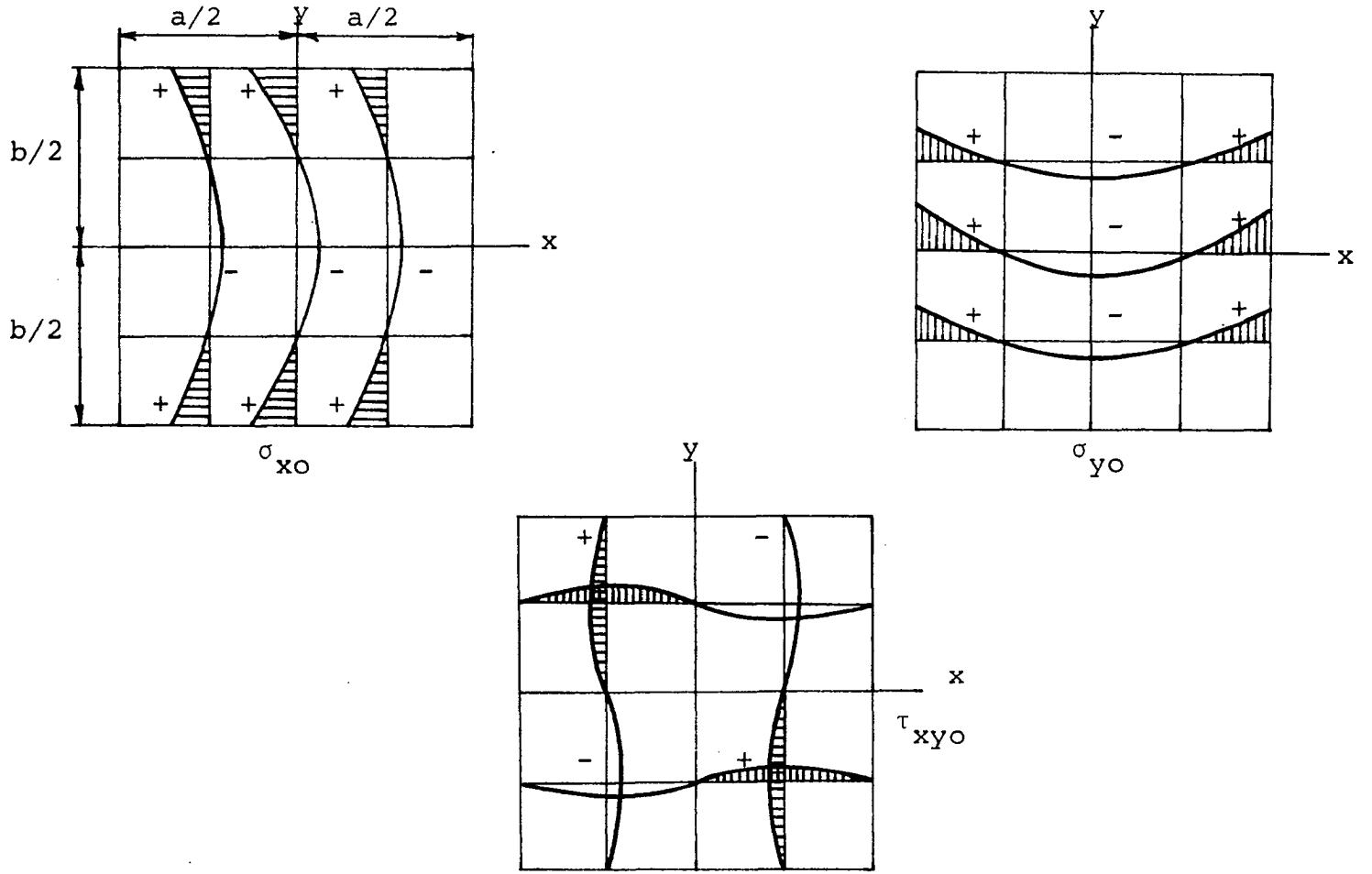

Figure 8. Residual stress distribution in a welded panel

$$\sigma_{yo} = -\frac{1}{2}\sigma_o\left[1 - 12\left(\frac{x'}{a}\right)^2\right]\left[1 - 4\left(\frac{y'}{b}\right)^2\right]^2$$

$$\tau_{xyo} = -8\sigma_o\frac{x'y'}{b^2}\left[1 - 4\left(\frac{x'}{a}\right)^2\right]\left[1 - 4\left(\frac{y'}{b}\right)^2\right]$$

The distributions of these stresses are illustrated in Figure 8.

Nondimensionalized Zero Order Equation in Terms of Displacements

The first and the second equations in Equations 26 have been analytically solved. Only the third equation in Equations 26 remains to be solved. The necessary boundary conditions are those presented for k = 0 in Equations 30.

Let N be the dimension of mesh points and

$$b = \lambda a$$

$$u^{(k)} = h\,\tilde{u}^{(k)}; \quad v^{(k)} = h\,\tilde{v}^{(k)}; \quad w^{(k)} = h\,\tilde{w}^{(k)} \qquad (k = 1,2,3)$$

$$w_o = A\,\tilde{w}_o$$

$$x = \frac{a}{N-1}\xi; \quad y = \frac{b}{N-1}\eta \quad \text{and} \quad x' = \frac{a}{N-1}\xi'; \quad y' = \frac{b}{N-1}\eta' \qquad (50)$$

$$\alpha = \sigma_o/E$$

$$\beta = a/h$$

$$\sigma_{xo} = \sigma_o\,\tilde{\sigma}_{xo}; \quad \sigma_{yo} = \sigma_o\,\tilde{\sigma}_{yo}; \quad \tau_{xyo} = \sigma_o\,\tilde{\tau}_{xyo}$$

Then, the nondimensionalized initial in-plane stresses are obtained as follows:

$$\tilde{\sigma}_{xo} = -\frac{1}{2\lambda^2}\left[1 - 4\left(\frac{\xi'}{N-1}\right)^2\right]^2\left[1 - 12\left(\frac{\eta'}{N-1}\right)^2\right]$$

$$\tilde{\sigma}_{yo} = -\frac{1}{2}\left[1 - 12\left(\frac{\xi'}{N-1}\right)^2\right]\left[1 - 4\left(\frac{\eta'}{N-1}\right)^2\right]^2 \qquad (51)$$

$$\tilde{\tau}_{xyo} = -\frac{8}{\lambda}\left(\frac{\xi'}{N-1}\right)\left(\frac{\eta'}{N-1}\right)\left[1 - 4\left(\frac{\xi'}{N-1}\right)^2\right]\left[1 - 4\left(\frac{\eta'}{N-1}\right)^2\right]$$

The equation of equilibrium in z-direction is then given by the following equation:

$$\left(\frac{\partial^4}{\partial\xi^4} + \frac{2}{\lambda^2}\frac{\partial^4}{\partial\xi^2\partial\eta^2} + \frac{1}{\lambda^4}\frac{\partial^4}{\partial\eta^4}\right)\tilde{w}^{(0)}$$

$$= 12\,\alpha\beta\,\frac{1-\nu^2}{(N-1)^2}\left(\tilde{\sigma}_{xo}\frac{\partial^2}{\partial\xi^2} + \frac{\tilde{\sigma}_{yo}}{\lambda^2}\frac{\partial^2}{\partial\eta^2} + 2\,\frac{\tilde{\tau}_{xyo}}{\lambda}\frac{\partial^2}{\partial\xi\partial\eta}\right)\tilde{w}_o \qquad (52)$$

The support conditions for $w^{(0)}$ which are shown in Equation 30 are nondimensionalized and presented in a later section.

Nondimensionalized Higher Order Equations in Terms of Displacements

Let

$$\zeta = \frac{\sigma_o}{\sigma_{Yw}}, \quad \text{and} \quad \mu = \frac{A}{h}, \qquad (53)$$

The higher order equations shown in Equations 27, 28 and 29 are first expressed in terms of displacements and then non-dimensionalized using Equations 50 and 53:

$$\begin{bmatrix} L_{uu} & L_{uv} & L_{uw} \\ L_{vu} & L_{vv} & L_{vw} \\ L_{wu} & L_{wv} & L_{ww} \end{bmatrix} \begin{bmatrix} \tilde{u}^{(1)} & \tilde{u}^{(2)} & \tilde{u}^{(3)} \\ \tilde{v}^{(1)} & \tilde{v}^{(2)} & \tilde{v}^{(3)} \\ \tilde{w}^{(1)} & \tilde{w}^{(2)} & \tilde{w}^{(3)} \end{bmatrix} = \begin{bmatrix} b_u^{(1)} & b_u^{(2)} & b_u^{(3)} \\ b_v^{(1)} & b_v^{(2)} & b_v^{(3)} \\ b_w^{(1)} & b_w^{(2)} & b_w^{(3)} \end{bmatrix} \tag{54}$$

where L_{ij} refers to a set of linear differential operators defined as follows:

$$L_{uu} = \frac{\partial^2}{\partial \xi^2} + \frac{1-\nu}{2\lambda} \frac{\partial^2}{\partial \eta^2}$$

$$L_{uv} = \frac{1+\nu}{2\lambda} \frac{\partial^2}{\partial \xi \partial \eta}$$

$$L_{uw} = (N-1) \left\{ \frac{\partial \tilde{w}_o}{\partial \xi} \frac{\partial^2}{\partial \xi^2} + \frac{1+\nu}{2\lambda^2} \frac{\partial \tilde{w}_o}{\partial \eta} \frac{\partial^2}{\partial \xi \partial \eta} + \frac{1-\nu}{2\lambda^2} \frac{\partial \tilde{w}_o}{\partial \xi} \frac{\partial^2}{\partial \eta^2} \right.$$

$$\left. + \left(\frac{\partial^2 \tilde{w}_o}{\partial \xi^2} + \frac{1-\nu}{2\lambda^2} \frac{\partial^2 \tilde{w}_o}{\partial \eta^2} \right) \frac{\partial}{\partial \xi} + \frac{1+\nu}{2\lambda^2} \left(\frac{\partial^2 \tilde{w}_o}{\partial \xi \partial \eta} \right) \frac{\partial}{\partial \eta} \right\} \left(\frac{\mu}{\beta} \right)$$

$$L_{vu} = \frac{1+\nu}{2\lambda} \frac{\partial^2}{\partial \xi \partial \eta}$$

$$L_{vv} = \frac{1}{\lambda^2} \frac{\partial^2}{\partial \eta^2} + \frac{1-\nu}{2} \frac{\partial^2}{\partial \xi^2}$$

$$L_{vw} = (N-1)\left(\frac{\mu}{\beta}\right)\left[\frac{1}{\lambda^3}\frac{\partial\tilde{w}_o}{\partial\eta}\cdot\frac{\partial^2}{\partial\eta^2} + \frac{1+\nu}{2\lambda}\frac{\partial\tilde{w}_o}{\partial\xi}\frac{\partial^2}{\partial\xi\partial\eta} + \frac{1-\nu}{2\lambda}\frac{\partial\tilde{w}_o}{\partial\eta}\frac{\partial^2}{\partial\xi^2}\right.$$

$$\left. + \left(\frac{1}{\lambda^3}\frac{\partial^2\tilde{w}_o}{\partial\eta^2} + \frac{1-\nu}{2\lambda}\frac{\partial^2\tilde{w}_o}{\partial\xi^2}\right)\frac{\partial}{\partial\eta} + \frac{1+\nu}{2\lambda}\left(\frac{\partial^2\tilde{w}_o}{\partial\xi\partial\eta}\right)\frac{\partial}{\partial\xi}\right]$$

$$L_{wu} = \left(\frac{\partial^2\tilde{w}_o}{\partial\xi^2} + \frac{\nu}{\lambda^2}\frac{\partial^2\tilde{w}_o}{\partial\eta^2}\right)\frac{\partial}{\partial\xi} + \frac{1-\nu}{\lambda^2}\frac{\partial^2\tilde{w}_o}{\partial\xi\partial\eta}\frac{\partial}{\partial\eta}$$

$$L_{wv} = \frac{1}{\lambda}\left(\frac{1}{\lambda^2}\frac{\partial^2\tilde{w}_o}{\partial\eta^2} + \nu\frac{\partial^2 w_o}{\partial\xi^2}\right)\frac{\partial}{\partial\eta} + \frac{1-\nu}{\lambda}\left(\frac{\partial^2\tilde{w}_o}{\partial\xi\partial\eta}\right)\frac{\partial}{\partial\xi}$$

$$L_{ww} = -\frac{1}{12}\left(\frac{N-1}{\beta\mu}\right)\left(\frac{\partial^4}{\partial\xi^4} + \frac{2}{\lambda^2}\frac{\partial^4}{\partial\xi^2\partial\eta^2} + \frac{1}{\lambda^4}\frac{\partial^4}{\partial\eta^4}\right)$$

$$+ (N-1)\left(\frac{\mu}{\beta}\right)\left[\frac{\partial\tilde{w}_o}{\partial\xi}\left(\frac{\partial^2\tilde{w}_o}{\partial\xi^2} + \frac{\nu}{\lambda^2}\frac{\partial^2\tilde{w}_o}{\partial\eta^2}\right) + \frac{1-\nu}{\lambda^2}\frac{\partial\tilde{w}_o}{\partial\eta}\frac{\partial\tilde{w}_o}{\partial\xi\partial\eta}\right]\frac{\partial}{\partial\xi}$$

$$+ (N-1)\left(\frac{\mu}{\beta}\right)\left[\frac{\partial\tilde{w}_o}{\partial\eta}\left(\frac{1}{\lambda^4}\frac{\partial^2\tilde{w}_o}{\partial\eta^2} + \frac{\nu}{\lambda^2}\frac{\partial^2\tilde{w}_o}{\partial\xi^2}\right)\right.$$

$$\left. + \frac{1-\nu}{\lambda^2}\frac{\partial\tilde{w}_o}{\partial\xi}\frac{\partial^2\tilde{w}_o}{\partial\xi\partial\eta}\right]\frac{\partial}{\partial\eta} + \alpha\left(\frac{\beta}{\mu}\right)\frac{1-\nu^2}{N-1}$$

$$\cdot\left[\tilde{\sigma}_{xo}\frac{\partial^2}{\partial\xi^2} + \frac{1}{\lambda^2}\tilde{\sigma}_{yo}\frac{\partial^2}{\partial\eta^2} + 2\frac{1}{\lambda}\tilde{\tau}_{xyo}\frac{\partial^2}{\partial\xi\partial\eta}\right]$$

and, $b_u^{(k)}$, $b_v^{(k)}$ and $b_w^{(k)}$ are constant vectors associated with the equations of equilibrium defined as follows:

$$b_u^{(1)} = 0; \quad b_v^{(1)} = 0; \quad b_w^{(1)} = 0$$

$$b_u^{(2)} = -\left(\frac{N-1}{\beta}\right)\left[\frac{\partial\tilde{w}^{(1)}}{\partial\xi}\frac{\partial^2\tilde{w}^{(1)}}{\partial\xi^2} + \frac{1+\nu}{2\lambda^2}\frac{\partial\tilde{w}^{(1)}}{\partial\eta}\frac{\partial^2\tilde{w}^{(1)}}{\partial\xi\partial\eta} + \frac{1-\nu}{2\lambda^2}\frac{\partial\tilde{w}^{(1)}}{\partial\xi}\frac{\partial^2 w^{(1)}}{\partial\eta^2}\right]$$

$$b_v^{(2)} = -\left(\frac{N-1}{\beta}\right)\left[\frac{1}{\lambda^3}\frac{\partial\tilde{w}^{(1)}}{\partial\eta}\frac{\partial^2\tilde{w}^{(1)}}{\partial\eta^2} + \frac{1+\nu}{2\lambda}\frac{\partial\tilde{w}^{(1)}}{\partial\xi}\frac{\partial^2\tilde{w}^{(1)}}{\partial\xi\partial\eta} + \frac{1-\nu}{2\lambda}\frac{\partial\tilde{w}^{(1)}}{\partial\eta}\frac{\partial^2\tilde{w}^{(1)}}{\partial\xi^2}\right]$$

$$b_w^{(2)} = -\left(\frac{\alpha\beta}{\mu\zeta}\right)\frac{1-\nu^2}{N-1}\left(\tilde{\sigma}_x^{(1)}\frac{\partial^2}{\partial\xi^2} + \frac{1}{\lambda^2}\tilde{\sigma}_y^{(1)}\frac{\partial^2}{\partial\eta^2} + 2\frac{1}{\lambda}\tilde{\tau}_{xy}^{(1)}\frac{\partial^2}{\partial\xi\partial\eta}\right)\tilde{w}^{(1)} - \left(\frac{N-1}{2\beta}\right)$$

$$\cdot\left[\left(\frac{\partial\tilde{w}^{(1)}}{\partial\xi}\right)^2 + \frac{\nu}{\lambda^2}\left(\frac{\partial\tilde{w}^{(1)}}{\partial\eta}\right)^2\right]\frac{\partial^2\tilde{w}_o}{\partial\xi^2}$$

$$-\left(\frac{N-1}{2\beta\lambda^2}\right)\left[\frac{1}{\lambda^2}\left(\frac{\partial\tilde{w}^{(1)}}{\partial\eta}\right)^2 + \nu\left(\frac{\partial\tilde{w}^{(1)}}{\partial\xi}\right)^2\right]\frac{\partial^2\tilde{w}_o}{\partial\eta^2}$$

$$-\left(\frac{N-1}{\beta}\right)\left(\frac{1-\nu}{\lambda^2}\right)\frac{\partial\tilde{w}^{(1)}}{\partial\xi}\frac{\partial\tilde{w}^{(1)}}{\partial\eta}\frac{\partial^2\tilde{w}_o}{\partial\xi\partial\eta}$$

$$b_u^{(3)} = -\left(\frac{N-1}{\beta}\right)\left[\frac{\partial\tilde{w}^{(1)}}{\partial\xi}\frac{\partial^2\tilde{w}^{(2)}}{\partial\xi^2} + \frac{1+\nu}{2\lambda^2}\frac{\partial\tilde{w}^{(1)}}{\partial\eta}\frac{\partial^2\tilde{w}^{(2)}}{\partial\xi\partial\eta}\right.$$

$$+ \frac{1-\nu}{2\lambda^2}\frac{\partial\tilde{w}^{(1)}}{\partial\xi}\frac{\partial\tilde{w}^{(2)}}{\partial\eta^2} + \frac{\partial^2\tilde{w}^{(1)}}{\partial\xi^2}\frac{\partial\tilde{w}^{(2)}}{\partial\xi}$$

$$\left. + \frac{1+\nu}{2\lambda^2}\frac{\partial^2\tilde{w}^{(1)}}{\partial\xi\partial\eta}\frac{\partial\tilde{w}^{(2)}}{\partial\eta} + \frac{1-\nu}{2\lambda^2}\frac{\partial^2\tilde{w}^{(1)}}{\partial\eta^2}\frac{\partial\tilde{w}^{(2)}}{\partial\xi}\right]$$

$$b_v^{(3)} = -\left(\frac{N-1}{\beta}\right)\left[\frac{1}{\lambda^3}\frac{\partial\tilde{w}^{(1)}}{\partial\eta}\frac{\partial^2\tilde{w}^{(2)}}{\partial\eta^2} + \frac{1+\nu}{2\lambda}\frac{\partial w^{(1)}}{\partial\xi}\frac{\partial^2 w^{(2)}}{\partial\xi\partial\eta}\right.$$

$$+ \frac{1-\nu}{2\lambda}\frac{\partial\tilde{w}^{(1)}}{\partial\eta}\frac{\partial^2\tilde{w}^{(2)}}{\partial\xi^2} + \frac{1}{\lambda^3}\frac{\partial^2 w^{(1)}}{\partial\eta^2}\frac{\partial\tilde{w}^{(2)}}{\partial\eta}$$

$$\left. + \frac{1+\nu}{2\lambda}\frac{\partial^2\tilde{w}^{(1)}}{\partial\xi\partial\eta}\frac{\partial\tilde{w}^{(2)}}{\partial\xi} + \frac{1-\nu}{2\lambda}\frac{\partial^2\tilde{w}^{(1)}}{\partial\xi^2}\frac{\partial\tilde{w}^{(2)}}{\partial\eta}\right]$$

$$b_w^{(3)} = -\left(\frac{\alpha\beta}{N-1}\right)\left(\frac{1-\nu^2}{\mu\zeta}\right)\left(\tilde{\sigma}_x^{(1)}\frac{\partial^2}{\partial\xi^2} + \frac{1}{\lambda^2}\tilde{\sigma}_y^{(1)}\frac{\partial^2}{\partial\eta^2}\right.$$

$$\left. + 2\frac{\tilde{\tau}_{xy}^{(1)}}{\lambda}\frac{\partial^2}{\partial\xi\partial\eta}\right)\tilde{w}^{(2)} - \left(\frac{\alpha\beta}{N-1}\right)\left(\frac{1-\nu^2}{\mu\zeta}\right)$$

$$\cdot\left(\tilde{\sigma}_x^{(2)}\frac{\partial^2}{\partial\xi^2} + \frac{1}{\lambda^2}\tilde{\sigma}_y^{(2)}\frac{\partial^2}{\partial\eta^2} + 2\frac{1}{\lambda}\tilde{\tau}_{xy}^{(2)}\frac{\partial^2}{\partial\xi\partial\eta}\right)\tilde{w}^{(1)}$$

$$-\left(\frac{N-1}{\beta}\right)\frac{\partial^2\tilde{w}_o}{\partial\xi^2}\left(\frac{\partial\tilde{w}^{(1)}}{\partial\xi}\frac{\partial\tilde{w}^{(2)}}{\partial\xi} + \frac{\nu}{\lambda^2}\frac{\partial\tilde{w}^{(1)}}{\partial\eta}\frac{\partial\tilde{w}^{(2)}}{\partial\eta}\right)$$

$$-\left(\frac{N-1}{\beta}\right)\frac{\partial^2\tilde{w}_o}{\partial\eta^2}\left(\frac{1}{\lambda^4}\frac{\partial\tilde{w}^{(1)}}{\partial\eta}\frac{\partial\tilde{w}^{(2)}}{\partial\eta}+\frac{\nu}{\lambda^2}\frac{\partial\tilde{w}^{(1)}}{\partial\xi}\frac{\partial\tilde{w}^{(2)}}{\partial\xi}\right)$$

$$-\left(\frac{N-1}{\beta}\right)\left(\frac{1-\nu}{\lambda^2}\right)\left(\frac{\partial\tilde{w}^{(1)}}{\partial\xi}\frac{\partial\tilde{w}^{(2)}}{\partial\eta}+\frac{\partial\tilde{w}^{(1)}}{\partial\eta}\frac{\partial\tilde{w}^{(2)}}{\partial\xi}\right)\frac{\partial^2\tilde{w}_o}{\partial\xi\partial\eta}$$

It was observed through many experiments that total initial deflection w_o is somewhat arbitrary in its shape and magnitude. Nevertheless, the following expression for w_o is found to approximate most total initial deflection surfaces and hence will be used in this study:

$$w_o = A\,\tilde{w}_o$$

$$\tilde{w}_o = (1 - \cos\omega\xi)\,(1 - \cos\omega\eta)$$

where (55)

$$\omega = \frac{2}{N-1}\pi$$

Upon substitution of this expression for $\tilde{w}_o$ into the previous relationships, Equations 54, the equations of equilibrium are obtained as follows:

$$\begin{bmatrix} L_{uu} & L_{uv} & L_{uw} \\ L_{vu} & L_{vv} & L_{vw} \\ L_{wu} & L_{wv} & L_{ww} \end{bmatrix} \begin{bmatrix} \tilde{u}^{(1)} & \tilde{u}^{(2)} & \tilde{u}^{(3)} \\ \tilde{v}^{(1)} & \tilde{v}^{(2)} & \tilde{v}^{(3)} \\ \tilde{w}^{(1)} & \tilde{w}^{(2)} & \tilde{w}^{(3)} \end{bmatrix} = \begin{bmatrix} \tilde{b}^{(1)} & \tilde{b}^{(2)} & \tilde{b}^{(3)} \\ \tilde{b}^{(1)} & \tilde{b}^{(2)} & \tilde{b}^{(3)} \\ \tilde{b}^{(1)} & \tilde{b}^{(2)} & \tilde{b}^{(3)} \end{bmatrix}$$

(56)

where $[L_{ij}]$ is a linear differential operator matrix,

$(\tilde{u}^{(k)}, \tilde{v}^{(k)}, \tilde{w}^{(k)})$ is a solution vector for k-th order approximation, and

$(\tilde{b}_u^{(k)}, \tilde{b}_v^{(k)}, \tilde{b}_w^{(k)})$ is a constant vector for k-th order approximation.

Elements of $[L_{ij}]$ are given as follows:

$$L_{uu} = \frac{\partial^2}{\partial\xi^2} + \frac{1-\nu}{2\lambda^2}\frac{\partial^2}{\partial\eta^2}$$

$$L_{uv} = \frac{1+\nu}{2\lambda}\frac{\partial^2}{\partial\xi\partial\eta}$$

$$L_{uw} = 2\pi\left(\frac{\mu}{\beta}\right)\left\{\sin\omega\eta(1-\cos\omega\eta)\frac{\partial^2}{\partial\xi^2} + \frac{1+\nu}{2\lambda^2}(1-\cos\omega\xi)\right.$$

$$\cdot\sin\omega\eta\frac{\partial^2}{\partial\xi\partial\eta} + \frac{1-\nu}{2\lambda^2}\sin\omega\xi\,(1-\cos\omega\eta)\frac{\partial^2}{\partial\eta^2}$$

$$+\omega\left[-\left(1+\frac{1-\nu}{2\lambda^2}\right)\cos\omega\xi\cos\omega\eta + \cos\omega\xi\right.$$

$$\left.\left.+\frac{1-\nu}{2\lambda^2}\cos\omega\eta\right]\frac{\partial}{\partial\xi} + \omega\left(\frac{1-\nu}{2\lambda^2}\right)\sin\omega\xi\sin\omega\eta\frac{\partial}{\partial\eta}\right\}$$

$$L_{vu} = \frac{1+\nu}{2\lambda}\frac{\partial^2}{\partial\xi\partial\eta}$$

$$L_{vv} = \frac{1}{\lambda^2}\frac{\partial^2}{\partial\eta^2} + \frac{1-\nu}{2}\frac{\partial^2}{\partial\xi^2}$$

$$L_{vw} = 2\pi\left(\frac{\mu}{\beta}\right)\left\{ \frac{1}{\lambda^3}(1 - \cos\omega\xi)\sin\omega\eta\frac{\partial^2}{\partial\eta^2} + \frac{1+\nu}{2\lambda}\sin\omega\xi \right.$$

$$\cdot(1 - \cos\omega\eta)\frac{\partial^2}{\partial\xi\partial\eta} + \frac{1-\nu}{2\lambda}(1 - \cos\omega\xi)\sin\omega\eta\frac{\partial^2}{\partial\xi^2}$$

$$+ \omega\left[-\frac{1}{\lambda}\left(\frac{1}{\lambda^2} + \frac{1-\nu}{2}\right)\cos\omega\xi\cos\omega\eta + \frac{1}{\lambda^3}\cos\omega\eta\right.$$

$$\left.\left. + \frac{1-\nu}{2\lambda}\cos\omega\xi\right]\frac{\partial}{\partial\eta} + \omega\left(\frac{1+\nu}{2\lambda}\right)\sin\omega\xi\sin\omega\eta\frac{\partial}{\partial\xi}\right\}$$

$$L_{wu} = 4\left\{\left[-\left(1+\frac{\nu}{\lambda^2}\right)\cos\omega\xi\cos\omega\eta + \cos\omega\xi + \frac{\nu}{\lambda^2}\cos\omega\eta\right]\frac{\partial}{\partial\xi}\right.$$

$$\left. + \frac{1-\nu}{\lambda^2}\sin\omega\xi\sin\omega\eta\frac{\partial}{\partial\eta}\right\}$$

$$L_{wv} = 4\left\{\left[-\frac{1}{\lambda}\left(\frac{1}{\lambda^2} + \nu\right)\cos\omega\xi\cos\omega\eta + \frac{1}{\lambda^3}\cos\omega\eta\right.\right.$$

$$\left.\left. + \frac{\nu}{\lambda}\cos\omega\xi\right]\frac{\partial}{\partial\eta} + \frac{1-\nu}{\lambda}\sin\omega\xi\sin\omega\eta\frac{\partial}{\partial\xi}\right\}$$

$$L_{ww} = -\frac{(N-1)^3}{12\pi^2\beta\mu}\left(\frac{\partial^4}{\partial\xi^4} + \frac{2}{\lambda^2}\frac{\partial^4}{\partial\xi^2\partial\eta^2} + \frac{1}{\lambda^4}\frac{\partial^4}{\partial\eta^4}\right)$$

$$+ 8\pi\left(\frac{\mu}{\beta}\right)\left\{ \sin\omega\xi\ (1 - \cos\omega\eta)\left[- \left(1 + \frac{\nu}{\lambda^2}\right)\cos\omega\xi\cos\omega\eta \right.\right.$$

$$\left. + \cos\omega\xi + \frac{\nu}{\lambda^2}\cos\omega\eta\right] + \frac{1-\nu}{\lambda^2}(1 - \cos\omega\xi)\sin^2\omega\eta$$

$$\left.\cdot\sin\omega\xi\right\}\frac{\partial}{\partial\xi} + 8\pi\left(\frac{\mu}{\beta}\right)\left\{(1 - \cos\omega\xi)\sin\omega\eta\left[- \frac{1}{\lambda^2}\right.\right.$$

$$\left.\left(\frac{1}{\lambda^2} + \nu\right)\cos\omega\xi\cos\omega\eta + \frac{1}{\lambda^4}\cos\omega\eta + \frac{\nu}{\lambda^2}\cos\omega\xi\right]$$

$$\left. + \frac{1-\nu}{\lambda^2}\sin^2\omega\xi\cdot\sin\omega\eta\,(1 - \cos\omega\eta)\right\}\frac{\partial}{\partial\eta}$$

$$+ \frac{1}{\pi^2}(1-\nu^2)(N-1)\left(\frac{\alpha\beta}{\mu}\right)\left[\tilde{\sigma}_{xo}\frac{\partial^2}{\partial\xi^2} + \frac{\tilde{\sigma}_{yo}}{\lambda^2}\frac{\partial^2}{\partial\eta^2}\right.$$

$$\left. + 2\frac{\tilde{\tau}_{xyo}}{\lambda}\frac{\partial^2}{\partial\xi\partial\eta}\right]$$

The constant vectors are given as follows:

$$\tilde{b}_u^{(1)} = 0; \quad \tilde{b}_v^{(1)} = 0; \quad \tilde{b}_w^{(1)} = 0$$

$$\tilde{b}_u^{(2)} = -\left(\frac{N-1}{\beta}\right)\left[\frac{\partial\tilde{w}^{(1)}}{\partial\xi}\frac{\partial^2\tilde{w}^{(1)}}{\partial\xi^2} + \frac{1+\nu}{2\lambda^2}\frac{\partial\tilde{w}^{(1)}}{\partial\eta}\frac{\partial^2\tilde{w}^{(1)}}{\partial\xi\partial\eta}\right.$$

$$+ \frac{1-\nu}{2\lambda^2} \frac{\partial \tilde{w}^{(1)}}{\partial \xi} \frac{\partial^2 \tilde{w}^{(1)}}{\partial \eta^2} \Bigg]$$

$$\tilde{b}_v^{(2)} = -\left(\frac{N-1}{\beta}\right) \Bigg[\frac{1}{\lambda^3} \frac{\partial \tilde{w}^{(1)}}{\partial \eta} \frac{\partial^2 \tilde{w}^{(1)}}{\partial \eta^2} + \frac{1+\nu}{2\lambda} \frac{\partial \tilde{w}^{(1)}}{\partial \xi} \frac{\partial^2 \tilde{w}^{(1)}}{\partial \xi \partial \eta}$$

$$+ \frac{1-\nu}{2\lambda} \frac{\partial \tilde{w}^{(1)}}{\partial \eta} \frac{\partial^2 \tilde{w}^{(1)}}{\partial \xi^2} \Bigg]$$

$$\tilde{b}_w^{(2)} = -(1-\nu^2)\left(\frac{N-1}{\pi^2}\right)\left(\frac{\alpha\beta}{\mu\zeta}\right)\left(\tilde{\sigma}_x^{(1)} \frac{\partial^2}{\partial \xi^2} + \frac{1}{\lambda^2} \tilde{\sigma}_y^{(1)} \frac{\partial^2}{\partial \eta^2}\right.$$

$$\left. + 2 \frac{\tilde{\tau}_{xy}^{(1)}}{\lambda} \frac{\partial^2}{\partial \xi \partial \eta}\right) \tilde{w}^{(1)} - 4\left(\frac{N-1}{\beta}\right) \Bigg\{ \frac{1}{2} \cos \omega\xi (1 - \cos \omega\eta)$$

$$\left[\left(\frac{\partial \tilde{w}^{(1)}}{\partial \xi}\right)^2 + \frac{\nu}{\lambda^2}\left(\frac{\partial \tilde{w}^{(1)}}{\partial \eta}\right)^2\right] + \frac{1}{2\lambda^2} (1 - \cos \omega\xi) \cos \omega\eta$$

$$\left[\frac{1}{\lambda^2}\left(\frac{\partial \tilde{w}^{(1)}}{\partial \eta}\right)^2 + \nu\left(\frac{\partial \tilde{w}^{(1)}}{\partial \xi}\right)^2\right] + \frac{1-\nu}{\lambda^2} \sin \omega\xi \sin \omega\eta$$

$$\frac{\partial \tilde{w}^{(1)}}{\partial \xi} \frac{\partial \tilde{w}^{(1)}}{\partial \eta} \Bigg\}$$

$$\tilde{b}_u^{(3)} = -\left(\frac{N-1}{\beta}\right) \Bigg[\frac{\partial \tilde{w}^{(1)}}{\partial \xi} \frac{\partial^2 \tilde{w}^{(2)}}{\partial \xi^2} + \frac{1+\nu}{2\lambda^2} \frac{\partial \tilde{w}^{(1)}}{\partial \eta} \frac{\partial^2 \tilde{w}^{(2)}}{\partial \xi \partial \eta}$$

$$+ \frac{1-\nu}{2\lambda^2} \frac{\partial \tilde{w}^{(1)}}{\partial \xi} \frac{\partial^2 \tilde{w}^{(2)}}{\partial \eta^2} + \frac{\partial^2 \tilde{w}^{(1)}}{\partial \eta^2} \frac{\partial \tilde{w}^{(2)}}{\partial \xi}$$

$$+ \frac{1+\nu}{2\lambda^2} \frac{\partial^2 \tilde{w}^{(1)}}{\partial \xi^2} \frac{\partial \tilde{w}^{(2)}}{\partial \eta} + \frac{1-\nu}{2\lambda^2} \frac{\partial^2 \tilde{w}^{(1)}}{\partial \eta^2} \frac{\partial \tilde{w}^{(2)}}{\partial \xi} \Big]$$

$$\tilde{b}_v^{(3)} = -\left(\frac{N-1}{\beta}\right) \Big[\frac{1}{\lambda^3} \frac{\partial \tilde{w}^{(1)}}{\partial \eta} \frac{\partial^2 \tilde{w}^{(2)}}{\partial \eta^2} + \frac{1+\nu}{2\lambda} \frac{\partial \tilde{w}^{(1)}}{\partial \xi} \frac{\partial^2 \tilde{w}^{(2)}}{\partial \xi \partial \eta}$$

$$+ \frac{1-\nu}{2\lambda} \frac{\partial \tilde{w}^{(1)}}{\partial \eta} \frac{\partial^2 \tilde{w}^{(2)}}{\partial \xi^2} + \frac{1}{\lambda^3} \frac{\partial^2 \tilde{w}^{(1)}}{\partial \eta^2} \frac{\partial \tilde{w}^{(2)}}{\partial \eta}$$

$$+ \frac{1+\nu}{2\lambda} \frac{\partial^2 \tilde{w}^{(1)}}{\partial \xi \partial \eta} \frac{\partial \tilde{w}^{(2)}}{\partial \xi} + \frac{1-\nu}{2\lambda} \frac{\partial^2 \tilde{w}^{(1)}}{\partial \xi^2} \frac{\partial \tilde{w}^{(2)}}{\partial \eta} \Big]$$

$$\tilde{b}_w^{(3)} = -(1-\nu^2)\left(\frac{N-1}{\pi^2}\right)\left(\frac{\alpha\beta}{\mu\zeta}\right)\Big(\tilde{\sigma}_x^{(1)} \frac{\partial^2}{\partial \xi^2} + \frac{1}{\lambda^2} \tilde{\sigma}_y^{(1)} \frac{\partial^2}{\partial \eta^2}$$

$$+ 2 \frac{1}{\lambda} \tilde{\tau}_{xy}^{(1)} \frac{\partial^2}{\partial \xi \partial \eta}\Big) \tilde{w}^{(2)} - (1-\nu^2)\left(\frac{N-1}{\pi^2}\right)\left(\frac{\alpha\beta}{\mu\zeta}\right)$$

$$\cdot \Big(\tilde{\sigma}_x^{(2)} \frac{\partial^2}{\partial \xi^2} + \frac{1}{\lambda^2} \tilde{\sigma}_y^{(2)} \frac{\partial^2}{\partial \eta^2} + 2 \frac{1}{\lambda} \tilde{\tau}_{xy}^{(2)} \frac{\partial^2}{\partial \xi \partial \eta}\Big) \tilde{w}^{(1)}$$

$$- 4\left(\frac{N-1}{\beta}\right) \Big\{ \cos \omega\xi \ (1 - \cos \omega\eta) \Big(\frac{\partial \tilde{w}^{(1)}}{\partial \xi} \frac{\partial \tilde{w}^{(2)}}{\partial \xi}$$

$$+ \frac{\nu}{\lambda^2} \frac{\partial \tilde{w}^{(1)}}{\partial \eta} \frac{\partial \tilde{w}^{(2)}}{\partial \eta}\Big) + (1 - \cos \omega\xi) \cos \omega\eta$$

$$\cdot \Big(\frac{1}{\lambda^4} \frac{\partial \tilde{w}^{(1)}}{\partial \eta} \frac{\partial \tilde{w}^{(2)}}{\partial \eta} + \frac{\nu}{\lambda^2} \frac{\partial \tilde{w}^{(1)}}{\partial \xi} \frac{\partial \tilde{w}^{(2)}}{\partial \xi}\Big) + \frac{1-\nu}{\lambda^2}$$

$$\cdot \sin \omega\xi \sin \omega\eta \left(\frac{\partial \tilde{w}^{(1)}}{\partial \xi} \frac{\partial \tilde{w}^{(2)}}{\partial \eta} + \frac{\partial \tilde{w}^{(1)}}{\partial \eta} \frac{\partial \tilde{w}^{(2)}}{\partial \xi}\right) \Bigg\}$$

The in-plane stresses appearing above are expressible in the following matrix form:

$$\begin{bmatrix} \tilde{\sigma}_x^{(1)} & \tilde{\sigma}_x^{(2)} & \tilde{\sigma}_x^{(3)} \\ \tilde{\sigma}_y^{(1)} & \tilde{\sigma}_y^{(2)} & \tilde{\sigma}_y^{(3)} \\ \tilde{\tau}_{xy}^{(1)} & \tilde{\tau}_{xy}^{(2)} & \tilde{\tau}_{xy}^{(3)} \end{bmatrix} = \frac{\zeta}{\alpha\beta} \frac{N-1}{1-\nu^2}$$

$$\begin{bmatrix} & & 2\pi\left(\frac{\mu}{\beta}\right)\left[\sin \omega\xi(1-\cos \omega\eta) \frac{\partial}{\partial \xi}\right. \\ \frac{\partial}{\partial \xi}, & \frac{\nu}{\lambda} \frac{\partial}{\partial \eta}, & \\ & & \left. + \frac{\nu}{\lambda^2} (1-\cos \omega\xi) \sin \omega\eta \frac{\partial}{\partial \eta}\right] \\ \cdots & \cdots & \cdots \\ & & 2\pi\left(\frac{\mu}{\beta}\right)\left[\frac{1}{\lambda^2} \sin \omega\eta(1-\cos \omega\xi) \frac{\partial}{\partial \eta}\right. \\ \nu\frac{\partial}{\partial \xi}, & \frac{1}{\lambda} \frac{\partial}{\partial \eta}, & \\ & & \left. + \nu \sin \omega\xi (1-\cos \omega\eta) \frac{\partial}{\partial \xi}\right] \\ \cdots & \cdots & \cdots \\ & & \pi(1-\nu)\left(\frac{\mu}{\beta}\right)\left(\frac{1}{\lambda}\right) \sin \omega\xi (1-\cos \omega\eta) \\ \frac{1-\nu}{2} \frac{\partial}{\partial \eta}, & \frac{1-\nu}{2} \frac{\partial}{\partial \xi}, & \\ & & \cdot\frac{\partial}{\partial \eta} + (1-\cos \omega\xi) \sin \omega\eta \frac{\partial}{\partial \xi}\Big] \end{bmatrix}$$

$$\cdot \begin{bmatrix} \tilde{u}^{(1)} & \tilde{u}^{(2)} & \tilde{u}^{(3)} \\ \tilde{v}^{(1)} & \tilde{v}^{(2)} & \tilde{v}^{(3)} \\ \tilde{w}^{(1)} & \tilde{w}^{(2)} & \tilde{w}^{(3)} \end{bmatrix} + \frac{\zeta}{\alpha\beta^2} \frac{(N-1)^2}{1-\nu^2}$$

$$\begin{bmatrix} \frac{1}{2}\left(\frac{\partial \tilde{w}^{(1)}}{\partial \xi}\right)^2 & & \\ 0, \quad + & \frac{\partial \tilde{w}^{(1)}}{\partial \xi} \frac{\partial \tilde{w}^{(2)}}{\partial \xi} + \frac{\nu}{\lambda^2} \frac{\partial \tilde{w}^{(1)}}{\partial \eta} \frac{\partial \tilde{w}^{(2)}}{\partial \eta} & \\ \frac{\nu}{2\lambda^2}\left(\frac{\partial \tilde{w}^{(1)}}{\partial \eta}\right)^2, & & \\ \cdots\cdots\cdots\cdots\cdots\cdots\cdots\cdots\cdots\cdots & & \\ \frac{1}{2\lambda^2}\left(\frac{\partial \tilde{w}^{(1)}}{\partial \eta}\right)^2 & & \\ 0, \quad + & \frac{1}{\lambda^2} \frac{\partial \tilde{w}^{(1)}}{\partial \eta} \frac{\partial \tilde{w}^{(2)}}{\partial \eta} + \nu \frac{\partial \tilde{w}^{(1)}}{\partial \xi} \frac{\partial \tilde{w}^{(2)}}{\partial \xi} & \\ \frac{\nu}{2}\left(\frac{\partial \tilde{w}^{(1)}}{\partial \xi}\right)^2, & & \\ \cdots\cdots\cdots\cdots\cdots\cdots\cdots\cdots\cdots\cdots & & \\ \frac{1-\nu}{2\lambda} & & \\ 0, \quad \times & \frac{1-\nu}{2\lambda}\left(\frac{\partial \tilde{w}^{(1)}}{\partial \xi} \frac{\partial \tilde{w}^{(2)}}{\partial \eta} + \frac{\partial \tilde{w}^{(1)}}{\partial \eta} \frac{\partial \tilde{w}^{(2)}}{\partial \xi}\right) & \\ \frac{\partial \tilde{w}^{(1)}}{\partial \xi} \frac{\partial \tilde{w}^{(1)}}{\partial \eta}, & & \end{bmatrix}$$

(57)

Nondimensionalized Boundary Conditions in Terms of Displacements

Let

$$\phi_f = \frac{A_f}{ah} \; ; \quad \phi'_f = \frac{A'_f}{ah}; \quad \phi_s = \frac{A_s}{ah}; \quad \phi'_s = \frac{A'_s}{ah}$$

$$\psi_f = 24\ (1-\nu)\left(\frac{J_f}{h^3\ a}\right); \quad \psi'_f = 24\ (1-\nu)\left(\frac{J'_f}{h^3\ a}\right) \tag{58}$$

$$\psi_s = 24\ (1-\nu)\left(\frac{J_s}{h^3\ a}\right); \quad \psi'_s = 24\ (1-\nu)\left(\frac{J'_s}{h^3\ a}\right)$$

$$\kappa_f = 64\ (1-\nu^2)\left(\frac{1}{\beta^2}\right)\left(\frac{i_f}{h^3\ a}\right); \quad \kappa'_f = 64\ (1-\nu^2)\left(\frac{1}{\beta^2}\right)\left(\frac{i'_f}{h^3\ a}\right)$$

Then the boundary conditions presented in Equations 30 through 40 are expressed in terms of displacements and then non-dimensionalized using Equations 50, 53 and 58.

1. Support conditions for w: The conditions are represented by the following differential equations:

$$L_w\ \tilde{w}^{(k)} = 0 \quad \text{along each boundary member}$$

where $L_w = \frac{1}{4}(N-1)\ \frac{\psi_s}{\lambda^2}\ \frac{\partial}{\partial\eta}\left(\frac{\partial^2}{\partial\xi\partial\eta}\right) - \frac{\partial^2}{\partial\xi^2} - \frac{\nu}{\lambda^2}\ \frac{\partial^2}{\partial\eta^2}$ along $x = 0$

$$L_w = \frac{1}{4}(N-1)\ \frac{\psi'_s}{\lambda^2}\ \frac{\partial}{\partial\eta}\left(\frac{\partial^2}{\partial\xi\partial\eta}\right) + \frac{\partial^2}{\partial\xi^2} + \frac{\nu}{\lambda^2}\ \frac{\partial^2}{\partial\eta^2} \quad \text{along } x = a$$

$$L_w = \frac{1}{4}(N-1)\ \frac{\psi_f'}{\lambda}\ \frac{\partial}{\partial\xi}\left(\frac{\partial^2}{\partial\xi\partial\eta}\right) - \frac{1}{\lambda^2}\ \frac{\partial^2}{\partial\eta^2} - \nu\frac{\partial^2}{\partial\xi^2} \qquad \text{along } y = 0$$

$$L_w = \frac{1}{4}(N-1)\ \frac{\psi_f}{\lambda}\ \frac{\partial}{\partial\xi}\left(\frac{\partial^2}{\partial\xi\partial\eta}\right) + \frac{1}{\lambda^2}\ \frac{\partial^2}{\partial\eta^2} + \nu\frac{\partial^2}{\partial\xi^2} \qquad \text{along } y = b, \tag{59}$$

also

$$\tilde{w}^{(k)} = 0 \quad \text{along each boundary member } (k=0,1,2,3) \tag{60}$$

2. Boundary conditions for in-plane displacements u and v:

Along x = 0

The conditions are given by the following matrix equation

$$(L_u,\ L_v)\begin{pmatrix} \tilde{u}^{(1)} & \tilde{u}^{(2)} & \tilde{u}^{(3)} \\ \tilde{v}^{(1)} & \tilde{v}^{(2)} & \tilde{v}^{(3)} \end{pmatrix} = (\tilde{b}^{(1)} \quad \tilde{b}^{(2)} \quad \tilde{b}^{(3)})$$

where $$L_u = \frac{1}{2\lambda(1+\nu)}\left(\frac{1}{\phi_s}\right)\ \frac{1}{N-1}\ \frac{\partial}{\partial\eta}$$

$$L_v = \frac{1}{\lambda^2}\ \frac{\partial^2}{\partial\eta^2} + \frac{1}{2(1+\nu)}\left(\frac{1}{\phi_s}\right)\ \frac{1}{N-1}\ \frac{\partial}{\partial\xi}$$

$$\tilde{b}^{(1)} = \frac{1}{(N-1)^2}\ \frac{\alpha\beta}{\zeta\phi_s} \tag{61}$$

$$\tilde{b}^{(2)} = -\frac{1}{2(1+\nu)\phi_s\lambda\beta}\ \frac{\partial w^{(1)}}{\partial\xi}\ \frac{\partial w^{(1)}}{\partial\eta}$$

$$\tilde{b}^{(3)} = -\frac{1}{2(1+\nu)\phi_s\lambda\beta}\left(\frac{\partial\tilde{w}^{(1)}}{\partial\xi}\ \frac{\partial\tilde{w}^{(2)}}{\partial\eta} + \frac{\partial\tilde{w}^{(1)}}{\partial\eta}\ \frac{\partial\tilde{w}^{(2)}}{\partial\xi}\right)$$

$$\text{also} \quad \tilde{u}^{(k)} = 0 \qquad (K = 1,2,3)$$

$$\text{and} \quad \tilde{v}^{(k)} \ (x = 0;\ y = 0) = 0 \qquad (k=1,2,3) \tag{62}$$

Along x = a

Similarly, the boundary conditions along x = a are given by:

$$(L_u,\ L_v) \begin{pmatrix} \tilde{u}^{(1)} & \tilde{u}^{(2)} & \tilde{u}^{(3)} \\ \tilde{v}^{(1)} & \tilde{v}^{(2)} & \tilde{v}^{(3)} \end{pmatrix} = \left(\tilde{b}^{(1)},\ \tilde{b}^{(2)},\ \tilde{b}^{(3)}\right)$$

where

$$L_u = -\frac{1}{2\lambda(1+\nu)}\left(\frac{1}{\phi_s'}\right)\frac{1}{N-1}\frac{\partial}{\partial\eta}$$

$$L_v = \frac{1}{\lambda^2}\frac{\partial^2}{\partial\eta^2} - \frac{1}{2\lambda(1+\nu)}\left(\frac{1}{\phi_s'}\right)\frac{1}{N-1}\frac{\partial}{\partial\xi}$$

$$\tilde{b}^{(1)} = -\frac{1}{(N-1)^2}\frac{\alpha\beta}{\zeta\phi_s'} \tag{63}$$

$$\tilde{b}^{(2)} = \frac{1}{2(1+\nu)\phi_s'\lambda\beta}\frac{\partial\tilde{w}^{(1)}}{\partial\xi}\frac{\partial\tilde{w}^{(1)}}{\partial\eta}$$

$$b^{(3)} = \frac{1}{2(1+\nu)\phi_s'\lambda\beta}\left(\frac{\partial\tilde{w}^{(1)}}{\partial\xi}\frac{\partial\tilde{w}^{(2)}}{\partial\eta} + \frac{\partial\tilde{w}^{(1)}}{\partial\eta}\frac{\partial\tilde{w}^{(2)}}{\partial\xi}\right)$$

$$\text{also} \quad \frac{\partial^2}{\partial\eta^2}\tilde{u}^{(k)} = 0 \qquad (k = 1,2,3) \tag{64}$$

Along y = 0

The conditions are divided into the bending equations and the shear equations. For this reason, the subscripts b and s are used in the following expression.

$$\begin{bmatrix} L_{ub} & L_{vb} \\ L_{us} & L_{vs} \end{bmatrix} \begin{bmatrix} \tilde{u}^{(1)} & \tilde{u}^{(2)} & \tilde{u}^{(3)} \\ \tilde{v}^{(1)} & \tilde{v}^{(2)} & \tilde{v}^{(3)} \end{bmatrix} = \begin{bmatrix} \tilde{b}_b^{(1)} & \tilde{b}_b^{(2)} & \tilde{b}_b^{(3)} \\ \tilde{b}_s^{(1)} & \tilde{b}_s^{(2)} & \tilde{b}_s^{(3)} \end{bmatrix}$$

where $L_{ub} = -\nu \frac{\partial}{\partial \xi}$

$$L_{vb} = \kappa_f' \frac{\partial^4}{\partial \xi^4} - \frac{1}{\lambda} \frac{\partial}{\partial \eta}$$

$$L_{us} = \frac{\partial^2}{\partial \xi^2} + \frac{1}{2(1+\nu)\phi_f' \lambda(N-1)} \frac{\partial}{\partial \eta}$$

$$L_{vs} = \frac{1}{2(1+\nu)\phi_f'(N-1)} \frac{\partial}{\partial \xi}$$

$$\tilde{b}_s^{(1)} = 0$$

$$\tilde{b}_s^{(2)} = -\frac{1}{2(1+\nu)\phi_f'\lambda\beta} \frac{\partial \tilde{w}^{(1)}}{\partial \xi} \frac{\partial \tilde{w}^{(1)}}{\partial \eta} \qquad (65)$$

$$\tilde{b}_s^{(3)} = -\frac{1}{2(1+\nu)\phi_f'\lambda\beta} \left(\frac{\partial \tilde{w}^{(1)}}{\partial \xi} \frac{\partial \tilde{w}^{(2)}}{\partial \eta} + \frac{\partial \tilde{w}^{(1)}}{\partial \eta} \frac{\partial \tilde{w}^{(2)}}{\partial \xi} \right)$$

$$\tilde{b}_b^{(1)} = 0$$

$$\tilde{b}_b^{(2)} = \left(\frac{N-1}{2\beta} \right) \left[\frac{1}{\lambda^2} \left(\frac{\partial \tilde{w}^{(1)}}{\partial \eta} \right)^2 + \nu \left(\frac{\partial \tilde{w}^{(1)}}{\partial \xi} \right)^2 \right]$$

$$\tilde{b}_b^{(3)} = \left(\frac{N-1}{\beta}\right)\left[\frac{1}{\lambda^2}\frac{\partial\tilde{w}^{(1)}}{\partial\eta}\frac{\partial\tilde{w}^{(2)}}{\partial\eta} + \nu\frac{\partial\tilde{w}^{(1)}}{\partial\xi}\frac{\partial\tilde{w}^{(2)}}{\partial\xi}\right]$$

Along y = b

The boundary conditions here are similar to those along y = 0.

$$\begin{bmatrix} L_{ub} & L_{vb} \\ L_{us} & L_{vs} \end{bmatrix}\begin{bmatrix} \tilde{u}^{(1)} & \tilde{u}^{(2)} & \tilde{u}^{(3)} \\ \tilde{v}^{(1)} & \tilde{v}^{(2)} & \tilde{v}^{(3)} \end{bmatrix} = \begin{bmatrix} \tilde{b}_b^{(1)} & \tilde{b}_b^{(2)} & \tilde{b}_b^{(3)} \\ \tilde{b}_s^{(1)} & \tilde{b}_s^{(2)} & \tilde{b}_s^{(3)} \end{bmatrix}$$

where

$$L_{ub} = \nu\frac{\partial}{\partial\xi}$$

$$L_{vb} = \kappa_f\frac{\partial^4}{\partial\xi^4} + \frac{1}{\lambda}\frac{\partial}{\partial\eta}$$

$$L_{us} = \frac{\partial^2}{\partial\xi^2} - \frac{1}{2(1+\nu)\phi_f\lambda(N-1)}\frac{\partial}{\partial\eta}$$

$$L_{vs} = -\frac{1}{2(1+\nu)\phi_f(N-1)}\frac{\partial}{\partial\xi}$$

$$\tilde{b}_s^{(1)} = 0$$

$$\tilde{b}_s^{(2)} = \frac{1}{2(1+\nu)\phi_f\lambda\beta}\frac{\partial\tilde{w}^{(1)}}{\partial\xi}\frac{\partial\tilde{w}^{(1)}}{\partial\eta} \qquad (66)$$

$$\tilde{b}_s^{(3)} = \frac{1}{2(1+\nu)\phi_f\lambda\beta}\left(\frac{\partial\tilde{w}^{(1)}}{\partial\xi}\frac{\partial\tilde{w}^{(2)}}{\partial\eta} + \frac{\partial\tilde{w}^{(1)}}{\partial\eta}\frac{\partial\tilde{w}^{(2)}}{\partial\xi}\right)$$

$$\tilde{b}_b^{(1)} = 0$$

$$\tilde{b}_b^{(2)} = -\left(\frac{N-1}{2\beta}\right)\left[\frac{1}{\lambda^2}\left(\frac{\partial\tilde{w}^{(1)}}{\partial\eta}\right)^2 + \nu\left(\frac{\partial\tilde{w}^{(1)}}{\partial\xi}\right)^2\right]$$

$$\tilde{b}_b^{(3)} = -\left(\frac{N-1}{\beta}\right)\left[\frac{1}{\lambda^2}\frac{\partial\tilde{w}^{(1)}}{\partial\eta}\frac{\partial\tilde{w}^{(2)}}{\partial\eta} + \nu\frac{\partial\tilde{w}^{(1)}}{\partial\xi}\frac{\partial\tilde{w}^{(2)}}{\partial\xi}\right]$$

3. Conditions of no net resultant forces

Along x = 0 or x = a

The condition is given by the following expression:

$$(L_u,\ L_v)\begin{bmatrix}\tilde{u}^{(1)} & \tilde{u}^{(2)} & \tilde{u}^{(3)}\\ \tilde{v}^{(1)} & \tilde{v}^{(2)} & \tilde{v}^{(3)}\end{bmatrix} = L_f\left(f_w^{(1)},\ f_w^{(2)},\ f_w^{(3)}\right)$$

where L_u, L_v and L_f are linear operators shown as follows

$$L_u = \frac{\lambda}{1-\nu^2}\int_0^{N-1} d\eta\ \frac{\partial}{\partial\xi} + \delta_\eta^{N-1}\,\phi_f\,(N-1)\,\frac{\partial}{\partial\xi} + \delta_\eta^{0}\,\phi_f'\,(N-1)\,\frac{\partial}{\partial\xi}$$

$$L_v = \frac{\nu}{1-\nu^2}\int_0^{N-1} d\eta\ \frac{\partial}{\partial\eta}$$

$$L_f = -\frac{\lambda}{1-\nu^2}\int_0^{N-1} d\eta \qquad (67)$$

and $\delta_\eta^Q = 1$ when $\eta = Q$

$= 0$ when $\eta \neq Q$

$f_w^{(1)}$, $f_w^{(2)}$ and $f_w^{(3)}$ are functions as shown below:

$$f_w^{(1)} = 0$$

$$f_w^{(2)} = \frac{1}{2}\left(\frac{N-1}{\beta}\right)\left[\left(\frac{\partial \tilde{w}^{(1)}}{\partial \xi}\right)^2 + \frac{\nu}{\lambda^2}\left(\frac{\partial \tilde{w}^{(1)}}{\partial \eta}\right)^2\right]$$

$$f_w^{(3)} = \left(\frac{N-1}{\beta}\right)\left[\frac{\partial \tilde{w}^{(1)}}{\partial \xi}\frac{\partial \tilde{w}^{(2)}}{\partial \xi} + \frac{\nu}{\lambda^2}\frac{\partial \tilde{w}^{(1)}}{\partial \eta}\frac{\partial \tilde{w}^{(2)}}{\partial \eta}\right]$$

Along y = 0 or y = b

The condition is given by the following expression:

$$(L_u', \quad L_v')\begin{bmatrix} \tilde{u}^{(1)} & \tilde{u}^{(2)} & \tilde{u}^{(3)} \\ \tilde{v}^{(1)} & \tilde{v}^{(2)} & \tilde{v}^{(3)} \end{bmatrix} = L_g\left(g_w^{(1)}, g_w^{(2)}, g_w^{(3)}\right)$$

where L_u, L_v and L_g are linear integro-differential operators shown as follows:

(68)

$$L_u' = \frac{\nu}{1-\nu^2}\int_0^{N-1} d\xi \frac{\partial}{\partial \xi}$$

$$L_v' = \frac{1}{1-\nu^2}\left(\frac{1}{\lambda}\right)\int_0^{N-1} d\xi \frac{\partial}{\partial \eta} + \frac{N-1}{\lambda}\frac{\partial}{\partial \eta}\left(\phi_s \delta_\xi^0 + \phi_s' \delta_\xi^{N-1}\right)$$

$$L_g = -\frac{1}{1-\nu^2}\int_0^{N-1} d\xi$$

and $\delta_\xi^Q = 1$ when $\xi = Q$

$= 0$ when $\xi \neq Q$

$g_w^{(k)}$ $(k = 1,2,3)$ are functions defined as follows:

$$g_w^{(1)} = 0$$

$$g_w^{(2)} = \frac{1}{2}\left(\frac{N-1}{\beta}\right)\left[\frac{1}{\lambda^2}\left(\frac{\partial \tilde{w}^{(1)}}{\partial \eta}\right)^2 + \nu\left(\frac{\partial \tilde{w}^{(1)}}{\partial \xi}\right)^2\right]$$

$$g_w^{(3)} = \left(\frac{N-1}{\beta}\right)\left[\frac{1}{\lambda^2}\frac{\partial \tilde{w}^{(1)}}{\partial \eta}\frac{\partial \tilde{w}^{(2)}}{\partial \eta} + \nu\frac{\partial \tilde{w}^{(1)}}{\partial \xi}\frac{\partial \tilde{w}^{(2)}}{\partial \xi}\right]$$

4. Bending moment conditions The bending moment is assigned a value at the edge x = a. On the other hand, the resultant bending moment should vanish along two edges: y = 0 and y = b, because of no external bending moments acting there. Considering the overall equilibrium of the panel, and referring to Figure 9, the following equation is obtained:

$$M\Big|_{x=a} - M\Big|_{x=0} = -Sa. \qquad (69)$$

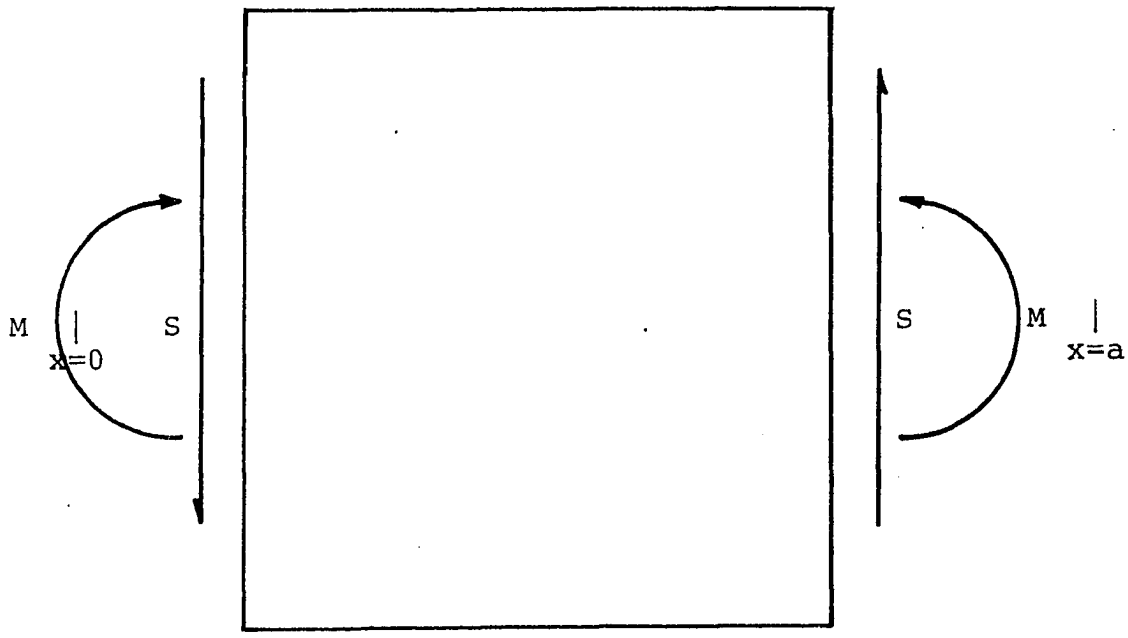

Figure 9. External force system

Let

$$\theta = \frac{b\ M}{a^2\ S}\ , \tag{70}$$

then,

$$M\ \Big|_{x=a} = M\ \Big|_{x=0} - S\ a = \left(\frac{a}{b}\ \theta\ -\ 1\right)\ S\ a = (\theta-\lambda)\tau h\ a^2 \tag{71}$$

The parameter θ indicates the interaction between the bending moment and the shearing stress. Therefore, the equation can be given in the following expression:

$$(L''_u,\ \ L''_v) \begin{pmatrix} \tilde{u}^{(1)} & \tilde{u}^{(2)} & \tilde{u}^{(3)} \\ \tilde{v}^{(1)} & \tilde{v}^{(2)} & \tilde{v}^{(3)} \end{pmatrix} = -\left(\frac{\alpha\beta\theta}{\zeta}\right)(1,\ 0,\ 0)$$

$$+\ L_{f\eta}\ \left(f_w^{(1)},\ f_w^{(2)},\ f_w^{(3)}\right)\quad \text{along } x = a. \tag{72}$$

Also,

$$(L'''_u,\ \ L'''_v) \begin{pmatrix} \tilde{u}^{(1)} & \tilde{u}^{(2)} & \tilde{u}^{(3)} \\ \tilde{v}^{(1)} & \tilde{v}^{(2)} & \tilde{v}^{(3)} \end{pmatrix} = L_{g\xi}\left(g_w^{(1)},\ g_w^{(2)},\ g_w^{(3)}\right) \tag{73}$$

along $y = 0$ or $y = b$.

where L''_u, L''_v and $L_{f\eta}$, and $L_{g\xi}$ are linear operators defined as follows:

$$L''_u = \frac{\lambda^2}{(N-1)(1-\nu^2)} \int_0^{N-1} \eta \, d\eta \, \frac{\partial}{\partial \xi} + \delta_\eta^{N-1} \, (N-1) \, \phi_f \, \frac{\partial}{\partial \xi}$$

$$L''_v = \frac{\lambda \, \nu}{(N-1)(1-\nu^2)} \int_0^{N-1} \eta \, d\eta \, \frac{\partial}{\partial \eta}$$

along x=a

$$L'''_u = \frac{\nu}{(N-1)(1-\nu^2)} \int_0^{N-1} \xi \, d\xi \, \frac{\partial}{\partial \xi}$$

$$L'''_v = \frac{1}{\lambda(N-1)(1-\nu^2)} \int_0^{N-1} \xi \, d\xi \, \frac{\partial}{\partial \eta} + \frac{\delta_\xi^{N-1}}{\lambda}(N-1) \, \phi'_s \, \frac{\partial}{\partial \eta}$$

along y=0 or y=b.

and

$$L_{f\eta} = - \frac{\lambda^2}{(N-1)(1-\nu^2)} \int_0^{N-1} \eta \, d\eta$$

$$L_{g\xi} = - \frac{1}{(N-1)(1-\nu^2)} \int_0^{N-1} \xi \, d\xi$$

Functions $f_w^{(k)}$ and $g_w^{(k)}$ have been defined in Equations 67 and 68.

Numerical Solutions by Means of Finite Difference Method

The purpose of this section is to illustrate the use of the finite difference method in solving Equations 52 and, 54 or 56, with appropriate boundary conditions mentioned in the

previous section. The reason for the use of this method rather than the closed-form solution is the complexity of the boundary conditions. In the finite different method, the basic differential equations as well as the boundary conditions are converted into sets of simultaneous algebraic equations.

Mesh point system

It was explained earlier that the displacement components u, v and w are selected as the unknowns. The structural system illustrated in Figure 4 is converted into sets of discrete points in a systematic manner. Figures 10 through 13 show the general numbering systems for N x N meshes. N designates the size (number of mesh lines in one direction) of the mesh point system. It should be noted that at one grid point, or mesh point, there are three unknowns, namely, u, v and w at that point. The total number of unknowns corresponding to the proposed mesh point system is $3N^2 + 7N - 7$ as can be seen from Figures 10 through 13.

In order to visualize the mesh point system clearly, the 5 x 5 mesh point system is shown in Figure 14 through Figure 17. As will be seen later, the 5 x 5 mesh point system is the one used in the actual numerical computations.

Finite difference formulas (Central difference)

Figures 18 and 19 illustrates some derivatives of a certain function Z. The double circles indicate the points

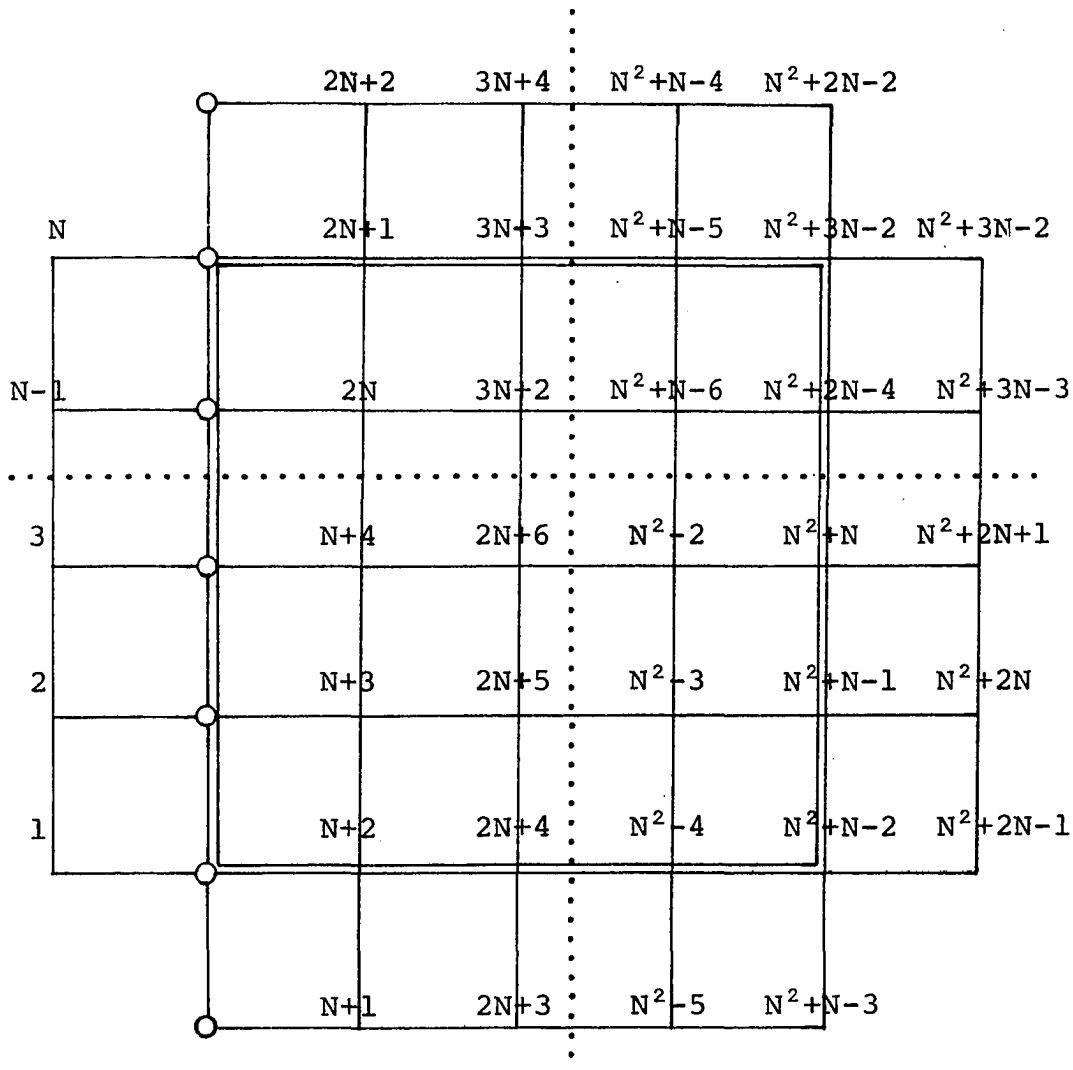

Figure 10. Generalized mesh point system for u

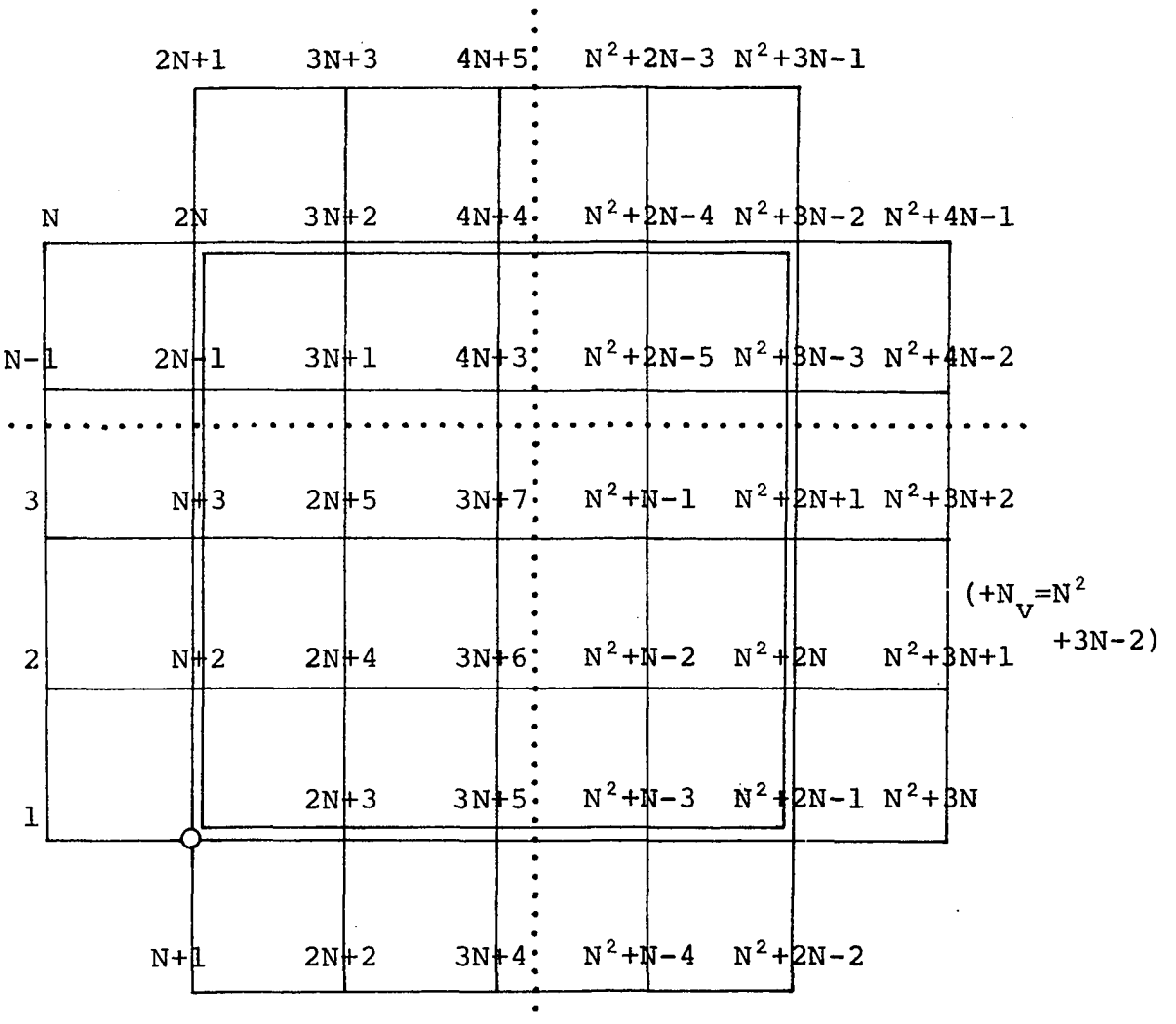

Figure 11. Generalized mesh point system for v

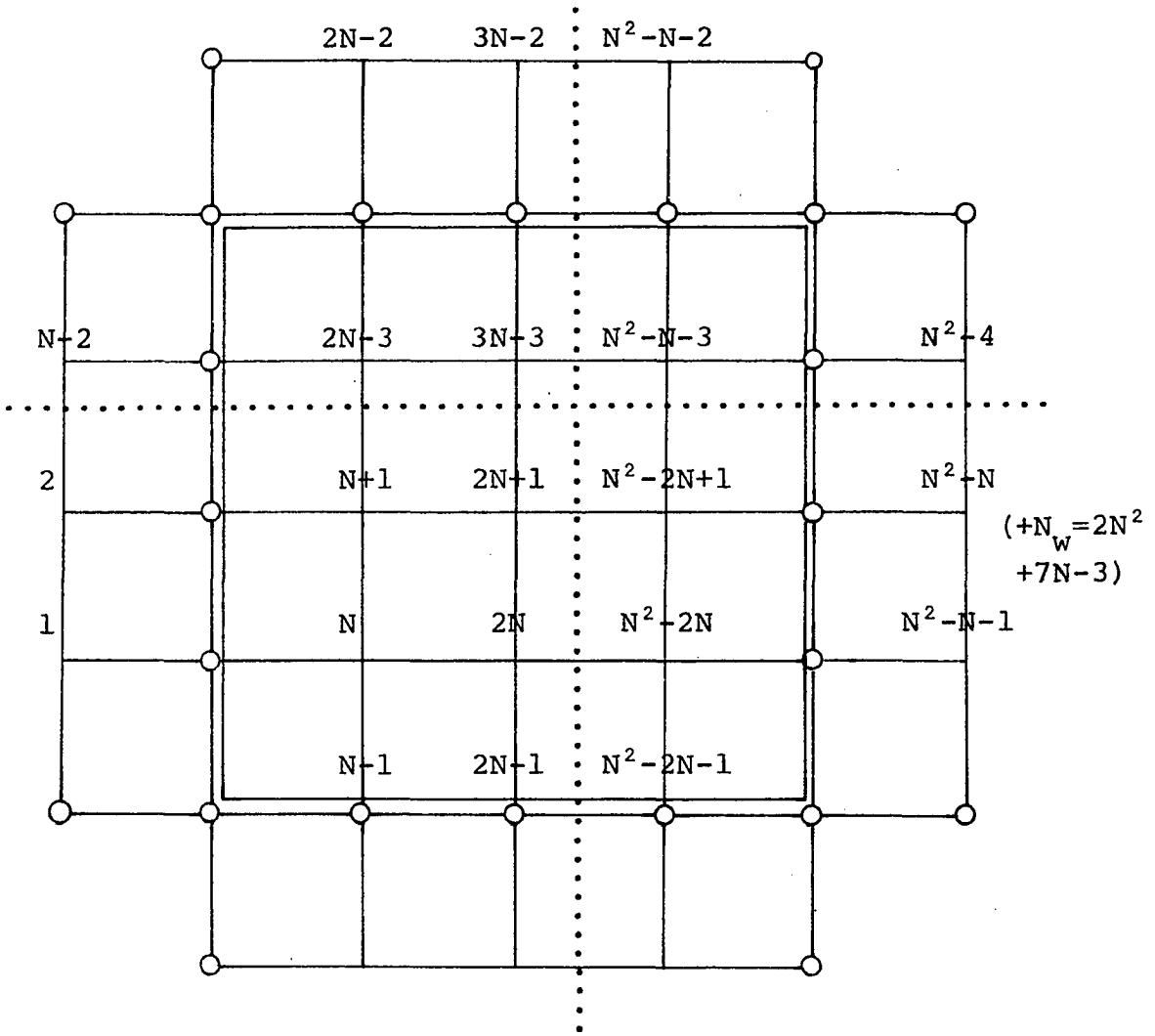

Figure 12. Generalized mesh point system for w

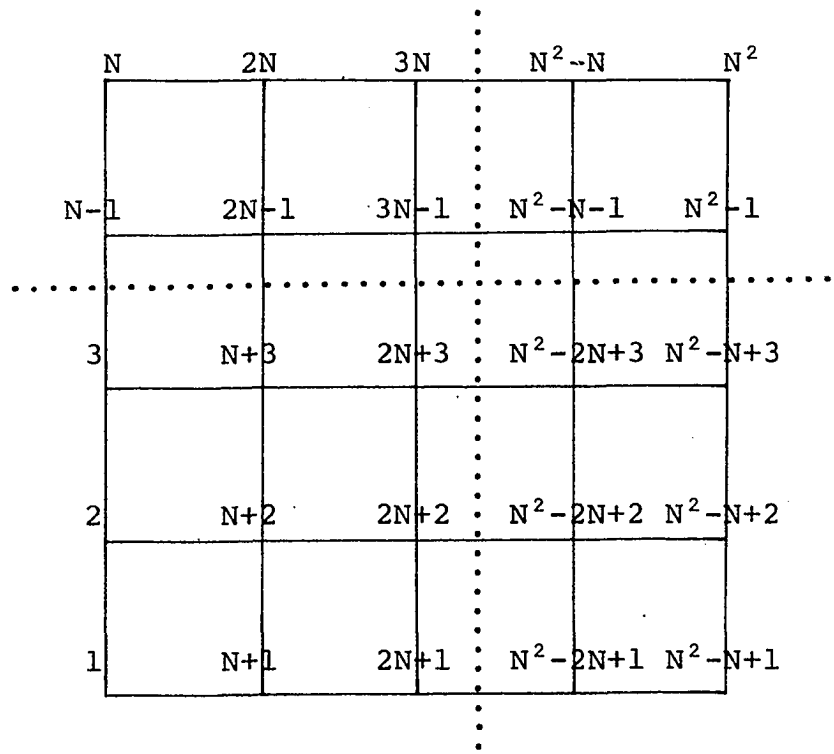

Figure 13. Generalized numbering system for stresses

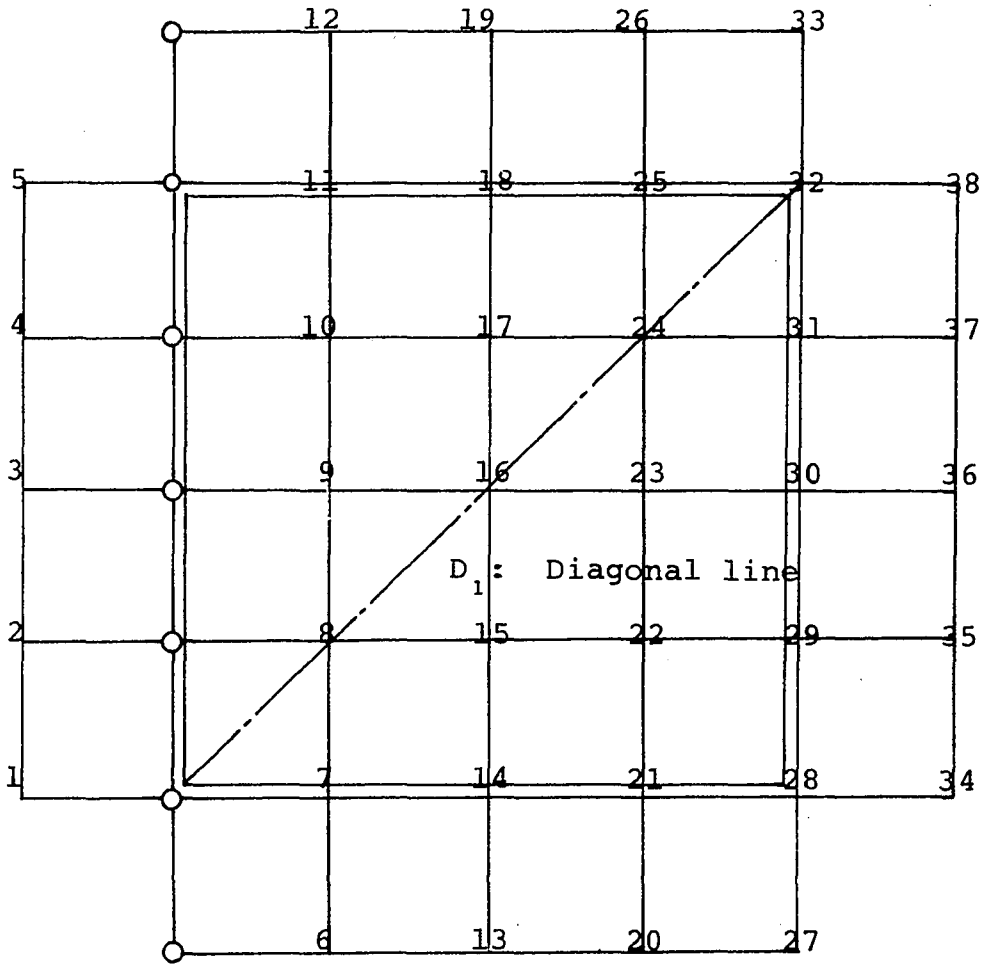

Figure 14. Numbering system for u
N = 5

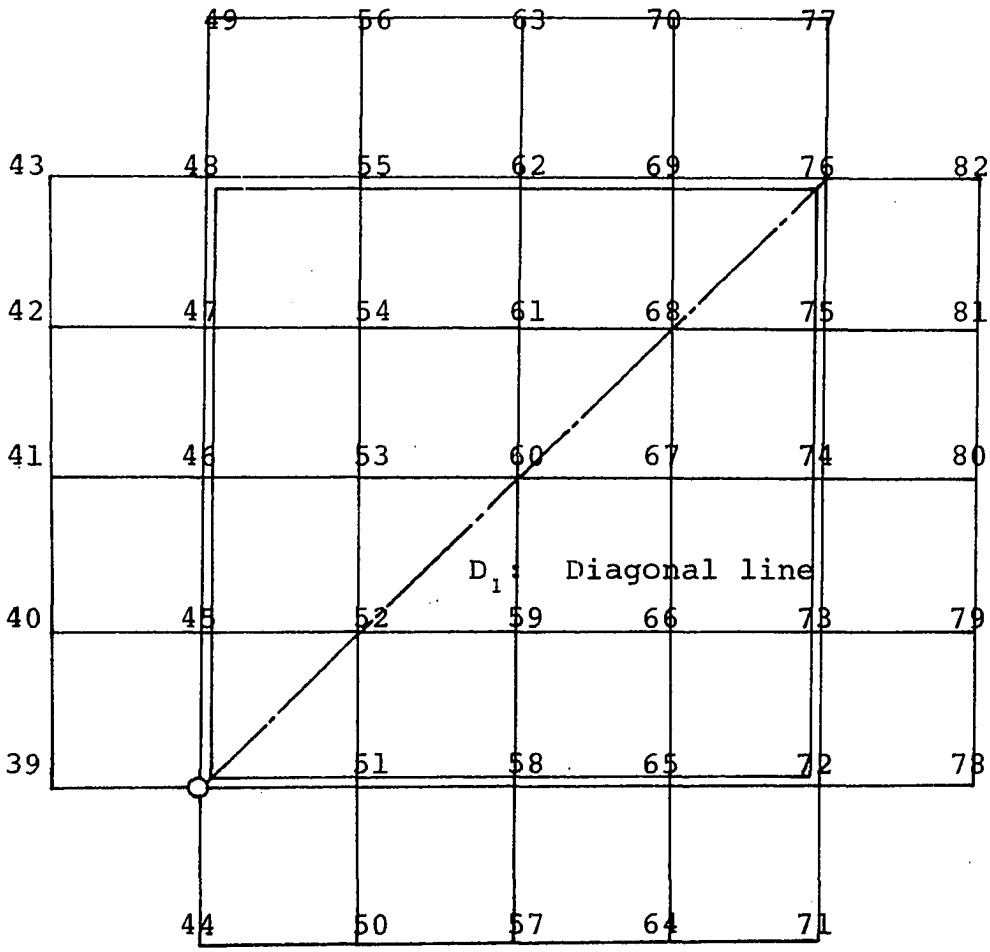

Figure 15. Numbering system for v
N = 5

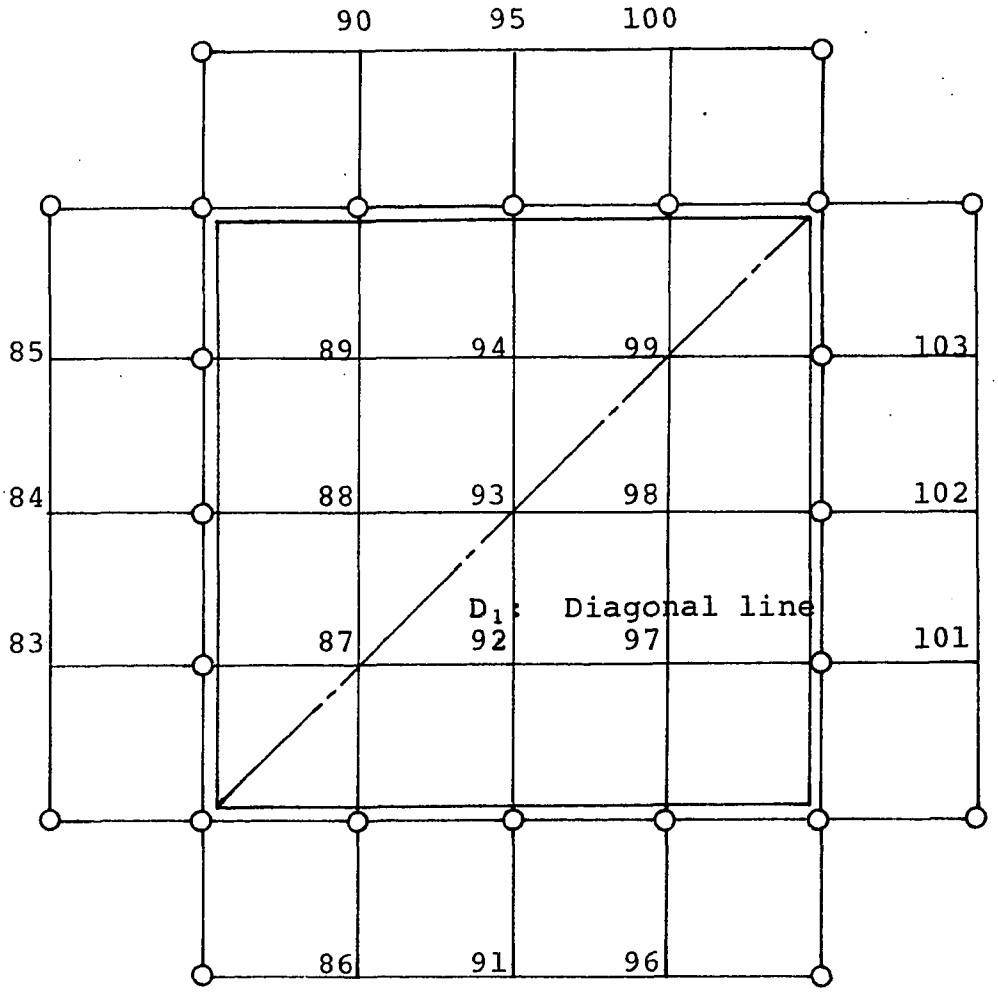

Figure 16. Numbering system for w
N = 5

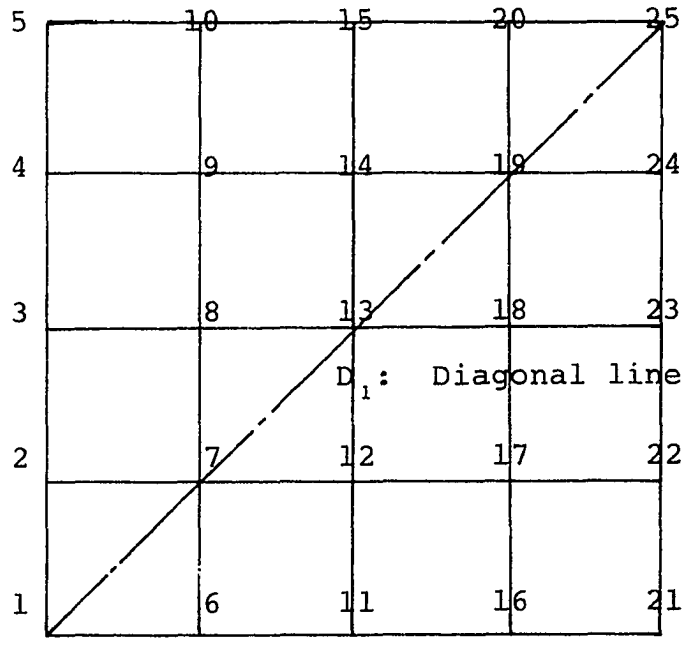

Figure 17. Numbering system for stresses
N=5

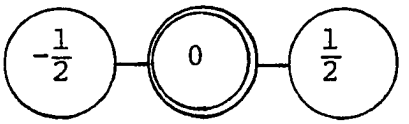

derivative $\frac{\partial Z}{\partial \xi}$

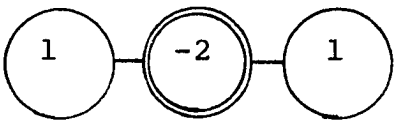

derivative $\frac{\partial^2 Z}{\partial \xi^2}$

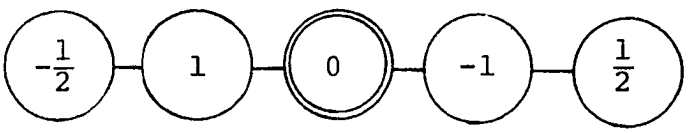

derivative $\frac{\partial^3 Z}{\partial \xi^3}$

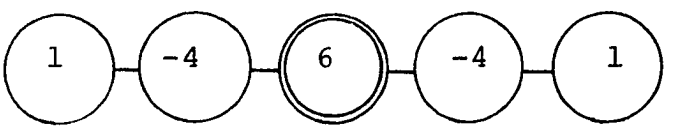

derivative $\frac{\partial^4 Z}{\partial \xi^4}$

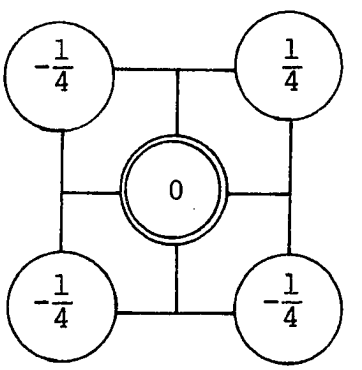

derivative $\frac{\partial^2 Z}{\partial \xi \partial \eta}$

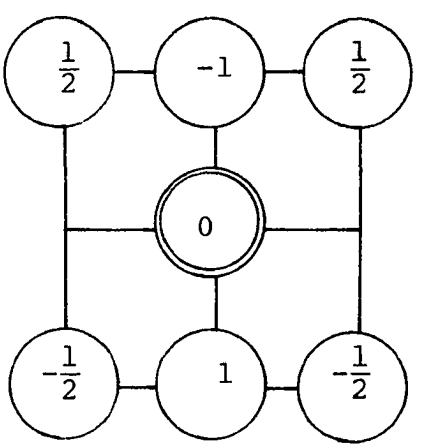

derivative $\frac{\partial^3 Z}{\partial \eta \partial \xi^2}$

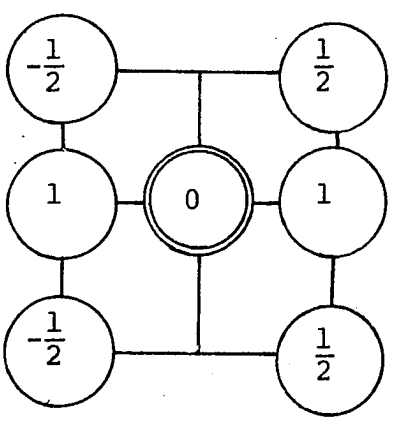

derivative $\frac{\partial^3 Z}{\partial \xi \partial \eta^2}$

Figure 18. Expressions for derivatives in terms of finite differences

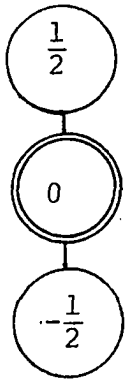

derivative $\frac{\partial Z}{\partial \eta}$

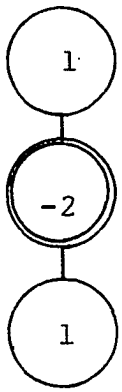

derivative $\frac{\partial^2 Z}{\partial \eta^2}$

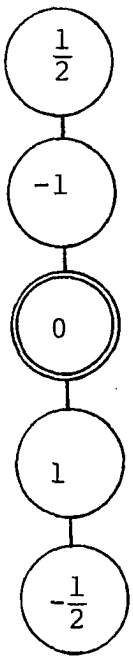

derivative

$\frac{\partial^3 Z}{\partial \eta^3}$

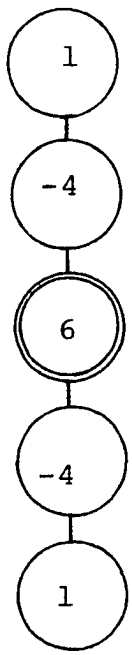

derivative

$\frac{\partial^4 Z}{\partial \eta^4}$

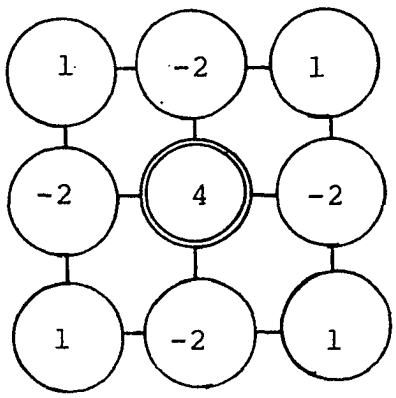

derivative $\frac{\partial^4 Z}{\partial \xi^2 \partial \eta^2}$

Figure 19. Expressions for derivatives in terms of finite differences

where the derivatives are being evaluated. It is to be noted that the interval between two adjacent points in vertical or horizontal direction is always unity by virtue of the non-dimensionalized coordinate system ξ and η defined in Equation 50.

Equations in terms of finite differences

The basic equations shown in Equations 52 and, 54 or 56, and the boundary conditions shown in Equations 59 through 73 can be expressed in terms of finite differences using the finite difference formulas mentioned above. The presentation of the whole equations in finite difference forms, is omitted here because of its bulkiness.

The equations used can be divided into five major groups. They are:

1. Equations of Equilibrium:

In x-direction	N^2-4 equations
In y-direction	N^2-4 equations
In z-direction	N^2-4N+4 equations

2. Boundary conditions excluding those at corner points:

Along x = 0	2N-4 equations
Along x = a	3N-6 equations
Along y = 0	3N-6 equations
Along y = b	3N-6 equations

3. Corner conditions:

At (0,0)	2 equations
At (0,b)	2 equations
At (a,0)	4 equations
At (a,b)	4 equations

4. Conditions of zero net forces:

Along x = 0	1 equation
Along x = a	1 equation
Along y = 0	1 equation
Along y = b	1 equation

5. Bending moment conditions:

Along x = a	1 equation
Along y = 0	1 equation
Along y = b	1 equation

Thus, the total number of equations is $3N^2+7N-7$. The boundary conditions used herein are those described in Equations 59 through 73 with the exception of the corner conditions. Special conditions are required at corner points. They are explained in the next subsection.

Corner conditions

The corner points provide special conditions for the in-plane displacement components u and v.

At (0,0) At this corner point, the boundary conditions for both x = 0 and y = 0 should be satisfied. Thus, the first, second, fifth and sixth equations of Equation 35 would be necessary. The first equation has been satisfied, however, since u has been set to be zero along y = 0 already. The fifth equation is a fourth order equation and this fourth derivative can not be evaluated at the corner. Therefore, the necessary conditions are the second and the sixth equations of Equation 35.

At (0,b) Similar to point (0,0), the necessary conditions at this point are the second and the eighth equations of Equation 35.

At (a,0) Similar consideration as was done for point (0,0) indicates that for this point the third, fourth and sixth equations of Equation 35 are used. Furthermore, since edge x = a is where the external bending moment, M, is assigned, better accuracy is desired to insure the equilibrium of this corner point. It has been assumed that the stiffeners do not have curvatures in y-direction. Thus, the moment equilibrium of the small corner element requires that

$$\frac{\partial^2 v}{\partial x^2} = 0 \tag{74}$$

This gives an additional condition for point (a,0).

At (a,b) Similar to point (a,0), the necessary conditions at this point are the third, fourth and eighth

equations of Equation 35, and Equation 74.

Computer programs

Appendix C provides a brief summary of computer programs used in the proposed analysis. This set of computer programs consists of a main program and twelve subroutine subprograms. The most important part in the programs is the solution of simultaneous algebraic equations corresponding to each order of approximation. These equations are solved by UGELG which is a library subroutine subprogram based on Gauss Reduction Method.

CHAPTER THREE: NUMERICAL ILLUSTRATIONS OF THE PROPOSED ANALYSIS AND DISCUSSION OF THE ANALYTICAL RESULTS

Description of Test Results Cited

To illustrate the proposed analysis numerically, some test results on plate girders are analyzed and compared with the results from the proposed analysis and with other theories. The experimental data is taken from, first, WEB BUCKLING TESTS ON WELDED PLATE GIRDERS (5), second, PROOF-TESTS OF TWO SLENDER-WEB WELDED PLATE GIRDERS (22) and third, THEORY AND EXPERIMENTS ON THE LOAD CARRYING CAPACITY OF PLATE GIRDERS (28). Hereafter, the first and the second series of tests are referred as Lehigh Tests and the third one is referred as Japanese Tests for convenience. Twelve tests are cited from Lehigh Tests and three tests are cited from Japanese Tests. These test girders are divided into three basic groups: moment panels, shear panels and combined panels.

1. Moment panels: These panels are mainly subjected to bending moment rather than shearing force. Seven girder panels are in this group. They are:

G1-T1; G2-T1; G3-T1; G4-T1; G5-T1 from Lehigh Tests, and

A-M; C-M from Japanese Tests.

2. Shear panels: These panels are mainly subjected to shearing force rather than bending moment. Five girder panels are in this group. They are:

G6-T1; G7-T1; F10-T2; F10-T3 from Lehigh Tests, and

B-Q from Japanese Tests.

3. Combined panels: These panels are subjected to both bending moment and shearing force. Three girder panels are in this group. They are:

G8-T1; G9-T1; F10-T1 from Lehigh Tests.

The description of the geometry and the mechanical properties of each of these girders is shown in Table 1. The cross sections of these girders are shown in Figure 20 and the loading setups are illustrated in Figure 21 through Figure 25. Among the test girders cited, G3-T1 and G5-T1 are of different cross sections because these two girders have compression flanges of tubular cross section.

Calculation of the Parameters in Test Girders Cited

All important parameters for the test girders cited are listed in Table 2. Parameters θ, α and ζ, μ are different for each case of computation. It is noted that the parameter θ does not appear in bending cases and does appear in both shear and combined cases.

Comparison of the Proposed Analysis with Test Results and with Basler's Theory

The plate girders cited in the previous sections are analysed by the proposed analysis. The results from these

Table 1. Description of test girders

Test Girder No.	Type of Loading[a]	Panel dimension a in.	Panel dimension b in.	Panel dimension h in.	Webplate σ_{Yw} ksi	Webplate max w_o in.
G1-T1	M	75.0	50.0	.270	33.0	.15
G2-T1	M	75.0	50.0	.270	35.3	.17
G3-T1	M	75.0	54.3	.270	33.7	.16
G4-T1	M	75.0	50.0	.129	43.4	.21
G5-T1	M	75.0	54.3	.129	45.7	.43
G6-T1	S	75.0	50.0	.193	36.7	.29
G7-T1	S	50.0	50.0	.196	36.7	.35
G8-T1	C	150.0	50.0	.197	38.2	.28
G9-T1	C	150.0	50.0	.131	44.5	.15
F10-T1	C	75.0	50.0	.257	38.7	.11
F10-T2	S	75.0	50.0	.257	38.7	.16
F10-T3	S	60.0	50.0	.257	38.7	.05
A-M	M	120.0[c]	120.0[c]	.450[c]	28.0[d]	.30[c]
B-Q	S	120.0	120.0	.450	50.0	.30
C-M	M	120.0	120.0	.600	50.0	.30

[a] M = moment, S = shear, and C = combined.

[b] For Girders G3-T1 and G5-T1 in which the compression flanges are tubular, t_f is the thickness of the hollow circular corss section, and d_f is the diameter.

[c] For Japanese tests, lengths are measured in terms of cm.

[d] For Japanese tests, stresses are measured in terms of kg/mm^2.

[e] For Japanese tests, loads are measured in ton.

Top flange			Bottom flange				Mode of Failure
t_f in.	d_f in.	σ_{Yf} ksi	t'_f in.	d'_f in.	σ'_{Yf} ksi	P_u kips	
.427	20.56	35.4	.760	12.25	35.8	81.0	Torsion
.769	12.19	38.6	.776	12.19	37.6	135.0	Lateral
.328[b]	8.62[b]	35.5	.770	12.19	38.1	130.0	Lateral
.774	12.16	37.6	.765	12.19	37.0	118.0	Lateral
.328[b]	8.62[b]	35.5	.767	12.25	37.0	110.0	Lateral
.778	12.13	37.9	.778	12.13	37.9	116.0	Diag. T
.769	12.19	37.6	.766	12.19	37.6	140.0	Diag. T
.752	12.00	41.3	.747	12.00	41.3	170.0	Diag. T
.755	12.00	41.8	.745	12.00	41.8	96.0	Diag. T
.997	16.05	28.8	.998	16.00	31.6	170.0	Diag. T
.997	16.05	28.8	.998	16.00	31.6	184.5	Diag. T
.997	16.05	28.8	.998	16.00	31.6	190.0	Diag. T
1.200[c]	24.00[c]	28.0[d]	1.200[c]	24.00[c]	28.0[d]	46.5[e]	Torsion
1.200	24.00	50.0	1.200	24.00	50.0	76.0	Diag. T
1.200	24.00	50.0	1.200	24.00	50.0	96.0	Torsion

Table 2. Calculation of parameters in test girders

Test No.	Type of Loading	λ= b/a	β= a/h	ϕ_f	ϕ'_f	ϕ_s	ϕ'_s
G1-T1	Moment	0.667	278	0.434	0.460	0.099	0.099
G2-T1	Moment	0.667	278	0.463	0.467	0.099	0.099
G3-T1	Moment	0.724	278	0.422	0.464	0.099	0.099
G4-T1	Moment	0.667	582	0.971	0.975	0.207	0.207
G5-T1	Moment	0.724	581	1.140	0.971	0.207	0.207
G6-T1	Shear	0.667	389	0.653	0.653	0.138	0.138
G7-T1	Shear	1.000	255	0.955	0.954	0.204	0.204
G8-T1	Combined	0.333	761	0.305	0.303	0.473	0.473
G9-T1	Combined	0.333	1145	0.461	0.455	0.710	0.710
F10-T1	Combined	0.667	292	0.830	0.830	0.312	0.081
F10-T2	Shear	0.667	292	0.830	0.830	0.081	0.081
F10-T3	Shear	0.833	234	1.037	0.036	0.101	0.101
A-M	Moment	1.000	267	0.533	0.533	0.400	0.400
B-Q	Shear	1.000	267	0.533	0.533	0.400	0.400
C-M	Moment	1.000	200	0.400	0.400	0.300	0.300

ψ_f	ψ'_f	ψ_s	ψ'_s	κ_f (10^{-4})	κ'_f (10^{-4})	μ_{ex}	Δ_{wcr}	Δ_u^{ex}
6.08	6.08	0.474	0.474	0.68	2.29	0.139	0.21	0.242
21.00	21.63	0.474	0.474	2.35	2.43	0.157	0.21	0.378
168.40	21.12	0.476	0.476	320.00	2.00	0.148	0.24	0.381
195.20	189.00	4.350	4.350	5.02	5.02	0.407	0.07	0.563
1536.00	191.90	4.340	4.340	669.00	4.17	0.833	0.08	0.495
59.40	59.40	1.299	1.299	3.40	3.40	0.376	0.08	0.328
79.00	81.60	1.863	1.863	11.00	10.90	0.446	0.11	0.389
25.00	24.40	23.300	23.300	0.37	0.37	0.355	0.11	0.226
85.60	82.60	78.900	78.900	0.56	0.55	0.286	0.04	0.165
69.90	70.00	6.590	0.670	7.09	7.10	0.108	0.12	0.342
69.90	70.00	0.670	0.670	7.09	7.10	0.157	0.16	0.371
87.40	87.40	0.833	0.833	20.00	20.00	0.053	0.19	0.382
21.30	21.30	8.950	8.950	2.60	2.60	0.167	0.22	0.640
21.30	21.30	8.950	8.950	2.60	2.60	0.167	0.10	0.282
8.95	8.95	3.780	3.780	1.95	1.95	0.125	0.19	0.555

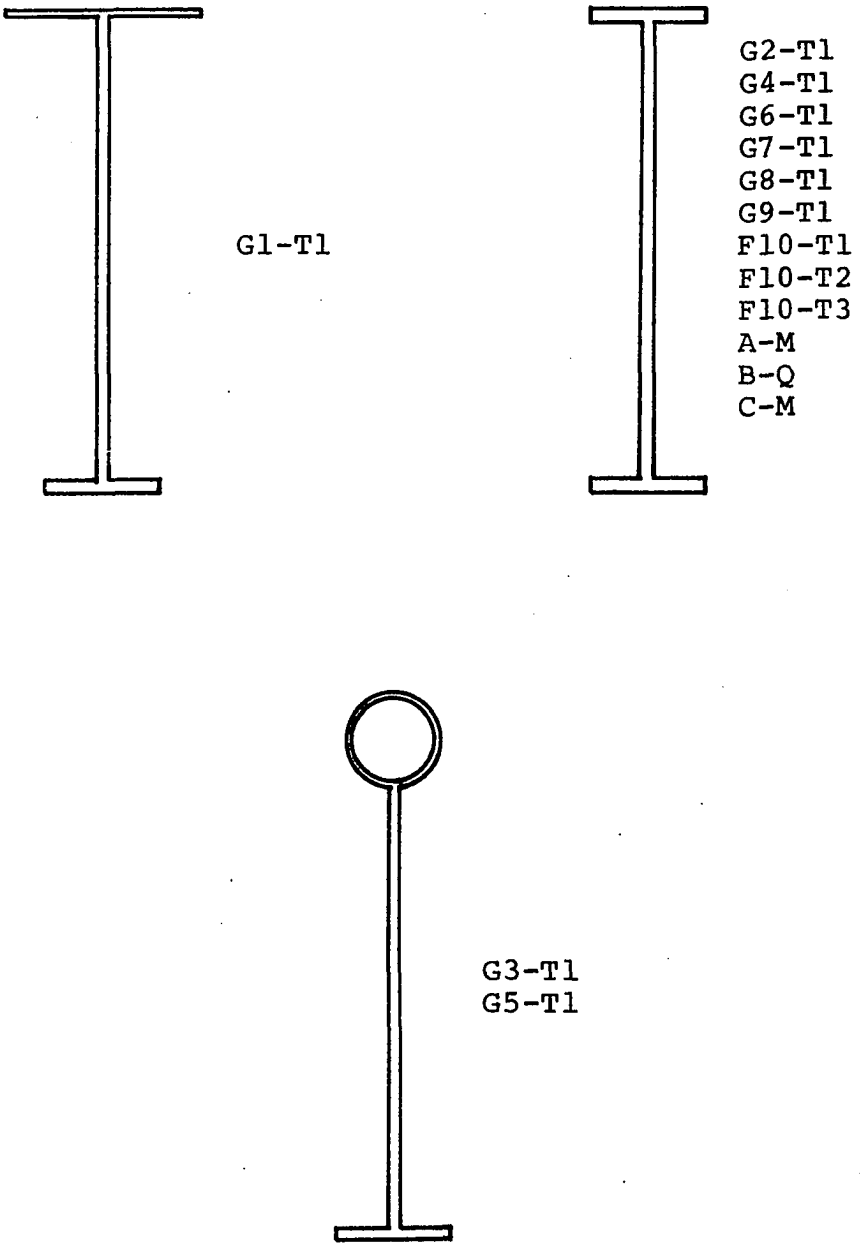

Figure 20. Cross sections of the tested girders cited

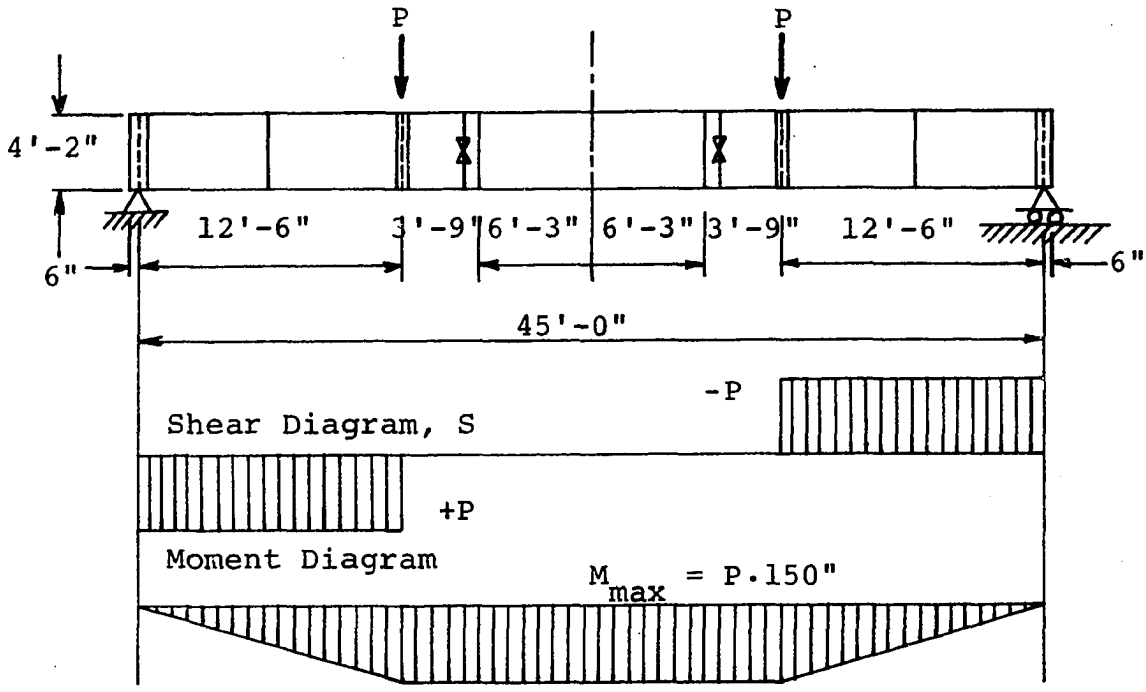

Figure 21. Test setup for bending panels: G1,G2,G3,G4,G5

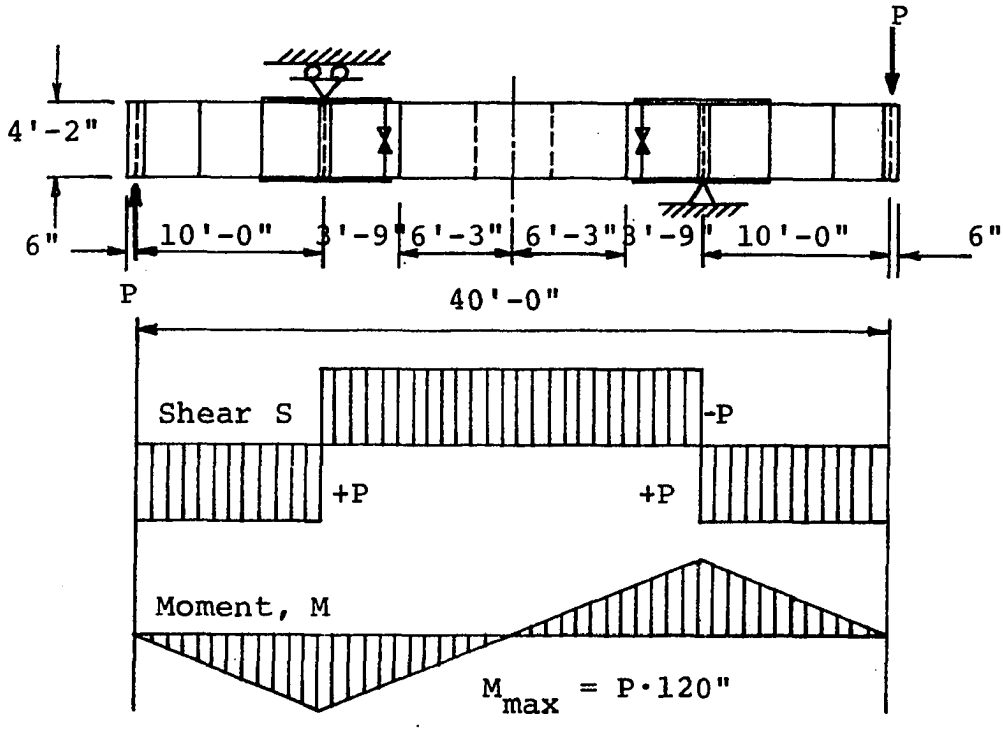

Figure 22. Test setup for shear panels: G6,G7

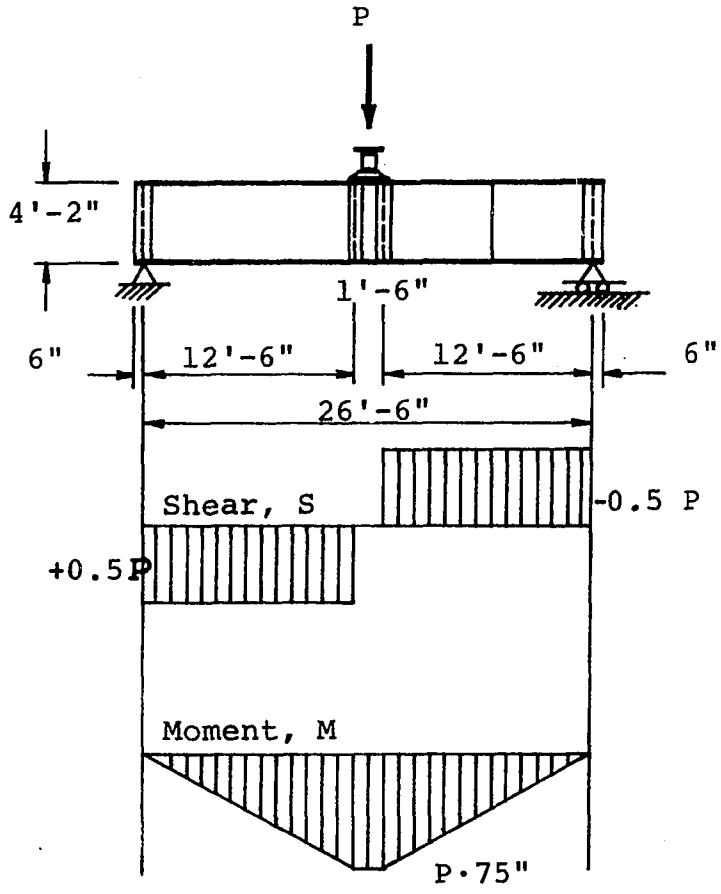

Figure 23. Test setup for girders under combined loading: G8,G9

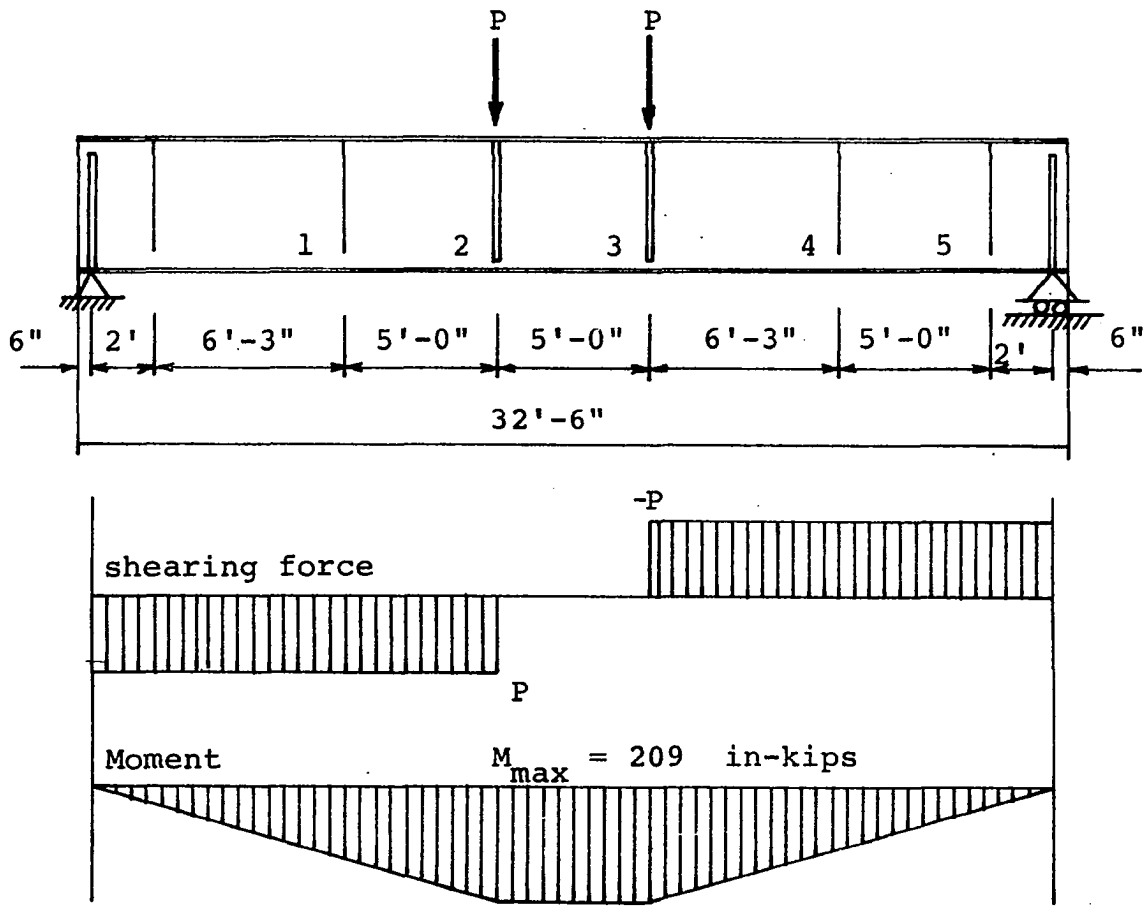

Figure 24. Test setup for F10 girder

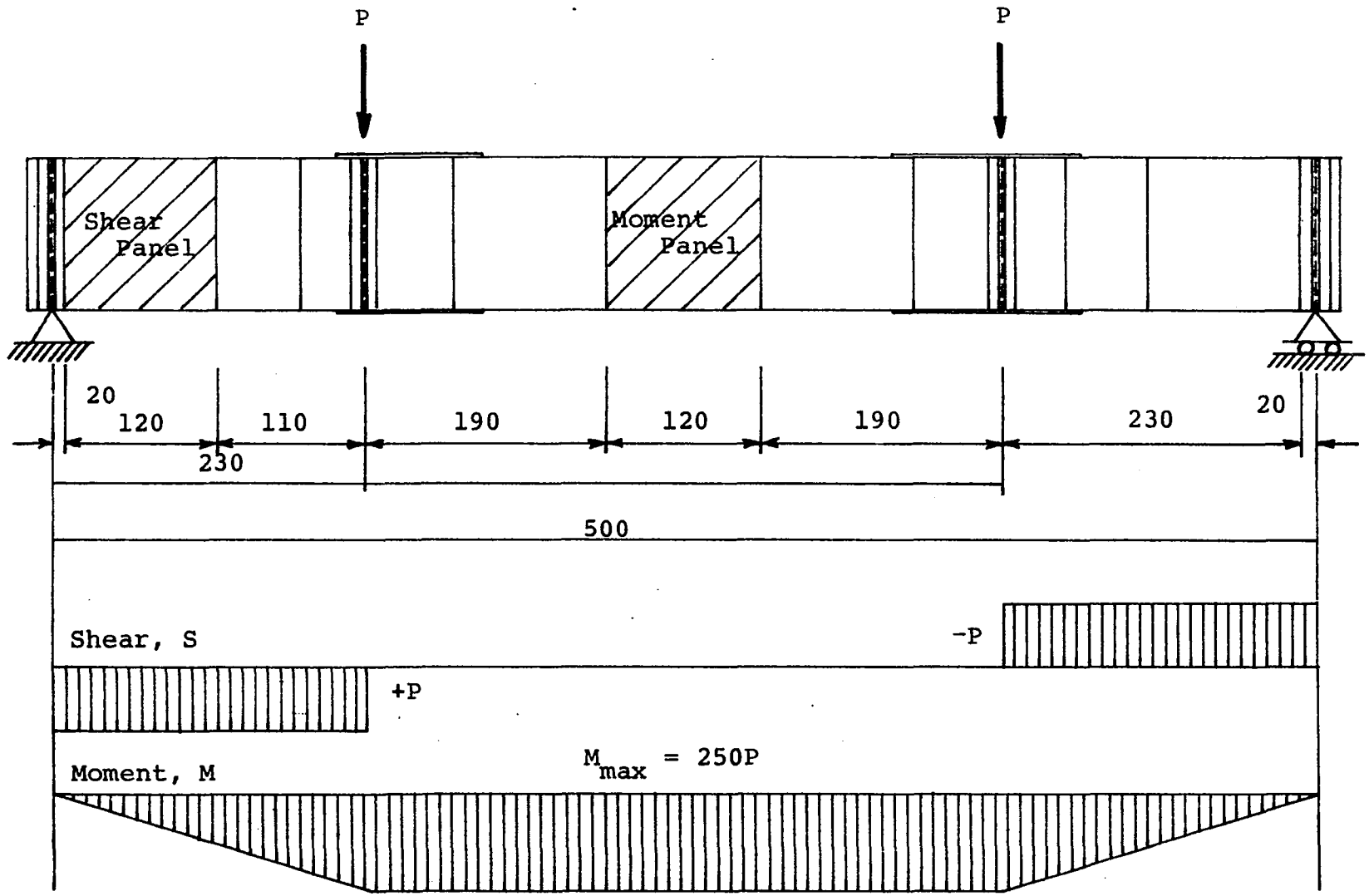

Figure 25. Test setup for shear and moment panels: A-M,B-Q,C-M (unit: cm)

analyses are presented herein with a view to finding out their correlation with the experimental results regarding the ultimate loads and the post-buckling behaviors of the test girder panels cited.

In the proposed analysis, the solution of a single problem, either bending, shear, or a combination of the two, consists of solving four different sets of simultaneous linear algebraic equations step by step from the lowest order to the highest order. Seventeen parameters are required as the input data to handle a single problem. These parameters are:

1. Type of loading: Bending moment, shear, or a combination of the two,
2. Aspect ratio: $\lambda=b/a$,
3. Slenderness ratio of webplate: $\beta=a/h$,
4. ϕ_f,
5. ϕ_f',
6. ϕ_s,
7. ϕ_s',
8. ψ_f,
9. ψ_f',
10. ψ_s,
11. ψ_s',
12. κ_f,
13. κ_f',
14. $\alpha= \sigma_o/E$,

(4 through 16 are rigidity parameters)

15. $\zeta=\sigma_o/\sigma_{Yw}$,

16. $\mu=A/h$

17. Magnitude of load: Δ.

After the problem is solved by the computer, the following results are printed in the computer output sheets for each mesh points on the webplate:

1. $\tilde{u}^{(1)}$, $\tilde{u}^{(2)}$ and $\tilde{u}^{(3)}$,

2. $\tilde{v}^{(1)}$, $\tilde{v}^{(2)}$ and $\tilde{v}^{(3)}$,

3. $\tilde{w}^{(0)}$, $\tilde{w}^{(1)}$, $\tilde{w}^{(2)}$ and $\tilde{w}^{(3)}$,

4. $\tilde{\sigma}_{xo}$, $\tilde{\sigma}_x^{(1)}$, $\tilde{\sigma}_x^{(2)}$ and $\tilde{\sigma}_x^{(3)}$,

5. $\tilde{\sigma}_{yo}$, $\tilde{\sigma}_y^{(1)}$, $\tilde{\sigma}_y^{(2)}$ and $\tilde{\sigma}_y^{(3)}$,

6. $\tilde{\tau}_{xyo}$, $\tilde{\tau}_{xy}^{(1)}$, $\tilde{\tau}_{xy}^{(2)}$ and $\tilde{\tau}_{xy}^{(3)}$,

7. $\tilde{\sigma}_{bx}^{(0)}$, $\tilde{\sigma}_{bx}^{(1)}$, $\tilde{\sigma}_{bx}^{(2)}$ and $\tilde{\sigma}_{bx}^{(3)}$,

8. $\tilde{\sigma}_{by}^{(0)}$, $\tilde{\sigma}_{by}^{(1)}$, $\tilde{\sigma}_{by}^{(2)}$ and $\tilde{\sigma}_{by}^{(3)}$,

9. $\tilde{\tau}_{bxy}^{(0)}$, $\tilde{\tau}_{bxy}^{(1)}$, $\tilde{\tau}_{bxy}^{(2)}$ and $\tilde{\tau}_{bxy}^{(3)}$,

10. $\tilde{u}^T$,

11. $\tilde{v}^T$,

12. $\tilde{w}_e^T$,

13. $\tilde{\sigma}_x^T$, $\tilde{\sigma}_y^T$, $\tilde{\tau}_{xy}^T$, $\tilde{\sigma}_{vM}^T$, $\tilde{\sigma}_1^T$, $\tilde{\sigma}_2^T$; $\tilde{\sigma}_{x1}^T$, $\tilde{\sigma}_{y1}^T$, $\tilde{\tau}_{xy1}^T$, $\tilde{\sigma}_{vM1}^T$; $\tilde{\sigma}_{x2}^T$, $\tilde{\sigma}_{y2}^T$, $\tilde{\tau}_{xy2}^T$ and $\tilde{\sigma}_{vM2}^T$.

All solutions given in this chapter are based on 5 x 5 mesh point system.

Analysis of panels subjected to bending

Past experiments show that the load carrying capacity of deep plate girder panels subjected to pure bending moment is most frequently governed by buckling, such as vertical buckling of flange, lateral buckling of beam and torsional buckling of flange plate, rather than by the yielding of the webplates. Consequently, these modes of buckling should be checked to insure the stability of the plate girder panels (4,6,14, 28).

The analysis of computed results from the proposed analysis of a bending girder panel consists of checking the above-mentioned possibilities of local buckling as well as checking the yielding of the webplates. It is to be noted that the proposed analysis loses its validity when yielding occurs anywhere in a plate girder panel under investigation. The procedure for the analysis of computed results is summarized as follows:

1. Evaluation of flange stresses using $\tilde{u}$,

2. Investigation of the yielding of webplate using von Mises yield criterion: $\tilde{\sigma}_{vM}$, $\tilde{\sigma}_{vM1}$ and $\tilde{\sigma}_{vM2}$,

3. Investigation of the possibility of vertical buckling of flange,

4. Investigation of the possibility of lateral buckling of beam,

5. Investigation of the possibility of torsional buckling of the compression flange.

The buckling criteria used in this study are given in Appendix A.

In each case, comparisons are made between the results obtained from the proposed analysis and the experimental values whenever these values are found useful and applicable regarding the post-buckling behaviors of girder panels such as load-σ_f and load-$\bar{\sigma}_x$ relationships. Furthermore, the simple beam theory is applied to find a possible indication of web-buckling in some of the plate girder panels cited. The simple beam theory assumes no web-buckling; in other words, web plates are assumed to keep their flatness during loading.

For the purpose of predicting the ultimate loads for the cited plate girder panels, Basler's theory (4) is also used for comparison. A brief summary of his theory has been presented in Chapter One. The format of the presentation of the theoretical results is demonstrated using cases 1 and 2 of test girder panel G1-T1. The results from all girder panels are presented in tables.

Test girder panel G1-T1 According to the test, the ultimate load is 81.0 Kips. This corresponds to $\Delta_u^{ex} = \underline{0.242}$. Furthermore, the failure mode is the torsional buckling of the compression flange. Assuming that the webplate is simply supported along four edges, $\Delta_{wcr} = \underline{0.210}$.

Computer result: Case 1 The maximum residual stress is assumed to be 0.5% of the yield strength of the webplate; while the maximum total initial deflection is assumed to be 10% of the webplate thickness. Then,

$$\alpha = 0.00000245; \quad \zeta = 0.00222; \quad \mu = 0.025$$

1. Flange stresses: In terms of finite differences, the flange stresses are given in the nondimensionalized form:

$$\tilde{\sigma}_f(\text{or } \tilde{\sigma}_f') = \frac{1}{2}(N-1)\left(\frac{\zeta}{\alpha\beta}\right)(\tilde{u}_{+1} - \tilde{u}_{-1}) ,$$

where $\tilde{u}_{+1}$ and $\tilde{u}_{-1}$ correspond to the displacement components in x-direction of the right and left points adjacent to the grid point concerned. Table 3 shows the stresses in flanges at $\Delta = 0.21$. The average stress in the compression flange is $\underline{-0.607}$.

2. In-plane stresses: Stresses at various locations in the webplate are computed and listed in Table 4 for $\Delta = 0.21$. The result shows that the webplate is not yielded at this load level.

Table 3. Computation of flange stresses: Case 1 of test girder panel G1-T1 at $\Delta = 0.21$

Pt. No.	$\tilde{u}_{+1}$	$\tilde{u}_{-1}$	$\tilde{u}_{+1}-\tilde{u}_{-1}$	$\tilde{\sigma}_f$	$\tilde{\sigma}'_f$
1	0.0473	-0.0446	0.0919	--	0.603
5	-0.0488	0.0460	-0.0948	-0.623	--
6	0.0930	0	0.0930	--	0.611
10	-0.0961	0	-0.0961	-0.631	--
11	0.1371	0.0473	0.0898	--	0.590
15	-0.1416	-0.0488	-0.0928	-0.609	--
16	0.1794	0.0930	0.0864	--	0.567
20	-0.1853	-0.0961	-0.0892	-0.586	--
21	0.2234	0.1371	0.0863	--	0.566
25	-0.2308	-0.1416	-0.0892	-0.586	

Average stress in compression flange $\tilde{\sigma}_{fav} = \underline{-0.607}$

Table 4. In-plane stresses: Case 1 of test girder panel G1-T1 at $\Delta = 0.21$

Pt. No.	$\tilde{\sigma}^T_x$	$\tilde{\sigma}^T_y$	$\tilde{\tau}^T_{xy}$	$\tilde{\sigma}^T_{vM}$	$\tilde{\sigma}^T_{vM1}$	$\tilde{\sigma}^T_{vM2}$	Yielding
1	0.6297	0.1023	0.0635	0.5959	0.6009	0.5914	--
5	-0.6500	-0.1058	-0.0645	0.6143	0.6186	0.6108	--
6	0.6099	0.0002	0.0374	0.6133	0.6140	0.6126	--
10	-0.6224	-0.0001	0.0371	0.6257	0.6255	0.6260	--
11	0.5905	0.0000	0.0386	0.5942	0.5963	0.5923	--
15	-0.5996	0.0000	0.0379	0.6032	0.6110	0.5709	--
16	0.5671	-0.0001	0.0427	0.5720	0.5731	0.5709	--
20	-0.5779	0.0000	0.0417	0.5825	0.5844	0.5808	--
21	0.5913	0.0964	-0.0390	0.5537	0.5550	0.5525	--
25	-0.6111	-0.0996	-0.0401	0.5721	0.5740	0.5706	--

3. Vertical buckling of flange: Referring to Equation A.1, $\beta_v = 404$; while $\beta' = 185$. Therefore, $\beta_v > \beta'$. This eliminates the possibility of vertical buckling.

4. Lateral buckling: The lateral buckling length, ℓ_k, is 100 in. The flange slenderness ratio, β_f, is 24.07 and the half width of the compression flange, c_f, is 10.28 in. Then, $2\beta_f = 48 > 12 + \ell_k/c_f = 16.85$. From Equation A.7, the torsional buckling is found to precede the lateral buckling.

5. Torsional buckling of the compression flange: Referring to Equation A.5, $\gamma = 1.329$; while $\gamma_p = 1.002$ by Equation A.6. Therefore, $\gamma_p < \gamma$. Using Equation A.5, the buckling stress is: $\tilde{\sigma}^T_{cr} = \sigma^T_{cr}/\sigma_{Yf} \times \sigma_{YF}/\sigma_{Yw} = \underline{0.608}$. Previously, the average stress in the compression flange is found to be $\underline{-0.607}$. Therefore, the buckling load is: $\Delta^T_{cr} = 0.21$.

In conclusion, the ultimate load is found to be $\underline{0.21}$ and the failure mode is the torsional buckling of the compression flange.

Computer result: Case 2 The maximum residual stress is assumed to be 50% of the yield strength of the web-plate; while, the maximum total initial deflection is assumed to be 10% of the webplate thickness. Then,

$\alpha = 0.000245$; $\zeta = 0.222$; $\mu = 0.025$

1. Flange stresses: Table 5 shows the flange stresses at $\Delta = 0.18$. The average stress in the compression flange is

-0.519.

2. In-plane stresses: Table 6 shows the in-plane stresses at $\Delta = 0.18$. Point 11 is found to be yielded at this load level.

3. Vertical buckling of flange: $\beta_v = 335 > \beta' = 185$. This eliminates the possibility of the vertical buckling.

4. Lateral buckling: $2\beta_f = 48 > 12 + \frac{1}{2}\ell_k/c_f = 16.85$. The torsional buckling precedes the lateral buckling.

5. Torsional buckling of the compression flange: $\gamma = 1.329 < \gamma_p = 1.414$. Equation A.6 gives n = 1.35. Therefore, $\tilde{\sigma}^T_{cr} = 0.567$. Previously, the average stress in the compression flange is found to be -0.519. Therefore, the torsional buckling has not occurred at $\Delta = 0.18$. A rough estimation of the ultimate load may be obtained by extending the elastic analysis beyond yielding load in the following manner:

$$\Delta^{th}_u = \Delta^{th}_{max} \left|\frac{\tilde{\sigma}^T_{cr}}{\tilde{\sigma}_{fav}}\right| = 0.18 \times \frac{0.567}{0.519} = 0.197 .$$

In conclusion, the maximum elastic load is found to be 0.18. Beyond this load, the girder panel enters the elasto-plastic range. The ultimate load is estimated as 0.197.

Basler's theory (4) In this theory, it is assumed that the residual stress has its maximum value of 50% of the yielding strength of the compression flange. The

Table 5. Computation of flange stresses: Case 2 of test girder panel G1-T1 at $\Delta = 0.18$

Pt. No.	$\tilde{u}_{+1}$	$\tilde{u}_{-1}$	$\tilde{u}_{+1}-\tilde{u}_{-1}$	$\tilde{\sigma}_f$	$\tilde{\sigma}'_f$
1	0.0405	-0.0384	0.0789	--	0.518
5	-0.0418	0.0392	-0.0810	-0.532	--
6	0.0797	0	0.0797	--	0.524
10	-0.0822	0	-0.0822	-0.540	--
11	0.1175	0.0405	0.0770	--	0.506
15	-0.1212	-0.0418	-0.0794	-0.522	--
16	0.1538	0.0797	0.0741	--	0.487
20	-0.1586	-0.0822	-0.0764	-0.502	--
21	0.1915	0.1175	0.0740	--	0.486
25	-0.1975	-0.1212	-0.0763	-0.501	--

Average stress in compression flange $\tilde{\sigma}_{fav} = \underline{-0.519}$

Table 6. In-plane stresses: Case 2 of test girder panel G1-T1 at $\Delta = 0.18$

Pt. No.	$\tilde{\sigma}^T_x$	$\tilde{\sigma}^T_y$	$\tilde{\tau}^T_{xy}$	$\tilde{\sigma}^T_{vM}$	$\tilde{\sigma}^T_{vM1}$	$\tilde{\sigma}^T_{vM2}$	Yielding
1	0.5407	0.0879	-0.0494	0.5098	0.5111	0.5086	--
5	-0.5549	-0.0903	-0.0593	0.5258	0.5260	0.5256	--
6	0.8936	0.0002	0.0312	0.8951	0.8981	0.8924	--
10	-0.1615	-0.0001	0.0319	0.1706	0.1695	0.1723	--
11	1.0009	0.0000	0.0327	1.0025	1.0089	0.9968	yes
15	-0.0183	0.0000	0.0320	0.0583	0.0638	0.0609	--
16	0.8574	-0.0001	0.0364	0.8598	0.8634	0.8564	--
20	-0.1237	0.0000	0.0354	0.1380	0.1355	0.1412	--
21	0.5072	0.0827	-0.0335	0.4749	0.4747	0.4750	--
25	-0.5232	-0.0853	-0.0344	0.4899	0.4912	0.4888	--

ultimate load is computed to be 73 Kips. Thus, $\Delta_u^B = \underline{0.218}$. The failure mode is the torsional buckling of the compression flange.

Figure 26 shows a load-$\tilde{\sigma}_f$ relationship, and Figure 27 shows a load-$\tilde{\sigma}_x$ relaticnship of girder panel G1-T1.

Test girder panels G2-T1 through C-M Similar computations are performed on these girder panels and the results are presented in Table 7. Figures 28 through 30, Figure 31, and Figure 32 show, respectively, load-$\tilde{\sigma}_x$ relationships, load-$\tilde{\sigma}_f$ relationship, and a total deflection surface, of girder panel G2-T1. Figure 33 illustrates a total elastic deflection surface of girder panel G3-T1. Figure 34, and Figures 35 through 38 show, respectively, a load-$\tilde{\sigma}_f$ relationship, and load-$\tilde{\sigma}_x$ relationships, of girder panel A-M. Figure 39 illustrates distributions of $\tilde{\sigma}_x$, $\tilde{\sigma}_{x1}$ and $\tilde{\sigma}_{x2}$, and Figure 40 shows a load-$\tilde{\sigma}_{bx}$ relationship of the same girder panel. Figure 41 shows a total deflection surface and Figure 42 shows an in-plane displacement configuration of girder panel A-M. Figure 43 shows a relationship of load-flange strain, ε_f, and Figure 44 shows a load-$\tilde{\sigma}_x$ relationship for girder panel C-M.

Analysis of panels subjected to shear

Many experiments have shown that the ultimate load of a shear panel is always governed by the yielding of the webplate along diagonal line D_1 (See Figures 14 through 17). This

Table 7. Prediction of ultimate load for bending panels

Girder	Δ_u^{ex}	Δ_{wcr}	Mode of Failure[a]	$(\mu)_{ex}$
G1-T1	0.242	0.210	T.B.	0.139
G2-T1	0.378	0.208	L.B.	0.157
G3-T1	0.381	0.240	L.B.	0.148
G4-T1	0.563	0.073	L.B.	0.407
G5-T1	0.495	0.080	L.B.	0.833
A-M	0.640	0.220	T.B.	0.167
C-M	0.555	0.186	T.B.	0.125

[a] T.B. = Torsional buckling and L.B. - lateral buckling.

[b] σ_r refers to the maximum residual stress and is given by: $\sigma_r=\sigma_o$ for $\lambda \geq 1$ and $\sigma_r=\sigma_o/\lambda^2$ for $\lambda \leq 1$.

$\left[\frac{\sigma_r}{\sigma_{Yw}}\right]^b_{th}$	$(\mu)_{th}$	$\lvert\frac{\tilde{\sigma}_{cr}}{\tilde{\sigma}_{fav}}\rvert$	Δ^{th}_{max}	Δ^{th}_{u}	Δ^{B}_{u}
0.005	0.025	1.00	0.21	0.21	0.22
0.500	0.025	1.09	0.18	0.20	0.22
0.500	0.139	1.21	0.18	0.22	0.22
0.005	0.025	1.13	0.35	0.40	0.39
0.500	0.025	1.80	0.20	0.36	0.39
0.005	0.125	1.17	0.36	0.42	0.39
0.500	0.157	1.94	0.20	0.39	0.39
0.005	0.157	1.29	0.33	0.42	0.39
0.005	0.025	1.08	0.39	0.42	0.37
0.005	0.025	1.02	0.60	0.61	0.56
0.005	0.125	1.50	0.39	0.59	0.56
0.005	0.025	1.26	0.54	0.68	0.48
0.005	0.100	1.57	0.42	0.66	0.48
0.005	0.025	1.06	0.65	0.69	0.63
0.125	0.025	1.09	0.64	0.70	0.63
0.500	0.125	1.74	0.42	0.73	0.63
0.500	0.025	1.54	0.45	0.69	0.63
0.001	0.167	1.17	0.56	0.66	0.63
0.125	0.167	1.74	0.36	0.63	0.63
0.003	0.025	1.03	0.54	0.56	0.46
0.150	0.125	1.52	0.33	0.50	0.46
0.003	0.125	1.03	0.48	0.49	0.46
0.250	0.125	(2.36)	(0.18)	0.43	0.46

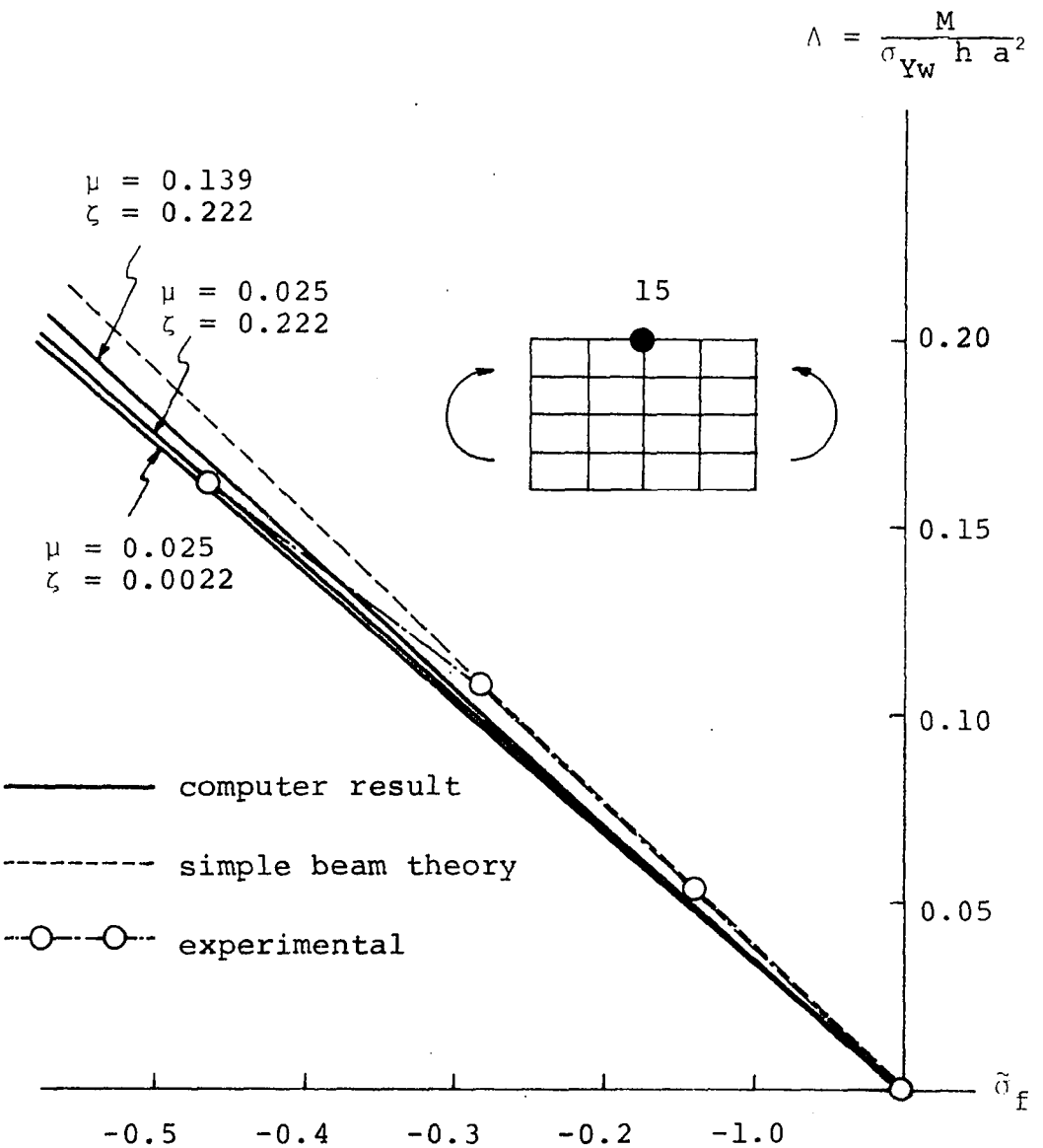

Figure 26. Load - $\tilde{\sigma}_f$ curve
Test girder panel G1-T1

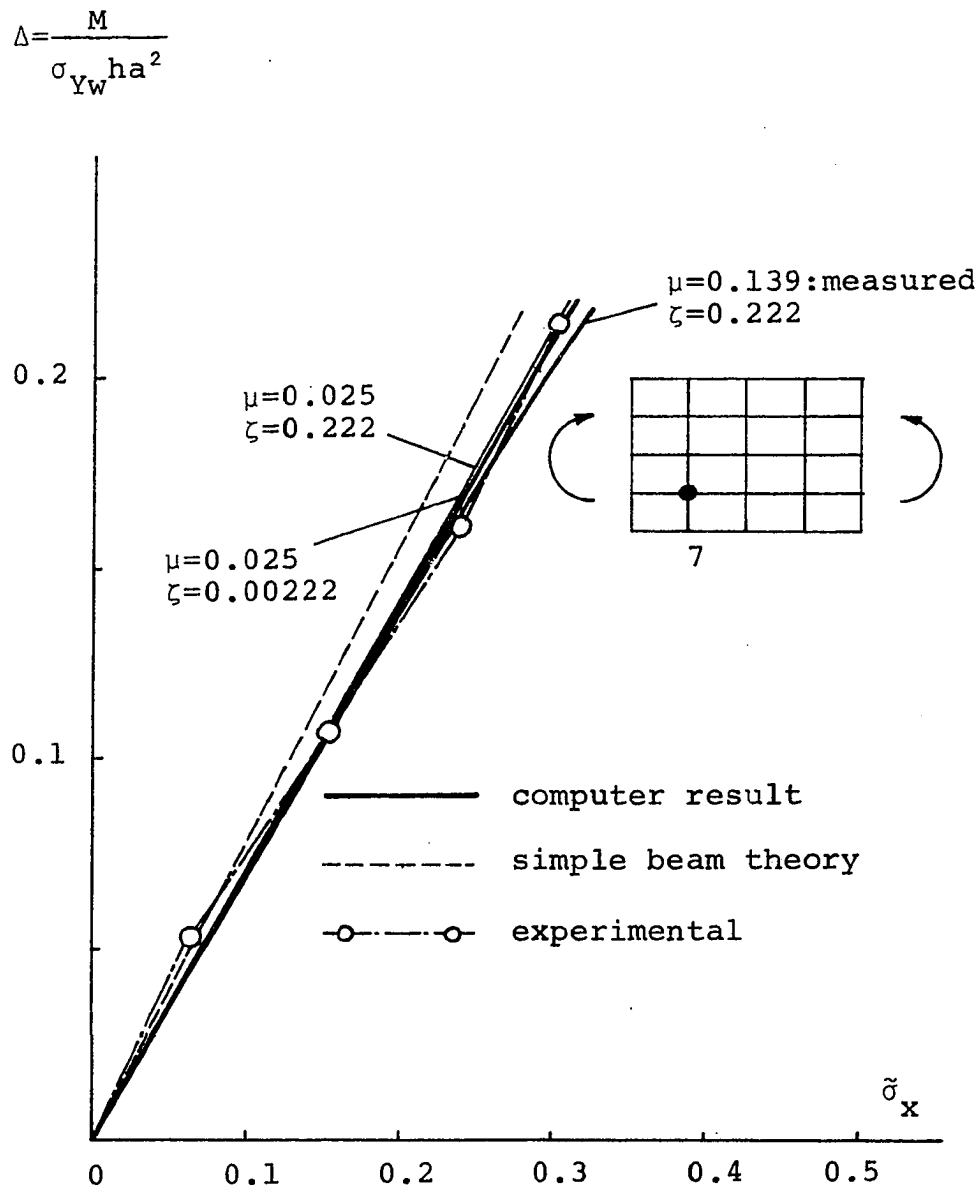

Figure 27. Load-$\tilde{\sigma}_x$ curve
Test girder G1-T1

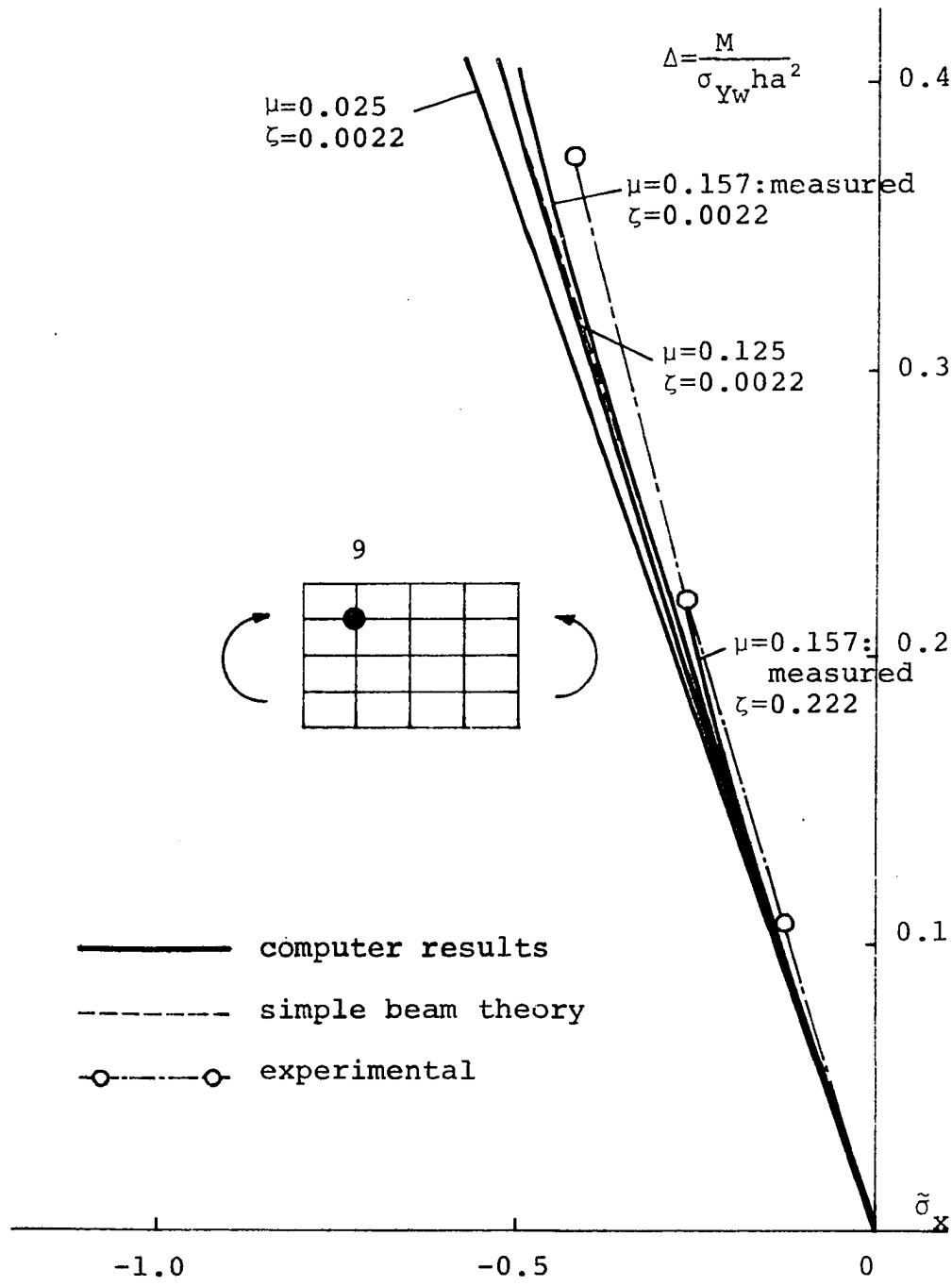

Figure 28. Load-$\tilde{\sigma}_x$ curve
Test girder G2-T1

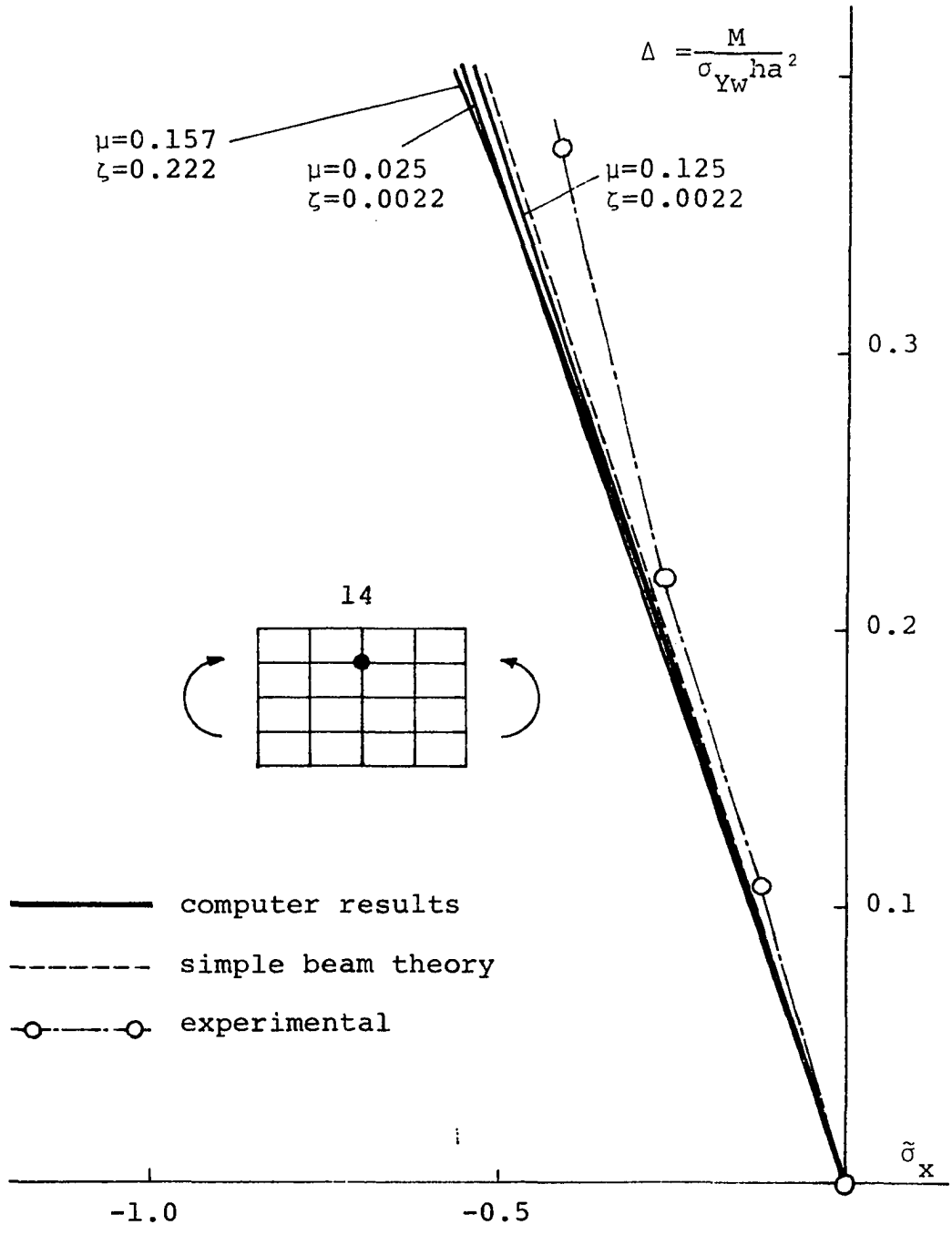

Figure 29. Load-σ_x curve
Test girder G2-T1

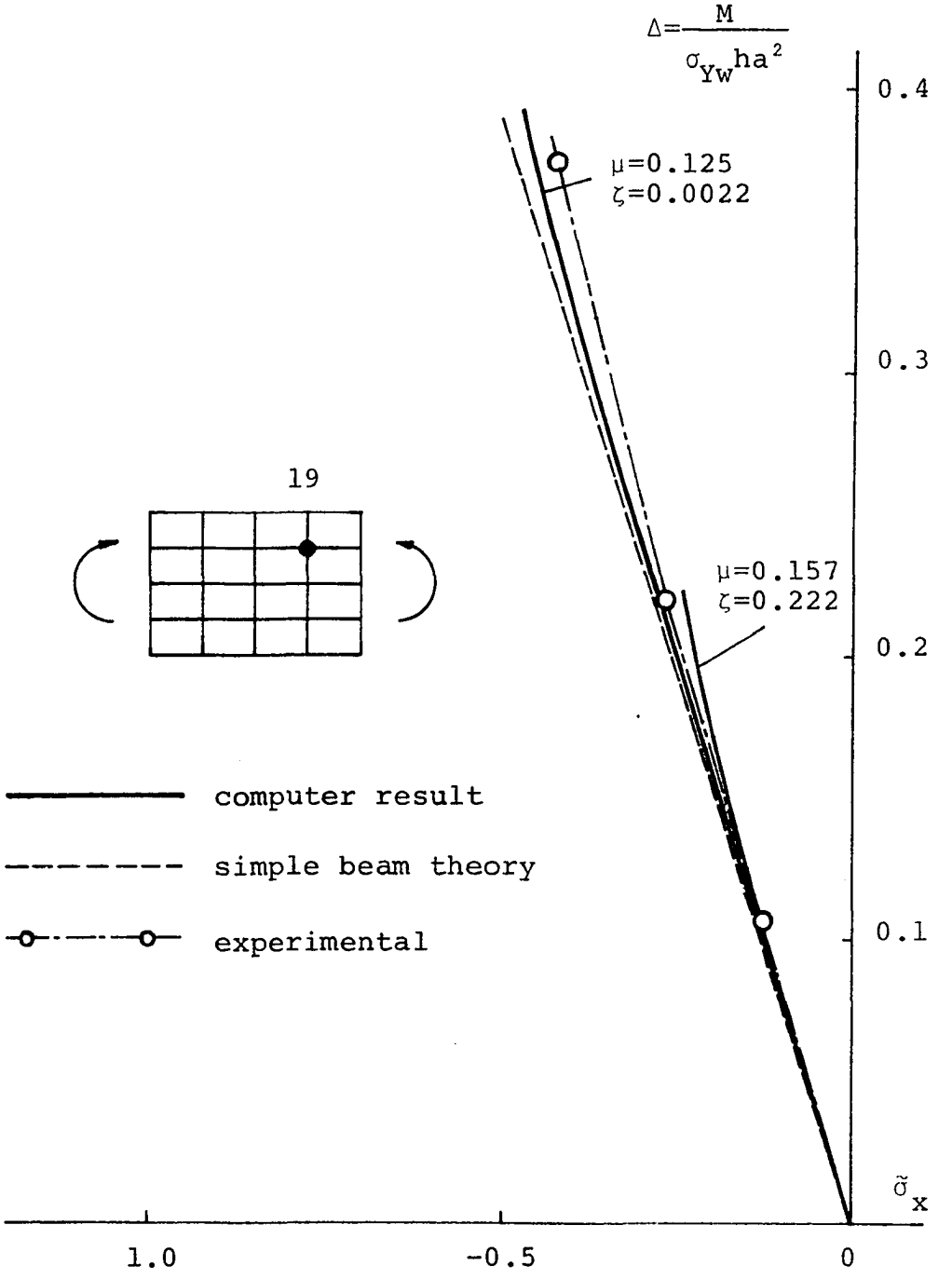

Figure 30. Load-$\tilde{\sigma}_x$ curve
Test girder G2-T1

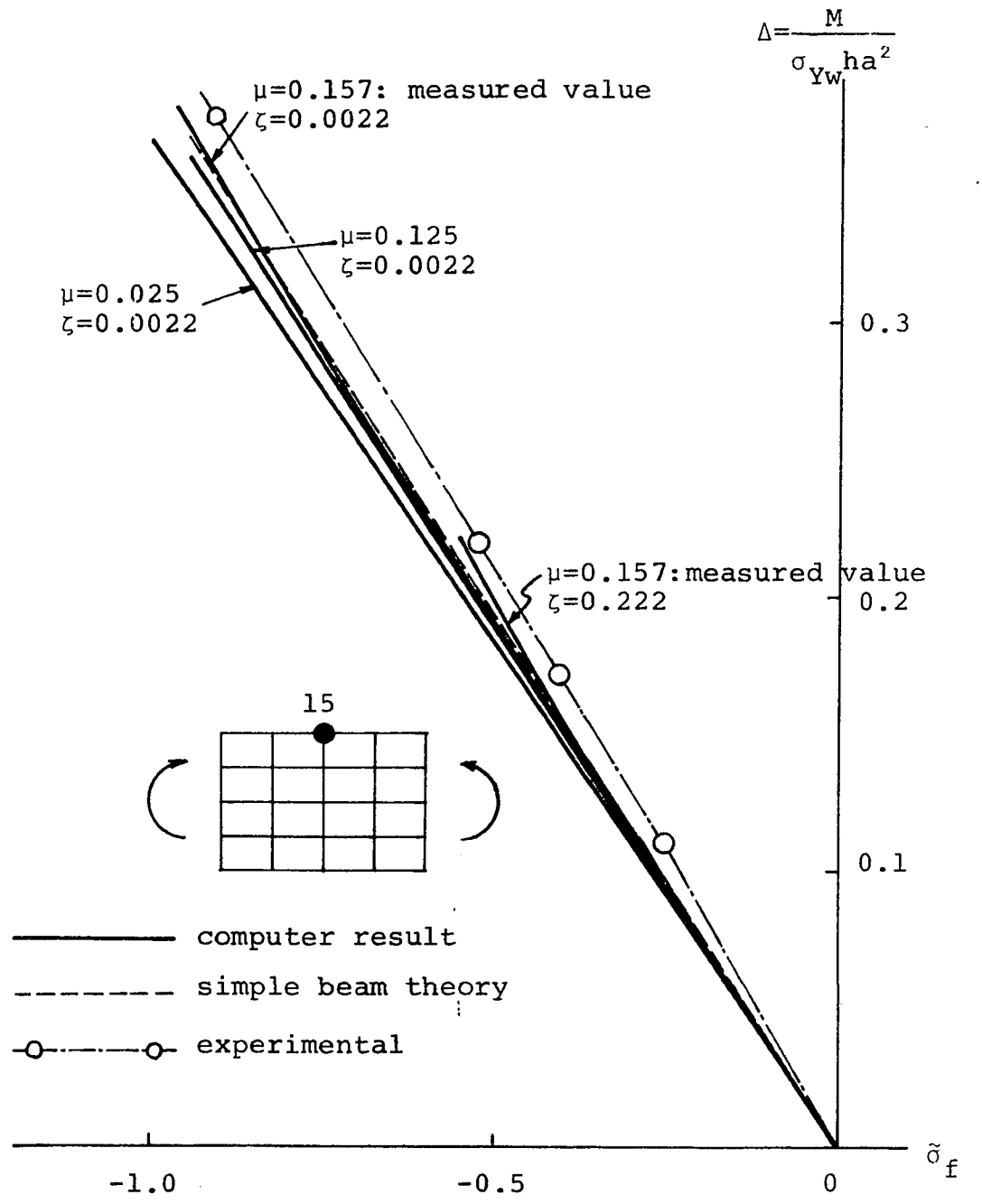

Figure 31. Load-$\tilde{\sigma}_f$ curve
Test girder G2-T1

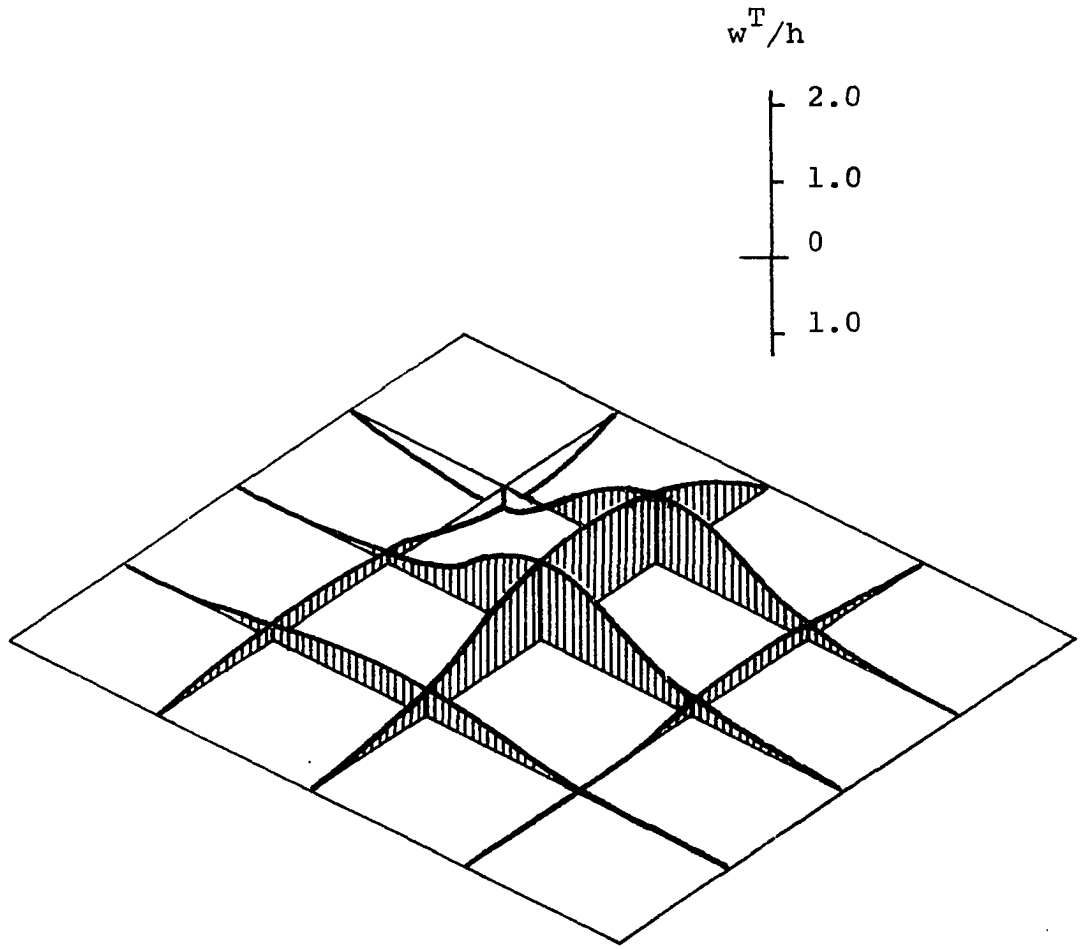

Figure 32. Total deflection w^T
Test girder G2-T1: μ=0.125; ζ=0.00222
Δ=0.36

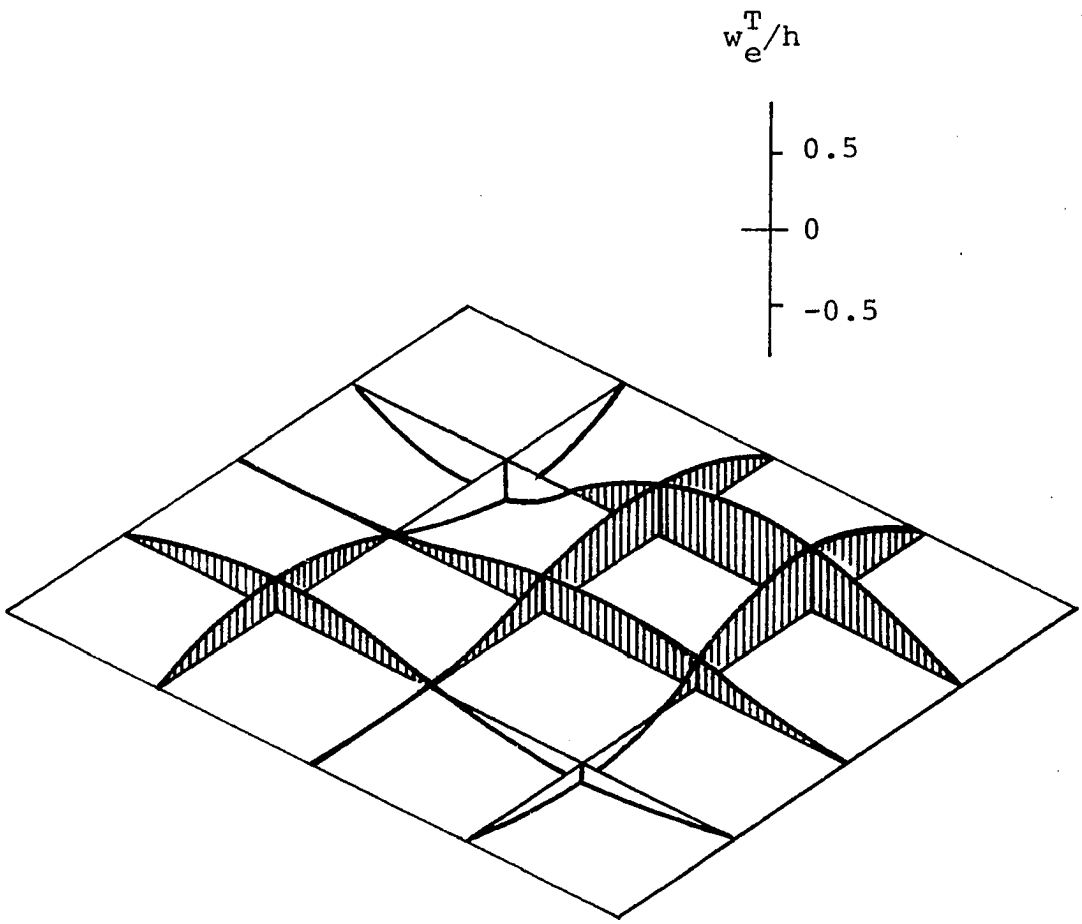

Figure 33. Total elastic deflection w_e^T
Test panel G3-T1: μ=0.025; ζ=0.00262
Δ=0.39

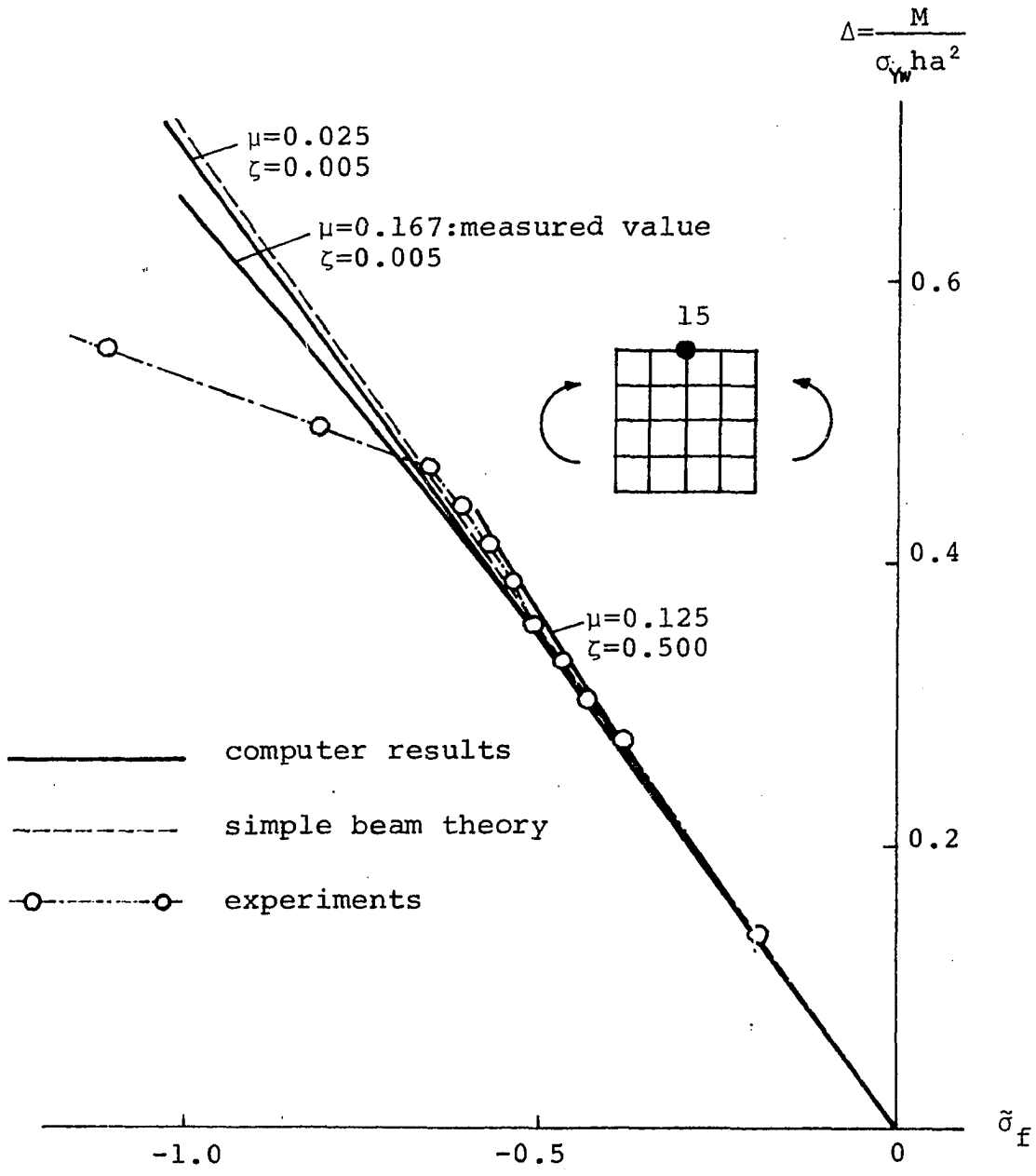

Figure 34. Load - flange stress $\tilde{\sigma}_f$ curve
Test girder A-M

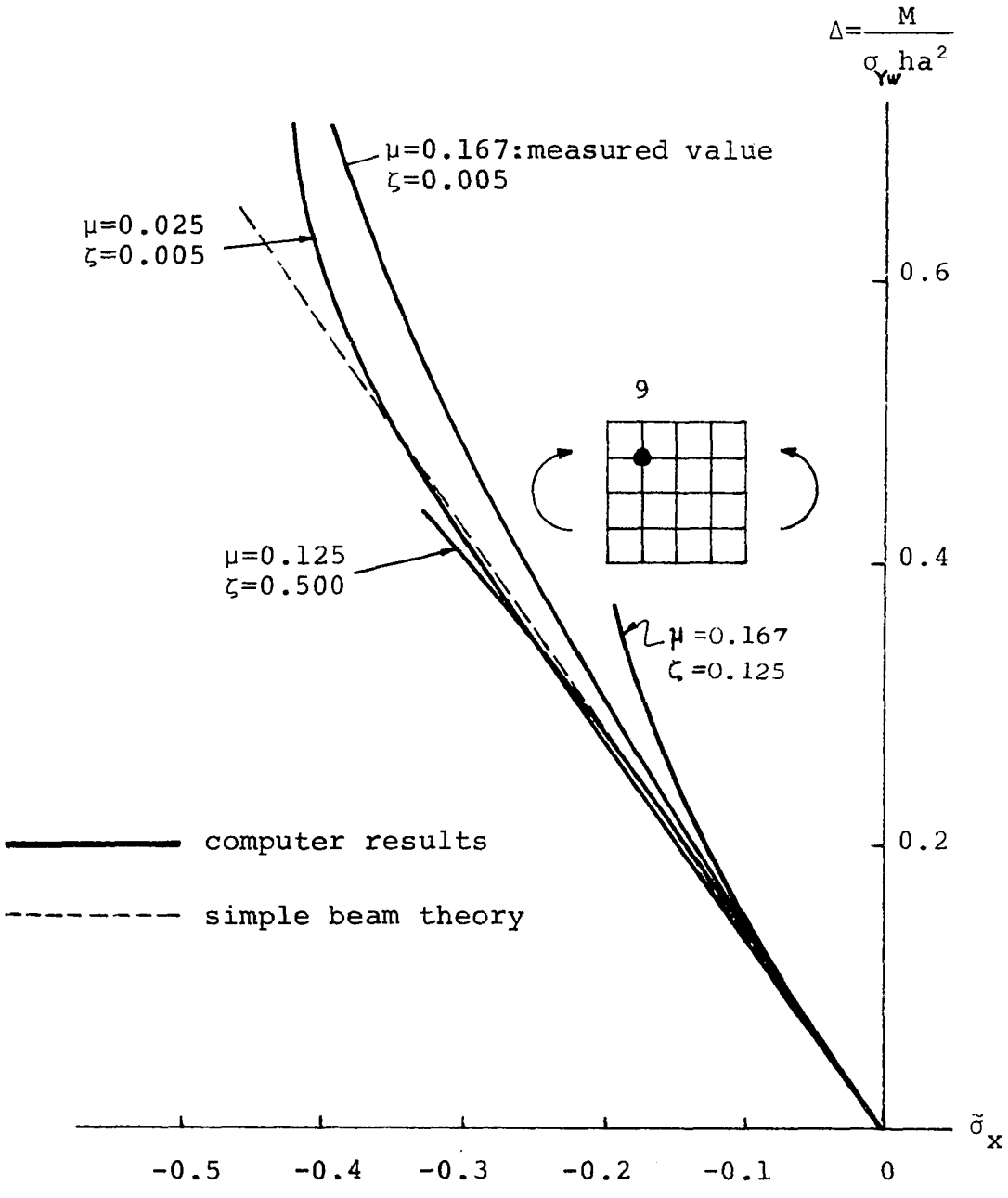

Figure 35. Load - $\tilde{\sigma}_x$ curve
Test girder A-M

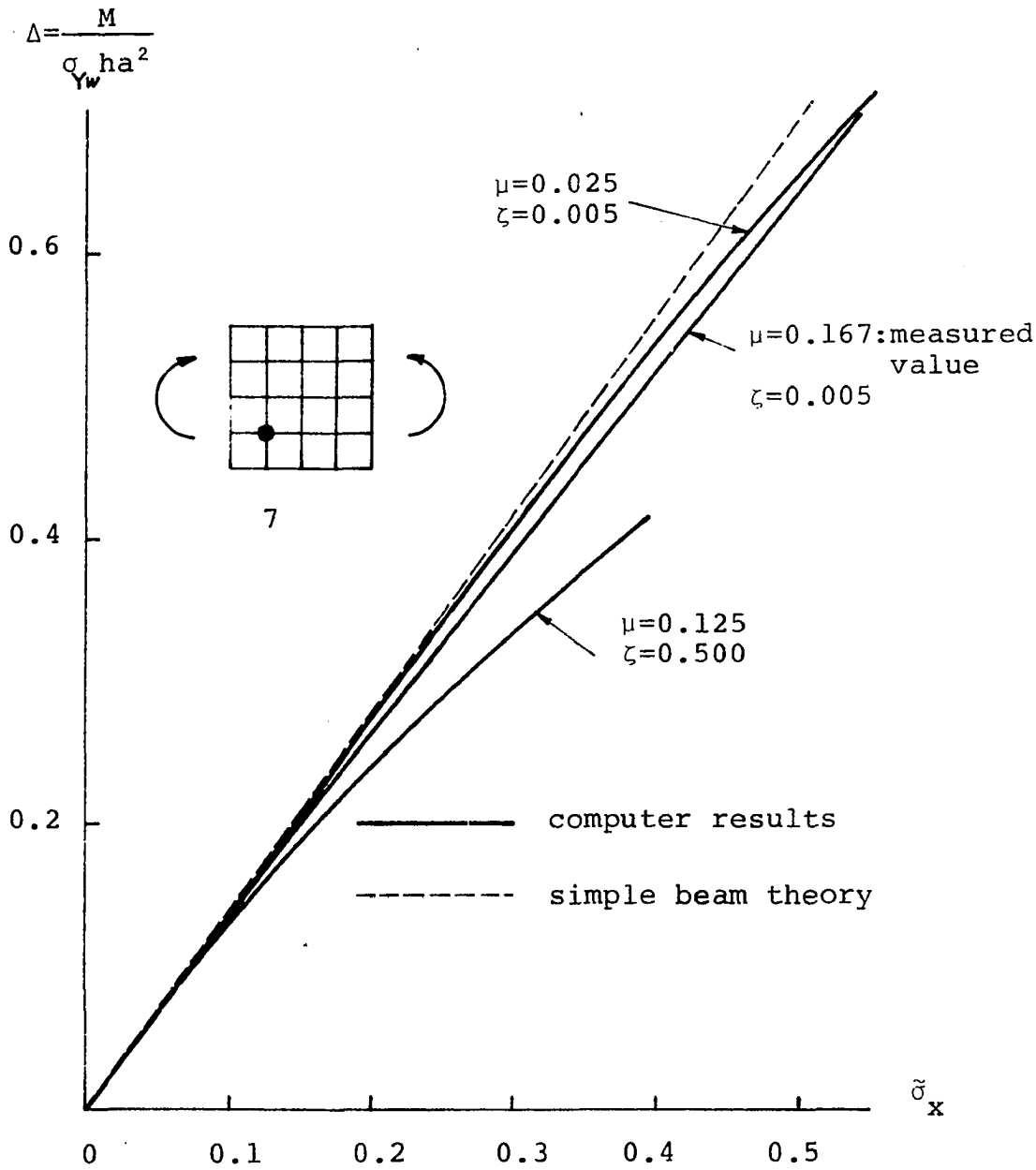

Figure 36. Load - $\tilde{\sigma}_x$ curve
Test girder A-M

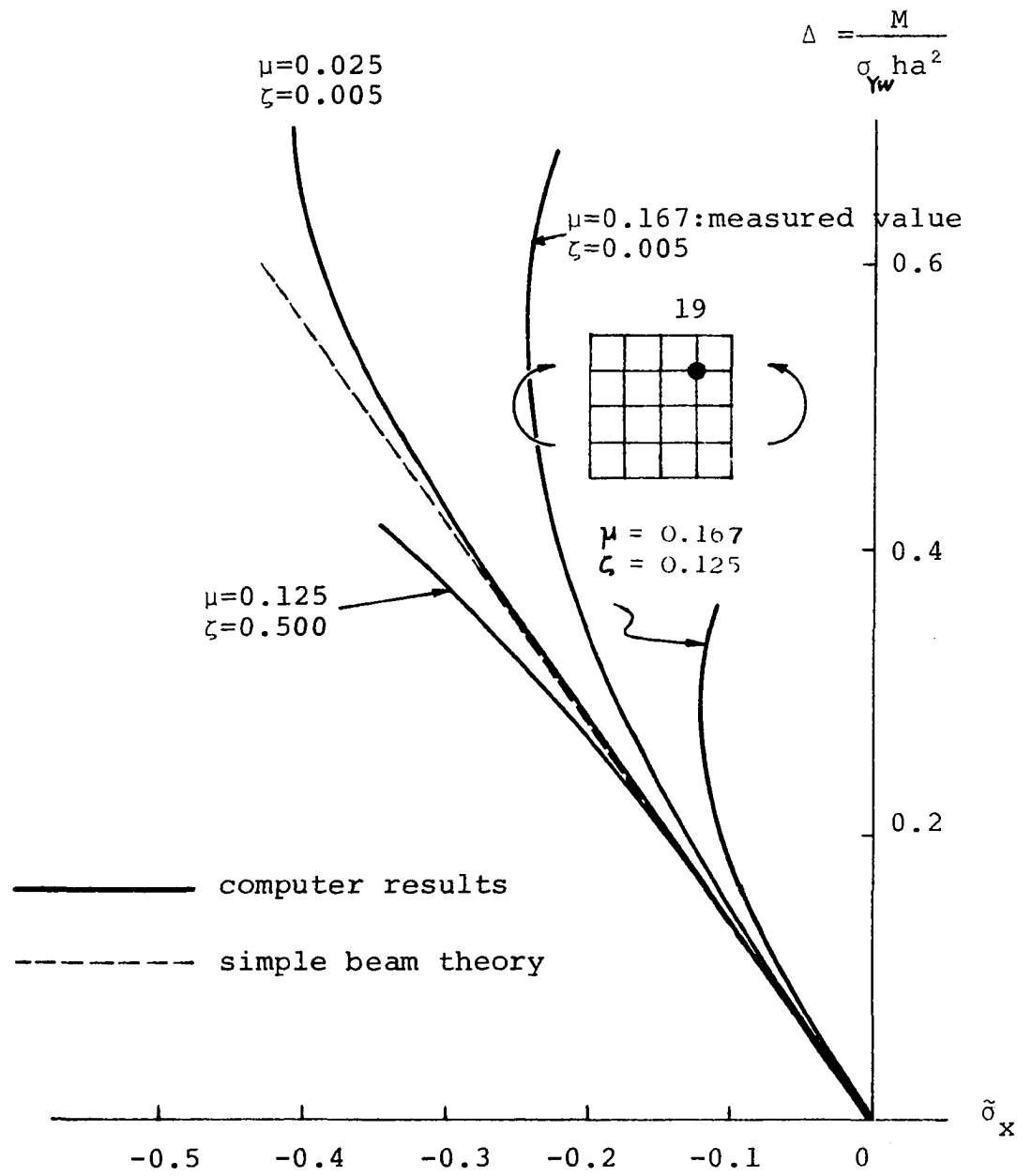

Figure 37. Load - $\tilde{\sigma}_x$ curve
Test girder A-M

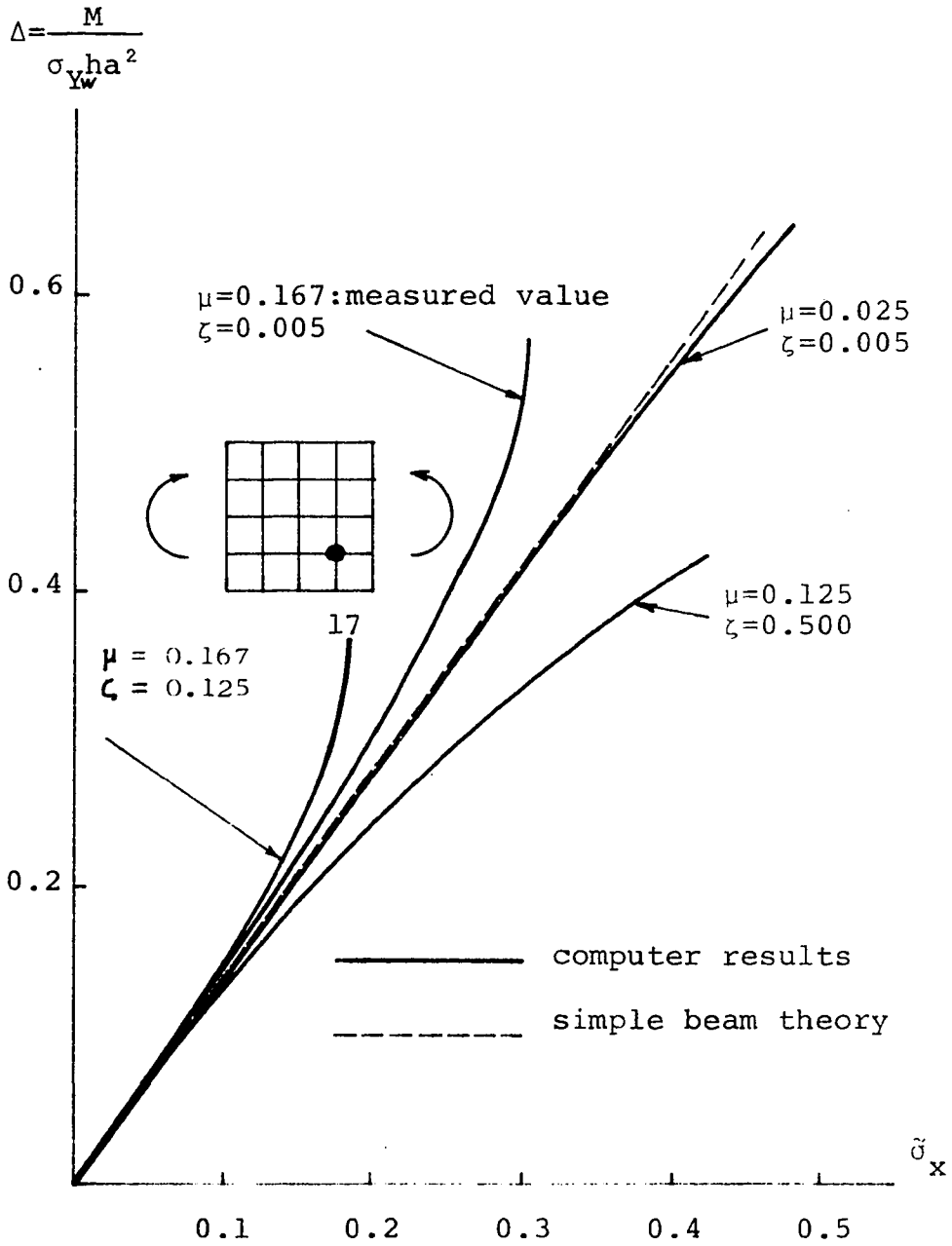

Figure 38. Load - $\tilde{\sigma}_x$ curve
Test girder A-M

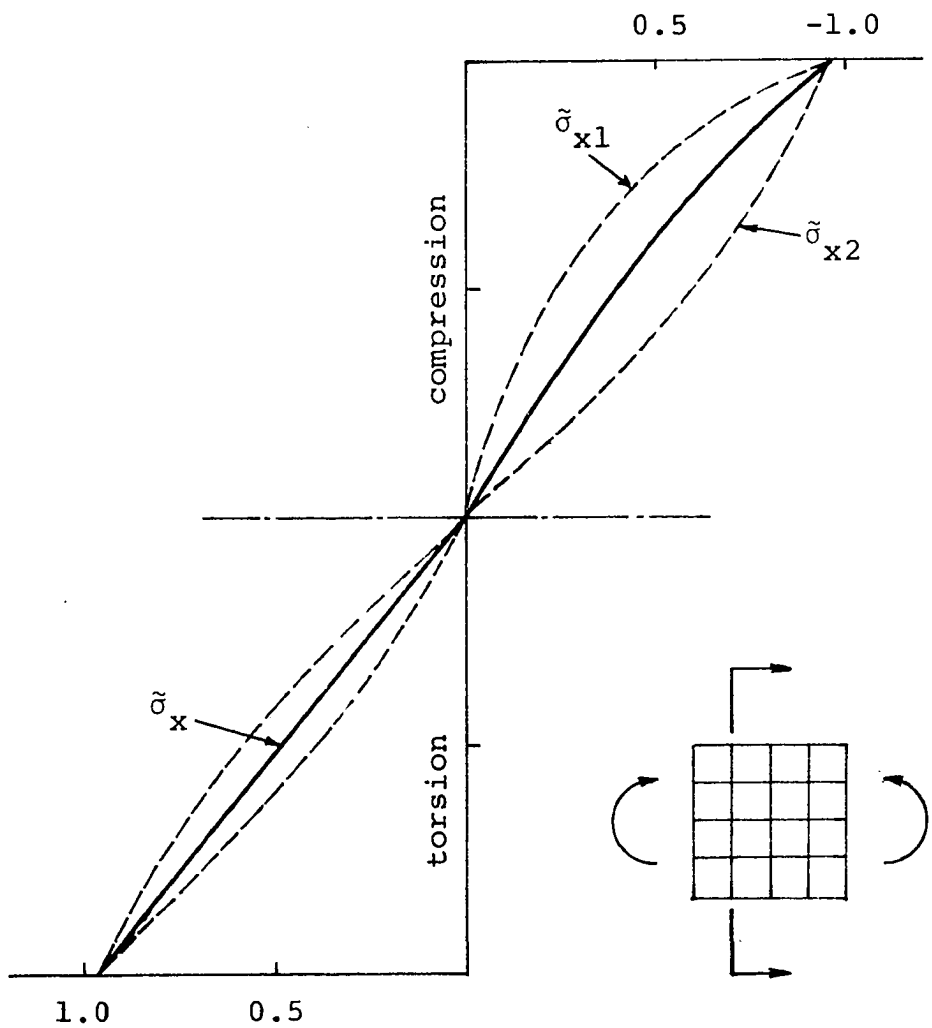

Figure 39. Distribution of $\tilde{\sigma}_x$, $\tilde{\sigma}_{x1}$ and $\tilde{\sigma}_{x2}$
Test girder A-M: μ=0.025; ζ=0.005
Δ=0.65

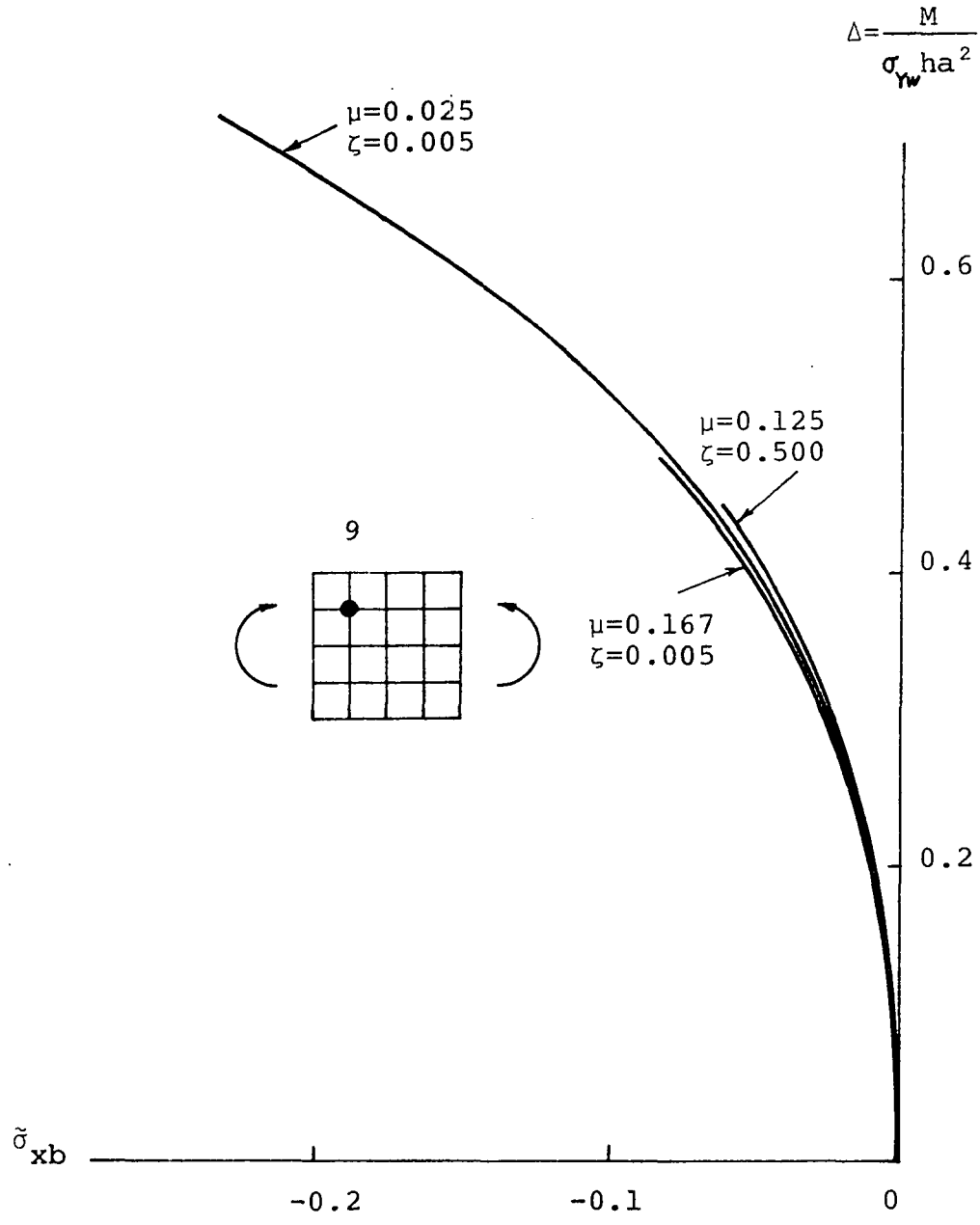

Figure 40. Load - bending stress $\tilde{\sigma}_{bx}$ curve
Test girder A-M

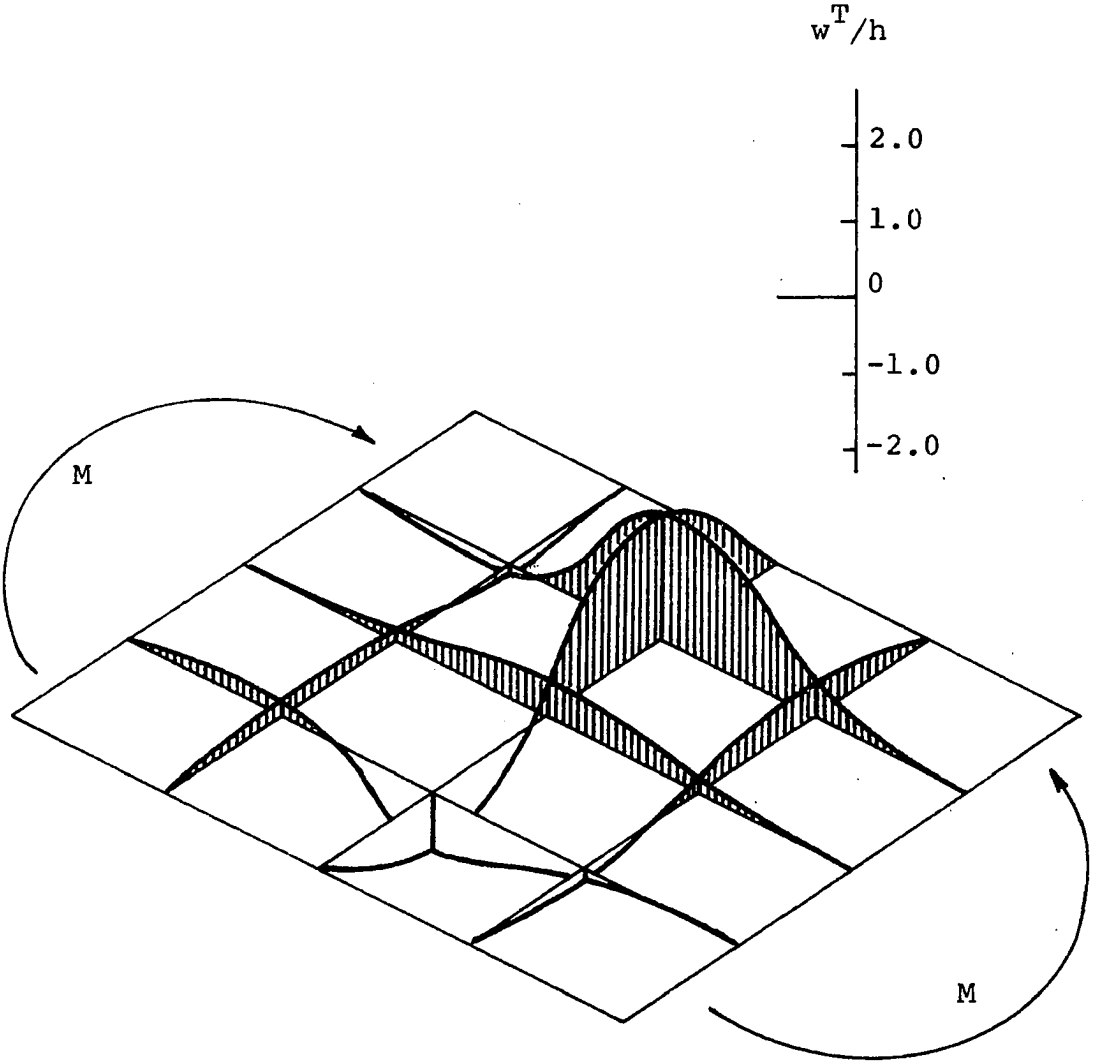

Figure 41. Total deflection w^T
Test girder A-M: μ= 0.025; ζ=0.005
Δ=0.65

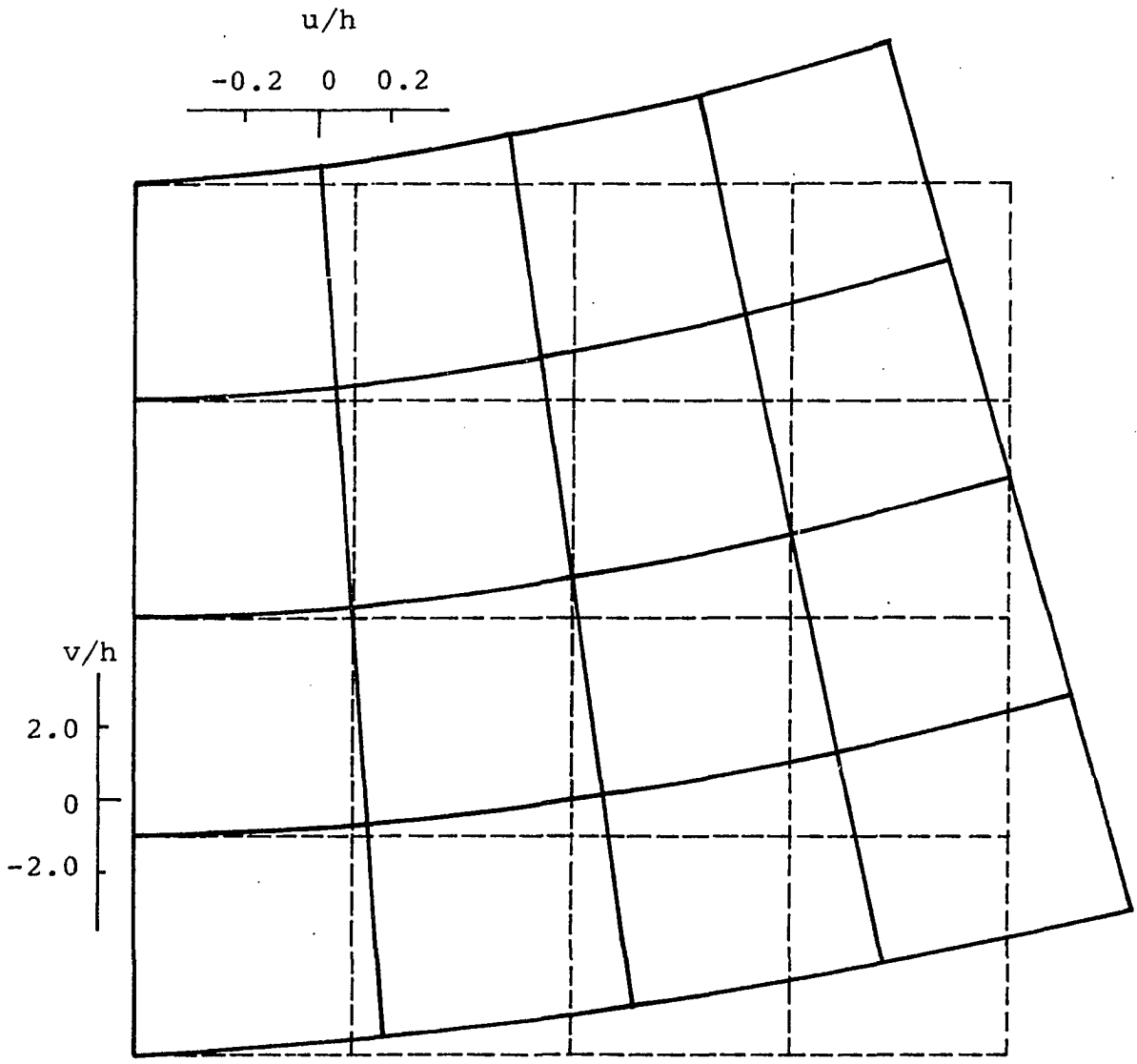

Figure 42. In-plane displacements u and v
Test girder A-M: μ=0.025; ζ=0.005
Δ=0.65

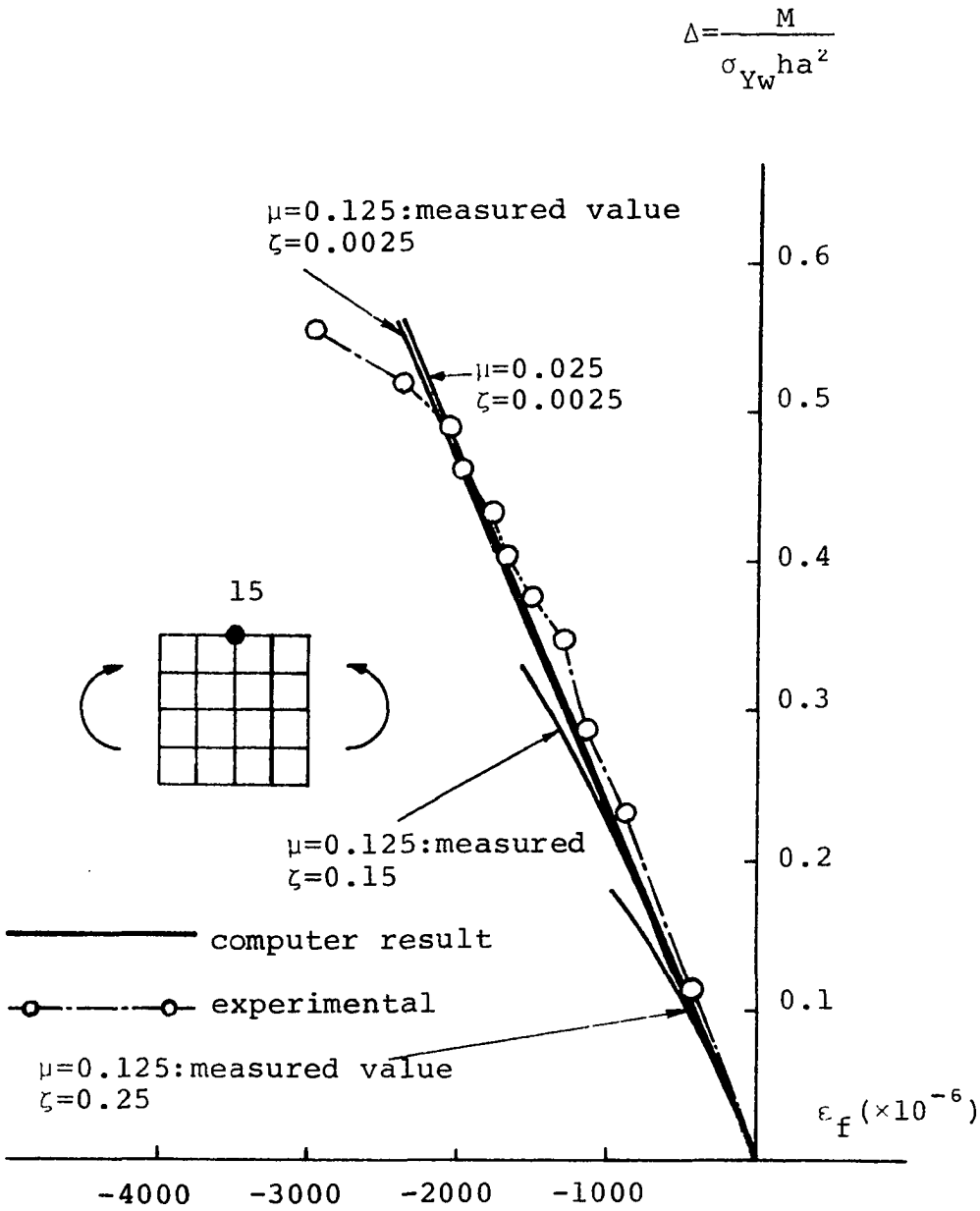

Figure 43. Load-flange strain, ε_f curve
Test girder C-M

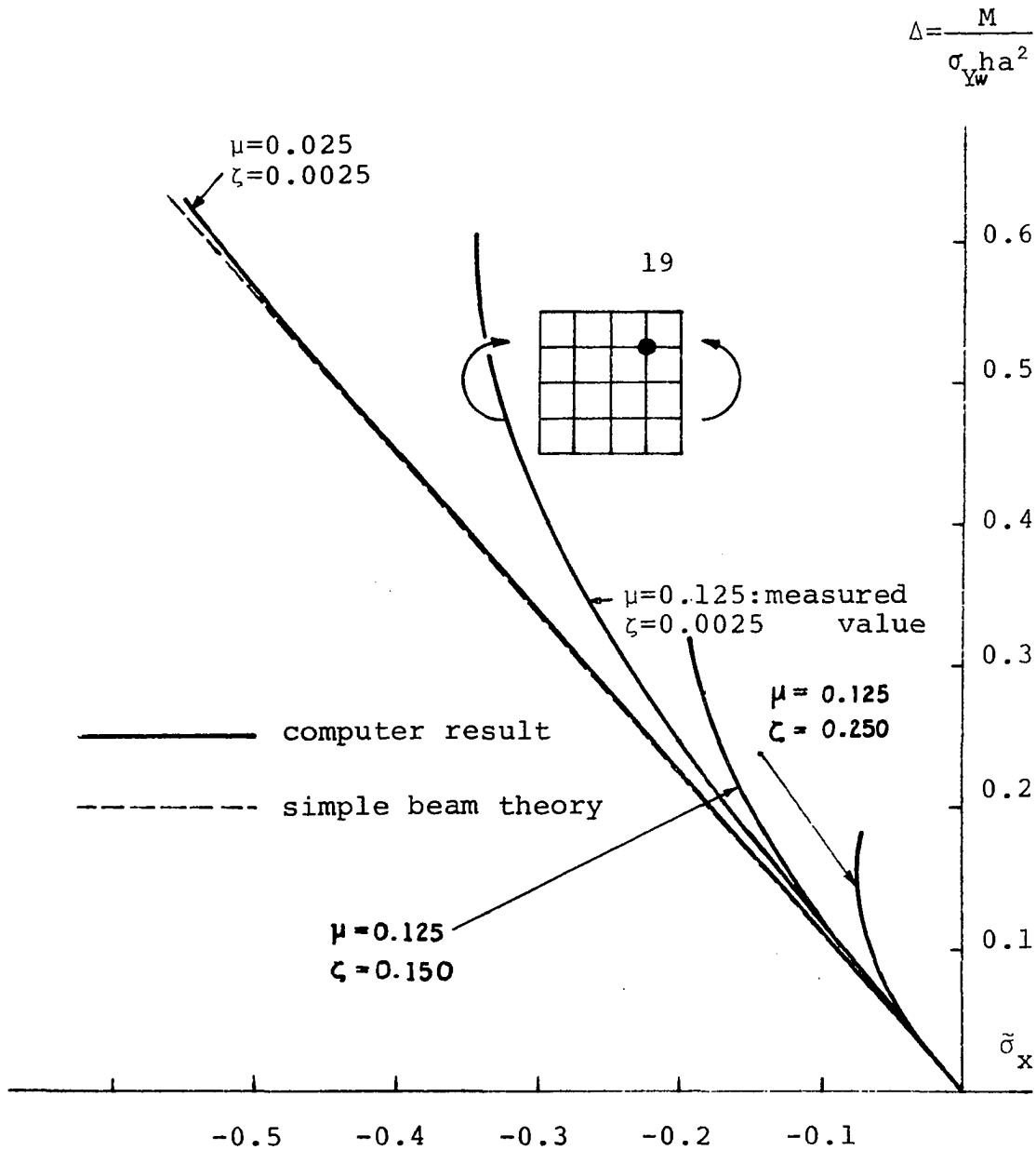

Figure 44. Load - $\tilde{\sigma}_x$ curve
Test girder C-M

yielding is caused by a significantly large tensile stress in the direction of diagonal line D_1. This phenomenon is ordinarily referred as a diagonal tension field action and is characterized by an outstanding bulge in the deflection surface along this diagonal line. Due to this buckled deflectional configuration of webplate it is generally believed that the minimum principal in-plane stress $\tilde{\sigma}_2$ does not increase too much with the increment of load along diagonal line D_1; on the other hand, the maximum principal in-plane stress $\tilde{\sigma}_1$ increases quite fast with the increment of load.

The analysis of computed results based on the proposed analysis consists of checking the deflectional surfaces, checking the yielding of diagonal line D_1, and investigating load-$\tilde{\sigma}_1$, $\tilde{\sigma}_2$ relationships. The ultimate load of a shear girder panel is evaluated by finding the load at which interior points on diagonal line D_1 initiate yielding. The yielding is checked by using von Mises comparison stresses $\tilde{\sigma}_{vM}$, $\tilde{\sigma}_{vM1}$ and $\tilde{\sigma}_{vM2}$.

Basler's theory (2) is used for comparison of the predicted ultimate strength. A brief summary of this has been presented in Chapter One. Overall behavior of a shear panel as predicted by the proposed theory is compared with simple pure shear case and with experimental data whenever available. The simple pure shear refers to the case of an ideal flat plate subjected to pure shear condition.

The format of the analysis of computed results for a shear panel is demonstrated using test girder panel G6-T1.

Test girder panel G6-T1 The experiment ultimate load is 116 Kips. Thus, Δ_u^{ex} = 0.328. Assuming that the webplate is simply supported along four boundaries, Δ_{wcr} = 0.077.

Computer result: Case 1 The maximum residual stress is assumed to be 0.5% of the yield strength of the webplate; while the maximum total initial deflection is assumed to be 50% of the thickness of the webplate. Also, $\theta = 0$. Then,

$$\alpha = 0.00000272; \quad \zeta = 0.00222; \quad \mu = 0.125; \quad \theta = 0.0$$

The in-plane stresses on diagonal line D_1 are listed in Table 8 for Δ = 0.26. Table 9 shows the computation of the flange stresses at the same load level. Table 10 shows the computation of the stiffener stresses at the same load level. It is seen that the entire portion of diagonal D_1 is yielded at Δ = 0.26.

Computer result: Case 2 The maximum residual stress is assumed to be 0.5% of the yield strength of the webplate; while, the maximum total initial deflection is assumed to be 40% of the thickness of webplate. Also, $\theta = 0$. Then,

$$\alpha = 0.00000272; \quad \zeta = 0.00222; \quad \mu = 0.100; \quad \theta = 0.0$$

The in-plane stresses are shown in Table 11 for Δ = 0.26. Table 12 shows the computation of the flange stresses at the same load level. Table 13 shows the computation of the stiffener

Table 8. In-plane stresses: Case 1 of test girder panel G6-T1 at $\Delta = 0.26$

Pt. No.	$\tilde{\tau}^T_{xy}$	$\tilde{\sigma}^T_{vM}$	$\tilde{\sigma}^T_{vM1}$	$\tilde{\sigma}^T_{vM2}$	$\tilde{\sigma}^T_1$	$\tilde{\sigma}^T_2$	Yielding
7	0.5745	1.0192	1.1318	1.1608	0.7874	-0.3638	yes
13	0.6226	1.0791	0.8593	1.3944	0.6495	-0.5962	yes
19	0.5622	1.0095	1.0909	1.1960	0.5991	-0.5665	yes

Table 9. Flange stresses: Case 1 of test girder panel G6-T1 at $\Delta = 0.26$

Pt. No.	$\tilde{u}_{+1}$	$\tilde{u}_{-1}$	$\tilde{u}_{+1}-\tilde{u}_{-1}$	$\tilde{\sigma}_f$	$\tilde{\sigma}'_f$
1	0.0800	0.0225	0.0575	-1.075	0.242
5	-0.0865	0.1668	-0.2533	-1.075	--
6	0.1344	0	0.1344	--	0.572
10	-0.1626	0	-0.1626	-0.691	--
11	0.1661	0.0800	0.0861	--	0.366
15	-0.2144	-0.0865	-0.1279	-0.544	--
16	0.1791	0.1344	0.0347	--	0.148
20	-0.2462	-0.1626	-0.0836	-0.356	--
21	0.1760	0.1661	0.0099	--	0.042
25	-0.2631	-0.2144	-0.0487	-0.207	--

Table 10. Stiffener stresses: Case 1 of test girder panel G6-T1 at $\Delta = 0.26$

Pt. No.	$\tilde{v}_{+1}$	$\tilde{v}_{-1}$	$\tilde{v}_{+1}-\tilde{v}_{-1}$	$\tilde{\sigma}_s$	$\tilde{\sigma}'_s$
1	0.1156	0.1215	-0.0059	-0.038	--
2	0.2129	0	0.2129	1.355	--
3	0.2993	0.1156	0.1837	1.170	--
4	0.3830	0.2129	0.1701	1.087	--
5	0.3188	0.2993	0.0195	0.124	--
21	1.2623	1.2636	-0.0013	--	-0.0083
22	1.2617	1.2567	0.0050	--	0.0318
23	1.2538	1.2623	-0.0085	--	-0.0541
24	1.2506	1.2617	-0.0111	--	-0.0707
25	1.2576	1.2538	0.0038	--	0.0242

Table 11. In-plane stresses: Case 2 of test girder panel G6-T1 at $\Delta = 0.26$

Pt. No.	$\tilde{\tau}^T_{xy}$	$\tilde{\sigma}^T_{vM}$	$\tilde{\sigma}^T_{vM1}$	$\tilde{\sigma}^T_{vM2}$	$\tilde{\sigma}^T_1$	$\tilde{\sigma}^T_2$	Yielding
7	0.5525	0.9814	1.0779	1.1159	0.7614	-0.3462	yes
13	0.6280	1.0884	0.8765	1.3906	0.6491	-0.6070	yes
19	0.5269	0.9509	1.0617	1.1706	0.5589	-0.5391	yes

Table 12. Flange stresses: Case 2 of test girder panel G6-T1 at $\Delta = 0.26$

Pt. No.	$\tilde{u}_{+1}$	$\tilde{u}_{-1}$	$\tilde{u}_{+1}-\tilde{u}_{-1}$	$\tilde{\sigma}_f$	$\tilde{\sigma}'_f$
1	0.0760	-0.0249	0.1009	--	0.423
5	-0.0857	0.1345	-0.2202	-0.925	--
6	0.1296	0	0.1296	--	0.544
10	-0.1571	0	-0.1571	-0.660	--
11	0.1602	0.0760	0.0842	--	0.354
15	-0.2045	-0.0857	-0.1188	-0.498	--
16	0.1727	0.1296	0.0428	--	0.180
20	-0.2334	-0.1571	-0.0763	-0.320	--
21	0.1695	0.1602	0.0093	--	0.039
25	-0.2479	-0.2045	-0.0434	-0.182	--

Table 13. Stiffener stresses: Case 2 of test girder panel G6-T1 at $\Delta = 0.26$

Pt. No.	$\tilde{v}_{+1}$	$\tilde{v}_{-1}$	$\tilde{v}_{+1}-\tilde{v}_{-1}$	$\tilde{\sigma}_s$	$\tilde{\sigma}'_s$
1	0.0601	0.0688	-0.0087	-0.055	--
2	0.1097	0	0.1097	0.690	--
3	0.1576	0.0601	0.0975	0.614	--
4	0.2069	0.1097	0.0972	0.612	--
5	0.1748	0.1576	0.0172	0.108	--
21	1.1420	1.1430	-0.0010	--	-0.0063
22	1.1417	1.1367	0.0050	--	0.0315
23	1.1350	1.1420	-0.0070	--	-0.0441
24	1.1323	1.1417	-0.0094	--	-0.0592
25	1.1385	1.1350	0.0035	--	0.0220

stresses at the same load level. It is observed that the entire portion of diagonal line D_1 is yielded at $\Delta = 0.26$.

Figure 45 shows the flange stress distribution and Figure 46 shows the stiffener stress distribution at $\Delta = 0.26$. Figure 47 shows a load-stiffener stress curve. Figure 48 shows the deflectional shape of the webplate.

Basler's theory (2) The ultimate load is computed to be 112 Kips. Thus, $\Delta_u^B = 0.317$.

Test girder panels G7-T1 through B-Q Similar computations are performed on these girder panels and the results are presented in Table 14. Figure 49 shows a load-$\tilde{\sigma}_1$, $\tilde{\sigma}_2$ relationship of girder panel G7-T1. Figures 50 and 51 show the distributions of flange stresses and stiffener stresses, respectively for girder panel F10-T2. Figure 52 illustrates a deflectional surface of the same girder panel. Figures 53, 54 and 55 show relationships of load-principal stresses, $\tilde{\sigma}_1$ and $\tilde{\sigma}_2$, respectively, and Figures 56 and 57 show the distributions of the maximum and minimum principal stresses, respectively, for girder panel B-Q. Figures 58 and 59 illustrate a total deflection surface and an in-plane displacement configuration, respectively, for the same girder panel.

Analysis of panels subjected to both bending moment and shear

Obviously, this case lies between two extreme cases, i.e., bending and shear cases. The load carrying capacity of a

Table 14. Prediction of ultimate load for shear panels

Girder	Δ^{ex}	Δ_{wcr}	Mode of Failure	$(\mu)_{ex}$	$(\frac{\sigma_r}{\sigma_{yw}})_{th}$	$(\mu)_{th}$	Δ_u^{th}	Δ_u^B	θ_{ex}	θ_{used}
G6-T1	0.328	0.077	Diag. T.	0.376	0.005	0.125	0.26	0.317	-0.667	-0.667
					0.005	0.100	0.26	0.317	-0.667	-0.667
G7-T1	0.389	0.105	Diag. T.	0.446	0.500	0.025	0.44	0.395	-1.500	-1.500
					0.500	0.025	0.45	0.395	-1.500	-0.500
					0.005	0.100	0.36	0.395	-1.500	-0.500
					0.005	0.125	0.32	0.395	-1.500	-0.500
F10-T2	0.371	0.159	Diag. T.	0.157	0.005	0.125	0.38	0.364	0.214	0.214
					0.005	0.125	0.40	0.364	0.214	-0.500
					0.500	0.125	0.40	0.364	0.214	0.214
F10-T3	0.382	0.185	Diag. T.	0.053	0.005	0.125	0.40	0.407	0.400	0.400
					0.005	0.100	0.42	0.407	0.400	0.400
					0.500	0.053	0.34	0.407	0.400	0.400
B-Q	0.282	0.022	Diag. T.	0.167	0.250	0.025	0.30	0.338	-1.167	-1.167
					0.003	0.025	0.38	0.338	-1.167	-1.167
					0.003	0.125	0.24	0.338	-1.167	-1.167
					0.250	0.050	0.32	0.338	-1.167	-0.500
					0.250	0.167	0.12	0.338	-1.167	-0.500
					0.003	0.025	0.38	0.338	-1.167	-0.500
					0.003	0.125	0.28	0.338	-1.167	-0.500

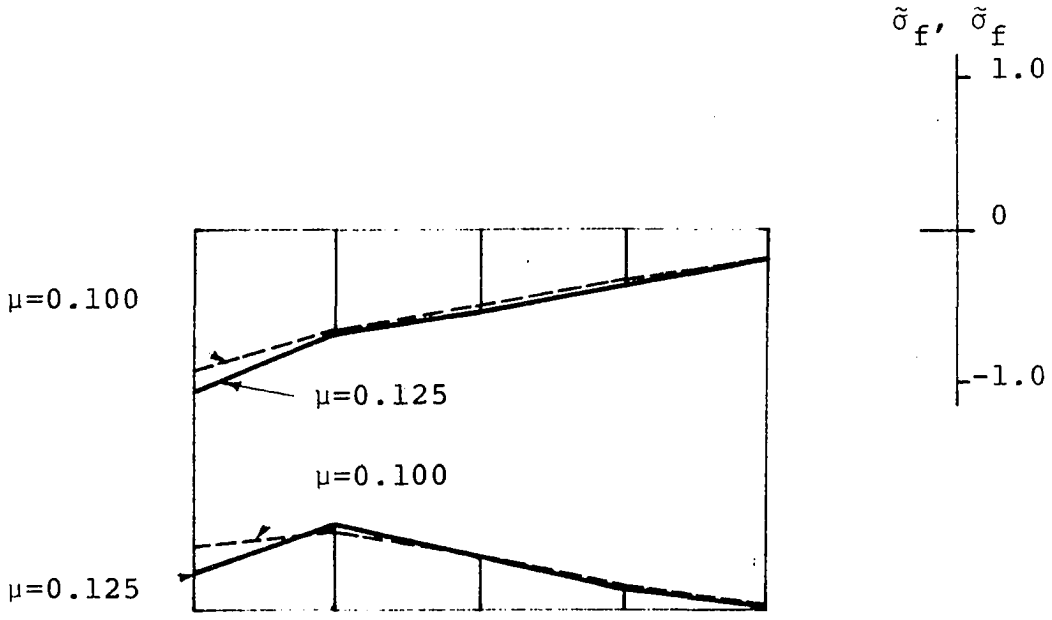

Figure 45. Flange stress distribution at Δ = 0.26
Test girder G6-T1: ζ=0.00222

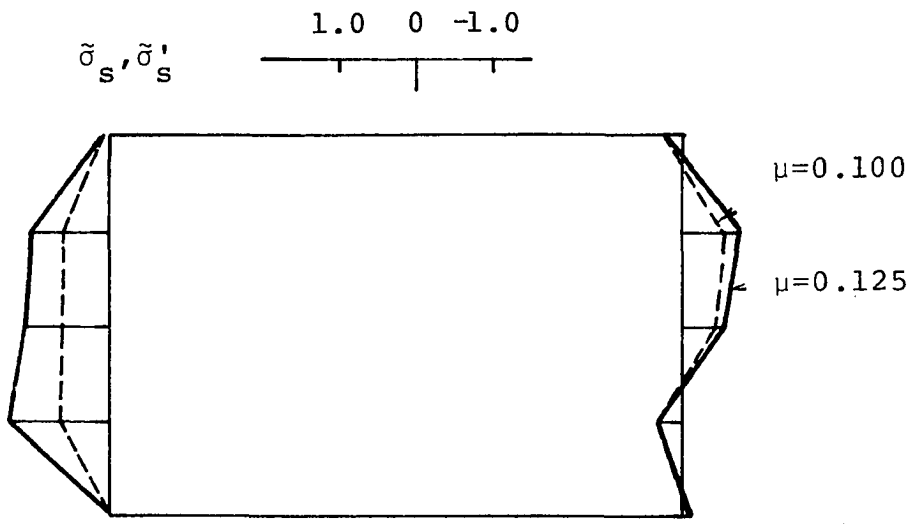

Figure 46. Stiffener stress distribution at Δ = 0.26
Test girder G6-T1: ζ=0.00222

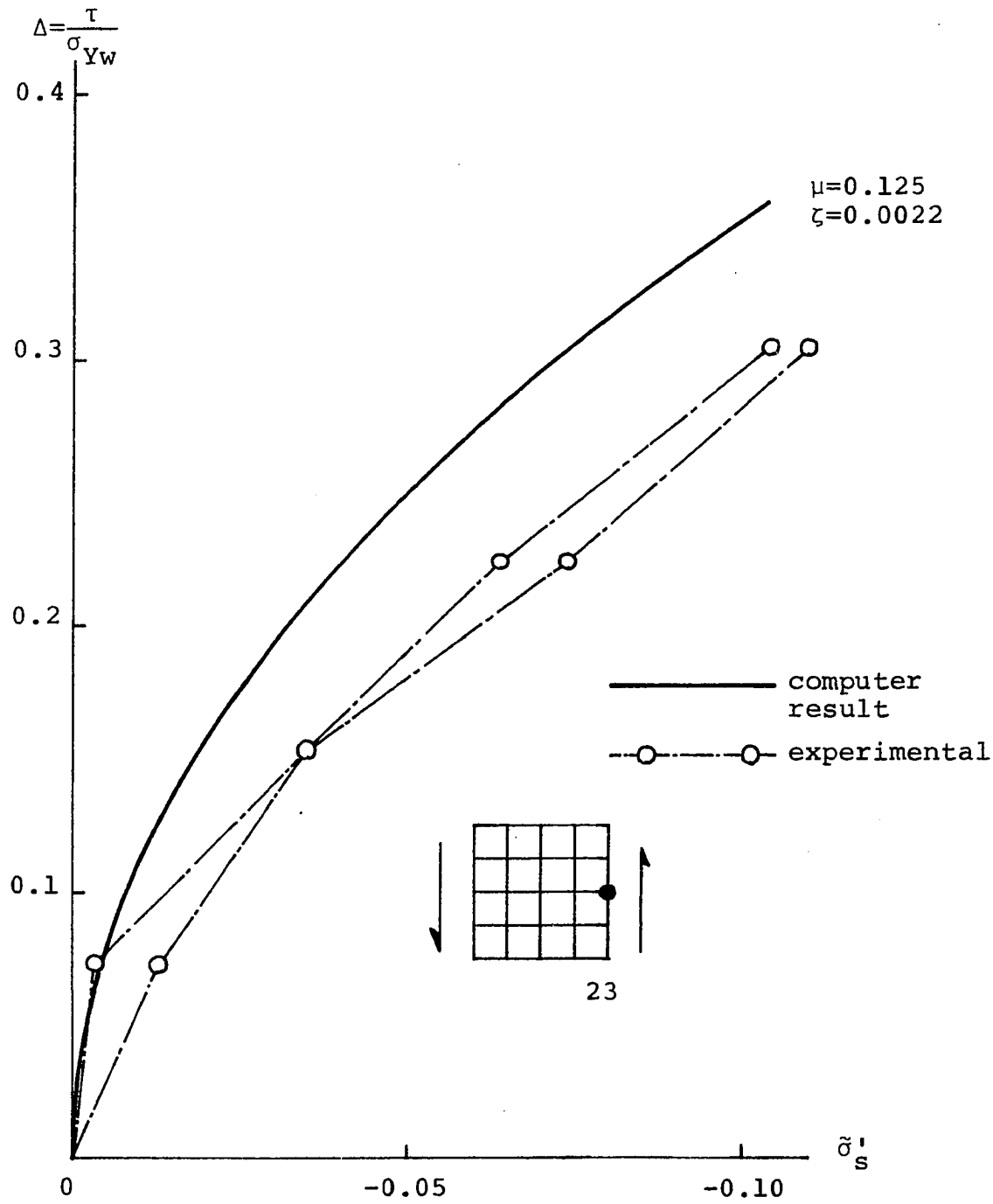

Figure 47. Load-stiffener stress $\tilde{\sigma}'_s$ curve
Test girder G6-T1

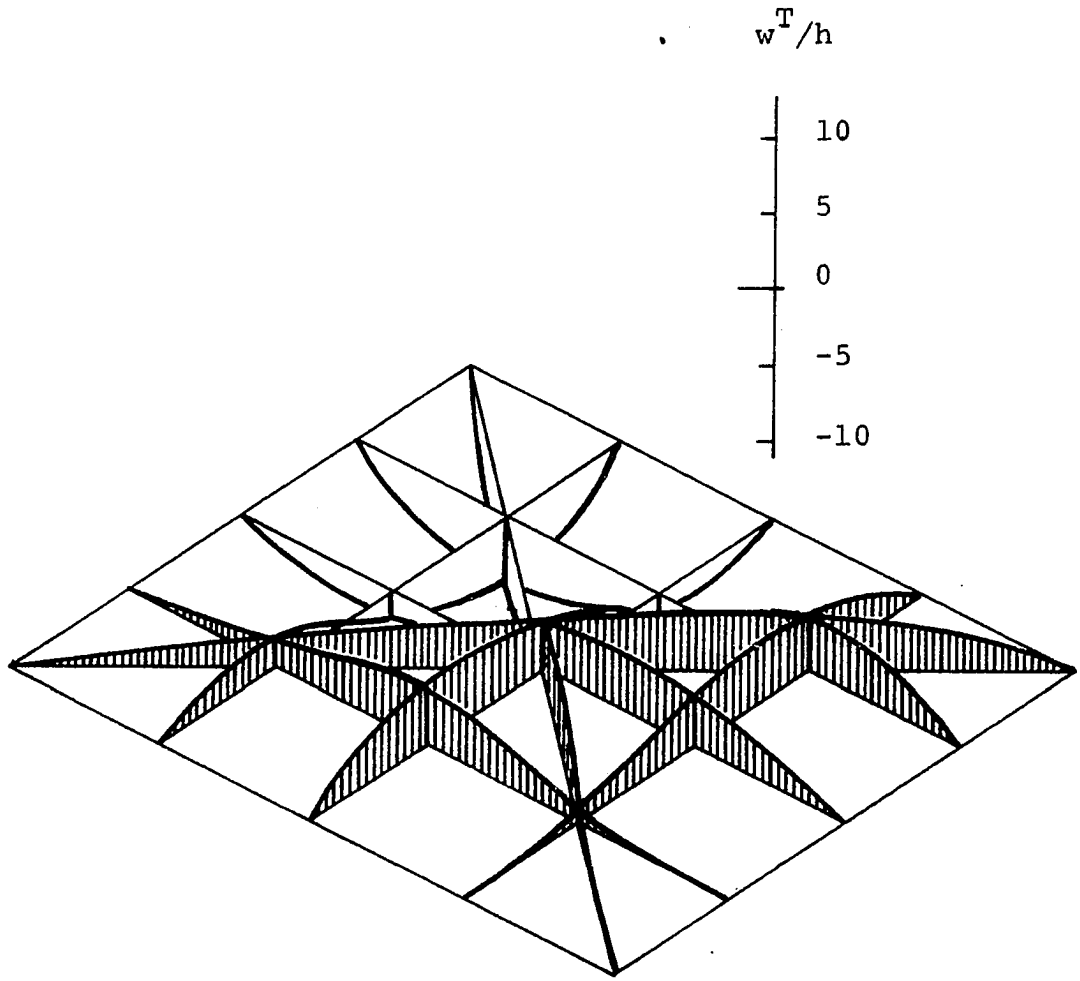

Figure 48. Total deflection w^T at $\Delta = 0.26$
Test girder panel G6-T1: μ=0.125;
ζ=0.00222

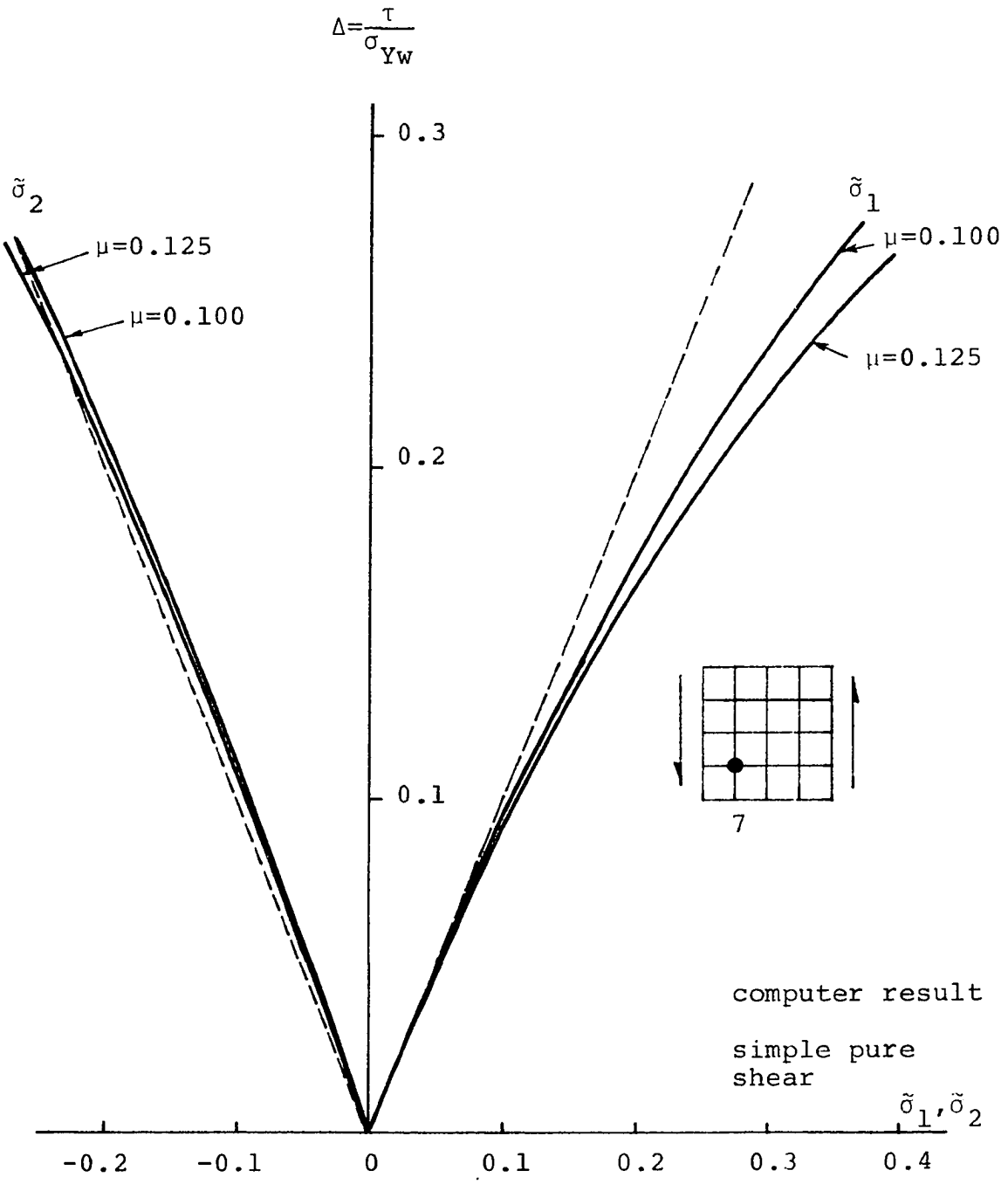

Figure 49. Load-principal stresses, $\tilde{\sigma}_1$ and $\tilde{\sigma}_2$
Test girder panel G7-T1: ζ=0.005

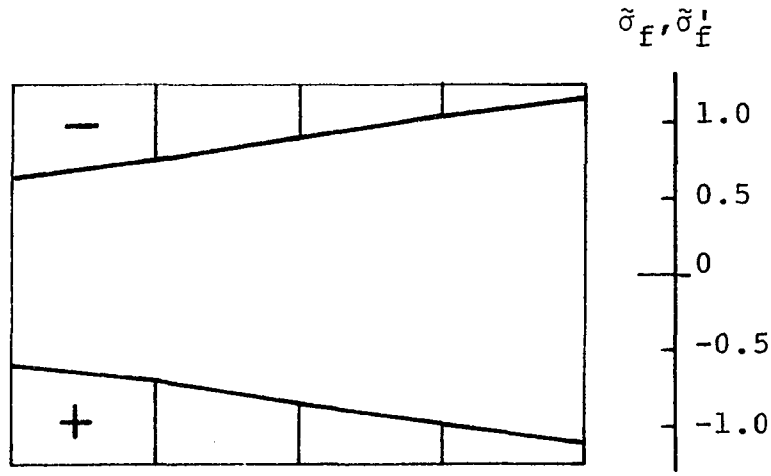

Figure 50. Flange stresses
Test girder panel F10-T2
μ=0.125; ζ=0.00222; θ=0.2135

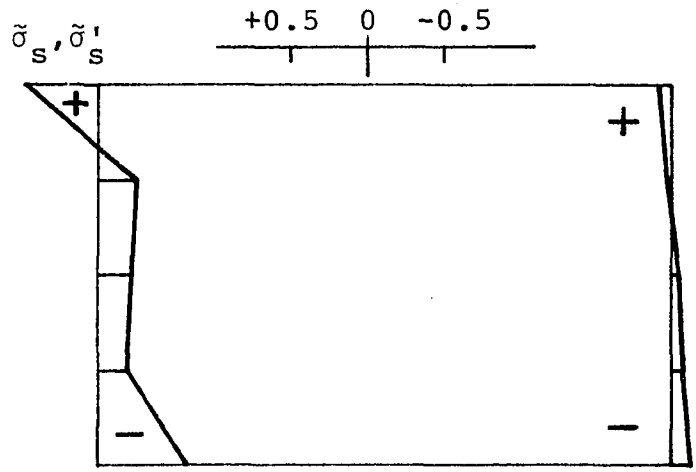

Figure 51. Stiffener stresses
Test girder panel F10-T2
μ=0.125; ζ=0.00222; θ=0.2135

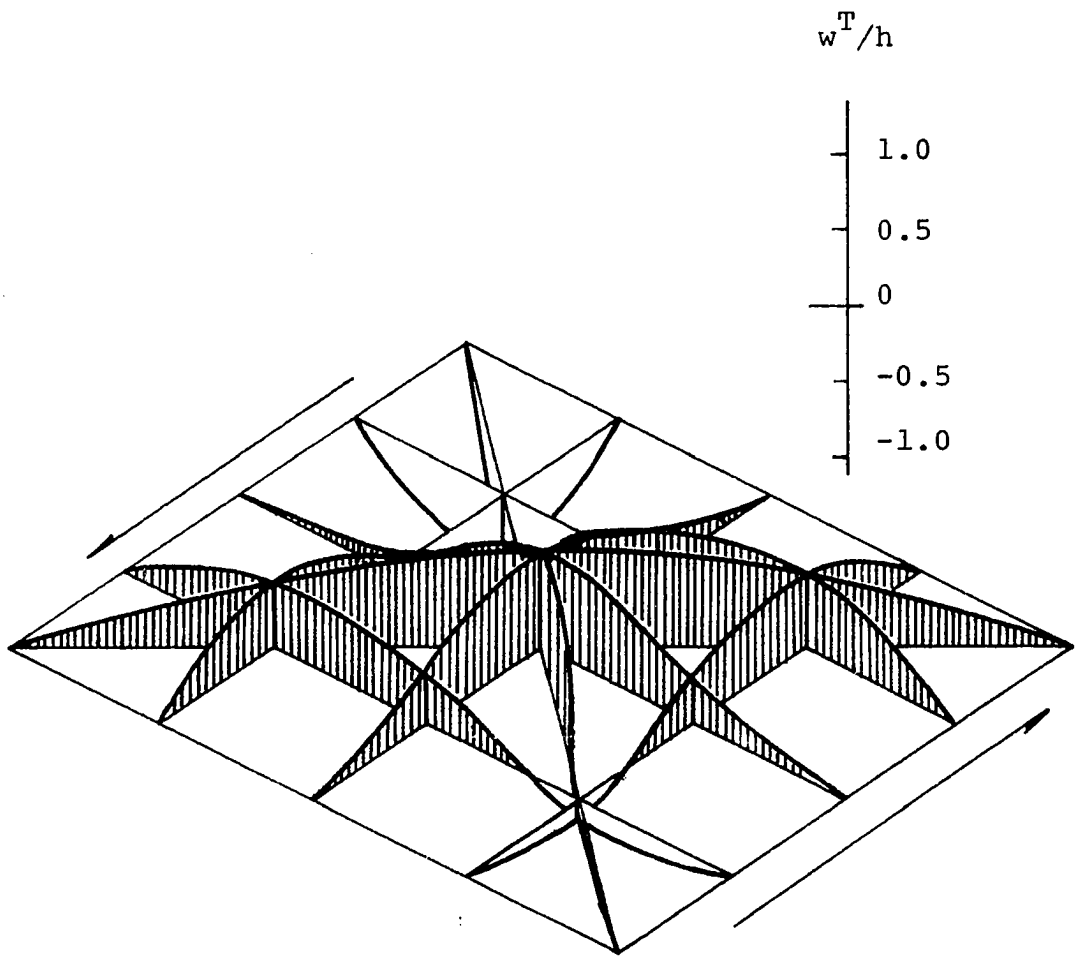

Figure 52. Total deflection surface at Δ=0.38
Test girder F10-T2: μ=0.125;
ζ=0.00222; θ=0.2135

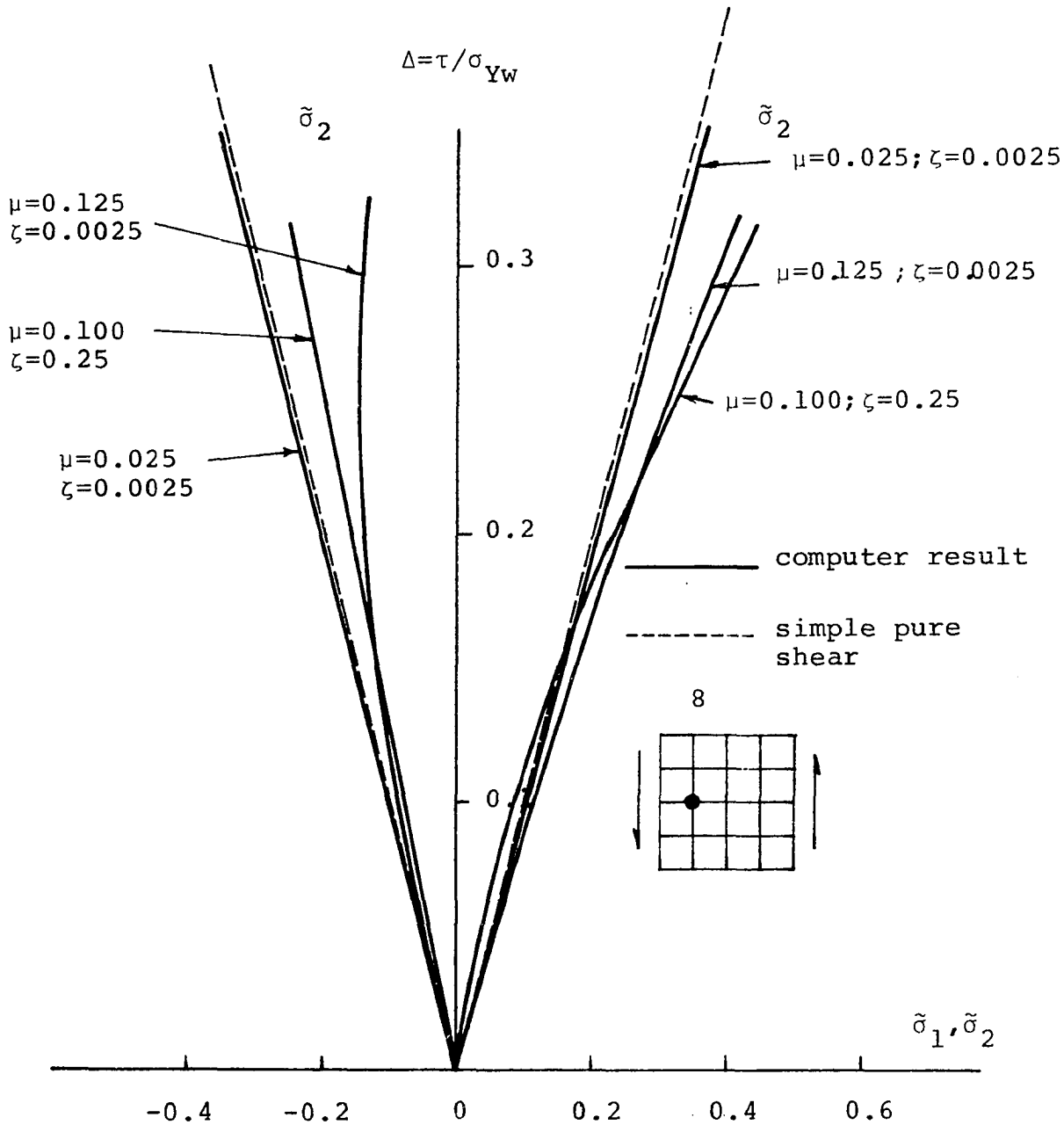

Figure 53. Load-principal stresses, $\tilde{\sigma}_1$ and $\tilde{\sigma}_2$
Test girder B-Q

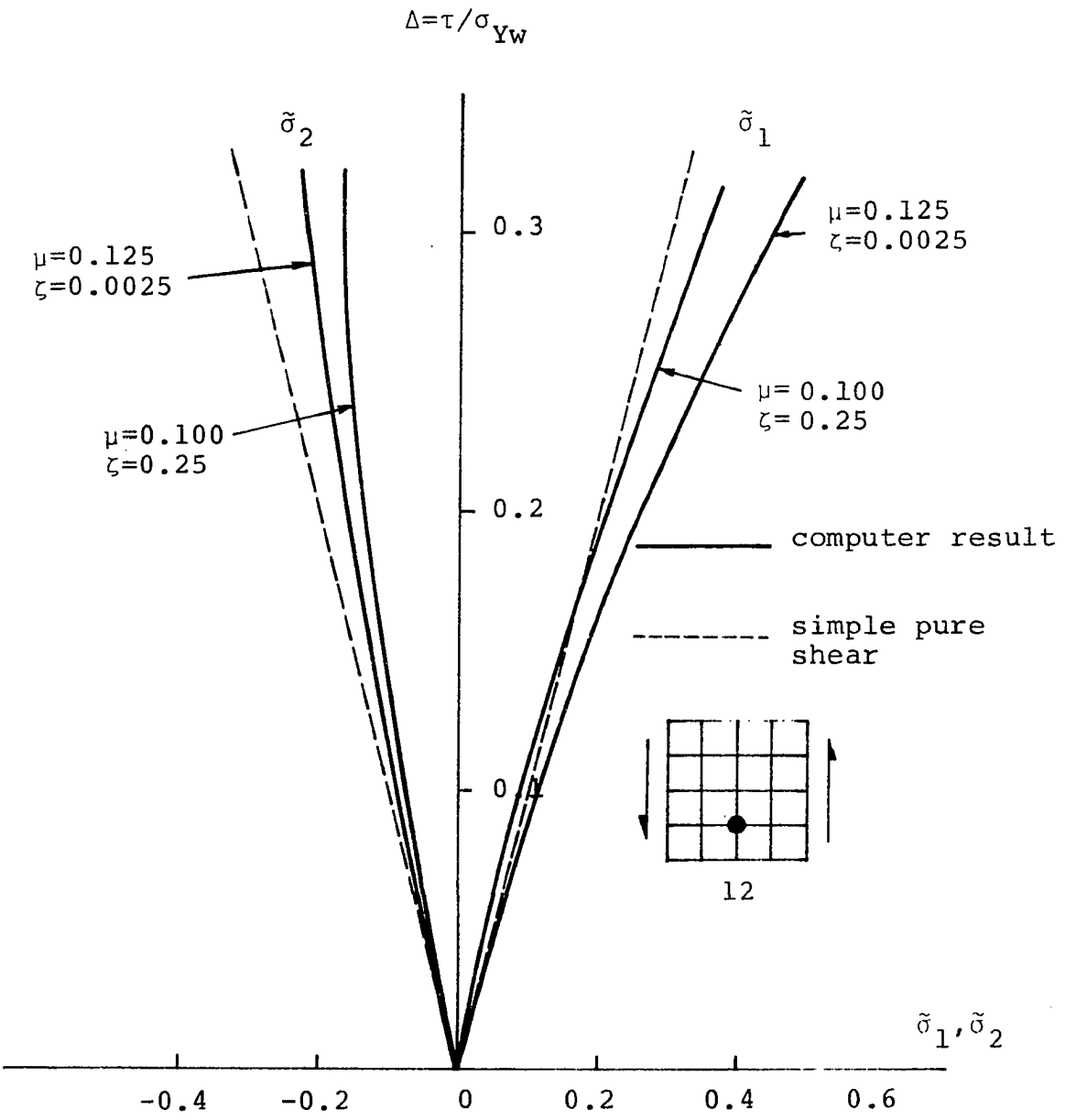

Figure 54. Load-principal stresses, $\tilde{\sigma}_1$ and $\tilde{\sigma}_2$
Test girder B-Q

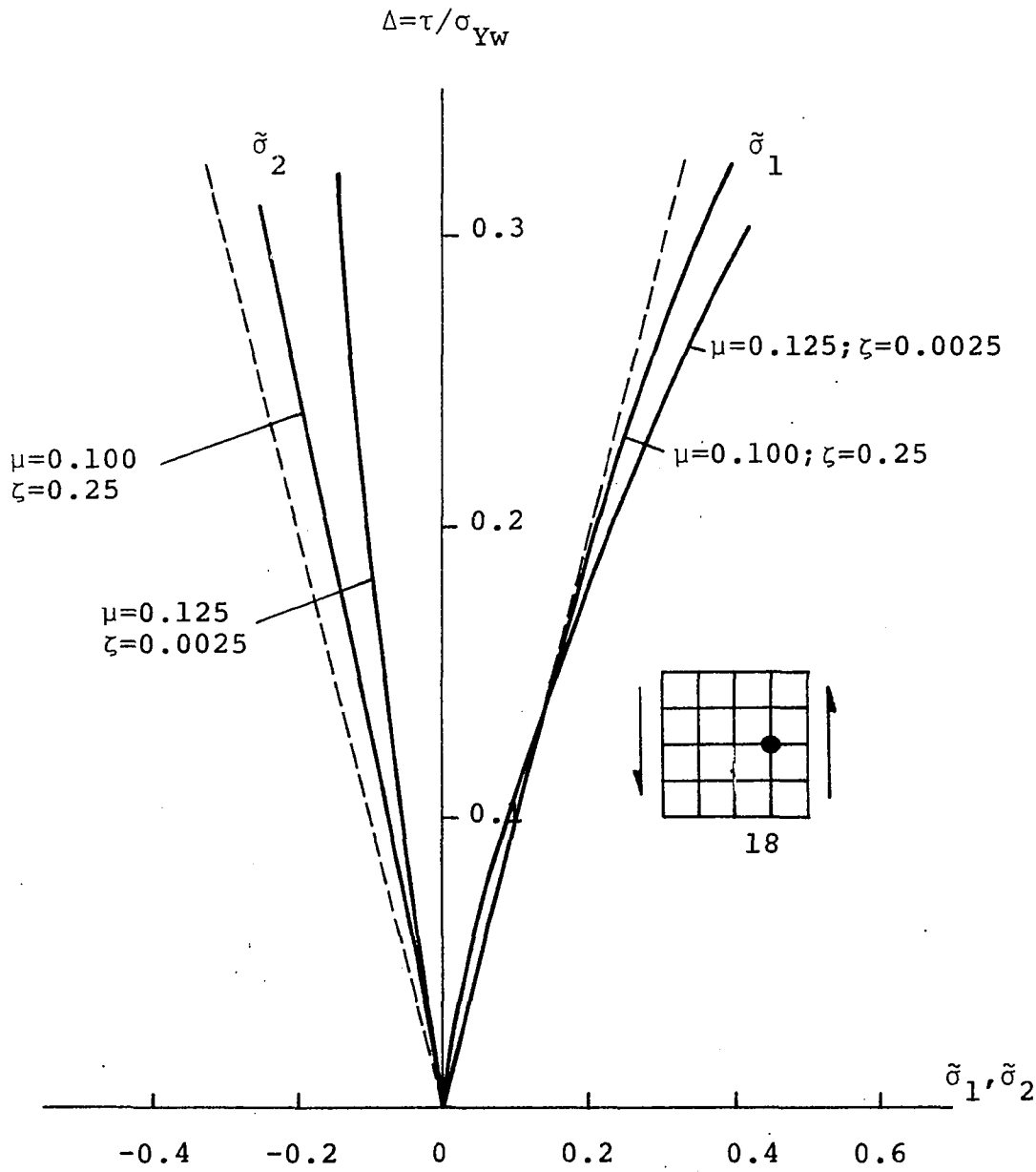

Figure 55. Load-principal stresses $\tilde{\sigma}_1, \tilde{\sigma}_2$
Test girder B-Q

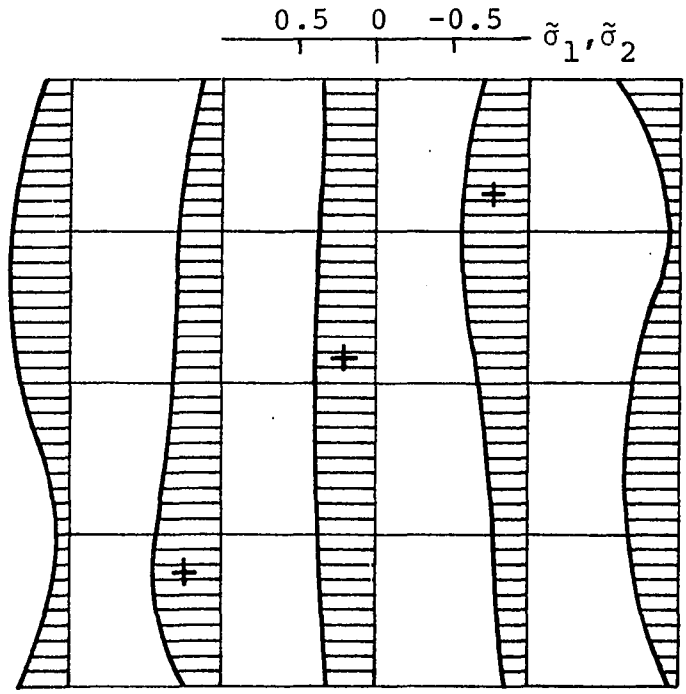

Figure 56. Maximum principal stress distribution $\tilde{\sigma}_1$ at Δ=0.28 Test girder B-Q: μ=0.125; ζ=0.0025

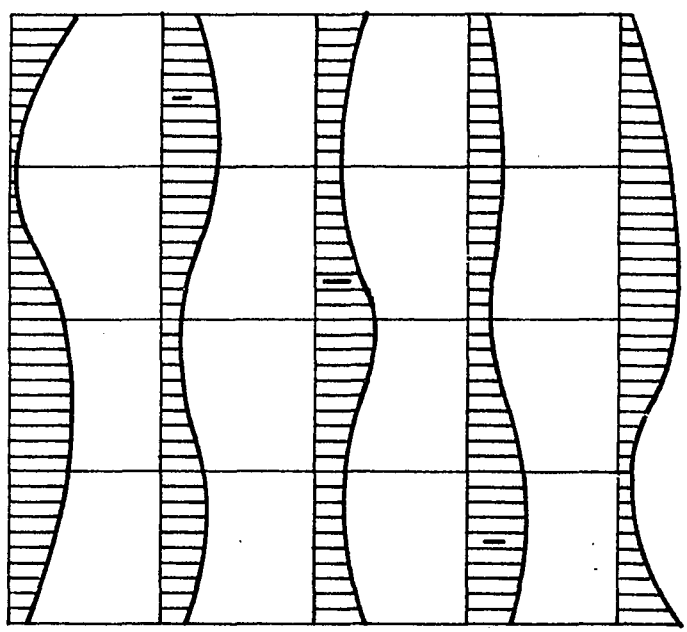

Figure 57. Minimum principal stress distribution $\tilde{\sigma}_2$ at Δ=0.28 Test girder B-Q: μ=0.125; ζ=0.0025

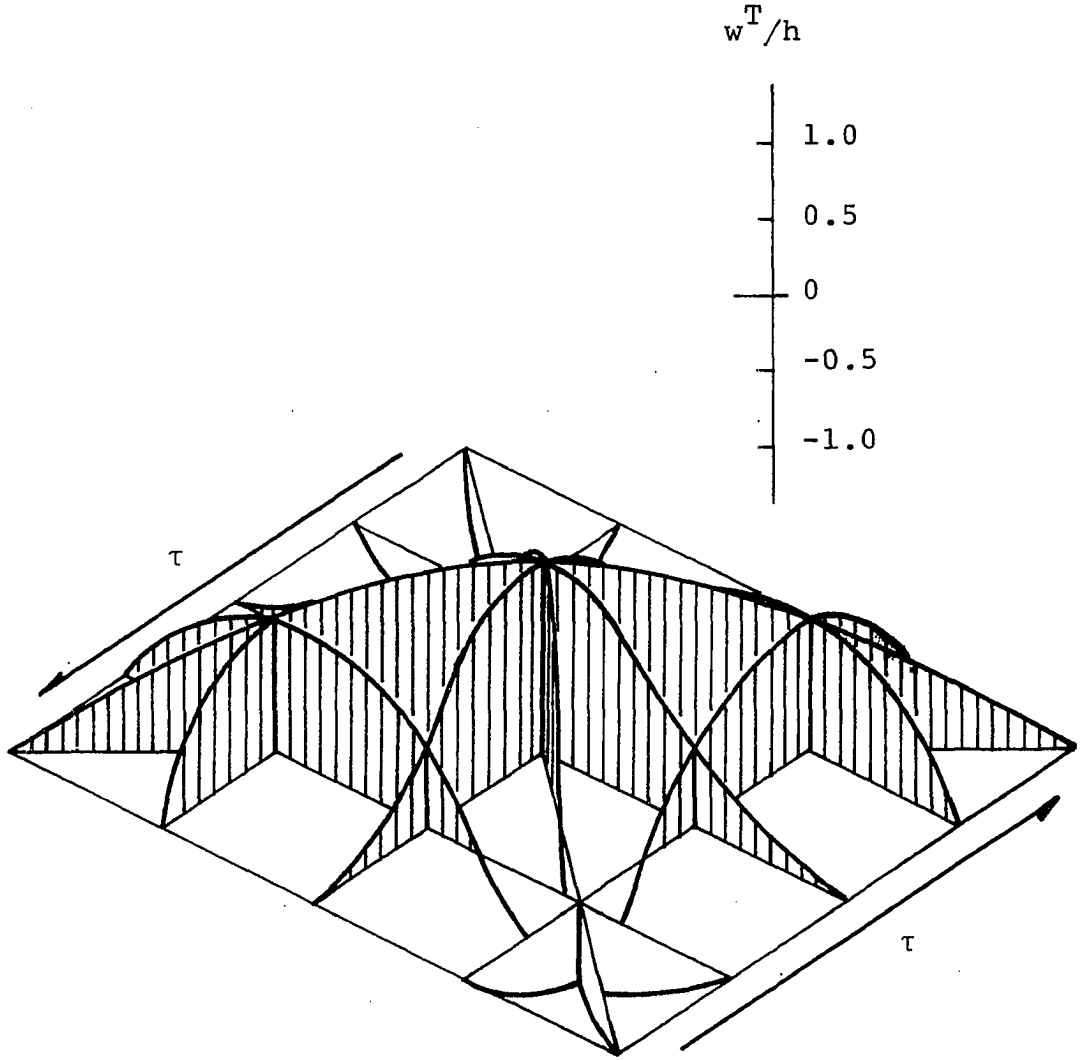

Figure 58. Total deflection surface
Test girder B-Q: $\mu=0.125; \zeta=0.0025$
$\Delta=0.28$

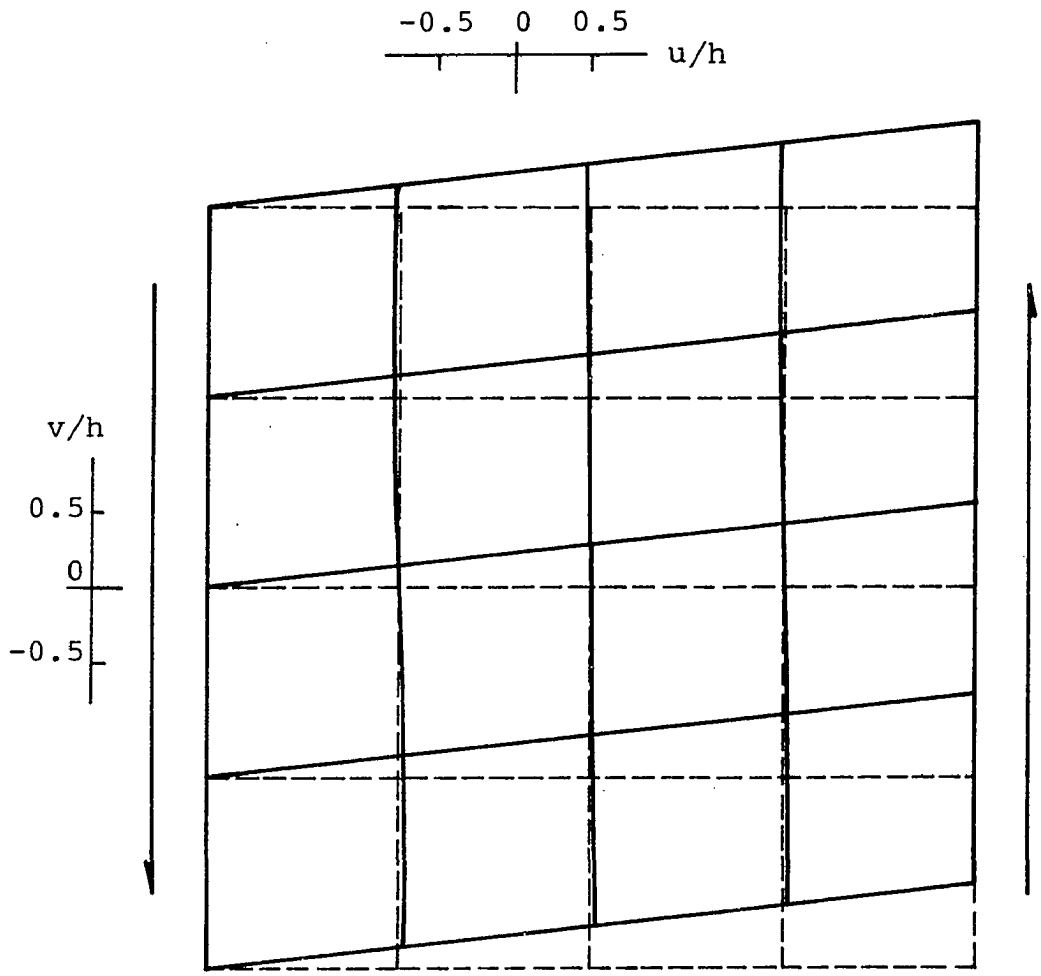

Figure 59. In-plane deformation u, v
Test girder B-Q: μ=0.025; ζ=0.25; θ=-0.5
Δ=0.32

bending panel is governed by the strength of the compression flange; while that of a shear panel is governed mainly by the strength of the webplate. In panels subjected to both bending and shear, past experiments show that failure is attained when a portion of webplate in the direction of diagonal tension has yielded, although this failure is not as obvious as in case of shear.

The prediction of the ultimate load in the combined case using the result of the proposed analysis consists of finding the load at which a certain region has yielded. It is seen that the mode of failure is not defined as clearly as for either bending or shear case. This is due to the nature of combination of two extreme cases.

Test girder panel G8-T1 The experimental ultimate load is 170 Kips. Thus, $\Delta_u^{ex} = \underline{0.226}$. The failure mode is the yielding of the diagonal line D_1. Assuming that the webplate is simply supported along four boundaries, $\Delta_{wcr} = \underline{0.110}$. The value of θ is 0.0.

Computer result: Case 1 The maximum residual stress is assumed to be 0.5% of the yield strength of the webplate; while, the maximum total initial deflection is assumed to be 50% of the thickness of the webplate. Then,

$$\alpha = 0.000000708; \quad \zeta = 0.000555; \quad \mu = 0.125; \quad \theta = 0.0$$

Table 15 shows the in-plane stresses at Δ=0.300. Diagonal

line D_1 is not completely yielded yet at this load level. Points 1 and 6 are yielded at this load level.

Computer result: Case 2 The maximum residual stress is assumed to be 0.5% of the yield strength of the webplate; while, the maximum total initial deflection is assumed to be 80% of the thickness of the webplate. Then,

$$\alpha = 0.000000708; \quad \zeta = 0.000555; \quad \mu = 0.200; \quad \theta = 0.0$$

Table 16 shows the in-plane stresses at $\Delta = 0.24$. Diagonal line D_1 is not completely yielded yet at this load level.

A load-v curve, an in-plane displacement configuration, and a deflectional shape of the webplate all at $\Delta = 0.26$ are shown in Figures 60 through 62, respectively.

Test girder panel G9-T1 and F10-T1 Similar computations are performed on these girder panels and the results are presented in Table 17. Figure 63 shows a load-v relationship for girder panel G9-T1.

Remakrs on the Feasibility of the Proposed Analysis

Since the solution of von Kármán's nonlinear partial differential equations is mainly based on the polynomial series and finite difference methods, it is necessary to show that the use of the polynomial series as well as the selection of 5 x 5 mesh point system for finite differences result in reasonably good accuracy. The result of a study on the convergence of

Table 15. In-plane stresses: Case 1 of test girder panel G8-T1 at Δ=0.300

Pt. No.	$\tilde{\tau}^T_{xy}$	$\tilde{\sigma}^T_{vM}$	$\tilde{\sigma}^T_{vM1}$	$\tilde{\sigma}^T_{vM2}$	$\tilde{\sigma}^T_1$	$\tilde{\sigma}^T_2$	Yielding
7	0.4195	0.8190	0.8806	0.9776	0.6606	-0.2558	--
13	0.4608	0.7982	0.7213	0.9512	0.4657	-0.4560	--
19	0.3560	0.6305	0.6704	0.6963	0.3228	-0.4037	--
1[a]	0.1632	0.9966	1.0101	0.9849	1.0942	0.2385	yes
5[a]	0.0767	0.9265	0.9384	0.9193	-0.2522	-1.0265	--
6[a]	0.3256	0.9647	1.1442	0.9805	0.9005	-0.1177	yes

[a]Points not on Diagonal line D_1.

Table 16. In-plane stresses: Case 2 of test girder panel G8-T1 at Δ=0.24

Pt. No.	$\tilde{\tau}^T_{xy}$	$\tilde{\sigma}^T_{vM}$	$\tilde{\sigma}^T_{vM1}$	$\tilde{\sigma}^T_{vM2}$	$\tilde{\sigma}^T_1$	$\tilde{\sigma}^T_2$	Yielding
7	0.3636	0.7111	0.9650	1.0734	0.5776	-0.2166	yes
13	0.4454	0.7721	0.6748	1.0263	0.4495	-0.4421	yes
19	0.3185	0.5608	0.6566	0.7084	0.2776	-0.3678	--
1[a]	0.2729	0.9945	1.0302	0.9627	1.0636	0.1567	yes
6[a]	0.2557	0.8145	1.2003	0.9794	0.7686	-0.0851	yes

[a]Points not on Diagonal line D_1.

Table 17. Prediction of ultimate load for panels both in bending and shear

Girder	Δ_u^{ex}	Δ_{wcr}	Mode of Failure	$(\mu)_{ex}$	$(\frac{\sigma_r}{\sigma_{Yw}})_{th}$	$(\mu)_{th}$	Δ_u^{th}	θ
G8-T1	0.226	0.110	Diag. T.	0.355	0.005	0.125	0.30	0.0
					0.005	0.200	0.24	0.0
					0.500	0.025	0.34	0.0
G9-T1	0.165	0.040	Diag. T.	0.286	0.005	0.125	0.20	0.0
					0.005	0.150	0.18	0.0
F10-T1	0.342	0.120	Diag. T.	0.108	0.005	0.125	0.32	0.747
					0.500	0.125	0.26	0.747
					0.500	0.108	0.26	0.747

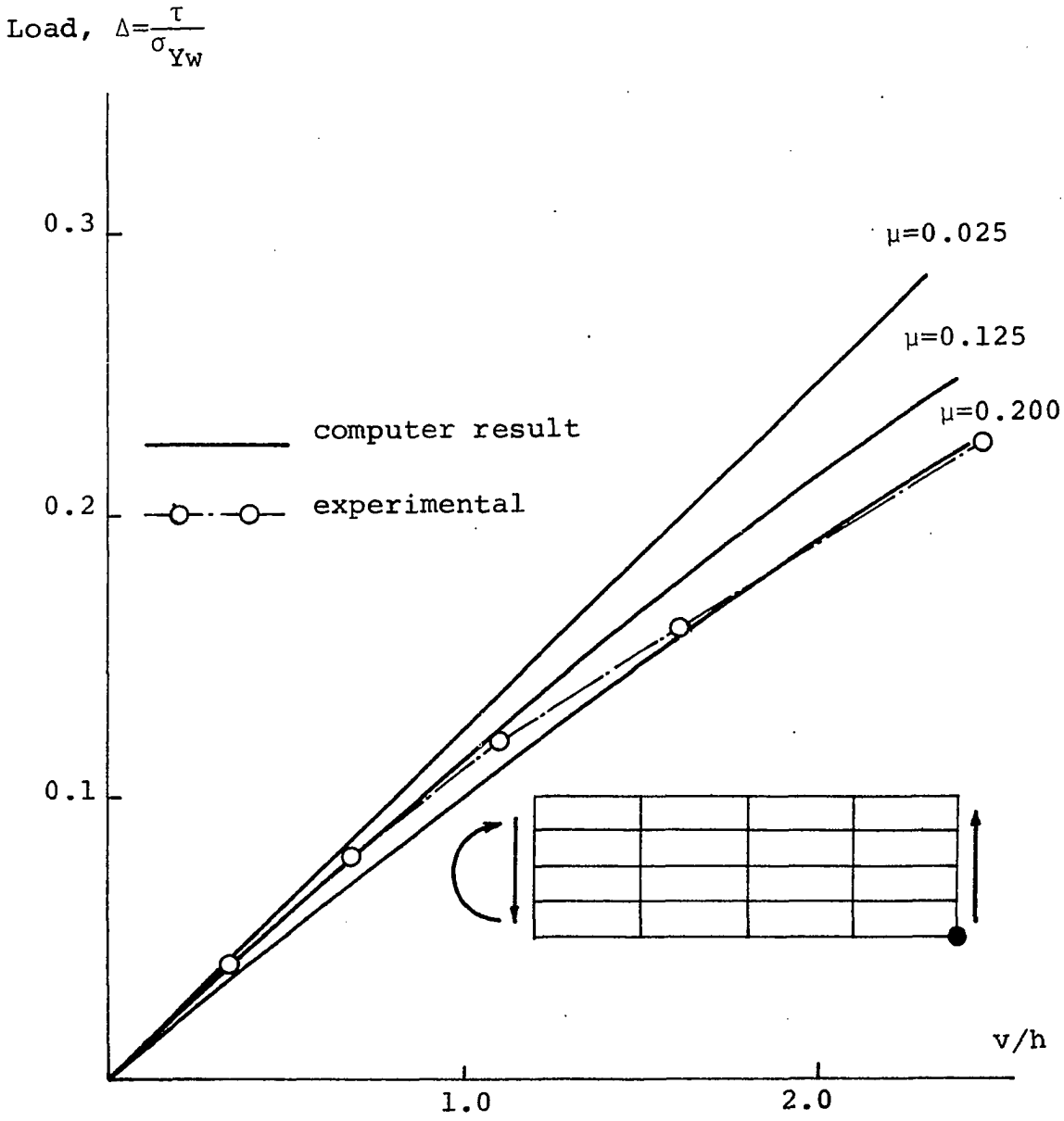

Figure 60. Load-vertical displacement, v curve
Test girder G8-T1: ζ=0.000555

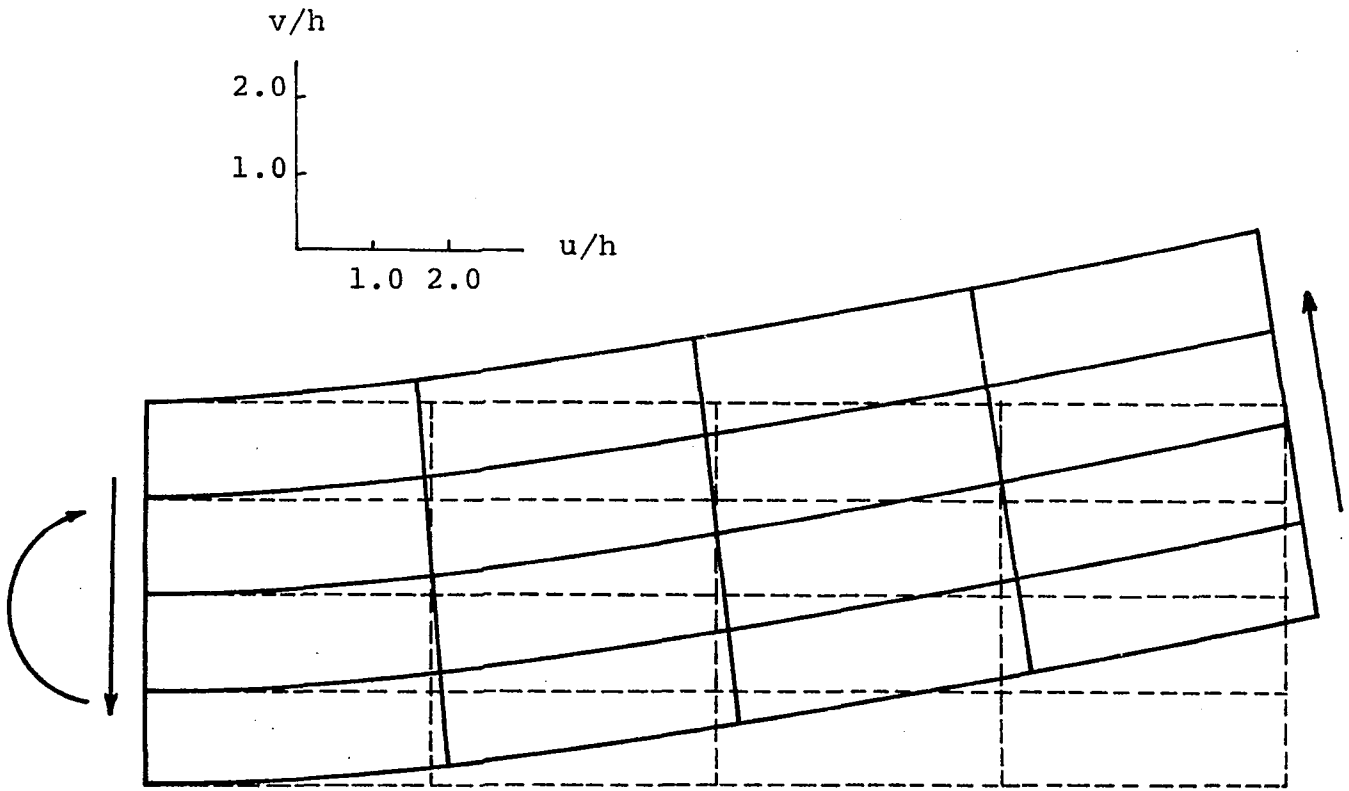

Figure 61. In-plane displacement configuration
Test girder G8-T1: μ=0.1250; ζ=0.000555
Δ=0.24

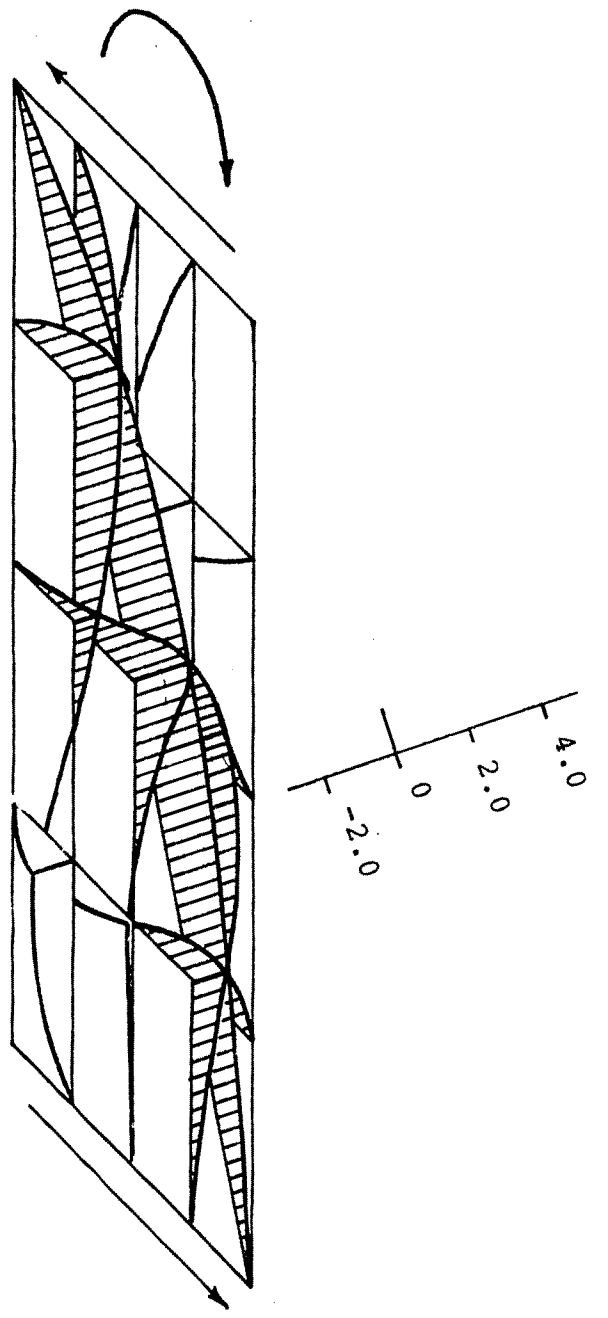

Figure 62. Deflection surface of test girder G8-T1 at $\Delta = 0.26$ w o max = 0.5hi $\sigma_r = 0.005\ \sigma_{yw}$

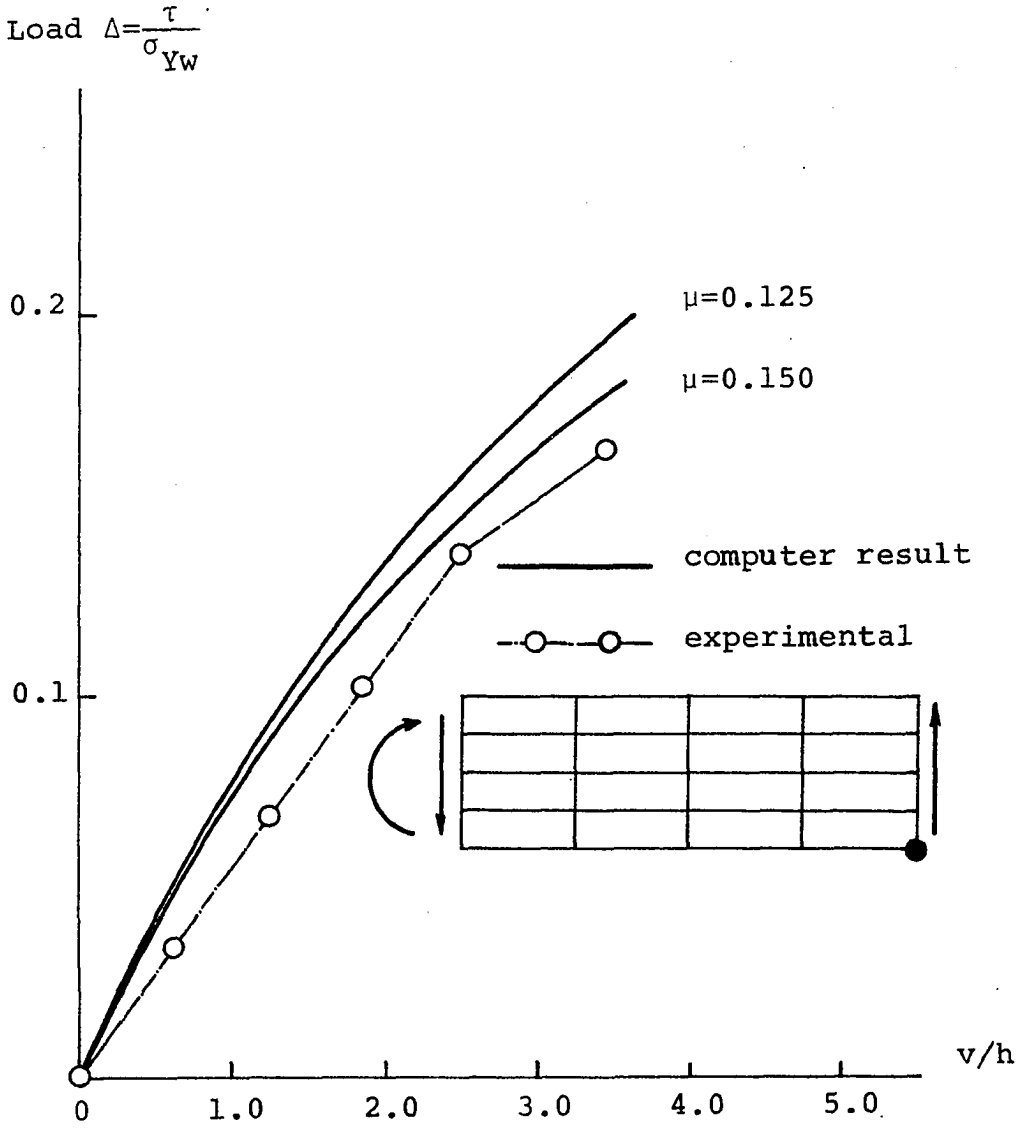

Figure 63. Load-vertical displacement, v curve
Test girder G9-T1: ζ=0.000555

the finite differences which is presented in Appendix B, shows that the 5 x 5 mesh point system gives sufficiently good convergence to the problems considered in this study.

Except for this, an analytical study of accuracy, however, is quite difficult because of the nonlinear nature of the problem. The only other way to establish the degree of accuracy would be by comparing computed results with available experimental results.

It is found through this study that the initial deflection and the initial in-plane stresses are the least known parameters among many parameters considered. The accuracy of the measurements of initial deflection, first of all, may be questioned. Besides, the initial in-plane stresses were not actually measured in any of the tests cited. Information on both of these parameters are needed in the proposed theoretical analysis. Thus, it is impossible to evaluate the accuracy of the method used in a quantitative manner. A discussion of accuracy from a qualitative viewpoint is given in the following based on the general correlation of the computed theoretical results with experimental data and with other theories. Various values of initial deflection and initial in-plane stresses are assumed for theoretical computation.

The load-$\tilde{\sigma}_x$ relationships presented in Figures 27 through 30 indicate that in general good correlations exist between the proposed theory and the experimental results. The load-$\tilde{\sigma}_f$

relationships presented in Figures 26, 31 and 34 and a load-$\tilde{\varepsilon}_f$ relationship presented in Figure 43 also indicate the same trend. Also, the deflectional shapes of webplates obtained by the proposed analysis are found to be governed by 2nd and 3rd order terms. The fact that these shapes are quite reasonable compared to the experimentally observed shapes suggests that the higher order terms are behaving properly. These good correlations indicate that the use of the polynomial series, as well as the use of the 5 x 5 mesh point system for finite differences are in general acceptable.

It is unfortunate that most available and most reliable test data is the ultimate load capacity. Since the proposed theory does not take into consideration the inelastic behavior, the direct correlation of theory and experiment using the ultimate load is impossible. However, advantage is taken of this fact in developing a means to predict ultimate strength using the proposed elastic theory. This is discussed in a later subsection.

Discussions on the Behavioral Results Obtained from the Numerical Computations

In bending case

Deflection surfaces shown in Figures 32, 33 and 41 indicate a fact that the deflection of webplate in the compression zone is more pronounced than that in the tension zone.

It is seen from these deflection surfaces, that the plate bending stress in this compression zone is quite significant.

In-plane displacement configurations show typical cylindrical bending deformation of beam such as the one shown in Figure 42. It is seen that the upper flange undergoes compression and the lower flange undergoes elongation. Furthermore, it is interesting to note that the points which are on a vertical line before loading remain also on the same line with a slope, and that the mesh lines which intersect orthogonally before loading remain orthogonal after loading.

Distributions of $\bar{\sigma}_x$ in general are such that they are almost linear in the tension zone and fairly curved in the compression zone in the webplate as is shown in Figure 39. Also, it is seen that the plate bending stresses σ_{x1} and σ_{x2} are more significant in the compression zone. It may be explained that the reduction of $\bar{\sigma}_x$ in the compression zone is caused by the significant deflection of webplate in this zone.

Load-average flange stress σ_f relationships in Figure 26, 31 and 34, and load-average ε_f relationship in Figure 43 show that these are approximately linear. Furthermore, these relationships are found not significantly affected by the initial deflection. This is thought as quite reasonable, because flanges are tightly connected with the webplate so that the webplate deflection is small near the joints of the flanges and the webplate.

Load-$\tilde{\sigma}_x$ relationships shown in Figures 27, 28, 29, 30, 35, 36, 37, 38 and 44 indicate in general that the portion of a webplate in the compression zone does not carry as much load as that in the tension zone does. In Figure 27, several computer solutions with different magnitudes of initial deflections and initial stresses all coincide approximately with the experimental values. The main reason is thought to be that the plate buckling load for this girder, G1-T1, is very close to the ultimate load so that the deflection of the webplate is not significantly large. In general, it could be observed that the larger the initial deflection is, the smaller $\tilde{\sigma}_x$ becomes in the compression zone.

Figure D.1 in Appendix D, and Figure 40 show P-ε_{bx} diagrams in test girder panel A-M. In Figure D.1, both the 2nd and the 3rd order approximations are shown for comparison. It may be seen that the 3rd order approximation is in better agreement with the experimental results with regard to the magnitude of ε_{bx} and the general trend.

The values of $\Delta_u^{ex}/\Delta_{wcr}$ varies from nearly 1 to 8 in the test girders cited indicating the existence of a significant post-buckling range.

In shear case

Deflection surfaces shown in Figures 48, 52 and 58 indicate outstanding oblique rise in the direction of Diagonal D_1; furthermore, the deflection surfaces are of typical three half-waves peculiar to the shear problem.

In-plane displacement configurations show typical shearing deformation of beam as is illustrated in Figure 59. This figure is seen to be completely different from a bending deformation shown in Figure 42.

Figures 56 and 57 show the distributions of principal stresses $\tilde{\sigma}_1$ and $\tilde{\sigma}_2$. The existence of the diagonal tension field may be seen from these figures together with Figure 58.

Load-$\tilde{\sigma}_1$, $\tilde{\sigma}_2$ relationships shown in Figures 49, 53, 54 and 55 show a general trend that the maximum principal stress tends to increase rapidly with load, while the minimum principal stress tends to creep with load. This trend is very prominent when the magnitude of initial deflection is large.

Figures 45, 46, 50 and 51 illustrate boundary stress distributions, of which Figures 45 and 50 show the effect of beam bending on the flange stress σ_f, and Figures 46 and 51 show the stiffener stresses. The accuracy of the computed stiffener stress is not as good as the in-plane stresses or the plate bending stress as shown in Figure 47. However, the same figure indicates the trend of load-stiffener stress relationship is fairly well represented.

The values of $\Delta_u^{ex}/\Delta_{wcr}$ varies from nearly 2 to 10 indicating the existence of a significant post-buckling range.

Combined case

An in-plane displacement configuration is shown in Figure 61. It is noted that this panel has large curvature

near the left edge and has little curvature near the right edge. This configuration is more or less the combination of the configurations illustrated by Figures 42 and 59.

Figure 60 shows computed and experimental load-v relationship. The trend of these curves coincides with that indicated in Figure 6. Figure 63 shows a relationship similar to Figure 60; however, in this case the relationship is almost linear for the range of Δ from 0 through 0.14.

A deflectional surface is shown in Figure 62. It is seen that this surface is similar to those shown in Figures 48, 52 and 58.

The values of $\Delta_u^{ex}/\Delta_{wcr}$ varies from nearly 2 to 4 indicating the existence of a significant post-buckling range.

Some Discussion on Effect of Parameters

The main parameters involved in the proposed analysis are presented in Chapter Two. Furthermore, parameters for the tested girder panels cited in this dissertation are listed in Table 2. Since the number of parameters involved is considerably large, study of all parameters leads to an enormous task. For this reason, and because of the lack of reliable information on initial deflection and residual stress, the effect of these parameters are studied. The effect of flange rigidity is also studied to some extent.

Range of parameters in the test girder panels

The maximum value and the minimum value of each parameter for the girder panels cited are indicated as follows:

1. Aspect ratio, λ: 0.33 - 1.000,
2. Slenderness ratio, β: 200 - 1145,
3. Rigidity parameters

ϕ_f: 0.305 - 1.140

ϕ'_f: 0.303 - 1.036

ϕ_s: 0.081 - 0.710

ϕ'_s: 0.081 - 0.710

ψ_f: 6.08 - 1536.0

ψ'_f: 6.08 - 191.9

ψ_s: 0.474 - 78.9

ψ_s: 0.474 - 78.9

κ_f: 0.000068 - 0.0669

κ'_f: 0.000037 - 0.0020

Effect of initial deflection

Theoretical determination of the initial deflectional pattern is very difficult because many factors are involved in a sophisticated manner. Previous experiments have shown that the initial deflectional patterns are quite complex and, to some extent arbitrary. Figures 64 and 65 present sketches of the initial deflectional patterns for the test girder panels cited. It is seen that these patterns are quite complex and by no means systematic. Furthermore, in some experiments the test girders were repaired after previous tests. In these cases, the initial deflection patterns depend on the loading history (5).

In all of the computations presented in this thesis, however, the initial deflectional pattern is assumed to be of a cosine wave shape as described by Equation 55. There are two main reasons for this assumption: First, previous experimental results indicate a fact that the most common initial deflectional shape is of one half wave in both x- and y-directions as seen from Figures 64 and 65. Secondly, flanges and

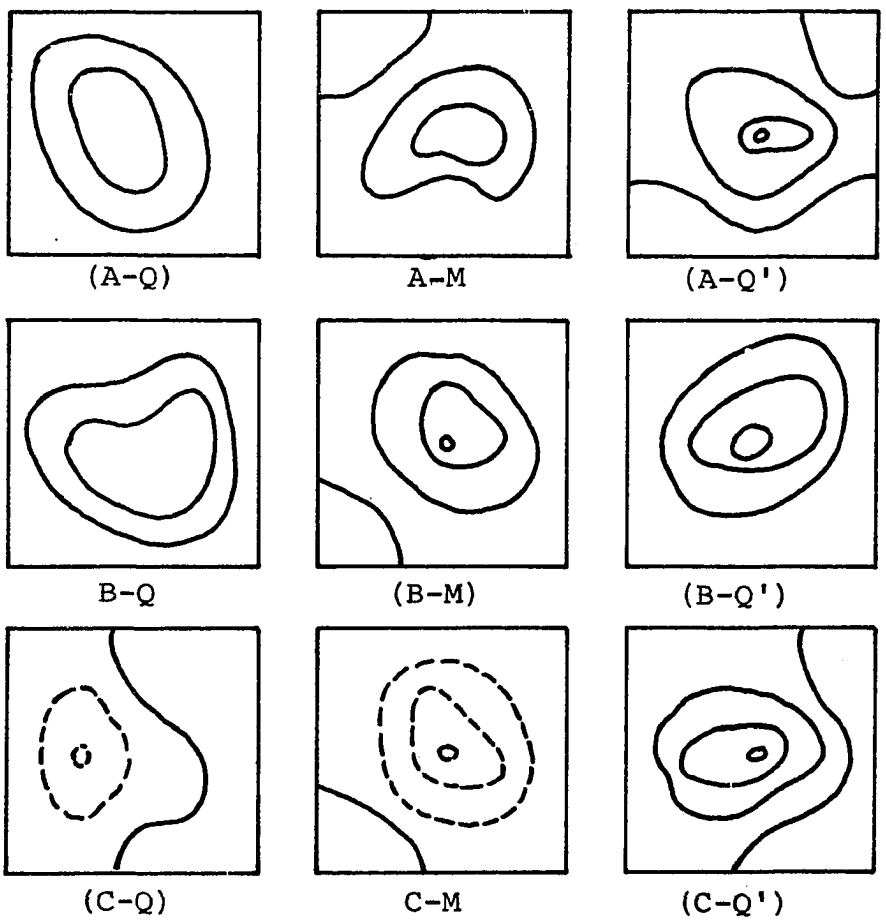

Figure 64. Sketches of total initial deflections for Japanese test girder panels

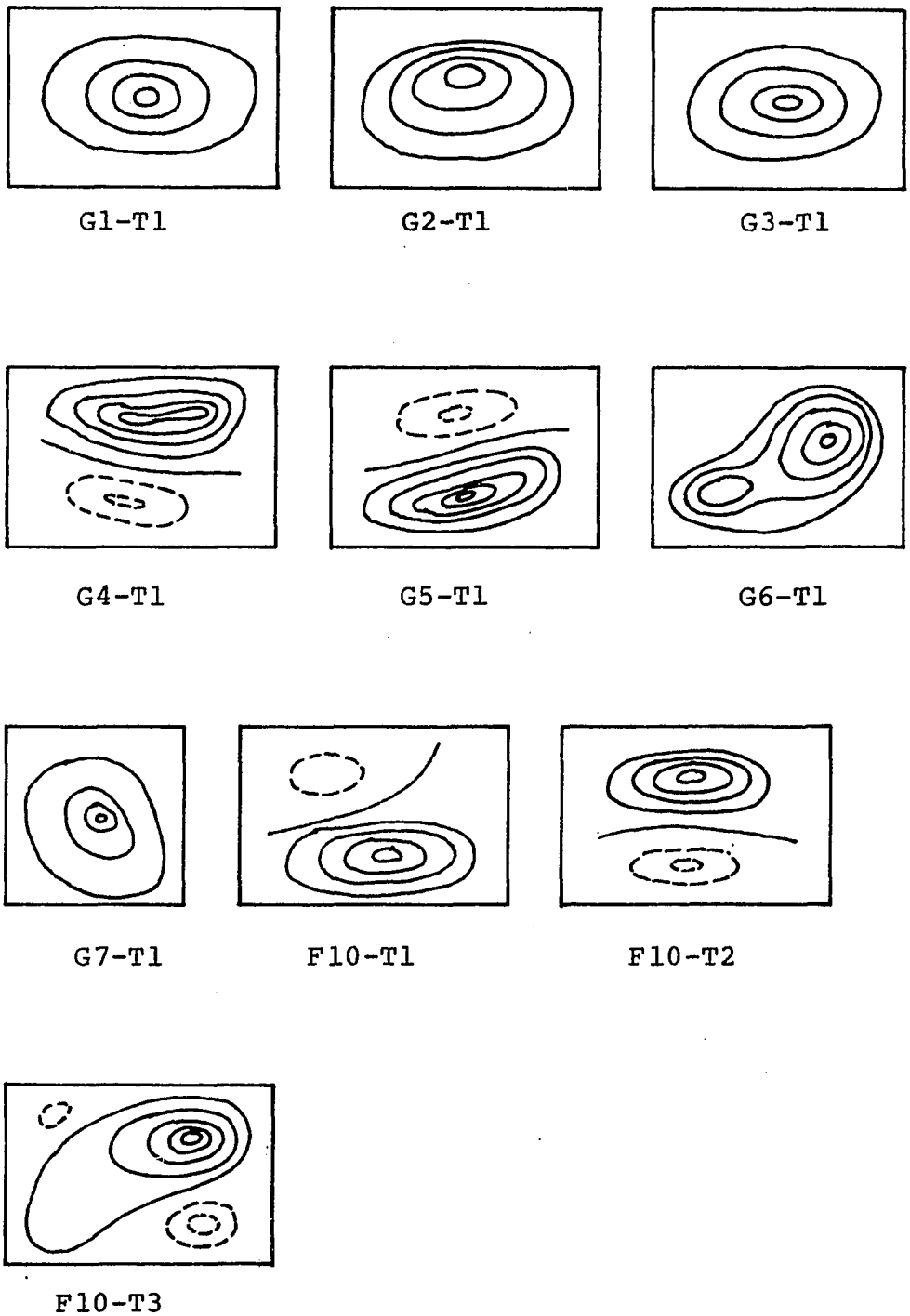

Figure 65. Sketches of total initial deflections for Lehigh test girder panels

stiffeners can be considered not to deform significantly before loads are applied. By virtue of Equation 55, flanges and stiffeners have zero initial deflectional slopes.

It has been assumed in the proposed analysis that the total initial deflection, w_o, consists of the initial elastic deflection, $w^{(0)}$, and the residual deflection of unknown nature. The solutions of the zero order equations indicate that the ratio of the initial elastic deflection, $w^{(0)}$, to the total initial deflection, w_o, is approximately 0.3 for ordinary plate girder panels when the maximum initial stress, σ_r, is one-half of the yield strength of webplate, σ_{Yw}.

The solutions of the higher order equations indicate that when the total initial deflection is 50% of the thickness of the webplate, the ratio of the bending stress component to the in-plane stress component at a point on the webplate can be as high as 40%. It is also found that the larger the initial deflections are, the larger the total deflections become, and that the in-plane displacement components u and v are not as significantly affected as deflection w is by the magnitude of the initial deflection.

Effect of initial in-plane stresses

In the proposed analysis, the distribution of the initial in-plane stresses, or residual stresses, has been determined by modifying that developed by Škaloud and Donea (25). Basler

and others assume that the maximum residual stress, σ_r, is approximately 50% of the yielding strength of steel (4,6). References 10 and 26 suggest that this percentage be lowered for high strength steel. In particular, Reference 28 assumes this percentage to be 50% for ordinary carbon steel and 25% for high strength steel.

The result of the analysis shows that larger residual stresses result in smaller yielding loads as expected. In bending problem, the magnitude of σ_r is found to be very significant with regard to the load at which a panel starts yielding. On the other hand, in shear problem, the maximum residual stress σ_r is found to have less significant effect with regard to the yielding load. Škaloud and Donea concluded in Reference 25 that the residual stresses, generally harmful, may in some cases, represent a real prestressing of webplates subjected to shear. This seems to agree with the statement just mentioned above.

Effect of flange rigidities

In order to see the effect of rigidities of flanges, a cover plate of 22 cm x 0.6 cm is assumed to be welded on top of both upper and lower flanges of test girder panel A-M. The rigidity parameters become larger than before and are given as follows:

$$\phi_f = 0.778; \quad \phi_f' = 0.778,$$

$$\psi_f = 23.7; \quad \psi_f' = 23.7,$$

$$\kappa_f = 0.008; \quad \kappa_f' = 0.008.$$

The result of analysis shows that the ultimate load, Δ_u^{th}, is now 0.95 compared with 0.69 obtained previously. Therefore, the ultimate load is considerably improved by reinforcing flanges as can be expected. Since the buckling load of web-plate remains essentially the same, larger ultimate load implies larger postbuckling strength.

Next, a shear girder panel is considered. Girder panel F10-T3 is chosen for this purpose. First, the thickness of the flanges is doubled. Then,

$$\phi_f = 2.074; \quad \phi_f' = 2.073; \quad \psi_f = 699.2; \quad \psi_f' = 699.2$$

$$\kappa_f = 0.0160; \quad \kappa_f' = 0.0160.$$

The analytical result shows that the ultimate load, Δ_u^{th}, is now 0.42 compared with 0.40 obtained previously. Secondly, the thickness of the flanges is quadrupled. Then,

$$\phi_f = 4.148; \quad \phi_f' = 4.144; \quad \psi_f = 5593.6; \quad \psi_f' = 5593.6$$

$$\kappa_f = 0.1280; \quad \kappa_f' = 0.1280.$$

However, the analytical result shows that Δ_u^{th} is still 0.42. This implies that excessive reinforcement on flanges does not lead to significant improvement on the load carrying capacity of girder panels in shear. In this respect, it is found that the flanges in the shear panels behave quite differently from flanges in the bending panels.

Prediction of Ultimate Load by the Proposed Analysis

A good correlation is found in the prediction of the ultimate load between the results from the proposed analysis and the experimental results when the maximum total initial deflection is assumed to be 10% of the thickness of webplate in the bending problem and 50% of the same in the shear problem, respectively, while initial in-plane stress is assumed to be negligibly small. It is also found that use of these assumed parameters results in good prediction of the post-buckling behavior. Table 18 shows the ultimate loads for the tested girder panels cited when the initial deflections and initial in-plane stresses are assumed as mentioned above. No similar correlation is given in the combined loading cases because of insufficient data.

Table 18. Prediction of ultimate load

Girder Panel	Type of Loading	Exp. Load Δ_u^{ex}	Basler's Δ_u^{B}	Proposed Δ_u^{th}
G1-T1	Moment	0.242	0.218	0.210
G2-T1	Moment	0.378	0.394	0.400
G3-T1	Moment	0.381	0.370	0.420
G4-T1	Moment	0.563	0.562	0.610
G5-T1	Moment	0.495	0.479	0.680
A-M	Moment	0.640	0.629	0.690
C-M	Moment	0.555	0.464	0.555
G6-T1	Shear	0.328	0.317	0.260
G7-T1	Shear	0.389	0.395	0.360
F10-T2	Shear	0.371	0.364	0.380
F10-T3	Shear	0.382	0.407	0.400
B-Q	Shear	0.282	0.338	0.280

$\frac{\Delta_u^{th}}{\Delta_u^{ex}}$	Initial Deflection μ	Residual Stress σ_r/σ_{Yw}	Theoretical Failure Mode
0.87	0.025	0.005	Torsional B.
1.06	0.025	0.005	Lateral B.
1.10	0.025	0.005	Lateral B.
1.08	0.025	0.005	Lateral B.
1.37	0.025	0.005	Lateral B.
1.08	0.025	0.005	Torsional B.
1.00	0.025	0.003	Torsional B.
0.79	0.125	0.005	Diag. Tens.
0.93	0.125	0.005	Diag. Tens.
1.02	0.125	0.005	Diag. Tens.
1.05	0.125	0.005	Diag. Tens.
0.99	0.125	0.003	Diag. Tens.

CHAPTER FOUR: SUMMARY AND CONCLUSIONS

Summary

A theoretical approach to the postbuckling problem of plate girder webplates is proposed and presented in this dissertation.

The purpose of the study is described and its significance in the light of past investigations is explained in Chapter One.

The basic concept, assumptions and the detailed method of approach to the problem are described in Chapter Two. The main feature of the proposed analysis is the use of a method similar to perturbation method as well as the finite difference method in solving a set of von Kármán's nonlinear partial differential equations.

A number of tested plate girder panels are reviewed and the comparison is made between the results from the proposed analysis and the experimental results in Chapter Three. Based on this comparison, the accuracy of the proposed analysis as well as the effect of parameters such as initial deflection, residual stresses and flange rigidities, are studied. To conclude the Chapter, prediction of the postbuckling behavior and the ultimate strength by means of the proposed analysis is discussed.

Conclusions

Fairly good agreement is found between the proposed theoretical analysis and the experimental results cited. This proves the validity and general accuracy of the proposed analysis. The mechanical model considered herein proves to be a satisfactorily good representation of the actual girder panels. The method of approach, especially the use of a perturbation method and a finite difference method, proves to be quite applicable.

Following conclusions are drawn based on the analysis of computed results presented in Chapter Three.

1. The larger the initial deflection is, the larger the final deflection becomes. The in-plane displacement components, however, are not significantly affected by the initial deflection.

2. Larger initial deflection causes more curved load-displacement and load-stress relationships.

3. The pattern of the initial deflection does not necessarily cause a similar deflectional shape in the webplate due to load.

4. Larger boundary rigidity leads, in general, to more stable behavior of the panel in the post-buckling range. However, excessive reinforcement of the boundary members does not prove to be beneficial in the case of shear problem.

5. The larger the yield strength of the steel is, the larger the post-buckling strength becomes.

6. The ultimate load carrying capacity of a bending panel is controlled by torsional buckling of the compression flange, or lateral buckling.

7. The ultimate load carrying capacity of a shear panel is controlled mainly by the yield strength of webplate. The mode of failure is the formation of diagonal tension field.

8. The ultimate load carrying capacity of a panel in shear and bending combined is controlled by the yielding in the diagonal tension action rather than lateral or torsional buckling.

9. The larger the residual stresses are, the sooner the webplate initiates yielding.

10. Good prediction of ultimate loads and post-buckling behavior of girder panels can be obtained by the proposed theory using the following values for the initial deflection and the residual stresses:

Maximum residual stress, σ_r: negligibly small=0.005 σ_{Yw} or less

Maximum total initial deflection, w_{omax}:

0.1 h for bending panels

0.5 h for shear panels.

Recommendation for Future Study

The proposed method of analysis limits itself to elastic behavioral study of plate girder panels. This restriction makes the prediction of the true load carrying capacity incomplete, since in most cases, the behavior of plate girder panels is elasto-plastic after certain loading levels.

Among parameters influencing the behavior of girder panels, two parameters deserve more extensive study. One is the initial residual stress distribution, and the other the initial deflection. In future experimental work, the more detailed study of these two parameters is highly recommended.

In summary, the following items are recommended for future work:

1. Elasto-plastic analysis making use of the plasticity laws and the large deflection theory of plates,

2. Investigation of initial stress due to welding in terms of its magnitude and distribution, and its effect on the post-buckling behavior of girder panels,

3. Investigation of initial deflection in terms of its causes, distribution shapes and magnitude as well as its effect on the post-buckling behavior of girder panels.

ACKNOWLEDGMENTS

The author wishes to express his hearty gratitude to one of his major professors, Dr. Ti-Ta Lee, for his direct guidance in the author's graduate program of study, precious directions and suggestions throughout the author's dissertation, his warm encouragement and strong patience which never failed. He also wishes to express his hearty gratitude to another major professor, Dr. R. E. Untrauer, for his kind guidance throughout the author's graduate program of study.

The author wishes to extend his appreciation to the author's former major professor, Dr. H. A. Elleby, for his precious suggestions in the author's dissertation.

The appreciation is also extended to his fellow student, J. G. Arendts, for his valuable suggestions and useful discussions on the author's dissertation.

This study is sponsored by the Engineering Research Institute of Iowa State University. The numerical computations were performed by IBM 360 at the Computer Center of Iowa State University, Ames, Iowa.

LITERATURE CITED

1. Alexeev, S. A. A postcritical study of flexible elastic plate. Applied Mathematics and Mechanics (Moscow) 20, No. 6: 673-679. 1956.

2. Basler, K. Strength of plate girders in shear. American Society of Civil Engineers Proceedings 87, No. ST7: 151-180. 1961.

3. Basler, K. Strength of plate girders under combined bending and shear. American Society of Civil Engineers Proceedings 87, No. ST7: 181-197. 1961.

4. Basler, K. and Thurlimann, B. Strength of plate girders in bending. American Society of Civil Engineers Proceedings 87 , No. ST6: 153-181. 1961.

5. Basler, K., Yen, B. T., Mueller, J. A. and Thurlimann, B. Web buckling tests on welded plate girders. Welding Research Council Bulletin Series 64. 1960.

6. Beedle, L. S., Blackman, J. H., Cooper, P. B., Driscoll, G. C., Jr. and Eney, W. J. Structural steel design. Ronald Press Inc., New York, New York. 1964.

7. Cook, I. T. and Rocky, K. C. Shear buckling of clamped and simply supported infinitely long plates reinforced by transverse stiffeners and a central longitudinal stiffener. Aeronautical Quarterly 13, No. 2: 95-114. 1962.

8. Cook, I. T. and Rocky, K. C. Shear buckling of clamped and simply supported infinitely long plates reinforced by closed-section transverse stiffeners. Aeronautical Quarterly 13, No. 3: 212-222. 1962.

9. Cook, I. T. and Rocky, K. C. Shear buckling of rectangular plates with mixed boundary conditions. Aeronautical Quarterly 14, No. 4: 349-356. 1963.

10. Cooper, P. B., Lew, H. S. and Yen, B. T. Welded constructional alloy steel plate girders. American Society of Civil Engineers Proceedings 90, No. ST1: 1-36. 1964.

11. Djubek, J. Lösung des nichtlinearen Problems bei Wanddeformationen. International Association for Bridges and Structural Engineering Publications 23: 91-110. 1963.

12. Frost, R. W. and Schilling, C. G. The behavior of hybrid beams subjected to static loads. American Society of Civil Engineers Proceedings 90, No. ST3: 55-88. 1964.

13. Gaylord, E. H. Discussion for strength of plate girders in shear. American Society of Civil Engineers Proceedings 88, No. ST2: 151-154. 1962.

14. Haaijer, G. and Thurlimann, B. On inelastic buckling in steel. American Society of Civil Engineers Proceedings 84, No. EM2: 308-344. 1958.

15. Kármán, von T. Festigkeitsprobleme im Maschinenbau. Encyklopadie der Mathematischen Wissenschaften IV, No. 4: 311-385. 1910.

16. Kármán, von T., Sechler, E. E. and Donnell, L. H. The strength of thin plates in compression. American Society of Mechanical Engineers Transactions 54, No. 2: 53-57.

17. Mansfield, E. H. The bending and stretching of plates. International Series of Monographs on Aeronautics and Astronautics 6. 1964.

18. Mansfield, E. H. Some identifies on structural flexibility after buckling. Aeronautical Quarterly 9: 300-304. 1958.

19. Massonnet, C. Buckling experiments on girders with stiffened web. International Association for Bridges and Structural Engineering Publications 14: 125-186.

20. Massonnet, C., Mas, E. and Maus, H. Buckling tests on two plate girders with tubular flanges and stiffeners. International Association for Bridges and Structural Engineering Publications 22: 183-228. 1962.

21. Mueller, J. A. and Yen, B. T. Girder web boundary stresses and fatigue. Welding Research Council Bulletin 127. 1968.

22. Patterson, P. J., Corrado, J. A., Huang, J. S. and Yen, B. T. Proof-tests of two slender-web welded plate girders. Fritz Engineering Laboratory, Department of Civil Engineering, Lehigh University, Fritz Engineering Laboratory Report No. 327.7. 1969.

23. Rao, N. R. N. and Tall, L. Residual stresses in welded plates. Fritz Engineering Laboratory, Department of Civil Engineering, Lehigh University, Fritz Engineering Laboratory Report No. 249.7. 1960.

24. Rockey, K. C. and Leggett, D. M. A. The buckling of plate girder web under pure bending when reinforced by a single longitudinal stiffener. Institution of Civil Engineering Proceedings 21: 161-188. 1962.

25. Škaloud, M. and Donea, J. Post-critical behavior of webs with residual stresses. International Association for Bridges and Structural Engineering Publication 23: 293-320. 1963.

26. Stein, M. Behavior of buckled rectangular plates. American Society of Civil Engineers Proceedings 86, No. EM2: 59-76. 1960.

27. Stein, M. Loads and deformations of buckled rectangular plates. National Aeronautics and Space Administration Technical Report No. R40. 1959.

28. Theory and Experiments on the load carrying capacity of plate girders (translated). Kansai Symposium on Bridges, Steel Frames and Welding. Nippon Publishing Company Inc., Osaka, Japan. 1965.

29. Timoshenko, S. P. and Gere, J. M. Theory of elastic stability. Second edition. McGraw-Hill Book Company, Inc., New York, New York. 1961.

30. Yamaki, N. Experiments on the postbuckling behavior of square plates loaded in edge compression. American Society of Mechanical Engineers Journal of Applied Mechanics 28: 238-244. 1961.

31. Yamaki, N. Postbuckling behavior of rectangular plates with small initial curvature loaded in edge compression. American Society of Mechanical Engineers Journal of Applied Mechanics 26: 407-414. 1959.

APPENDIX A: CRITERIA FOR BUCKLING

Vertical Buckling of Flange

When a plate girder is bent, the deflectional curvature gives rise to transverse flange force components. As a result, a uniform compressive stress acts on the upper and lower edge of the webplate through the flanges. Therefore, it is possible for this compressive stress to cause the webplate to buckle just like a column. It has been found (4) that if the webplate has a slenderness ratio β' less than the following value:

$$\beta_v = \sqrt{\frac{\pi^2 E}{24(1-\nu^2)} \frac{A_w}{A_f} \frac{1}{\sigma_f \varepsilon_f}} = 0.673\ E \sqrt{\frac{\lambda}{\phi_f} \frac{1}{\sigma_{Yf}(\sigma_{Yf}+\sigma_r)}}\ , \qquad (A.1)$$

then, it is safe against the vertical buckling of flange.

Lateral Buckling of Girder

When a plate girder is subjected to bending, this mode of failure sometimes governs the strength of the girder. The mode of failure is such that the whole cross section of the girder rotates about the axis of the tension flange. A typical buckling curve is shown in Figure A.1 (4). This curve is based on the maximum value of residual stress σ_r = 0.5 σ_{Yf}. Curve I is a transition curve from an Euler's

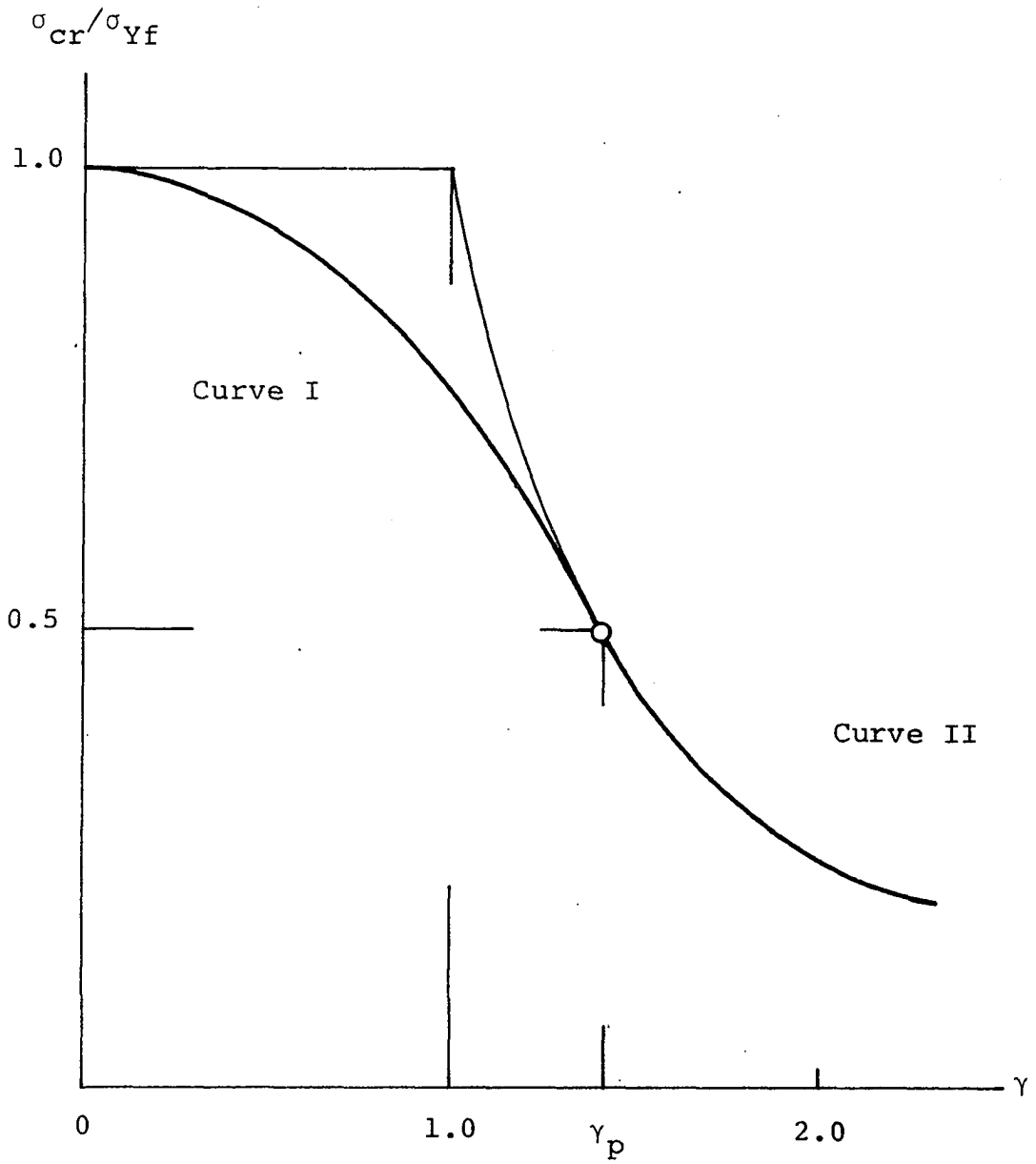

Figure A.1. Lateral buckling curve

buckling curve and reflects the significant effect of residual stress. Curve II is the Euler's buckling curve. For this case of maximum residual stress $\sigma_r = 0.5\ \sigma_{Yf}$, the buckling stress is obtained by Basler (4) as follows:

$$\frac{\sigma^L_{cr}}{\sigma_{Yf}} = 1 - \frac{1}{4}\gamma^2 \qquad \text{for } 0 < \gamma \leq \gamma_p = \sqrt{2}$$

$$= \frac{1}{\gamma^2} \qquad \text{for } \gamma > \gamma_p = \sqrt{2} \qquad \text{(A.2)}$$

where

$$\gamma = \frac{\ell_k}{r}\sqrt{\frac{\varepsilon_Y}{\pi^2}} = \frac{k}{\pi}\sqrt{\frac{6A_f + A_w}{6I_f} \cdot \varepsilon_Y}$$

However, for some different value of the maximum residual stress, σ_r, a different transition curve should be used. It is reasonable to assume this transition curve in the following general form (14).

$$\frac{\sigma^L_{cr}}{\sigma_{Yf}} = 1 - \frac{\sigma_r}{\sigma_{Yf}}\left(\frac{\gamma}{\gamma_p}\right)^n \qquad \text{(A.3)}$$

The term on the left assumes a value of 1.0 when $\gamma = 0$, and $1.0 - \sigma_r/\sigma_{Yf}$ when $\gamma = \gamma_p$. It is required that the Euler's curve and the transition curve intersect and their tangents be the same at $\gamma = \gamma_p$. From these two conditions, the power index n and the parameter γ_p are determined as follows (14):

$$\gamma_p = \frac{1}{\sqrt{1.0 - \sigma_r/\sigma_{Yf}}} \text{ , and}$$

$$n = 2\ (\sigma_{Yf}/\sigma_r - 1) \qquad \text{(A.4)}$$

Torsional Buckling of Compression Flange

This failure is also one of the typical failures in plate girders subjected to bending moment. The compression flange by itself buckles as a plate in this failure. Similar to the case of lateral buckling, the buckling stress can be obtained as follows (14):

$$\frac{\sigma^T_{cr}}{\sigma_{Yf}} = 1 - \frac{\sigma_r}{\sigma_{Yf}} \left(\frac{\gamma-\gamma_o}{\gamma_p-\gamma_o}\right)^n \qquad \text{for } \gamma_o<\gamma<\gamma_p$$

$$= 1/\gamma^2 \qquad \text{for } \gamma>\gamma_p$$

where

$$\gamma = \frac{c_f}{t_f}\sqrt{\frac{12(1-\nu^2)\varepsilon_y}{\pi^2 K}} \qquad \text{(A.5)}$$

with the value of K suggested to be taken as 0.425 (4). It is required that the Euler's curve and the transition curve intersect and their tangents be the same at $\gamma = \gamma_p$. From these conditions, γ_p and n are determined as follows (14):

$$\gamma_p = 1/\sqrt{1.0-\sigma_r/\sigma_{Yf}} \quad , \quad \text{and}$$

$$n = 2\,\frac{\gamma_p - \gamma_o}{\gamma_p(\gamma_p^2-1)} \tag{A.6}$$

It is suggested that the value of γ_o be taken as 0.46 (4).

Figure A.2 provides a typical torsional buckling curve. Curve II is the Euler's buckling curve, and Curve I is the transition curve.

In order that the torsional buckling precedes the lateral buckling of girder the following inequality should be satisfied (4):

$$2\beta_f > 12 + \frac{1}{2}\,\frac{\ell_k}{c_f}$$

where $\beta_f = c_f/t_f$

ℓ_f = lateral buckling length (A.7)

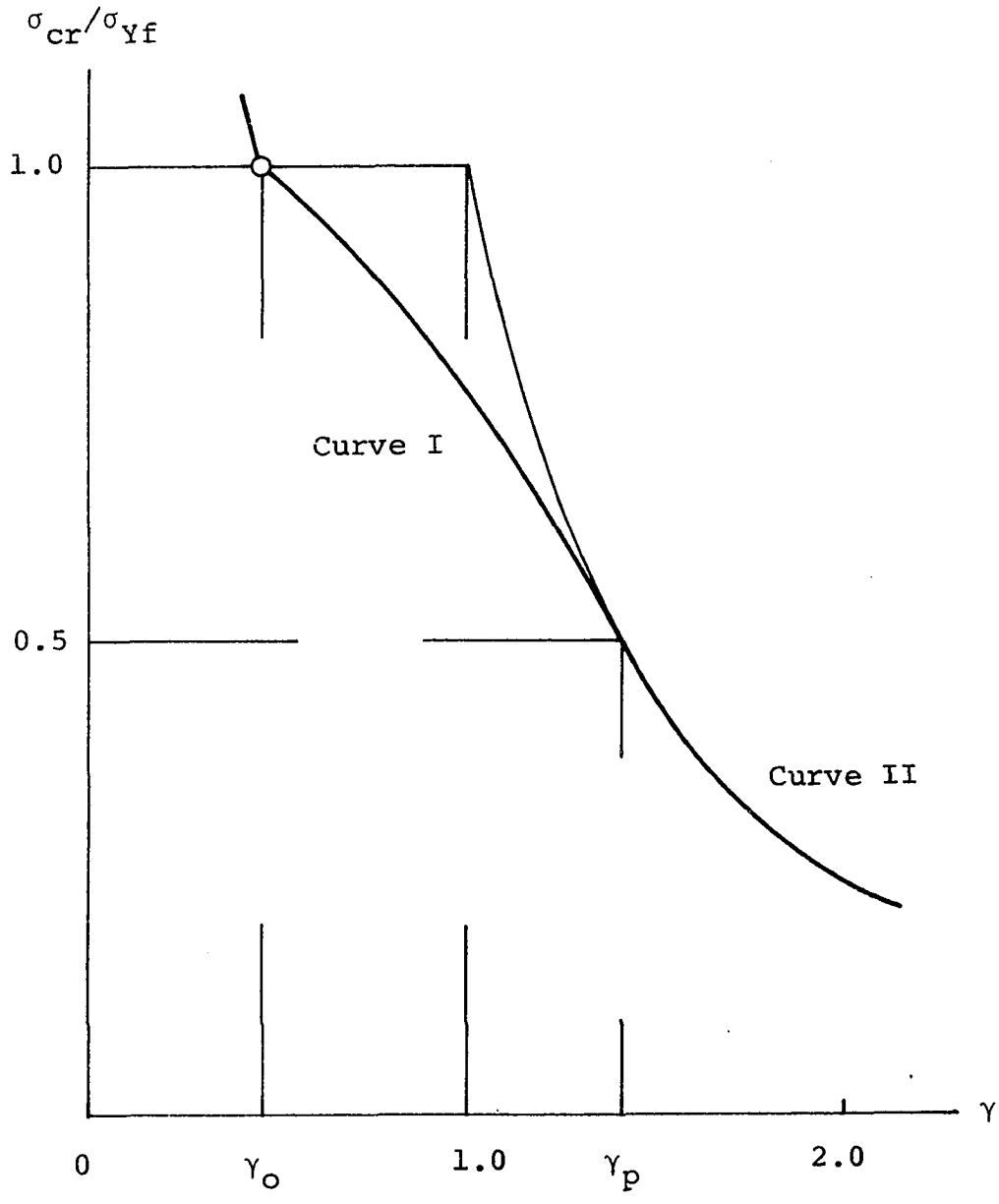

Figure A.2. Torsional buckling curve

APPENDIX B: CONVERGENCE CHECK WITH RESPECT TO DIMENSION OF MESH POINT SYSTEM

Choice of 5 x 5 Mesh Point System

The computer program developed in this study is generally applicable for any dimension of mesh point system, N. In Chapter Three, the computations are based on 5 x 5 mesh point system. In this appendix, it is shown that the choice of N = 5 is a good representation of the mechanical model used in the study. It is true that the larger the value of N, the more accurate the solutions get. On the other hand, the value of N should be determined so that the solution yields reasonably good accuracy and yet does not require excessive computer time.

The convergence for the zero order equation is studied first. This is followed by the convergence study for the higher order equations.

Zero order equation

Equation 52 is solved repeatedly by varying the value of N. The parameters used for this purpose are as follows:

$\alpha = 0.000667$; $\zeta = 0.5$; $\mu = 0.67$; $\lambda = 1.0$; $\beta = 266.7$

$\psi_f = 21.3$; $\psi_f' = 21.3$; $\psi_s = 10.8$; $\psi_s' = 10.8$

The result of the convergence study is presented in Figure B.1. Judging from the convergence curve, the true value for the

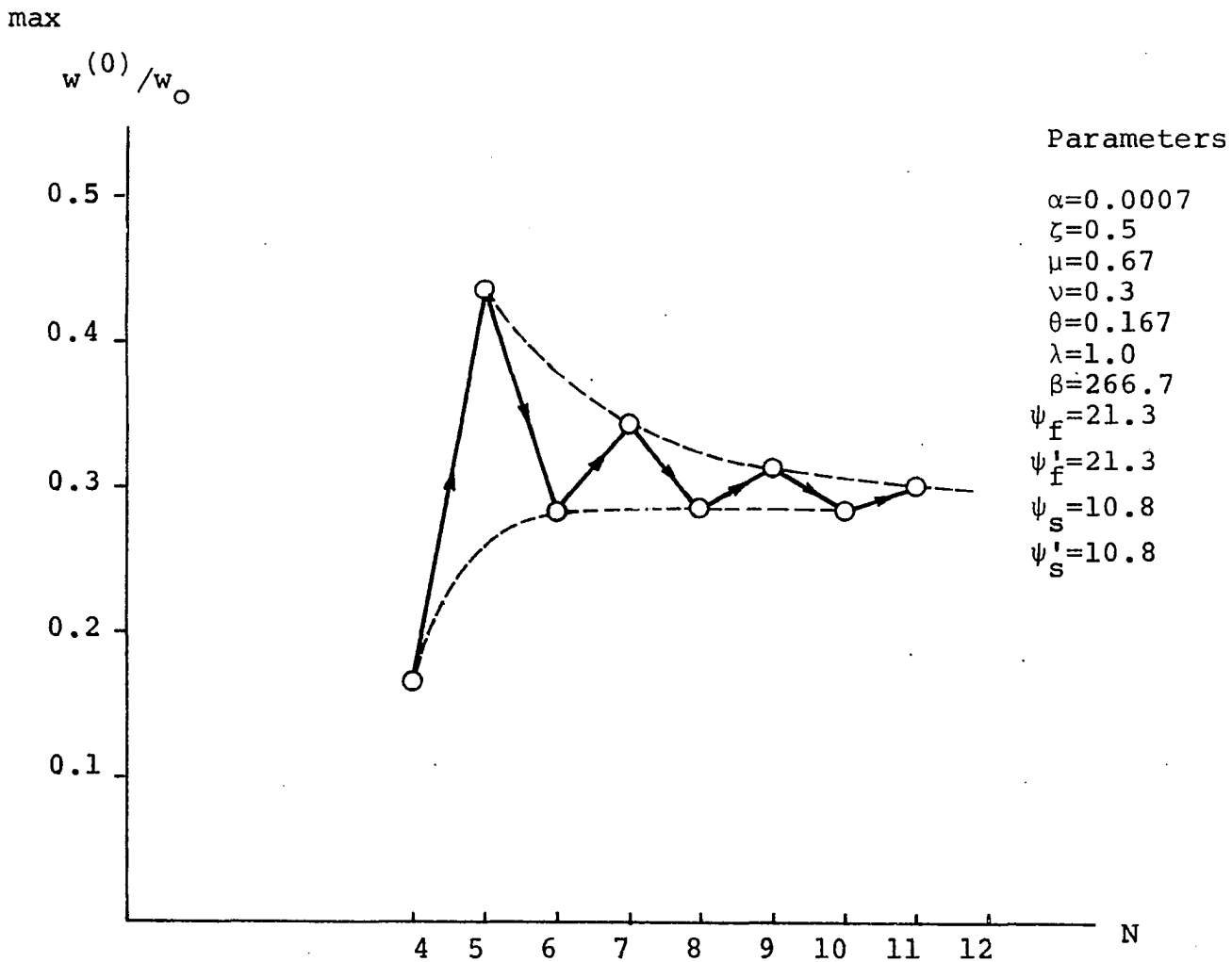

Figure B.1. Convergence curve for maximum $w^{(0)}/w_o$

maximum $w^{(0)}$ would be 0.299 by observation. The convergence is obtained in the following manner:

N	4	5	6	7	8	9	10	11
$w^{(0)}_{max}$	0.167	0.436	0.284	0.345	0.286	0.315	0.286	0.301
$w^{(0)}_{max}/.299$	0.559	1.460	0.950	1.155	0.957	1.055	0.957	1.008

Therefore, the use of the 5 x 5 mesh point system overestimates the true solution by 46% error. The use of the 7 x 7 mesh point system overestimates the true solution by 15.5% error. Although the zero order approximation yields 46% of error on the 5 x 5 mesh point system, the solution $w^{(0)}$, however, affects only the zero order plate bending stress components. The contribution of the zero order plate bending stress components is less than 10% of the total plate bending stresses.

Higher order equations

The convergence check is done for Girder A-M, a girder in bending; and for Girder B-Q, a girder in shear.

Girder A-M in bending The parameters used are as follows:

$\alpha = 0.00000667$; $\zeta = 0.005$; $\mu = 0.167$; $\lambda = 1.000$

$\beta = 267$; $\phi_f = 0.533$; $\phi'_f = 0.533$; $\phi_s = 0.400$; $\phi'_s = 0.400$

$\psi_f = 21.3$; $\psi'_f = 21.3$; $\psi_s = 8.95$; $\psi'_s = 8.95$; $\psi'_s = 8.95$

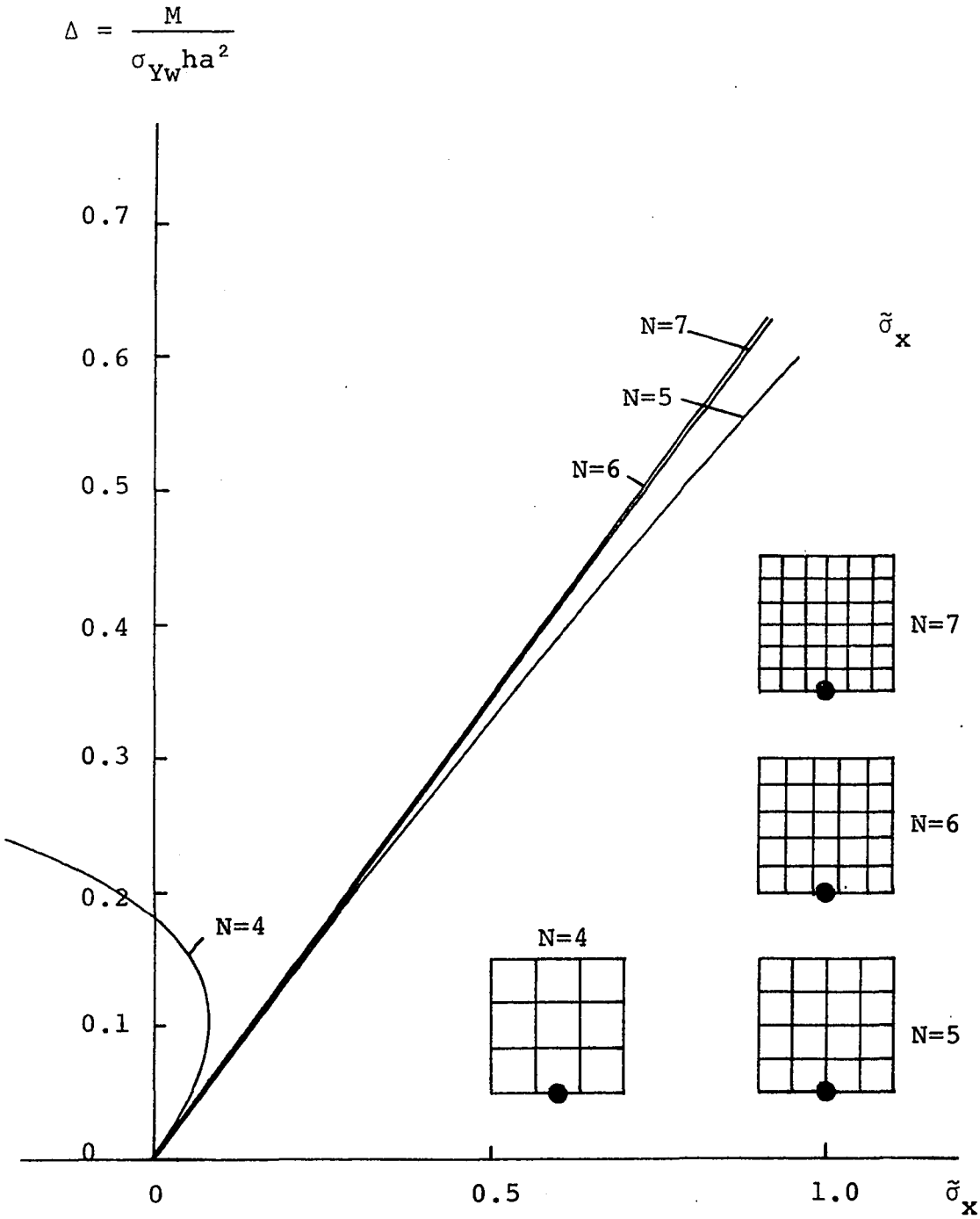

Figure B.2. Load-$\tilde{\sigma}_x$ curve: Test girder panel A-M

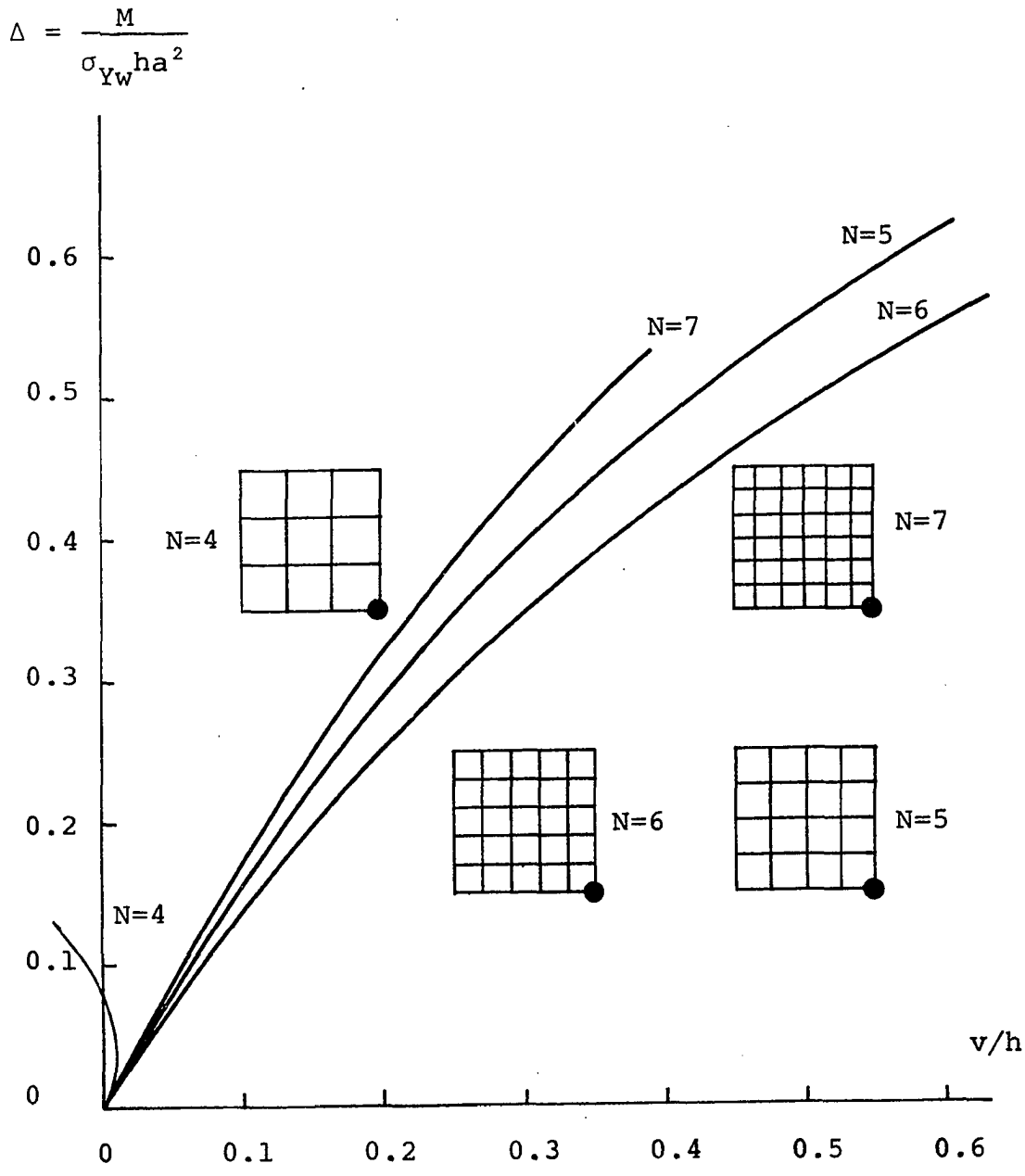

Figure B.3. Load-$\tilde{v}$ curve: Test girder panel A-M

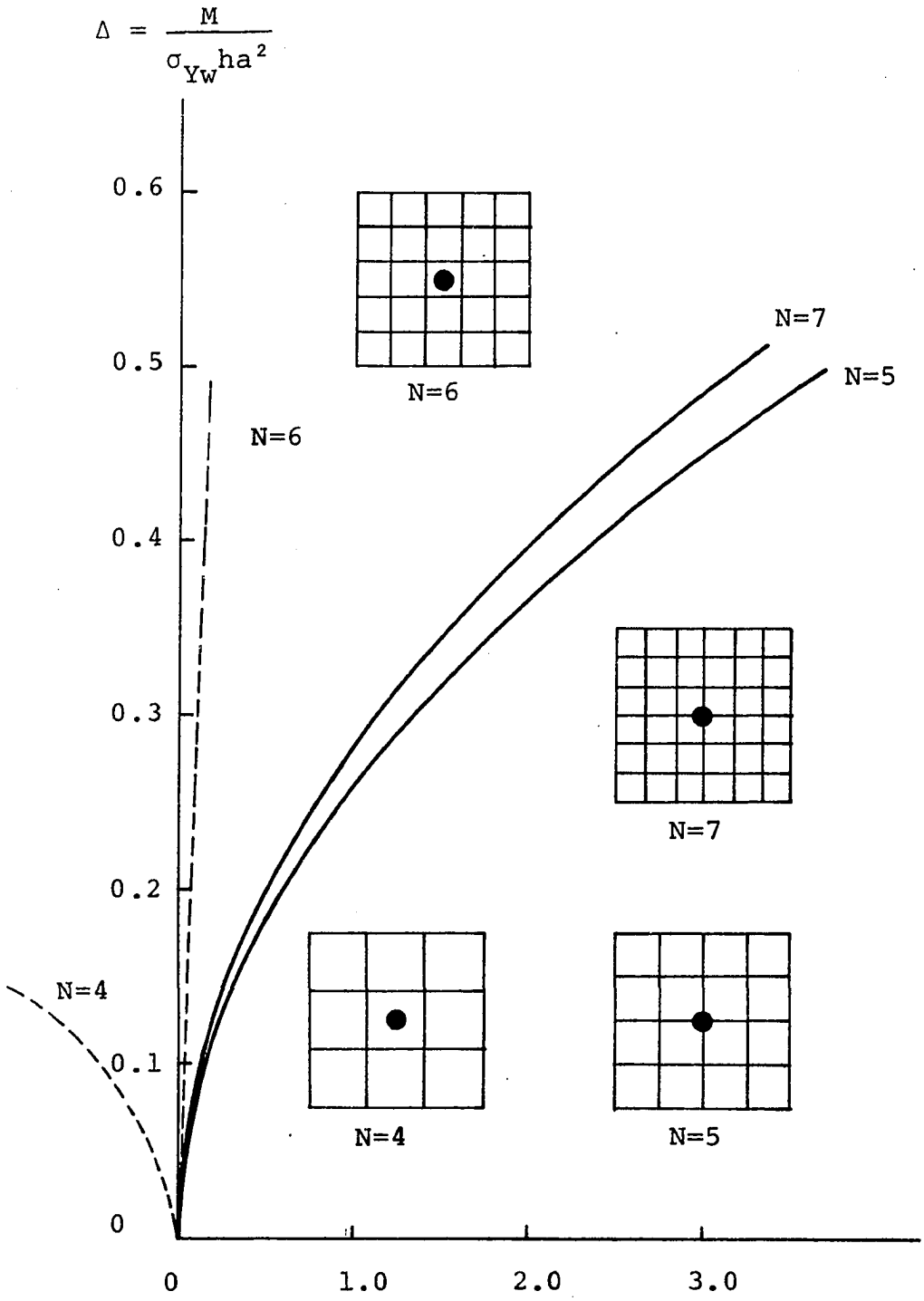

Figure B.4. Load-deflection curve: Test girder panel A-M

values of N. It is found that the 4 x 4 mesh point system is too coarse and the results are far off from those results for N = 5. It is seen that the 5 x 5 mesh point system is a fairly good representation.

Girder B-Q in shear The parameters used are as follows:

$\alpha = 0.00000595$; $\zeta = 0.0025$; $\mu = 0.025$; $\theta = 0.1667$

$\lambda = 1.00$; $\beta = 266.7$; $\phi_f = 0.533$; $\phi_f' = 0.533$; $\phi_s = 0.400$

$\phi_s' = 0.400$; $\psi_f = 21.3$; $\psi_f' = 21.3$; $\psi_s = 8.95$; $\psi_s' = 8.95$

$\kappa_f = 0.00026$; $\kappa_f' = 0.00026$

Figure B.5 shows the convergence of the von Mises comparison stresses, $\tilde{\sigma}_{vM}$, $\tilde{\sigma}_{vM1}$ and $\tilde{\sigma}_{vM2}$. It is seen that $\tilde{\sigma}_{vM}$ converges very rapidly. Figure B.6 and Figure B.7 show the convergence for the in-plane displacement component, v. Figure B.7 shows that the 5 x 5 mesh point system is a good representation. Figure B.8 shows the convergence of the deflection, w. Results for N=4 and N=6 are not presented because of the fact that the central point is not included in these mesh point systems. Fairly good convergence is observed.

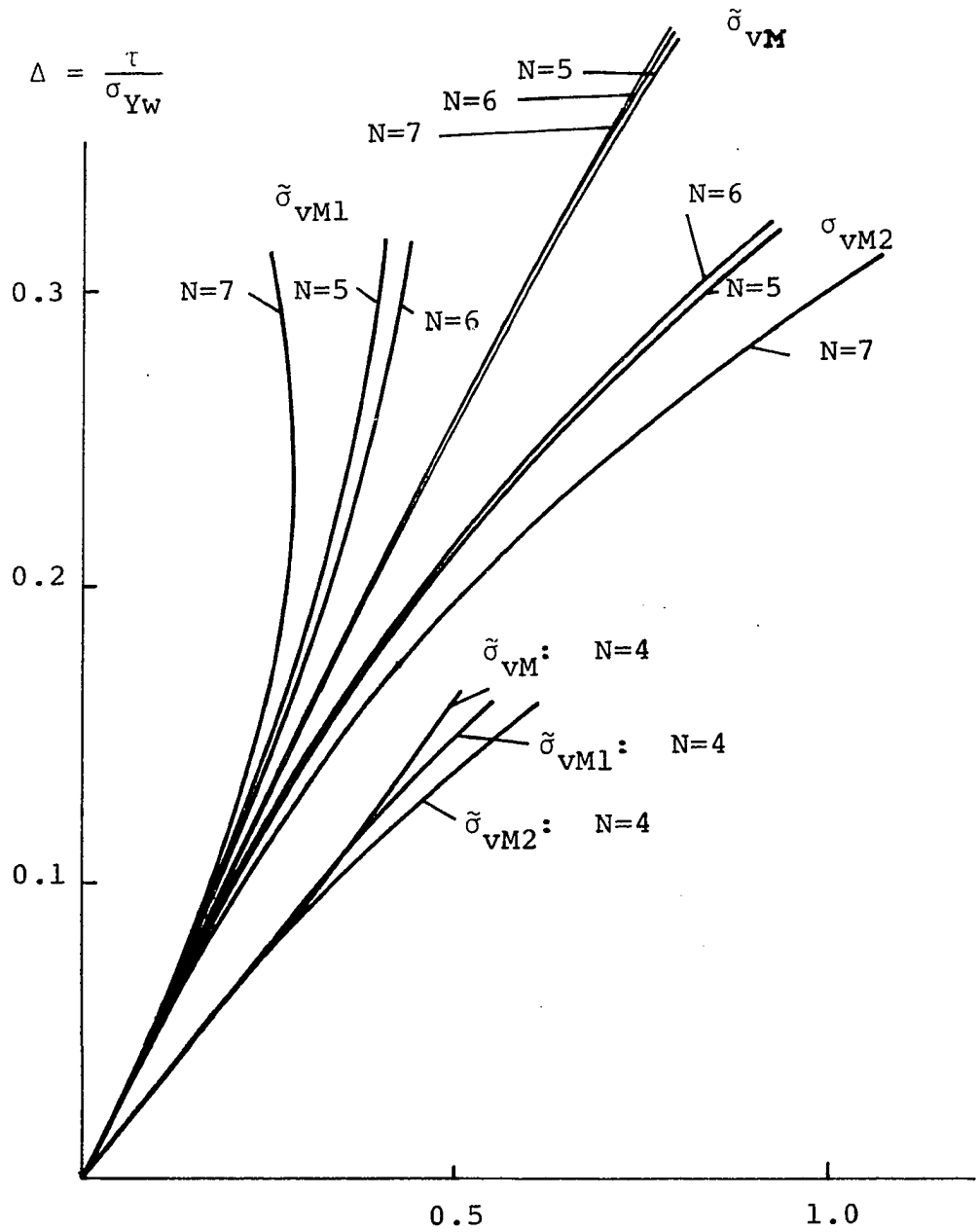

Figure B.5. Convergence of von Mises stresses, $\tilde{\sigma}_{vM}$, $\tilde{\sigma}_{vM1}$ and $\tilde{\sigma}_{vM2}$ at the center of the webplate Loading: shear

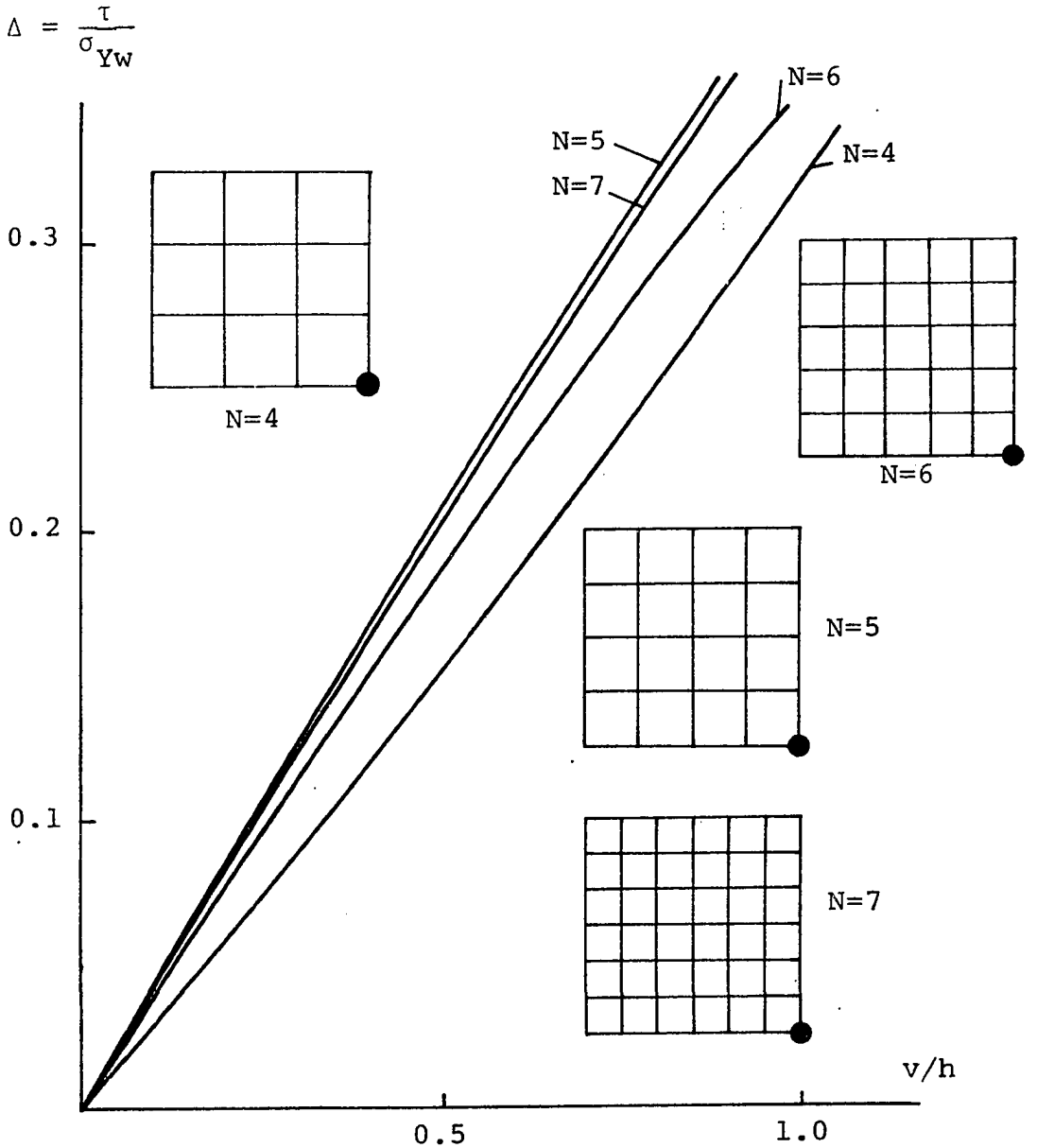

Figure B.6. Load-displacement v curve
Convergence check Loading: shear

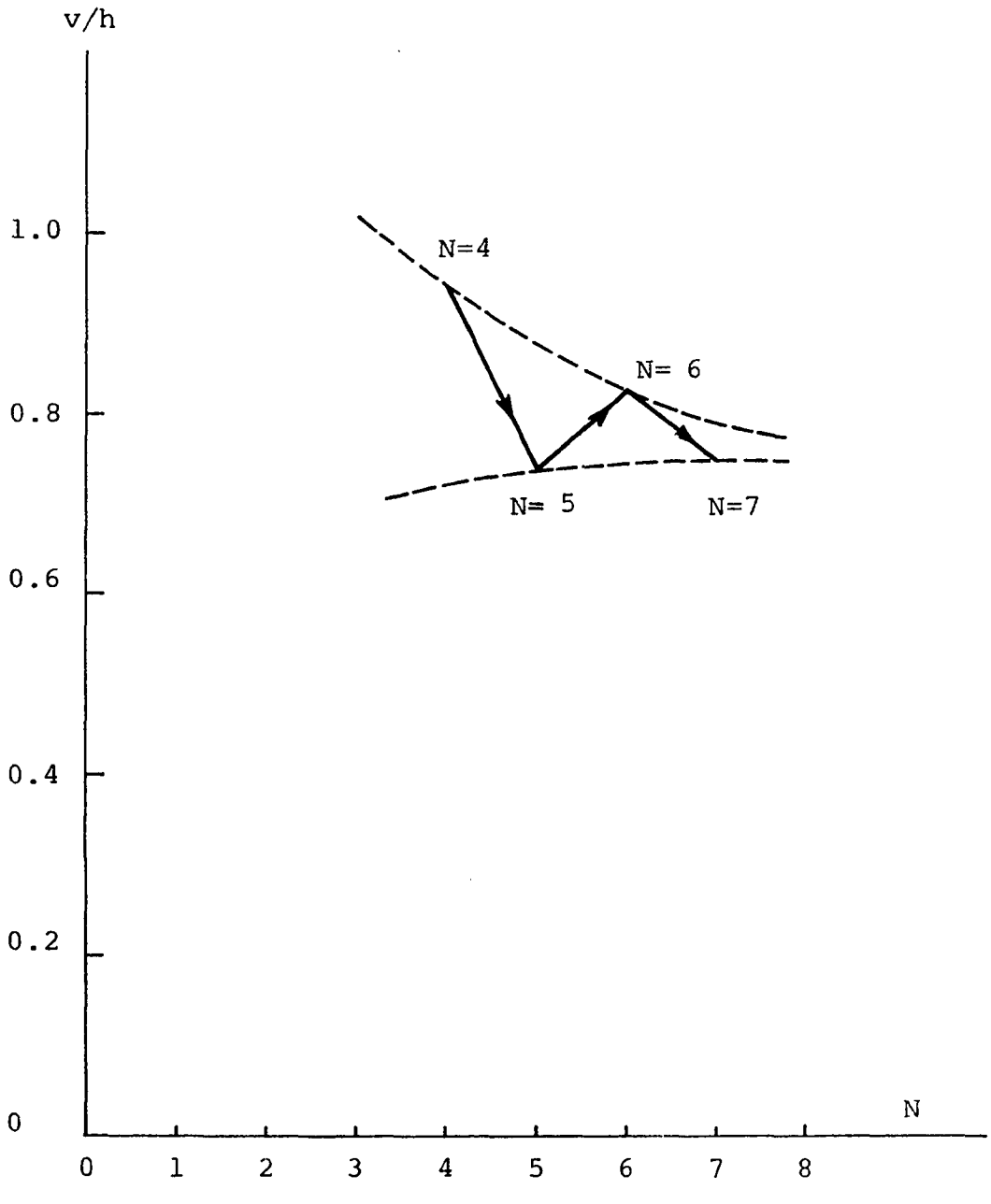

Figure B.7. Convergence curve for v
Test girder B-Q at Δ=0.30

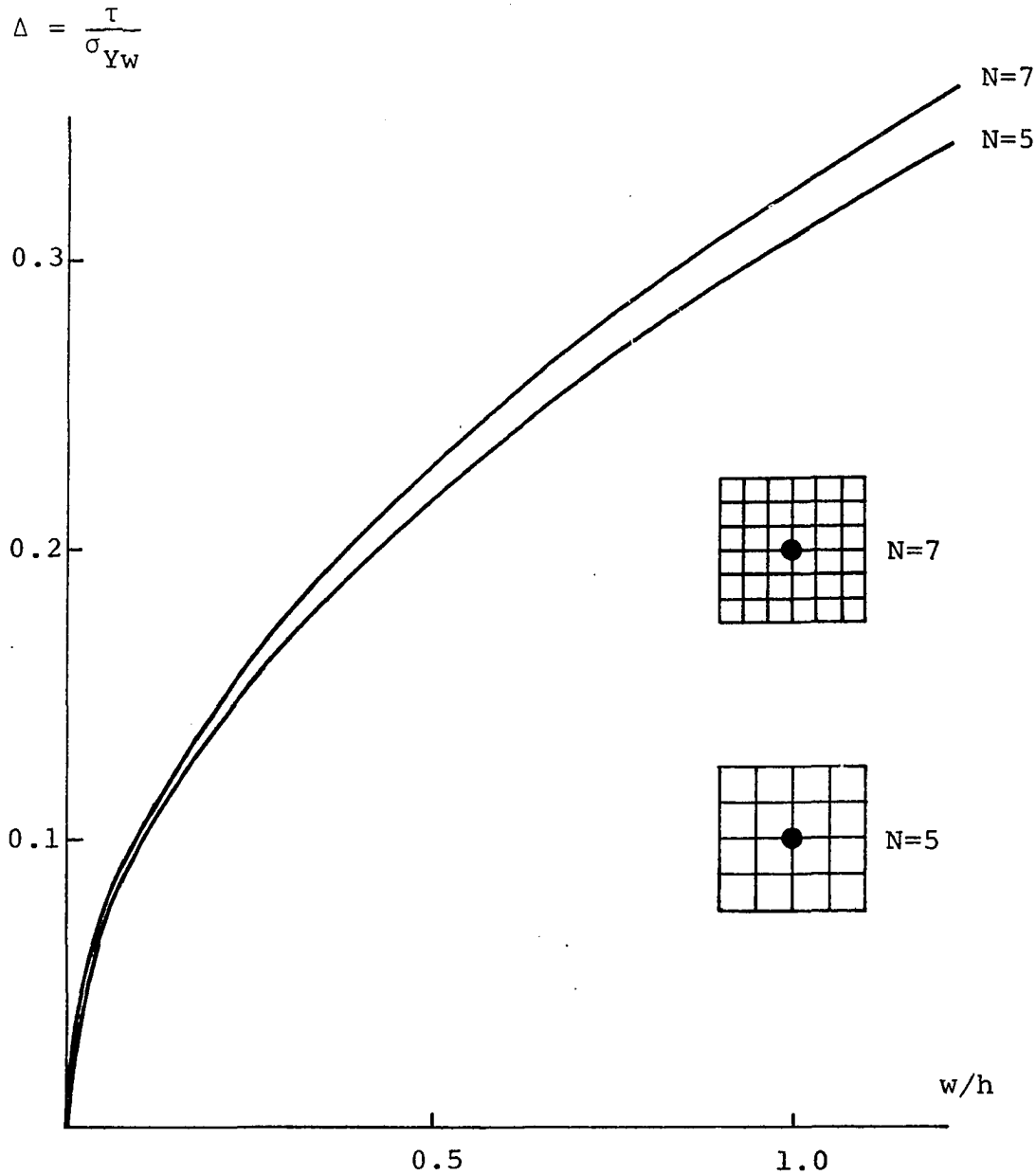

Figure B.8. Convergence for deflection w at the center of webplate Loading: shear

APPENDIX C: COMPUTER PROGRAMS

General Remarks

The computer programs used in this study consist of a main program and 12 subroutine subprograms. The computer program flow chart is shown in Figure C.1. The subroutine subprograms are shown in capitalized letters in this figure, except for UGELG, which is a library subroutine subprogram for solving a set of simultaneous equations by means of Gauss Reduction Method, each program is explained in the following.

Main program

This program serves as a medium by which subroutine subprograms are organized and input-output jobs carried out. It calls UGELG four times to solve sets of simultaneous algebraic equations.

Input The input data consists of four cards and includes the following quantities:

1. First card:

   ALPH (α); ZETA (ζ); AM (μ); AN (ν); TH (θ); AL (λ); BET (β),

2. Second card:

   FF (ϕ_f); FF1 (ϕ_f'); FS (ϕ_s); FS1 (ϕ_s'),

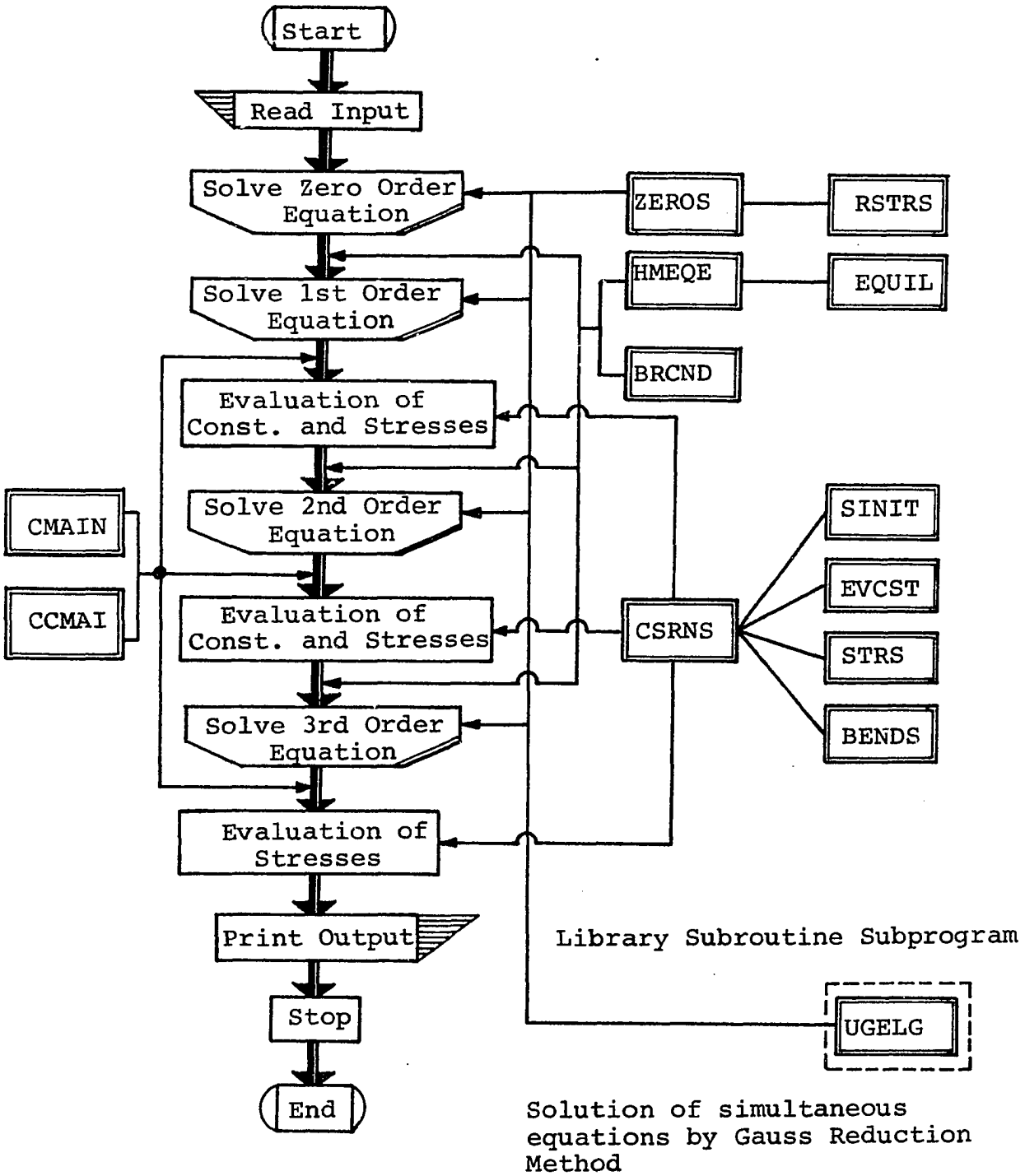

Figure C.1. Computer program flow chart

3. Third card:

PF (ψ_f); PF1 (ψ_f'); PS (ψ_s); PS1 (ψ_s'); AKF (κ_f); AKF1 (κ_f'),

4. Fourth card:

N; LEVEL; AMINL; ILD; INLD; KMAX,

where N = Dimension of mesh point system

LEVEL = Number of load levels

AMINL = Minimum load level, also used as load increment

ILD = Index showing the type of loading: 1 for shear or combined case, 2 for bending case

INLD = Index for the initial load level, usually 1

KMAX = Maximum order of approximation, usually 4

Output The output has been explained in Chapter Three.

Subroutine CMAIN

This program is a continuation of the main program and serves to evaluate derivatives for 2nd and 3rd order constants of simultaneous equations and to evaluate stresses along boundaries excluding those at corner points.

Subroutine CCMAI

This is also a continuation of the main program and serves in the same way as CMAIN except that this is for corner points.

Subroutine HMEQE

This forms matrix elements of simultaneous equations for the higher order equations of equilibrium.

Subroutine BRCND

This forms matrix elements of simultaneous equations for the higher order boundary conditions.

Subroutine ZEROS

This solve zero order equations.

Subroutine RSTRS

This program is for the evaluation of residual stress components.

Subroutine STRS

This program is for the evaluation of the in-plane stress components.

Subroutine BENDS

This program is for the evaluation of the bending stress components.

Subroutine EQUIL

This program is for the formation of linear operators for the equations of equilibrium for higher orders.

Subroutine EVCST

This program is for the detailed evaluation of constants of simultaneous equations for higher orders.

Subroutine SINIT

This program is for the initialization of constants and stresses.

Subroutine CSRNS

This program serves as a coordinator between SINIT, EVCST, STRS and BENDS.

APPENDIX D: DISCUSSIONS ON THE EXPANSION OF DISPLACEMENT COMPONENTS IN TERMS OF AN ARBITRARY PARAMETER

Discussions

In this thesis, the unknown displacement components u, v and w are assumed to have the form of power series of order three as shown by Equation 22. Consequently, the in-plane stress components and the plate bending stress components are also expressed in the form of power series of order three. If $u^{(3)}$, $v^{(3)}$ and $w^{(3)}$ are not considered as Equation 41 shows, then the expressions of stresses should include no third power, either.

In this section, the significance of the third order power terms are investigated by comparing two approximations, the second and the third approximations. The second approximation considers the terms only up to the second powers; on the other hand, the third approximation also takes into account the third powers. The contribution of each term is evaluated as follows:

Suppose, $\bar{\sigma}_x^T$ is to be considered. Then from Equations 1 and 23,

$$\bar{\sigma}_x^T = \sigma_{xo} + \bar{\sigma}_x^{(1)} \Delta + \bar{\sigma}_x^{(2)} \Delta^2 + \bar{\sigma}_x^{(3)} \Delta^3.$$

The contribution of the k-th power (k = 1,2,3) is evaluated by the following quantity:

$$|\bar{\sigma}_x^{(k)} \Delta^k| \Big/ \left[|\sigma_{xo}| + |\bar{\sigma}_x^{(1)} \Delta| + |\bar{\sigma}_x^{(2)} \Delta^2| + |\bar{\sigma}_x^{(3)} \Delta^3| \right] .$$

For all three types of loading considered in this thesis, the following results are found to be true:

1. The contribution of the 3rd power terms in the in-plane displacement components u and v is usually less than 10% of the total of the 1st through the 3rd power terms.

2. The contribution of the 3rd power term in the deflection w can be sometimes as high as 30% of the total deflection w^T. Furthermore, the 2nd power term of w is usually the greatest for webplates with relatively long post-buckling range and zero power term is the greatest for web-plates with large initial deflection and relatively short range of post-buckling.

3. The contribution of the 3rd power terms in the in-plane stress components $\bar{\sigma}_x$, $\bar{\sigma}_y$ and $\bar{\tau}_{xy}$ is usually small, say, less than 5% of the total of zero through the 3rd power terms. Furthermore, the 1st power terms are usually greater than the 2nd and 3rd power terms.

4. The contribution of the 3rd power terms in the plate bending stress components σ_{bx}, σ_{by} and τ_{bxy} is approximately in the same order of the 1st and 2nd power terms. By retaining these 3rd power terms better agreement with the experimental results can be obtained. Figure D.1 shows a comparison between the 2nd and the 3rd order approximations for test girder A-M.

It is seen that the 3rd order approximation is in better agreement with the experimental results. Similar remarks can be made with the other test girders cited in this thesis.

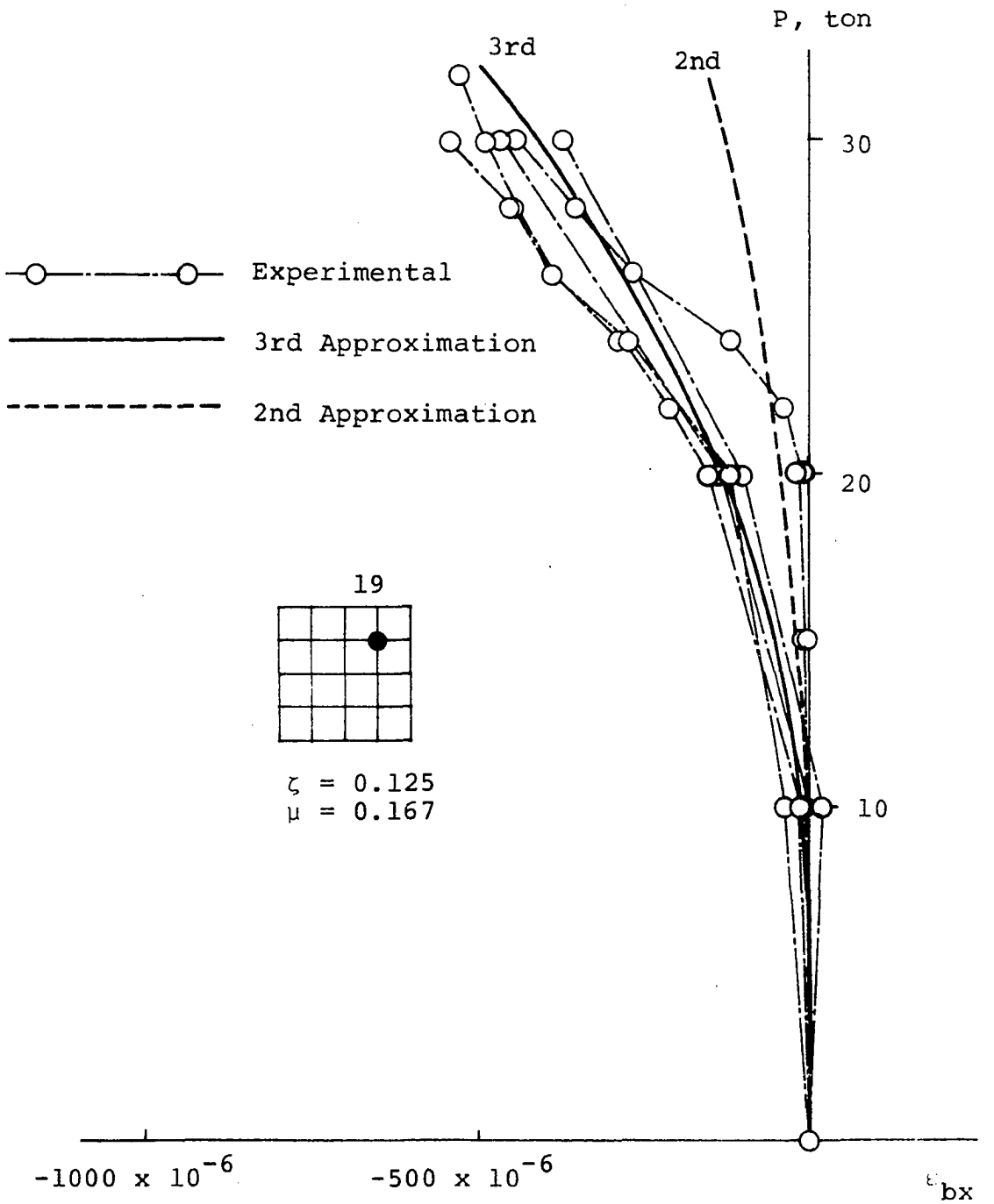

Figure D.1. P - ε_{bx} relationship: Test girder A-M
2nd and 3rd order approximations